

Tauno Vähä-Heikkilä

MEMS tuning and matching  
circuits, and millimeter wave  
on-wafer measurements



VTT PUBLICATIONS 596

# **MEMS tuning and matching circuits, and millimeter wave on-wafer measurements**

Tauno Vähä-Heikkilä

*Dissertation for the degree of Doctor of Science in Technology to be presented  
with due permission of the Department of Electrical and Communications  
Engineering for public examination and debate in Auditorium S4  
at the Helsinki University of Technology (Espoo, Finland)  
on the 27th of March, 2006, at 12 o'clock noon.*



ISBN 951-38-6704-8 (soft back ed.)

ISSN 1235-0621 (soft back ed.)

ISBN 951-38-6705-6 (URL: <http://www.vtt.fi/inf/pdf/>)

ISSN 1455-0849 (URL: <http://www.vtt.fi/inf/pdf/>)

Copyright © VTT Technical Research Centre of Finland 2006

JULKAISIJA – UTGIVARE – PUBLISHER

VTT, Vuorimiehentie 3, PL 1000, 02044 VTT

puh. vaihde 020 722 111, faksi 020 722 4374

VTT, Bergsmansvägen 3, PB 1000, 02044 VTT

tel. växel 020 722 111, fax 020 722 4374

VTT Technical Research Centre of Finland, Vuorimiehentie 3, P.O. Box 1000, FI-02044 VTT, Finland

phone internat. +358 20 722 111, fax +358 20 722 4374

VTT, Tietotie 3, PL 1000, 02044 VTT

puh. vaihde 020 722 111, faksi 020 722 7012

VTT, Tietotie 3, PB 1000, 02044 VTT

tel. växel 020 722 111, fax 020 722 7012

VTT Technical Research Centre of Finland, Tietotie 3, P.O. Box 1000, FI-02044 VTT, Finland

phone internat. +358 20 722 111, fax +358 20 722 7012

Vähä-Heikkilä, Tauno. MEMS tuning and matching circuits, and millimeter wave on-wafer measurements [Mikromekaaniset viritys- ja sovituspierit sekä millimetrialtoalueen suoraan kiekolta tehtävät mittaukset]. Espoo 2006. VTT Publications 596. 86 p. + app. 82 p.

**Keywords** RF MEMS, on-wafer measuring techniques, millimeter wave devices, impedance tuning, instrumentation, noise parameter measurements, reconfigurable matching networks, W-band measurement, double-stub tuners, triple-stub tuners, amplifier applications

## Abstract

The focus of this thesis is on the development of on-wafer measurement techniques for millimeter wave device and circuit characterization as well as on the development of MEMS based impedance tuning circuits both for measurement and telecommunication applications. Work done in this thesis is presented with eight scientific articles written by the author. The summary of the thesis introduces the field of on-wafer measurements and impedance tuning methods, and is followed by the articles.

Wide-band on-wafer measurement systems have been developed for noise parameter measurement at room temperature at W-band, and for cryogenic S-parameter measurements at 50–110 GHz and 20–295 K. Using the developed systems, noise parameters of an InP HEMT have been measured and results are shown in the frequency band of 79–94 GHz. These are the first published noise parameter measurement results for an active device at W-band, and first on-wafer measurement results at cryogenic conditions and at 50–110 GHz.

Novel RF MEMS impedance tuners have been developed for instrumentation and measurement applications to improve measurement automation and accuracy in on-wafer measurements. Several integrated impedance tuners have been realized to cover 6–120 GHz frequency range. RF MEMS technology has also been used for reconfigurable matching networks. Reconfigurable distributed 4–18 GHz and 30–50 GHz matching networks have been designed, fabricated, and characterized. These are based on switched 4 or 8 MEMS capacitors producing 16 or 256 different impedances. The matching networks are ideal for multi-band and wide impedance range amplifier as well as for antenna matching and tuning applications. Both the tuners and matching networks have shown state-of-the-art performance for circuits realized with integrated circuit technologies.

Vähä-Heikkilä, Tauno. MEMS tuning and matching circuits, and millimeter wave on-wafer measurements [Mikromekaaniset viritys- ja sovituspiirit sekä millimetriaaltoalueen suoraan kiekolta tehtävät mittaukset]. Espoo 2006. VTT Publications 596. 86 s. + liitt. 82 s.

**Avainsanat** RF MEMS, on-wafer measuring techniques, millimeter wave devices, impedance tuning, instrumentation, noise parameter measurements, reconfigurable matching networks, W-band measurement, double-stub tuners, triple-stub tuners, amplifier applications

## Tiivistelmä

Väitöskirjatyössä kehitettiin suoraan kiekolta tehtäviä millimetriaaltoalueen mittauksia sekä mikromekaanisia (MEMS) impedanssin säätö- ja sovituspiirejä.

Mittauslaitteistoja ja -menetelmiä kehitettiin suoraan kiekolta tehtäviin mittauksiin millimetriaaltoalueelle. Kohinaparametrien mittaamiseksi kehitettiin laitteisto W-alueelle (75–110 GHz), ja mittaustulokset esitetään InP HEMT -transistorille 79–94 GHz taajuusalueella. Sirontaparametrien mittaamiseksi kryogeenisissä olosuhteissa kehitettiin laitteisto W-alueelle, ja laajakaistaiset sekä kahden aaltoputkikaistan kattavat mittaustulokset esitetään InP HEMT -transistoreille 50–110 GHz:n taajuusalueella ja 20–295 K:n lämpötiloissa. Sekä molemmat mittauslaitteistot että esitettävät tulokset ovat ainutlaatuisia näillä taajuuksilla.

Kohinaparametrimittauslaitteistojen kehittämiseksi ja mittausten automatisoimiseksi väitöskirjatyössä suunniteltiin ja valmistettiin integroituja mikromekaanisia impedanssiviritimiä. Impedanssiviritimillä tuotetaan erilaisia impedansseja, ja niitä voidaan kontrolloida sähköisesti. Impedanssin säätö perustuu MEMS-kondensaattoreihin, ja kehitetyillä piireillä saadaan tuotettua tuhansia erilaisia impedansseja riippuen MEMS-kondensaattoreiden lukumäärästä. Impedanssiviritimiä kehitettiin usealle eri taajuusalueelle taajuuksien 6 ja 120 GHz välille. Virittimien tuottama heijastuskerroin on parhaimmillaan lähellä yhtä mitatun seisovan aallon suhteen ollessa 199 taajuudella 30 GHz. Työssä myös sovellettiin MEMS-kondensaattoreita impedanssinsovituspiireihin tehovahvistimen ja antennin sovittamiseksi. Piireissä integroidun siirtolinjan sähköistä pituutta ja impedanssia muutetaan. Mitatut tulokset osoittavat, että piireillä voidaan sovittaa paljon erilaisia impedansseja pienin häviöin ja lineaarisesti.

# Preface

I would like to thank everyone who allowed me to meet this important goal in my life. I wish to thank my advisor Research Professor Jussi Tuovinen at VTT for all his support, leadership, and encouragement during the thesis work.

Professor Antti Räisänen at the Helsinki Univ. of Technology contributed to this thesis in the finalization of the thesis and in the review process. His valuable comments are greatly appreciated.

I'm very thankful for Proferssor Gabriel M. Rebeiz for taking me to his group, sharing all his knowledge, guiding me during my stay at the Univ. of Michigan and also after that, and his friendship.

I am grateful to Dr. Jeremy Muldavin and Dr. Michael Schlechtweg for their valuable comments and pre-examination of the thesis. I'm also thankful to the opponent Prof. Herbert Zirath for agreeing to examine the thesis.

I would like to thank all people in MilliLab and the former Radio Technology Group at VTT: Alpo Ahonen, Hannu Hakojärvi, Markku Jenu, Mikko Kantanen, Timo Karttaavi, Anna Karvonen, Dr. Arttu Luukanen, Ilkka Marttila, Pekka Rantakari, Markus Rintamäki, Hannu Salminen, Dr. Jussi Varis, and Juha Volotinen, as well as people in other teams at VTT: Ari Alastalo, Prof. Hannu Kattelus, Anu Kärkkäinen, Markku Sipilä, Jussi Säily, and Mari Ylönen. I'm very thankful for Research Professor Aarne Oja for his guidance and support during my stay at VTT. I would like to thank Aija Kaski and Milja Heimonen for arranging my numerous travels all around the world.

I am grateful to all people of TICS group that I had possibility to get to know you in Michigan. First of all, Dr. Jad Rizk, who was my mentor in the clean room and Lebanese culture, and with whom I experienced many things both inside and outside of the clean room. Also, I have enjoyed the friendship of other lab-mates, Dr. Laurent Dussopt, Dr. Jose Canillas, Dr. Abbas Abbaspoor-Tamijani, Dr. Bernhard Schoenlinner, Dr. Kamran Entesari, Dr. Bryan Hung, Dr. Timothy Hancock, Dr. Andrew Brown, Dr. Kiran Nimmagada, Noriyo Nishijima, Koen van Caekenberghe, Michael Chang, Carson White, Chris Galbraight, San-June Park, Byung-Wook Min, Philip Grajek, and Helena Chan.

I would like to thank all of my Lebanese friends who were my family during my stay in the US. In addition to Gabriel and Jad, I'm thankful for Elias Abboud, Pierre Assouad, Walid El Asmar, Fadi Zoghby, Prof. Imad Btaich, and Tony Nawar.

I wish to thank Dr. Tapani Närhi from ESA, ESTEC, for his valuable comments in European Space Agency (ESA) funded projects as well as his encouragement during this thesis work.

This work has been carried out in 2000–2005 at MilliLab, VTT Technical Research Centre of Finland and the University of Michigan in projects funded by VTT, ESA, and DARPA IRFEE program. I would also like thank Graduate School of Electronics, Telecommunications, and Automation (GETA), Nokia Foundation, and Foundation of the Finnish Society of Electronics Engineers.

I would like to thank my parents Mirja-Leena and Jorma as well my sister Kaisa and brothers Kalle and Frans for their support. Finally, I would like to thank my wife Sini for her support and patience during the years.

Tauno Vähä-Heikkilä, Espoo, March 2005.

## List of publications

- [P1] T. Vähä-Heikkilä, M. Lahdes, M. Kantanen, and J. Tuovinen, "On-wafer noise parameter measurements at W-band." *IEEE Transactions on Microwave Theory and Techniques*, Vol. 51, no. 6, pp. 1621–1628, 2003.
- [P2] T. Vähä-Heikkilä, J. Varis, H. Hakojärvi, and J. Tuovinen, "Cryogenic on-wafer measurements at 50–110 GHz and at 20–295 K." *Proceedings of the 33rd European Microwave Conference*, Munich, Germany, 2003. Pp. 1167–1170.
- [P3] T. Vähä-Heikkilä, K. Van Caekenberghe, J. Varis, J. Tuovinen, and G.M. Rebeiz, "RF MEMS impedance tuners for 6–24 GHz applications." *Accepted for publication in International Journal of RF and Microwave Computer-Aided Engineering*, February 2006.
- [P4] T. Vähä-Heikkilä, J. Varis, J. Tuovinen, and G.M. Rebeiz, "A 20–50 GHz RF MEMS single-stub impedance tuner." *IEEE Microwave and Wireless Components Letters*, vol. 15, no. 4, pp. 205–207, 2005.
- [P5] T. Vähä-Heikkilä, J. Varis, J. Tuovinen, and G.M. Rebeiz, "A V-band single-stub RF MEMS impedance tuner." *Proceedings of the 34th European Microwave Conference*, Amsterdam, Netherlands, 2004. Pp. 1301–1304.
- [P6] T. Vähä-Heikkilä, J. Varis, J. Tuovinen, and G.M.Rebeiz, "W-band RF MEMS double and triple-stub impedance tuners." *2005 IEEE MTT-S International Microwave Symposium Digest*, Long Beach, CA, USA, 2005. Pp. 923–926.
- [P7] T. Vähä-Heikkilä, and G.M. Rebeiz, "A 4–18 GHz reconfigurable RF MEMS matching network for power amplifier applications." *International Journal of RF and Microwave Computer-Aided Engineering*, Vol. 14, no. 4, pp. 356–372, 2004.

- [P8] T. Vähä-Heikkilä, and G.M. Rebeiz, "A 20–50 GHz reconfigurable matching network for power amplifier applications." *2004 IEEE MTT-S International Microwave Symposium Digest*, Forth Worth, TX, USA, 2004. Pp. 717–721.

Contribution of the author in [P1–P8] is described on the next page. Furthermore, work relevant to the thesis including contribution of the author is also presented in [1–6].

## Contribution of author

Contribution of the author of this thesis is the following in publications P1–P8:

- [P1] The author developed the set-up and computational methods used in noise parameter measurements, under the supervision of M. Lahdes, M. Kantanen, and Prof. J. Tuovinen.
- [P2] The author developed the system together with the co-authors. The author carried out measurements and data analysis. Dr. J. Varis and Prof. J. Tuovinen supervised the work.
- [P3] The author designed, fabricated, and measured circuits under the supervision of Prof. G. M. Rebeiz. Dr. J. Varis and Prof. J. Tuovinen collaborated in the preliminary selection of tuner topologies and definitions of specifications. K. Van Caekenberghe built a bias control board.
- [P4] The author designed, fabricated, and measured circuits under the supervision of Prof. G. M. Rebeiz. Dr. J. Varis and Prof. J. Tuovinen collaborated in the preliminary selection of tuner topologies and definitions of specifications.
- [P5] The author designed, fabricated, and measured circuits under the supervision of Prof. G. M. Rebeiz. Dr. J. Varis and Prof. J. Tuovinen collaborated in the preliminary selection of tuner topologies and definitions of specifications.
- [P6] The author designed, fabricated, and measured circuits under the supervision of Prof. G. M. Rebeiz. Dr. J. Varis and Prof. J. Tuovinen collaborated in the preliminary selection of tuner topologies and definitions of specifications.
- [P7] The author designed, fabricated, and measured circuits. Prof. G. M. Rebeiz supervised the work.
- [P8] The author designed, fabricated, and measured circuits. Prof. G. M. Rebeiz supervised the work.

# Contents

Abstract.....	3
Tiivistelmä.....	4
Preface.....	5
List of publications.....	7
Contribution of author.....	9
Abbreviations.....	12
List of symbols.....	15
1. Introduction.....	17
1.1 Short introduction to millimeter wave low noise receivers.....	18
1.2 Research problem of this thesis.....	20
1.3 Scope and contents of this thesis.....	21
1.4 New scientific results.....	22
2. Millimeter wave on-wafer measurement techniques.....	23
2.1 Cryogenic on-wafer measurements at V- and W-band.....	23
2.2 On-wafer noise parameter measurements.....	26
3. Reconfigurable RF MEMS impedance tuners and matching networks.....	34
3.1 Tuner topologies.....	39
3.1.1 Stub-based impedance tuners.....	39
3.1.2 Slug tuners.....	43
3.2 Components for electrically controllable impedance tuners.....	44
3.2.1 Varactor diodes and transistors.....	44
3.2.2 MEMS switches and varactors.....	45
3.2.3 Sliding planar backshorts.....	54
3.3 Realized impedance tuners.....	55
3.3.1 Active device based impedance tuners and matching networks.....	55
3.3.2 Impedance tuners based on sliding planar backshorts.....	55
3.3.3 Stub-based impedance tuners and matching networks realized with MEMS switches.....	55

3.3.4 Distributed impedance tuners and matching networks realized with MEMS switches .....	63
4. Summary of publications .....	67
5. Conclusion .....	70
References.....	72

## Appendices

Appendix A: Detailed surface MEMS fabrication procedure used in this thesis  
Publications P1–P8

# Abbreviations

ALMA	Atacama Large Millimeter Array
Au	Gold
CPS	CoPlanar Stripline
CPW	CoPlanar Waveguide
DC	Direct Current
DMTL	Distributed MEMS Transmission Line
DUT	Device Under Test
ESA	European Space Agency
ESTEC	European Space Research and Technology Centre
GPIB	General-Purpose Interface Bus
HEMT	High Electron Mobility Transistor
HTS	High Temperature Superconductor
LNA	Low Noise Amplifier
LO	Local Oscillator
LRRM	Line-Reflect-Reflect-Match
MAM	Metal-Air-Metal
MAP	Microwave Anisotropy Probe
MEMS	MicroElectroMechanical Systems

MilliLab	Millimeter Wave Laboratory of Finland – MilliLab
MIM	Metal-Insulator-Metal
MMIC	Monolithic Microwave Integrated Circuit
PC	Personal Computer
PECVD	Plasma Enhanced Chemical Vapor Deposition
PMMA	Polymethylmethacrylate
RF	Radio Frequency
RIE	Reactive Ion Etching
SDA	Scratch Drive Actuator
SiCr	Silicon Chrome
Si <sub>x</sub> N <sub>y</sub>	Silicon Nitride
SOLT	Short-Open-Load-Thru
S-parameter	Scattering parameter
SPB	Sliding Planar Backshort
Ti	Titanium
TRL	Thru-Reflect-Line
V-Band	50–75 GHz waveguide frequency band
VLBA	Very Long Baseline Array
VNA	Vector Network Analyzer
VSWR	Voltage Standing Wave Ratio

VTT	Valtion Teknillinen Tutkimuskeskus, Technical Research Centre of Finland
W-Band	75–110 GHz waveguide frequency band
WLAN	Wireless Local Area Network
WR-10	75–110 GHz waveguide
WR-15	50–75 GHz waveguide

## List of symbols

$A$	Area of electrodes in a capacitor
$C$	Capacitance of a capacitor
$C1$	Fixed capacitance
$C2$	Fixed capacitance
$C3$	Fixed capacitance
$C_{\text{FIXED}}$	Capacitance of a fixed capacitor
$C_{\text{MAM}}$	Capacitance of a metal-air-metal capacitor
$C_{\text{MEMS}}$	Capacitance of a MEMS switch or varactor
$C_{\text{TOT}}$	Total capacitance
$F$	Noise figure
$F_{\text{min}}$	Minimum noise figure
$l$	Transmission line length
$L_1...L_5$	Electrical length of a transmission line
$L_{\text{MEMS}}$	Inductance of a MEMS switch or varactor
$N$	Number of elements
$R_{\text{FIXED}}$	Resistance of a fixed capacitor
$R_{\text{MEMS}}$	Resistance of a MEMS switch or varactor
$r_n$	Normalized noise resistance

S1–S11	Switch numbers
$Z_0$	Characteristic impedance of a transmission line
$Z_1...Z_3$	Impedance of a transmission line
$\beta$	Propagation constant
$\delta$	Distance between electrodes in a capacitor, gap
$\epsilon_0$	Permittivity of vacuum
$\epsilon_r$	Relative dielectric constant
$\Gamma_i$	Source reflection coefficient
$\Gamma_{MAX}$	Maximum reflection coefficient
$\Gamma_{opt}$	Optimum reflection coefficient

# 1. Introduction

Millimeter wave (30–300 GHz) technology has been traditionally used mostly in scientific and military applications, but during the last decade this technology has been applied also to commercial applications. Examples of several planned or realized radio astronomical and cosmological missions are WMAP [7], Planck [8], VLBA [9], and ALMA [10]. Commercial applications at millimeter wave lengths are, for example, automotive radars around 77 GHz e.g. [11, 12], mobile broadband telecommunication systems operating in the 62–63 GHz and 65–66 GHz bands, wireless local area networks (WLAN) in the 59–62 GHz band in Europe, and radio links at 38, 42, 58 and 94 GHz e.g. [13–16]. Millimeter wave imaging systems have also been developed both for commercial and defense applications, and they operate around 94 GHz e.g. [17–19].

High performance receivers are needed in all above mentioned applications at millimeter wave lengths. Low noise amplifiers (LNA) are key elements in these receivers and their performances have to be optimized, at least, in terms of noise, gain, and power consumption. LNAs are based on transistors, which need to be characterized and modeled before low noise amplifiers can be designed. With on-wafer measurements, devices and circuits are characterized directly from a chip or wafer. On-wafer measurements play an important role at millimeter wave frequencies and in cryogenic conditions.

As a part of integrated circuit technologies, micromachining and micro-electromechanical systems (MEMS) technologies have made their breakthrough also to millimeter wavelengths. MEMS are micro scale mechanically movable elements that are controlled electrically. The MEMS technology is applied at millimeter wavelengths, for example, for switching [20–24], phase shifting [21, 22, 24–30], filtering [31–34], impedance tuning [35, P4, P5], tunable antennas [36], and multilines-TRL calibration standards [37].

## 1.1 Short introduction to millimeter wave low noise receivers

Receivers have an important role in all millimeter wave scientific, defense, and commercial applications [38–41]. A simple millimeter wave receiver contains at least an antenna and a detector (Figure 1a). This kind of receiver is called a direct detection receiver. The diode detector after the antenna directly converts the millimeter wave power to voltage. In addition to the frequency selectivity of the antenna or a possible filter between the antenna and detector, the direct detection receiver does not have frequency selectivity. It is mostly suitable for applications, where the total power information of a certain frequency band is needed like in millimeter wave imaging applications or as a wideband receiver together with a narrowband swept source e.g. [17–19, 38, 39, 41]. The sensitivity of the receiver can be improved by using a low noise amplifier before the diode detector (Figure 1b). Up to-date, LNAs have been developed up to G-band (140–220 GHz) frequencies [49–51].

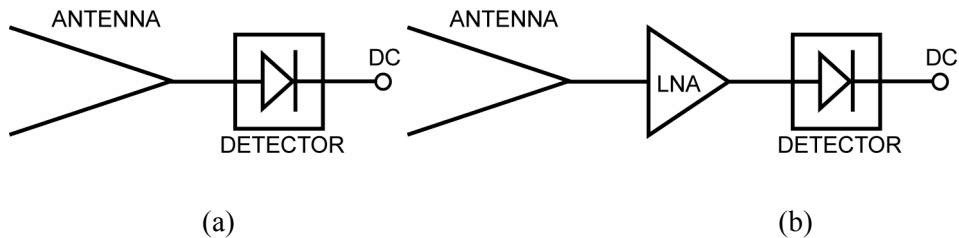


Figure 1a. Schematics of a direct detection receiver, b) a direct detection receiver with an LNA.

Another common type of a receiver, used in millimeter wave applications, is a superheterodyne receiver. The millimeter wave part of the simplest superheterodyne receiver consists of an antenna, mixer, and local oscillator (LO). A millimeter wave signal is received with the antenna, and is down-converted from millimeter wave frequencies to intermediate frequencies (IF) using the mixer with the LO. The local oscillator is also used for the selection of the millimeter wave frequency down-converted to the IF. This kind of frequency selectivity is an important property, which has been used intensively, for example, in millimeter wave spectroscopy of  $\text{H}_2\text{O}$  and  $\text{O}_2$ , at 60 GHz, 118.75 GHz, and 183.5 GHz [38].

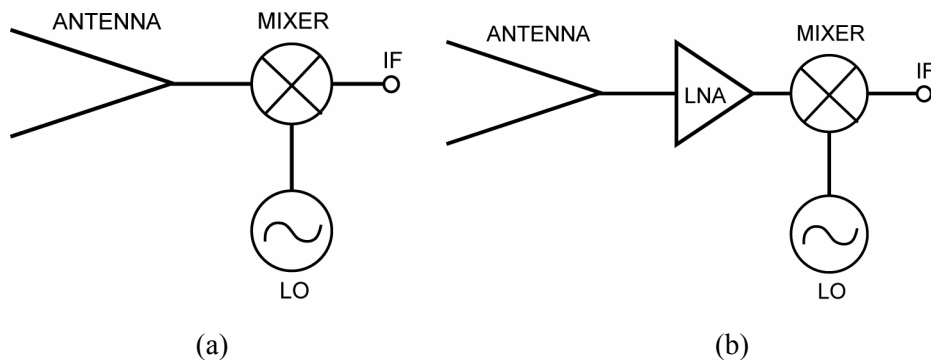


Figure 2. a) Schematics of a superheterodyne receiver, and b) a superheterodyne receiver with an LNA.

High stability low noise receivers used in advanced applications, like in the Planck mission, are more complicated than receivers in Figures 1 and 2. The Planck Surveyor has three channels at 30, 44, and 70 GHz in its low frequency instrument [42]. Figure 3 shows the schematics of these low noise receivers. The receiver front-end is cooled down to 20 K and the back-end is at 300 K. The receiver is based on direct detection, and it has about 60 dB gain.

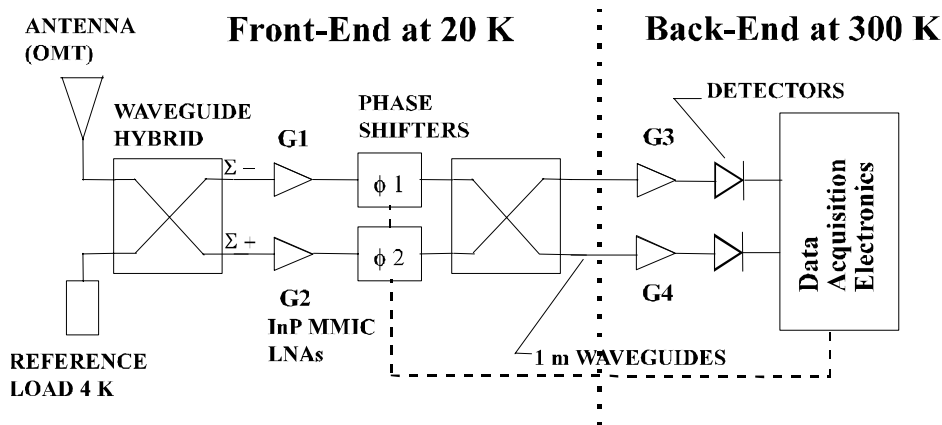


Figure 3. Schematics of low noise receivers used in the Planck mission at 30, 44, and 70 GHz [42].

Having low noise figure and high gain, low noise amplifiers are very important circuits in low noise receivers increasing their sensitivity. Currently, the use of

an LNA is beneficial before a mixer in low noise receivers up to about 200 GHz at room temperature and up to about 100 GHz at cryogenic temperatures [42]. Figure 4 shows a photograph of an LNA developed in the Planck Surveyor project. The LNA consists of four transistors. Cryogenic cooling lowers a temperature dependent resistance in transistors thus lowering their noise figure and increasing their gain.

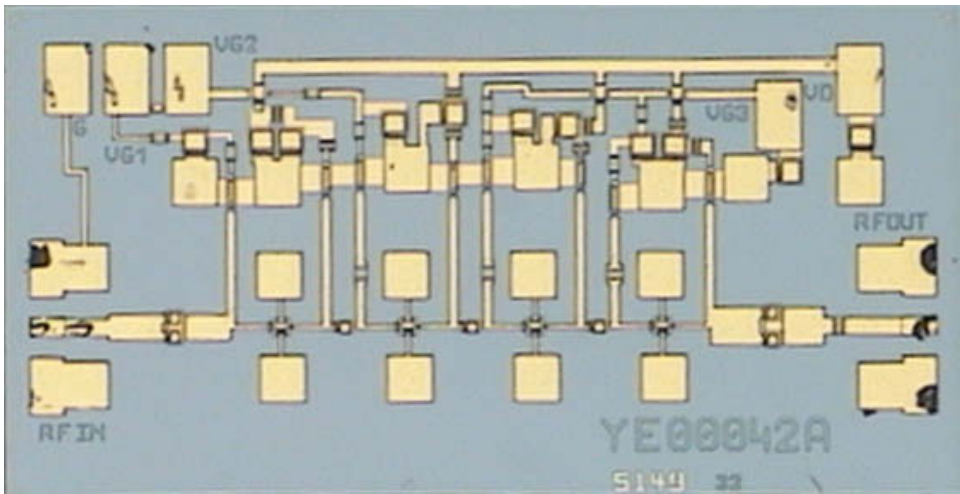


Figure 4. Photograph of a four-stage LNA developed in the Planck mission. The size of the chip is about 1.1 mm x 2.1 mm.

## 1.2 Research problem of this thesis

To design low noise amplifiers, models for transistors are needed. Transistors used in low noise amplifiers are treated as linear two-ports, and both the S- and noise parameters of the transistors are needed in the design of LNAs [43]. These can be obtained with simulations, but often on-wafer measurements are the most practical and accurate way to get them at millimeter wavelengths. After the design and fabrication of an LNA, its performance needs also to be measured, because it will be used as a part of a receiver. These measurements are usually done using on-wafer measurement methods. If LNAs are used in cooled cryogenic applications as in the Planck Surveyor, cryogenic on-wafer measurements are also needed both for transistors in the design phase and for fabricated LNAs in the receiver building phase.

The lack of commercially available on-wafer measurement systems for cryogenic and noise parameter measurements at W-band was the first practical research problem in this thesis work. Also, the level of measurement automation and accuracy could be increased with electrically controllable impedance tuners. To study suitable technologies and develop such integrated impedance tuners was the second research problem in this thesis work.

### **1.3 Scope and contents of this thesis**

The focus of this thesis is on the development of on-wafer measurement techniques for millimeter wave device and circuit characterization as well as on the development of MEMS based circuits both for measurement and telecommunication applications. The research has been carried out at the Millimeter Wave Laboratory of Finland – MilliLab, VTT Technical Research Centre of Finland and at the Radiation Laboratory, University of Michigan, Ann Arbor, USA.

This thesis is divided into two parts: a summary and eight scientific articles. The summary gives introduction to the research area and results presented in the scientific articles. Introduction gives also a short introduction to low noise receivers, and shows how this thesis is connected to the low noise receiver development. In the summary, Chapter 2 discusses basic techniques related to on-wafer noise parameter measurements as well as on-wafer S-parameter measurements in cryogenic conditions. Chapter 3 gives introduction to integrated impedance tuners, presents several technologies used in impedance tuners, and compares existing integrated impedance tuners. Chapter 4 summarizes the work carried out in publications [P1–P8]. Both conclusions and future work are presented in Chapter 5.

Publications [P1, P2] and Chapter 2 present a cryogenic on-wafer S-parameter measurement systems for the 50–110 GHz frequency band, and noise parameter measurement system for W-band frequencies both developed in this thesis work. Both the S- and noise parameters of transistors needed in the LNA design can be measured with the measurement system. To improve on-wafer noise parameter measurement systems, MEMS based impedance tuners have also been developed in this thesis work. This development work is presented in Chapter 4

and publications [P3–P8]. Other publications related to this thesis work [1–5] present on-wafer measurement systems for transistor and LNA characterization. All these on-wafer measurement systems have been an important part of low noise receiver development at MilliLab as well as commercially available on-wafer measurement services provided by MilliLab.

## **1.4 New scientific results**

This thesis has produced new knowledge and scientific results in the following areas:

- 1) cryogenic on-wafer measurements at millimeter wavelengths;
- 2) on-wafer noise parameter measurement methods and a system for W-band device characterization;
- 3) novel impedance tuners for measurement applications based on RF MEMS technology;
- 4) novel reconfigurable matching networks for telecommunication applications based on RF MEMS technology.

## **2. Millimeter wave on-wafer measurement techniques**

On-wafer measurements are used for electrical characterization of components and circuits directly from a wafer or chip. On-wafer measurement techniques have been used in component characterization as long as integrated circuit techniques have been used in component fabrication. Component properties like DC-curves have been measured with needles already tens of years. Scattering (S-) parameter measurement is a basic tool in microwave and millimeter wave circuit characterization. The first wideband on-wafer measurement systems at microwave frequencies were presented at the beginning of 80's [44, 45]. Since that time, development work to extend on-wafer measurements to the millimeter wave frequencies have been carried out. Development has been driven mostly by scientific and military applications. On-wafer S-parameter measurement systems for W-band component and circuit characterization were presented in the beginning of nineties reaching 110 GHz [46–48]. In the late nineties and in the beginning of this century, on-wafer S-parameter measurements reached 200 GHz [48–51]. However, progress in on-wafer noise figure measurements has not been so fast. On-wafer measurement systems for noise figure and gain measurements at W-band have been published covering just part of the whole waveguide band [53–55]. For the first time, wideband 50–110 GHz on-wafer noise figure and gain measurements has been demonstrated in this work covering both the V- and W-bands [3]. In addition measurements over a wide frequency band, automated wafer scale measurements can be carried out with the developed measurement set-ups.

### **2.1 Cryogenic on-wafer measurements at V- and W-band**

Especially in radio astronomical applications, active components and circuits are cooled down to low temperatures (10–100 K) in order to obtain as high performance as possible [8]. Also, on-wafer measurements are often the easiest and most straightforward way to get models for transistors and high temperature superconductor (HTS) devices at low temperatures and at millimeter wavelengths. For example, measured transistor models at cryogenic temperatures are needed in the design of cooled low noise amplifiers. Cryogenic on-wafer

measurement systems have been developed in other research groups mostly for frequencies below 50 GHz [56–58]. The first on-wafer measurement set-up for above 50 GHz for S-parameter measurements was developed at MilliLab [59]. In this thesis work, the V-band measurement system has been extended to W-band [1], and also, wideband 50–110 GHz cryogenic on-wafer S-parameter measurements of HEMTs have been demonstrated [P2, 5].

The developed cryogenic measurement system is based on a commercial cryogenic on-wafer system by Nagase Co originally designed for measurements below 50 GHz. The Nagase system consists of a stainless steel vacuum chamber, vacuum pump, cryocooler, cold plate (chuck) for the test devices, and a temperature controller. In addition to the Nagase system, a video microscope and a temperature monitor with four silicon diode temperature sensors have been acquired. All the installations necessary for waveguide based measurements above 50 GHz have been designed and built in-house.

The vacuum chamber has several feed throughs for both mechanical manipulators and electrical connections (Figure 5). Three of these are for RF and bias probe holders connected to xyz translation stages and one is for y-directional translation arm used for moving the chuck in that direction. The probes can be moved with the manipulators about the area of 25 mm x 25 mm. The probe holders are connected to a 10 K cold head with cold fingers. Two of the feed throughs have been built in-house for connecting WR-10 or WR-15 waveguides.

Inside the vacuum chamber, special in-house built spiral-shape metal waveguides are used for connecting the two feed throughs to the RF probes (see Figure 5). Each of the waveguides is about 450 mm long and consists of three sections. Two of the sections are gold-plated copper, and the third one is gold-plated stainless steel. The steel section is about 200 mm long, and it is provided for reasons of temperature isolation as well as mechanical flexibility. The feed throughs are in room temperature, whereas the device under test (DUT) can have a temperature as low as 15 K. The steel sections reduce heat flow to the DUT helping to maintain the wanted testing temperature. This flexibility of the steel sections makes it possible to adjust the positions of the RF probes.

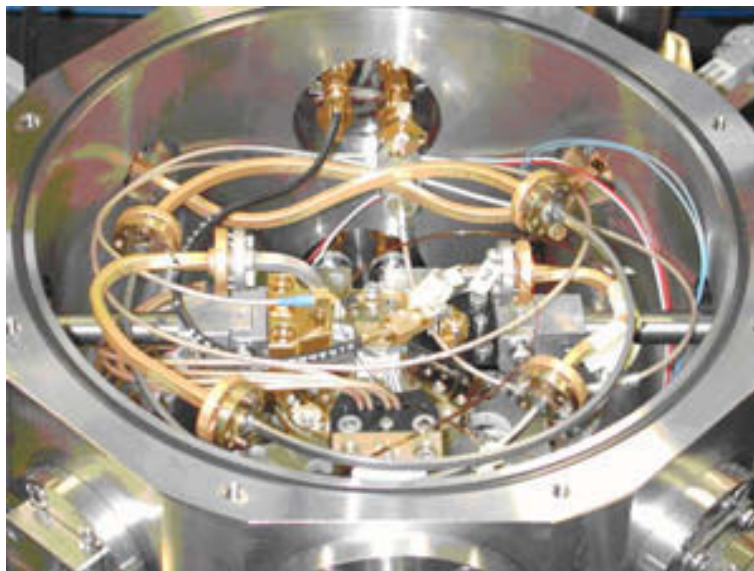
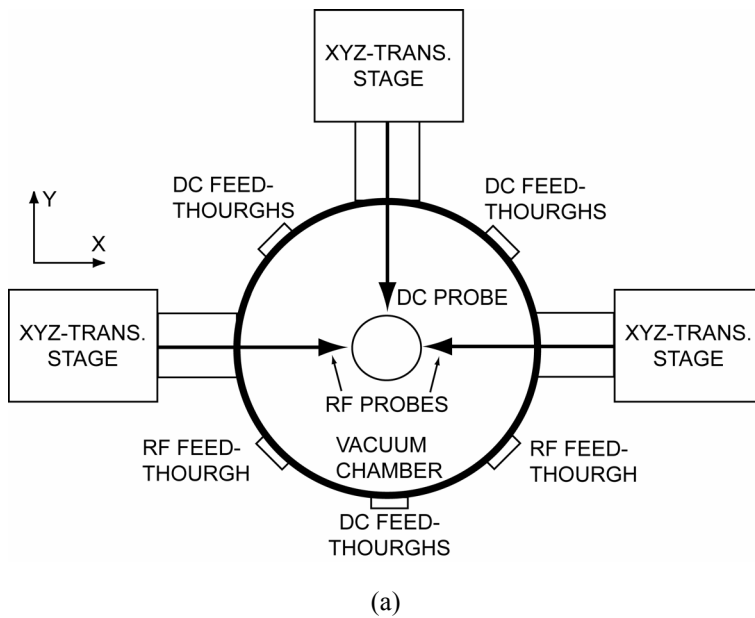


Figure 5. a) A schematic drawing of the cryogenic measurement station. b) A photograph showing the RF and bias probes with waveguide installations inside the vacuum chamber.

Publication [P2] describes the measurement systems and procedures for cryogenic on-wafer measurements at 50–110 GHz. The S-parameters of HEMTs (DaimlerChrysler and HRL) were measured at W-band and temperatures between 20 K and 295 K using the developed system [P2, 1]. HEMTs were also characterized in the 50–110 GHz frequency band and 20–295 K. Results showed good continuity between V and W-bands. For the first time, a cryogenic on-wafer measurement system and measurement results were presented at W-band and 50–110 GHz, being only published results for at this frequency range [1, 5, P2].

Error analysis for cryogenic S-parameter measurements was carried out in this work. Repeatability of on-wafer calibration and sensitivity for probe movements were investigated [5]. Repeatability of on-wafer calibration was moderate at W-band and good at V-band. The W-band measurement system was sensitive for x-directional probe movement, which caused the most significant errors. These errors were most probably due to the mechanical bending of the spiral waveguides. As a result of error analysis carried out in [5], the measurement system has been decided to be further develop. This includes the replacement of the spiral waveguides by straight waveguides to avoid bending of the waveguides.

## 2.2 On-wafer noise parameter measurements

Noise properties of a two-port can be presented using noise parameters. Noise parameters describe how the noise figure of the two-port changes as a function of source reflection coefficient. For example, noise figure of a HEMT varies as a function of source reflection coefficient. This is important information in the design of low noise amplifiers, because the LNA should provide a low noise figure and high gain at the same time.

The noise figure of a linear two-port as a function of source reflection coefficient  $\Gamma_i$  is given by [60]:

$$F = F_{\min} + \frac{4r_n}{1 - |\Gamma_i|^2} \left| \frac{\Gamma_i - \Gamma_{\text{opt}}}{1 + \Gamma_{\text{opt}}} \right|^2 \quad (1)$$

where  $F_{\min}$  is the minimum noise figure of the two-port,  $r_n$  is the normalized (with reference impedance) noise resistance, and  $\Gamma_{\text{opt}}$  is the optimum reflection coefficient. Variables  $F_{\min}$ ,  $r_n$  and  $\Gamma_{\text{opt}}$  are called noise parameters. Graphical three-dimensional representation of Equation (1) in Figure 6 shows the noise paraboloid over the Smith chart. The minimum noise figure can be achieved with the optimum reflection coefficient.

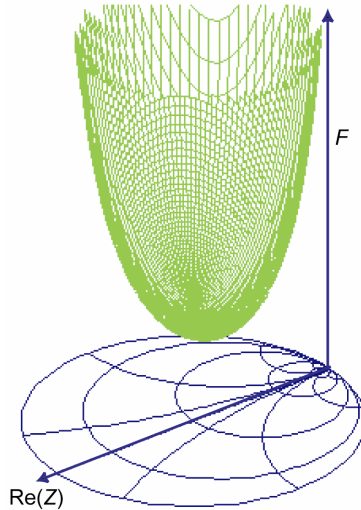


*Figure 6. Graphical presentation of noise the figure paraboloid.*

Noise parameters cannot be measured directly. In order to measure them, the input reflection coefficient of a device under test, DUT, is changed, and the corresponding noise figure of the DUT is measured. During late fifties and sixties, an experimental searching method for minimum noise figure and corresponding optimum reflection coefficient was used [61]. However, this method was found to be slow and inaccurate [62]. Alternatively, the noise figure paraboloid and noise parameters can be obtained by fitting Equation (2.1) to the measured data [62]. In order to do the fitting, the noise figure of the DUT should be measured at least with four different  $\Gamma_i$  values because  $\Gamma_{\text{opt}}$  is a complex quantity. Several methods have been developed for the noise parameter extraction purpose [62–66]. Lane’s method [62] uses a least-squares data fitting technique, and it is used in this work [P1].

The schematics of a noise figure and traditional noise parameter measurement set-ups are shown in Figure 7 [61]. In noise figure measurements, a noise source producing two different noise temperatures is connected to the input of the device under test, and corresponding noise powers are measured with the noise receiver. This kind of measurement system is used for noise characterization with a 50- $\Omega$  reference impedance. In this work, similar systems have been used for wideband on-wafer noise figure and gain measurements of low noise amplifiers [2, 3, 5]. This kind of a set-up has also been used as a basis of the so-called F50 noise parameter extraction method [67–69]. The F50 method is a tunerless method, where wideband noise figure measurements are carried out, and transistors noise models are fitted to this data. These set-ups are simpler because impedance tuners are not needed but on the other hand, wideband measurements are necessary as well as accurate noise models for transistors. Suitability of the F50 method for noise characterization and modeling purposes has also been criticized due to the lack of accurate noise models at millimeter wavelengths [70].

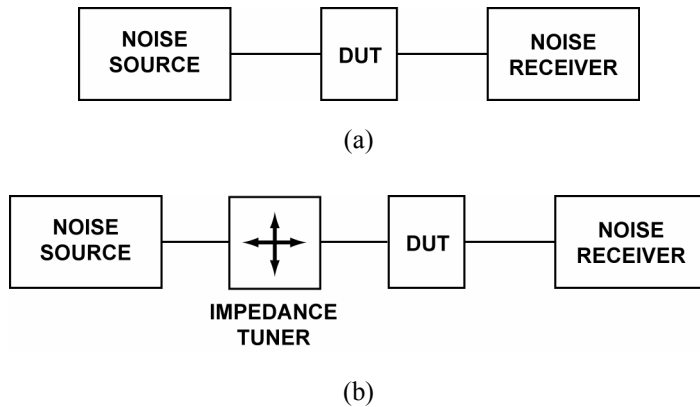


*Figure 7. Schematics of a) noise figure measurement system and b) traditional noise parameter measurement system.*

The traditional noise parameter measurement system has an impedance tuner between the noise source and DUT in order to generate impedances differing from 50- $\Omega$  (Figure 7b). The loss of the two-port tuner increases at the same time when the magnitude of the reflection coefficient is increased. This is problematic because the noise power delivered to DUT is reduced lowering the measurement accuracy [71].

Improved measurement systems for noise parameter measurements are shown schematically in Figure 8. These systems are based on the cold-source method, because the noise source is used here only for the calibration of the noise receiver, and is not needed for the noise measurements of DUT [71–73]. If the noise source is at the input side of DUT (Figure 8a), the device under test is replaced with thru connection in receiver calibration. If the noise source is at the output side of DUT (Figure 8b), then just a switch is needed to connect the noise source to the noise receiver. The later method is used in this work [P1].

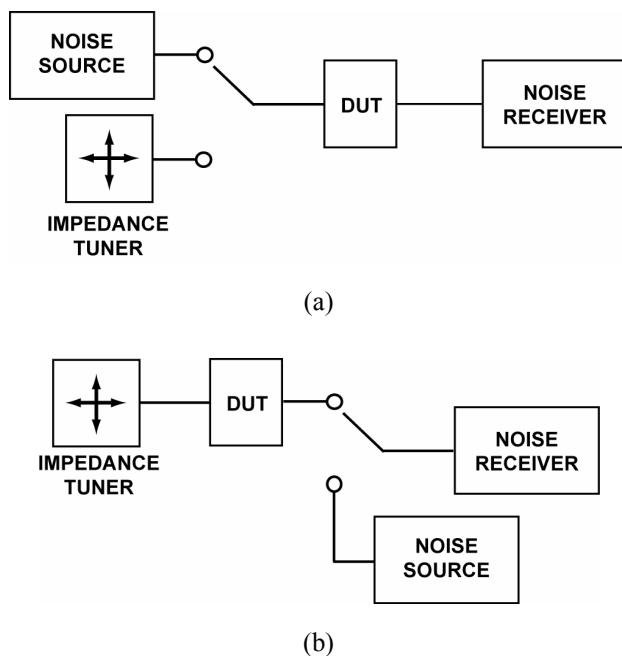


*Figure 8. Schematics of the cold-source measurement set-ups for noise parameter measurements.*

Waveguide based (WR-10) on-wafer measurement set-up used in this work is presented schematically in Figure 9 [P1, 6]. Also, the reference planes A, B, C, D, and E are shown there. DUT is connected to the measurement system using waveguide probes. By including two waveguide switches, both noise and S-parameter measurements can be done without breaking any connections. Only a simple uncalibrated 1-port impedance tuner is needed at the input side of the device under test. This is possible due to the switch 1. The 1-port tuner consists of an adjustable waveguide backshort and attenuator. System characterization

and the S-parameter measurements of DUT are done using a HP8510C vector network analyzer. Also, the VNA is needed during noise measurements of DUT to measure the reflection coefficient of the impedance tuner. The noise source is used here only during the calibration of the noise receiver. The noise receiver calibration can also be done during long measurement sessions without breaking any connections due to the switch 2. An LNA is used for increasing the sensitivity of the noise receiver. The LNA was obtained through the Planck Surveyor collaboration [8]. The mixer is used for downconverting the noise power from W-band to the measurement region of a HP8970A noise figure meter. The local oscillator (LO) chain consists of a HP83650A synthesized sweeper, HP8349B microwave amplifier, and HP83558A mm-wave source module. All measurement instruments are controlled using a PC via GPIB line. The PC and in-house written software make automatic data acquisition and complex calculations possible.

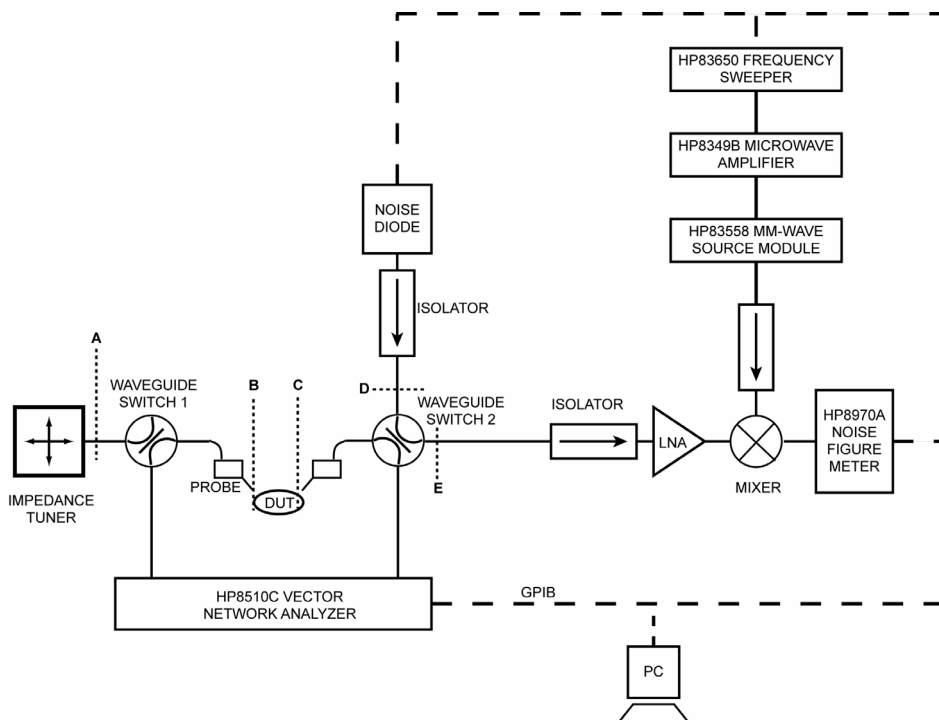
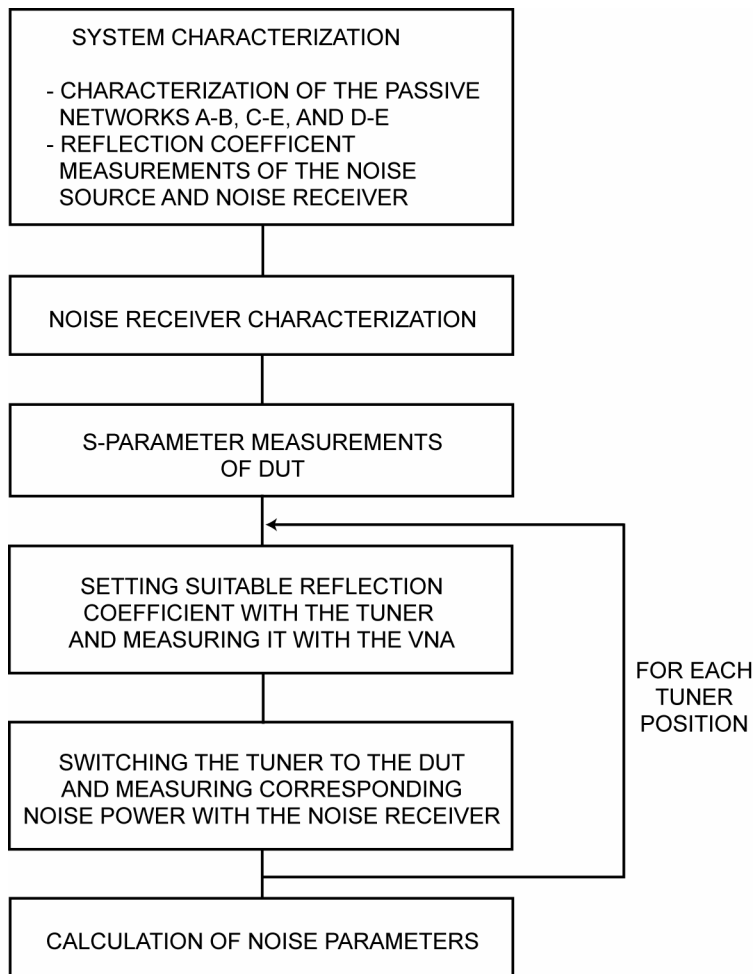


Figure 9. Schematics of the W-band on-wafer measurement system used in this work. Reference planes A, B, C, D, and E are also shown [P1].

On-wafer noise parameter measurements consist of several steps as shown in Figure 10. In system characterization, both waveguide and on-wafer calibrations are needed. To characterize the noise receiver, the noise source is connected to the noise receiver as in Figure 9. After this, the S-parameters of the device under test are measured. At this point, the VNA is calibrated to the reference planes B and C using on-wafer calibration. Typically, on-wafer Line-Reflect-Reflect-Match (LRRM) [74], Short-Open-Load-Thru (SOLT) [75], or Thru-Reflect-Line (TRL) [76] calibration method is used at MilliLab. The first step in actual noise measurements of DUT is to set suitable source reflection coefficient with the manual tuner. At that time, the tuner is switched to the VNA so that the reflection coefficient can be set and measured with the VNA. After this, the tuner is switched to DUT and corresponding noise power is measured with the noise receiver. The two latest steps are repeated for all different tuner positions. All these steps need to be done at all frequency points of interest. Finally, complicated calculation routines are performed and noise parameters are calculated. In this work, data analysis, calculation routines, and statistical analysis were done with self-written programs in Matlab<sup>1</sup>.

---

<sup>1</sup> Matlab is a product of Mathworks, [www.mathworks.com](http://www.mathworks.com)



*Figure 10. Measurement flow for noise parameter measurements.*

Only a few noise parameter measurement results have been published for frequencies above 50 GHz. Webster et al. have presented noise parameter measurement results at V-band up to 60 GHz in coaxial systems [77], and V-band on-wafer noise parameter measurement systems and results have been published only by researchers from MilliLab [72–74]. Lahdes et al. have developed measurement system based on the cold source method and uncalibrated manual impedance tuner in MilliLab [78–80]. Kantanen et al. have developed wideband automated on-wafer measurement system for V-band noise parameter measurements, which uses commercial motorized V-band impedance tuner [4]. Before this work, only single frequency on-wafer noise parameter

measurement results have been published at W-band by Alam et al. and only for a passive device [81, 82]. Measurement results presented in this work are unique, being the only published wideband results at W-band.

In this work, an on-wafer noise parameter measurement set-up has been developed for W-band device characterization. Detailed description of the developed measurement system and procedures has been given. The noise parameters of an InP HEMT (DaimlerChrysler  $2 \times 40 \mu\text{m}$ ) have been measured, and measurement results have been presented in 79–94 GHz frequency band. A similar device has been measured at V-band [4], and good agreement has been reached between the measurements [P1, 5]. It has also been shown in this work that wideband measurements are often the best way to find out possible errors in measurements of active devices [P1, P2, 2–5]. Especially, if measurements are carried out with different set-ups and at several frequency bands, possible measurement errors can be more easily identified. Also, wideband fitting can be done to the wideband results in order to get better models for devices.

The measurement set-up can be further improved to get more wideband results, and also the automation of the set-up can be increased. A drawback of the current W-band noise parameter measurement set-up is that the measurements are done manually, because of the manual impedance tuner. This requires presence of a person at all times during the measurements. To improve the measurement system, an automated W-band impedance tuner would be needed. This kind of automated measurement set-up based on a motorized impedance tuner has been successfully developed at MilliLab by Kantanen et al. for wideband on-wafer noise parameter measurements at V-band [4]. More detailed development plans for integrated impedance tuners are given in the next chapter.

### 3. Reconfigurable RF MEMS impedance tuners and matching networks

A manual impedance tuner is currently used in the W-band on-wafer noise parameter measurement system (Figure 11) [P1]. Currently, the tuner consists of an adjustable waveguide backshort and attenuator, and high reflection coefficients can be produced with such a tuner. However, the maximum reflection coefficient that can be obtained at the probe tip (reference plane B in Figure 8) is limited by the loss of the passive network between the impedance tuner and device under test. In practice, the maximum reflection coefficient that can be reached with the set-up at the probe tip is from 0.7 to 0.72 depending on the frequency.

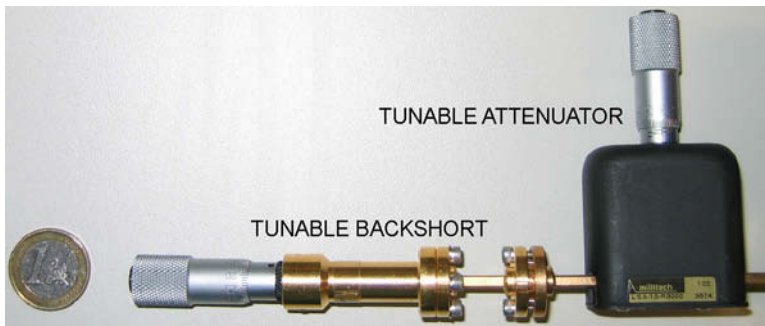


*Figure 11. Manual impedance tuner used in W-band noise parameter measurements consisting of an adjustable waveguide backshort and attenuator.*

A commercial motorized impedance tuner is used in a V-band on-wafer measurement set-up at MilliLab [4]. Similar tuners have also been developed for W-band systems [83]. Step motors are used for moving a probe inside a waveguide in the tuner thus changing the tuner output impedance. It is evident that the level of measurement automation can be increased with a motorized tuner. A further step would be to develop an electrically controllable impedance tuner packaged into a waveguide split-block, and a size comparison between the motorized impedance tuner and the waveguide split-block is shown in Figure 12. The size of the motorized impedance tuner is about 110 mm  $\times$  125 mm  $\times$  130 mm with a weight of about 0.5 kg. In comparison, the waveguide split-block is quite small (12 mm  $\times$  15 mm  $\times$  20 mm) and is easy to use with coplanar probes and

probe stations in on-wafer measurement systems. The maximum achievable reflection coefficient,  $|\Gamma_{MAX}|$ , which can be generated using waveguide tuners, is very high (about 0.97) but this is referred to the tuner output. For on-wafer measurements, the loss of the connecting waveguide sections and RF probe can limit  $|\Gamma_{MAX}|$  to about 0.7–0.8 at 50–110 GHz [4, P1]. Despite the size benefit of an integrated tuner inside the split-block, the maximum reflection cannot be increased significantly because the probe still remains between the tuner and DUT. A major improvement would be to place an integrated tuner inside a measurement probe. In this case, the loss between the tuner and DUT could be minimized. This is shown schematically in Figure 13.



*Figure 12. A photograph of a motorized waveguide impedance tuner and a waveguide split-block.*

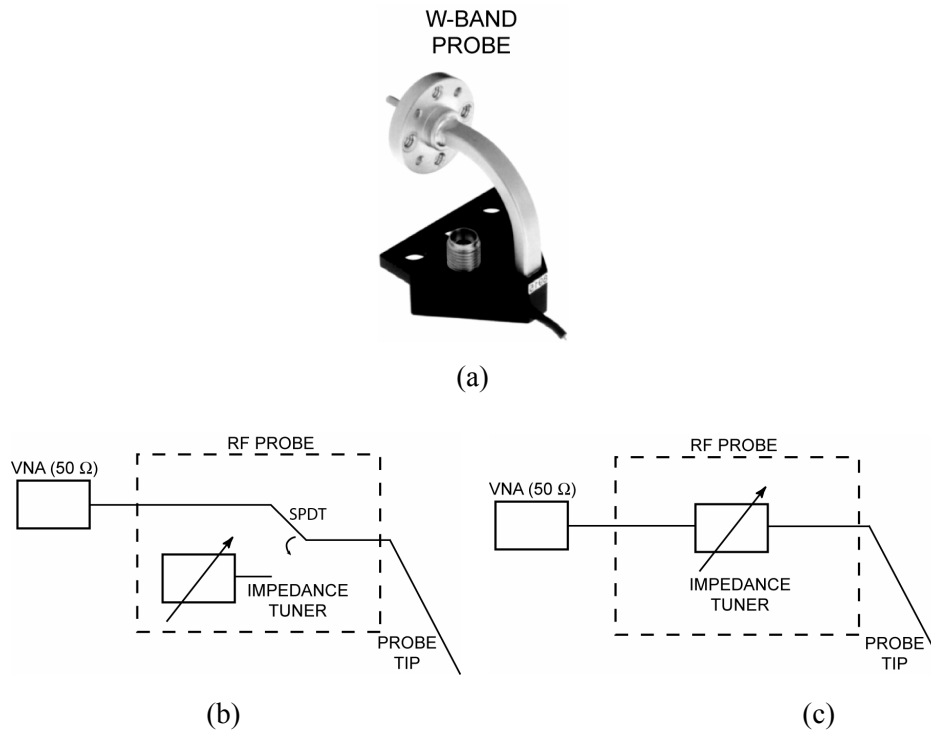


Figure 13. a) W-band on-wafer measurement probe<sup>2</sup>, b) schematics of a reflection, and c) a transmission type impedance tuner inside a probe.

In addition to measurement applications, impedance tuners can be used in telecommunication and defense applications for reconfigurable matching networks or impedance tuners. Reconfigurable matching networks are beneficial in multi-band and reconfigurable systems. Figure 14 presents a conventional and reconfigurable multi-band front-end. Portable handsets already use multiple frequency bands since they need to be functional on many continents with different frequency allocations. Also, the number of frequency bands is expected to increase in the near future because new applications (GPS, WLAN etc.) are being integrated into handsets. Also at microwave and millimeter wave frequencies, radio links are using many different frequency bands including bands around 7, 8, 13, 15, 18, 23, 26, 28, 38, 42, and 58 GHz, and reconfigurable circuits would allow the radio to operate at several bands.

<sup>2</sup> www.ggb.com

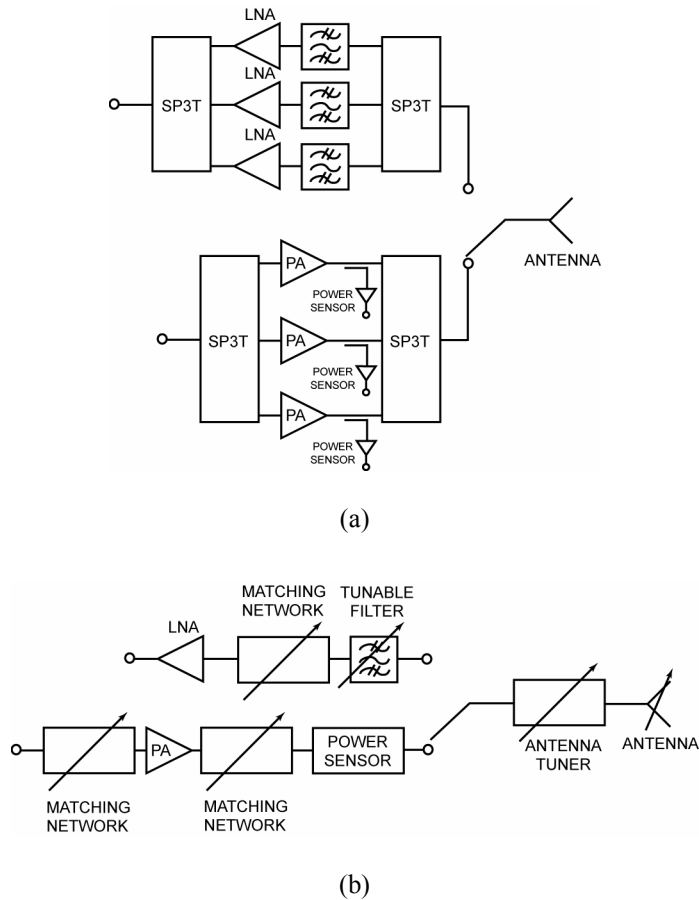


Figure 14. a) Conventional and b) reconfigurable multi-band front-end.

Other types of problems, existing both in single- and multi-band systems especially in mobile phones, are proximity effects. A typical situation is that a user places a mobile phone next to his head during a call (Figure 15). In this case, the antenna resonance frequency is shifted due to near-field coupling with the human head resulting in an impedance change at the operation frequency. This also creates a mismatch between the power amplifier (PA) and the antenna, thus reducing the output power. These effects could be decreased using a reconfigurable matching network between the PA and the antenna or using an antenna tuner inside the antenna to maintain the same resonance frequency. Mobile phone antennas with antenna tuners based on transistor switches are already commercially available, and their use is expected to increase in the near future due to the of multi-radio phones.



*Figure 15. When a person uses his mobile phone, the performance of the mobile phone front-end is changed because the phone is next to the head.*

Specifications for impedance tuners depend on the application. In noise parameter measurements, transmission loss is not very critical but it is beneficial to have a good impedance coverage over a wide frequency range, and these impedance tuners can be both reflection and transmission-type circuits (see Figure 13). On the other hand, matching networks and antenna tuners should have as low loss as possible still producing impedances needed in changing matching conditions. In most cases, matching networks and antenna tuners are transmission type circuits. These components should also have good RF power handling capabilities in case they are used with power amplifiers. Furthermore, linearity is one of the most important properties in receiver or transmitter applications, and it is important that the reconfigurable circuits produce very little additional distortion. This chapter presents several topologies and realizations for integrated electronically controllable impedance tuners.

## 3.1 Tuner topologies

### 3.1.1 Stub-based impedance tuners

Stub-based matching networks are mature matching technology in microwave and millimeter wave applications, especially in coaxial implementations [84–87]. Lumped element tuners and matching networks can be used at frequencies below 6 GHz. Also, integrated-circuit technologies have made possible to realize stubs with integrated capacitors and inductors at microwave frequencies. Stub matching networks are quite narrowband circuits, because the lengths of stubs and distances between them are proportional to the wavelength. They can be made tunable by using screws, tunable backshorts, and other tuning elements. In this work, emphasis has been in the development of reconfigurable electrically controllable integrated impedance tuners for several frequency bands. Standard single-, double-, or triple-stub matching networks can be made tunable by integrating tuning elements into these circuits. Next, some possible stub-based impedance tuner topologies are shown, and several tuning methods are presented.

#### *Stub topologies*

Stub-based impedance tuners/matching circuits are based on single-, double-, or triple-stub topologies [84]. In order to make the stub-circuits tunable, the electrical length and/or impedance of the stubs needs to be tuned. The sections between stubs can also be tunable for achieving wider impedance coverage. Figure 16 presents some possible stub-based impedance tuner topologies. Parameters  $L_1$ ,  $L_2$ ,  $L_3$ ,  $L_4$ , and  $L_5$  are the electrical lengths of the stubs and sections between them, meaning that their electrical length as well as their impedance can be tuned.

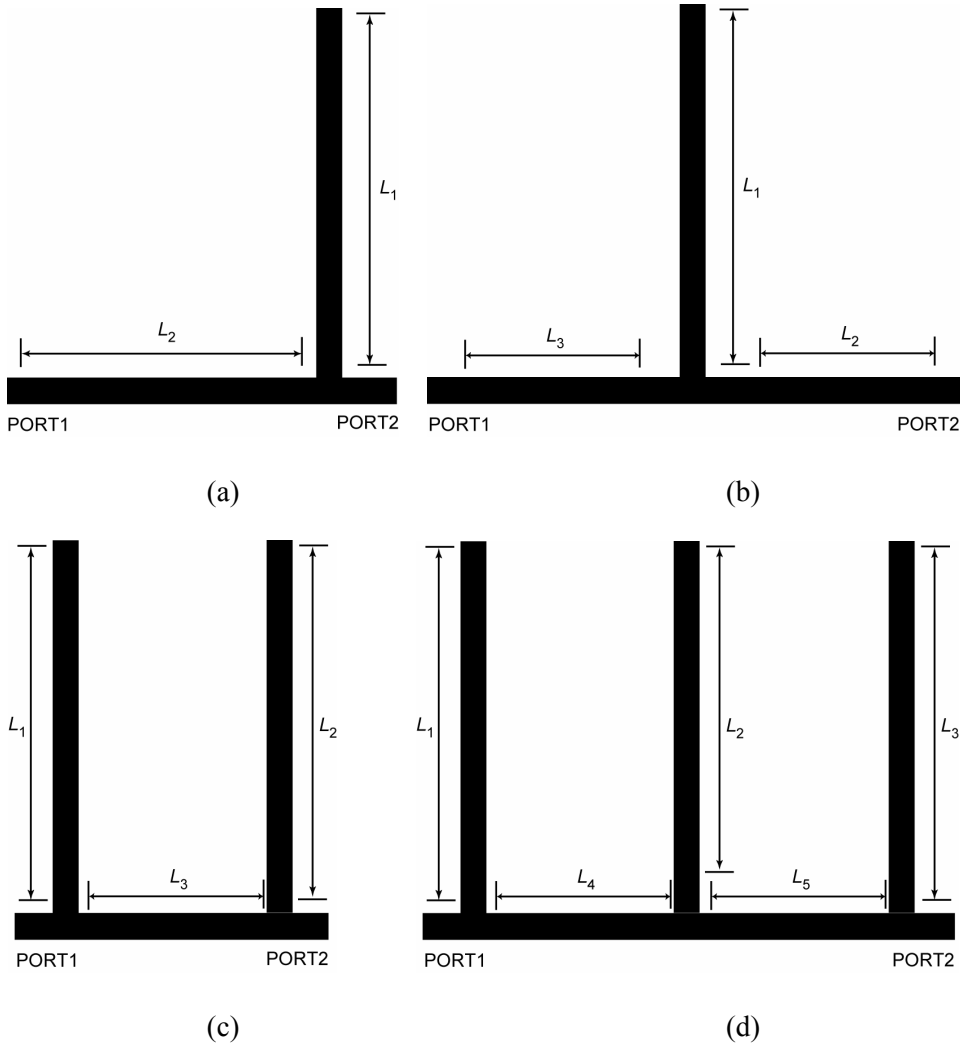


Figure 16. Tuning the electrical lengths of the stub-based circuits.

### ***Tuning methods***

Tuning possibilities are divided here into two main categories: digital and analog tuning. Digital tuning means that impedances are generated in a discrete manner using, for example, switches or capacitor banks with several fixed capacitances. Analog tuning is a continuous tuning which is realized, for example, with varactors having continuous tunability. Some possible analog and digital tuning

methods for changing the electrical length and/or impedance of stubs are shown in Figures 17 and 18, respectively [87].

By having a capacitor bank (Figure 17a) or a varactor (Figure 18a) at the end of the stub, the electrical length of the stub can be tuned. Also, the impedance of the stub is changed locally in the end of the stub because of increased capacitive loading. An other way to realize analog tuning (both electrical length and impedance), is to distribute many varactors along stub allowing larger tuning compared to just a single varactor at the end of the stub (Figure 18b). Also, stubs with different lengths or impedances can be switched to provide different impedances (Figure 17b and c). Straightforward methods for controlling the electrical length of the stub are to use series switches to connect transmission line sections (Figure 17d) or movable short circuit realized with switches in this case (Figure 17e). Both the electrical length and impedance of the stub can be controlled simultaneously with switched capacitor-based loading (Figure 17f).

If the capacitor bank at the end of the stub (Figure 17a) is realized with three switches then  $2^3 = 8$  ( $2^N$  impedances,  $N =$  number of switches) different impedances can be generated. In this case, the total loading capacitance is  $C_{TOT} = 0, C_1, C_2, C_3, C_1+C_2, C_1+C_3, C_2+C_3, \text{ or } C_1+C_2+C_3$ . The same amount of different impedances ( $2^N$ ) can be generated also with the designs in Figures 17b, c, and f. Designs in Figures 17 d and e produce  $N+1$  different impedances. The difference between the two methods,  $2^N$  vs.  $N+1$  impedances, becomes significant if a larger amount of switches is used. For example, if  $N = 8$ , then the first type of tuning produces 256 impedances and the latter only 9 (this assumes that capacitances should be chosen correctly in the first type of tuning). In theory, unlimited number of impedances can be generated using analog type tuning as in Figure 18. However, this tuning range is limited in practice by the tuning range of a single varactor, parasitics of the varactors, and the number of varactors used. Also, the loss of the circuit is increased when the number of tuning elements is increased. This reduces the maximum available reflection coefficient.

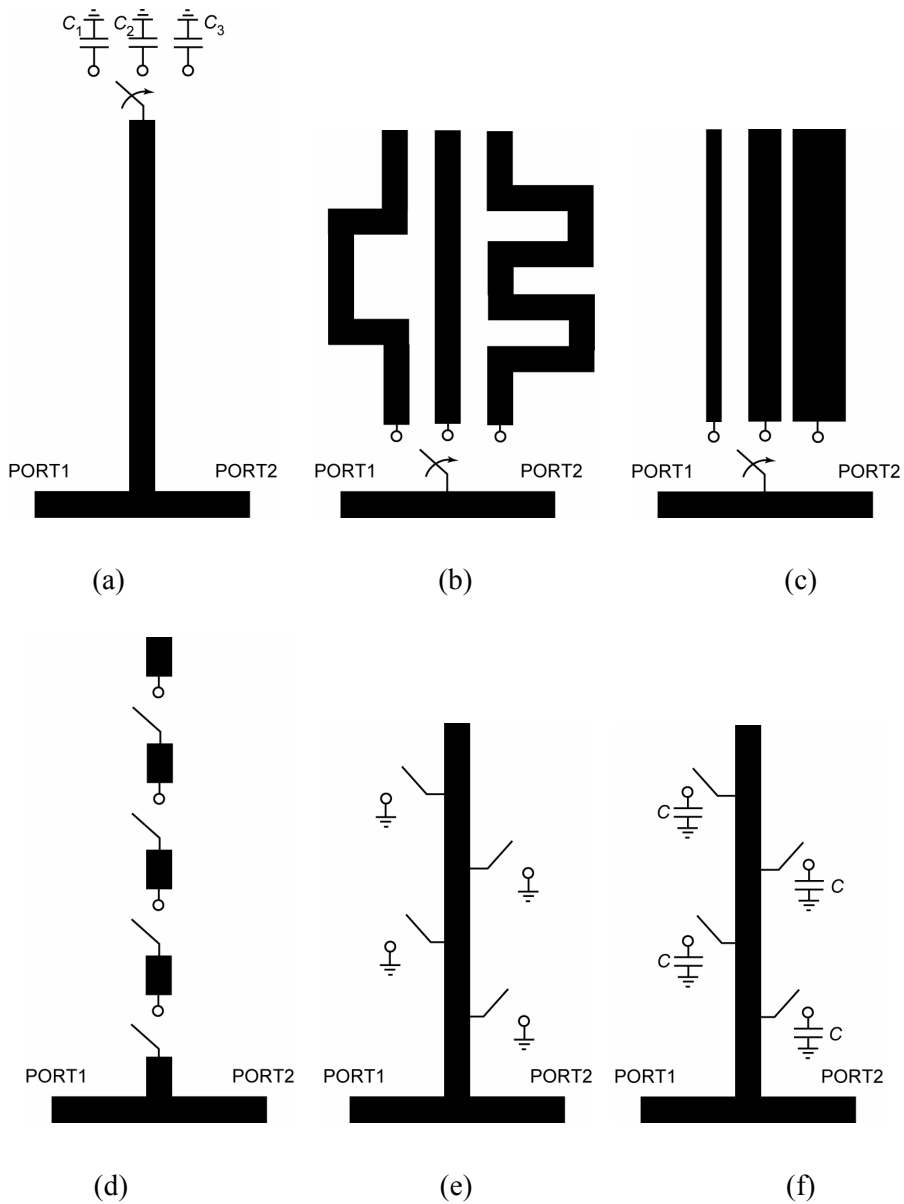
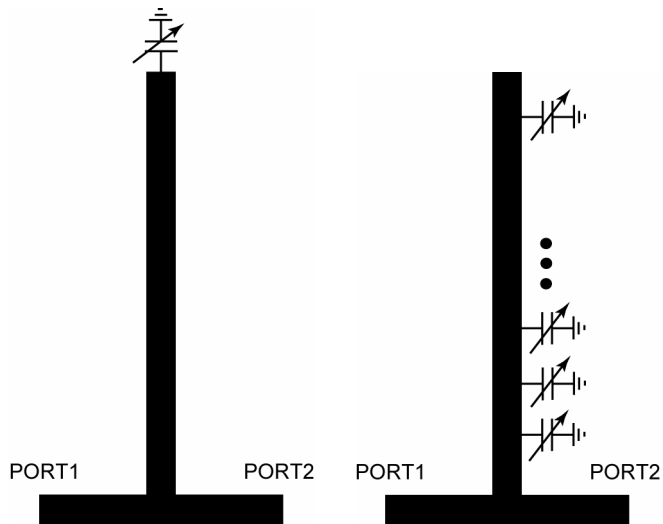


Figure 17. Electrically tunable stubs with digital type tuning. Tuning realized with a) capacitor bank at the end of the stub, b) switchable stubs with different electrical lengths, c) switchable stubs with different transmission-line impedance, d) series switches in a stub for different stub lengths, e) shunt switches in a stub for different stub lengths, and f) switched capacitors in a stub.



*Figure 18. Electrically tunable stubs with analog type tuning. Tuning realized with a) a varactor in the end of the stub and b) many varactors distributed along the stub.*

The electrical distance between the stubs and the impedance of these sections can be controlled electrically to increase impedance coverage of a tuner, and the same tuning methods which are used with stubs can be applied to sections between, before, and after the stubs.

Just some possible solutions for tuning have been shown here. By combining topologies shown in Figure 16 to tuning methods in Figures 17 and 18, several new impedance tuners can be realized. New tuners can be created easily using innovative stub structures as in [88–90]. Also, by coupling or connecting stubs together in the double- or triple-stub topologies, novel tuners can be developed. The most limiting factors in impedance tuner design are probably imagination and creativity of designers.

### 3.1.2 Slug tuners

Double-slug tuners have been used for a long time in coaxial systems [84]. Figure 19 shows the principle of the double-slug tuner topology two movable short circuits or sections having different impedance from the transmission line

impedance. By changing the distance between the short circuits or impedance sections ( $L_2$ ) and distance from the port 1 ( $L_1$ ), different reflection coefficients can be generated. Maximum reflection coefficient is defined by the impedance ratios between the transmission line impedance and impedance section having the highest value in the case of the short circuit.

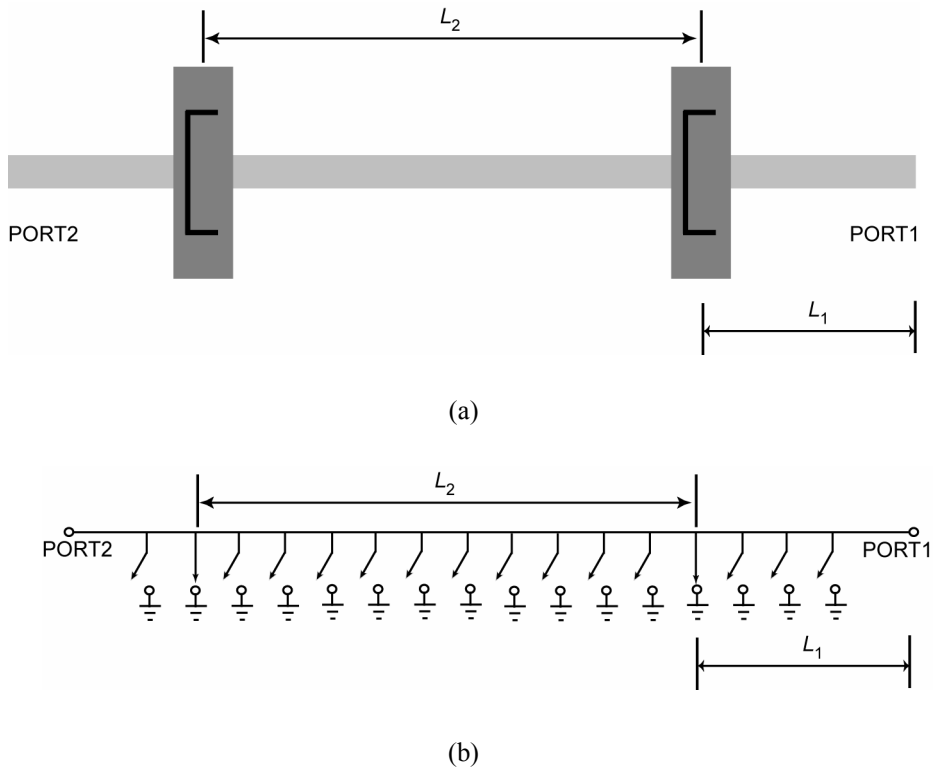


Figure 19. a) Schematic drawing of a double-slug tuner. b) Electrically tunable short circuits realized with switches.

## 3.2 Components for electrically controllable impedance tuners

### 3.2.1 Varactor diodes and transistors

All topologies presented above can be realized with active devices such as transistors or diodes. Active devices based on diodes and transistors can be used

as switches, or their capacitance can be changed as in varactor diodes. Their benefits are, at least, that the technology of active devices is already well established and tens of foundries exist for the fabrication of MMICs. Also, they have a low control voltage (0–10 V), they are fast (ns), produce gain (transistors only), and integration of other circuits like LNAs, PAs, mixers, and multipliers is possible in the same process. However, they also have several drawbacks when used in impedance tuners and matching networks. The best performance active devices at millimeter wavelengths are based on Indium Phosphide (InP) processes which are very expensive. Also, active devices generate noise and non-linearities, decreasing the system performance. The generation of noise and nonlinearities is problematic for applications in systems before the large gain stages, such as tuning for antennas and amplifier input matching. From the impedance tuner point of view, the biggest disadvantage of millimeter wave diode varactors is their quite high resistance [91] being lossy and limiting available impedance coverage. Noise can cause problems in noise parameter measurements, because any unwanted noise coming from the measurement system should be minimized to avoid additional calibration steps.

### **3.2.2 MEMS switches and varactors**

MEMS technology offers the possibility to use mechanically movable micro scale elements that can be controlled electrically in microwave and millimeter wave applications. MEMS technologies have been applied to accelerometers and sensors (pressure, gas, and temperature) already from 1970s, and several commercial products have been available since the early nineties. The first MEMS switch and varactor for microwave applications have been presented in 1991 [92]. MEMS technologies have been applied to microwave and millimeter wavelengths mostly after 1995, and packaged MEMS switches are commercially available from several companies such as Radant MEMS<sup>3</sup>, Teravicta<sup>4</sup>, and Magfusion<sup>5</sup>. An extensive introduction and also, deep analysis of RF MEMS technology, components and circuits can be found in [87]. In this thesis work,

---

<sup>3</sup> [www.radantmems.com](http://www.radantmems.com)

<sup>4</sup> [www.teravicta.com](http://www.teravicta.com)

<sup>5</sup> [www.magfusion.com](http://www.magfusion.com)

capacitive MEMS switches are used. In addition to the capacitive MEMS switch, other kinds of switches are also used in other research groups. Especially DC metal-to-metal contact switches are used in many applications below 5 GHz. Commercially available MEMS switches by Radant MEMS, Teravicta, and Magfusion are metal-to-metal contact switches.

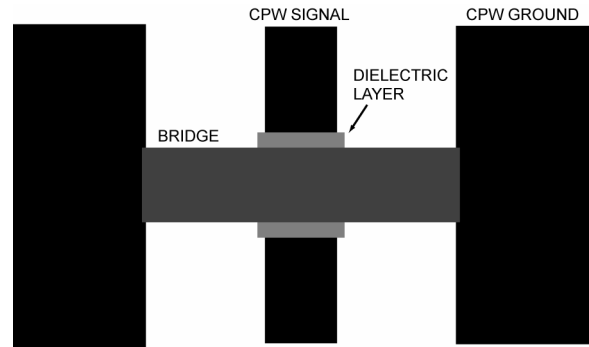
### *Capacitive MEMS switches and varactors*

Figure 20 shows one possible layout and schematical cross-sectional view for a capacitive shunt switch. This is very similar to a standard air bridge used in integrated circuits, but with a movable bridge.

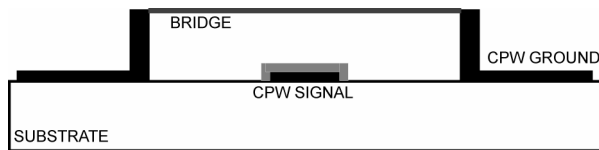
If a voltage is applied between the CPW center conductor (signal) and ground, the bridge starts to curve towards the signal line. From the electrical point of view, this means that the capacitance between the CPW signal and ground is changed. If the voltage is increased, then the bridge collapses to the down-state position, also called "pull-down". Pull-down occurs, when the distance between the bridge and the signal line is reduced to 2/3 of its original distance [81]. The Voltage needed to pull-down the bridge is called pull-down voltage and is:

$$V_p = \sqrt{\frac{8k\delta^3}{27\varepsilon_0 A}} \quad (2)$$

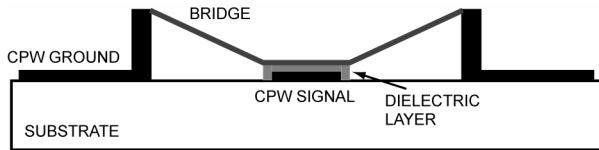
where  $k$  is the spring constant of the bridge,  $\varepsilon_0$  is the permittivity of vacuum,  $A$  is the overlapping area of the electrodes, and  $\delta$  is the distance (gap) between the electrodes.



(a)



(b)



(c)

Figure 20. Shunt switch in a CPW configuration: a) top view, b) side-view in the up-state, and c) side-view in the down-state. The size of a MEMS bridge (switch) used in [P3, P7] is  $80 \mu\text{m} \times 280 \mu\text{m}$ .

Capacitance of a MEMS switch or varactor can be calculated approximately with the parallel-plate capacitor equation

$$C_{\text{MEMS}} = \frac{\epsilon_0 \epsilon_r A}{\delta} \quad (3)$$

where  $\epsilon_r$  is the relative dielectric constant of the material between the electrodes. A thin dielectric layer is used for covering the bottom electrode of a MEMS

switch to get high down-state capacitance and prevent DC contact between the electrodes (Figure 20). The previous equation can be used for calculating both the up and down-state capacitances approximately. If it is used in the down-state, then  $\delta$  and  $\epsilon_r$  are the thickness and relative dielectric constant of the dielectric layer. In practice, the actual up-state capacitance is 20–40 % higher than calculated from Equation (3) due to fringing fields.

The capacitance ratio of a capacitive MEMS switch between the up and down-states is typically between 20–100 depending mostly from the gap,  $\delta$ , thickness of the dielectric layer, quality of the dielectric layer, smoothness of all layers, and contact force between the surfaces in the down-state [87, 94–98].

Equivalent circuits for a MEMS switch or varactor is shown in Figures 21 and 22, where  $R_{MEMS}$  and  $L_{MEMS}$  are the resistance and inductance of the MEMS component, and  $Z_0$ ,  $\beta$ , and  $l$  are the transmission line impedance, propagation constant, and length, respectively.

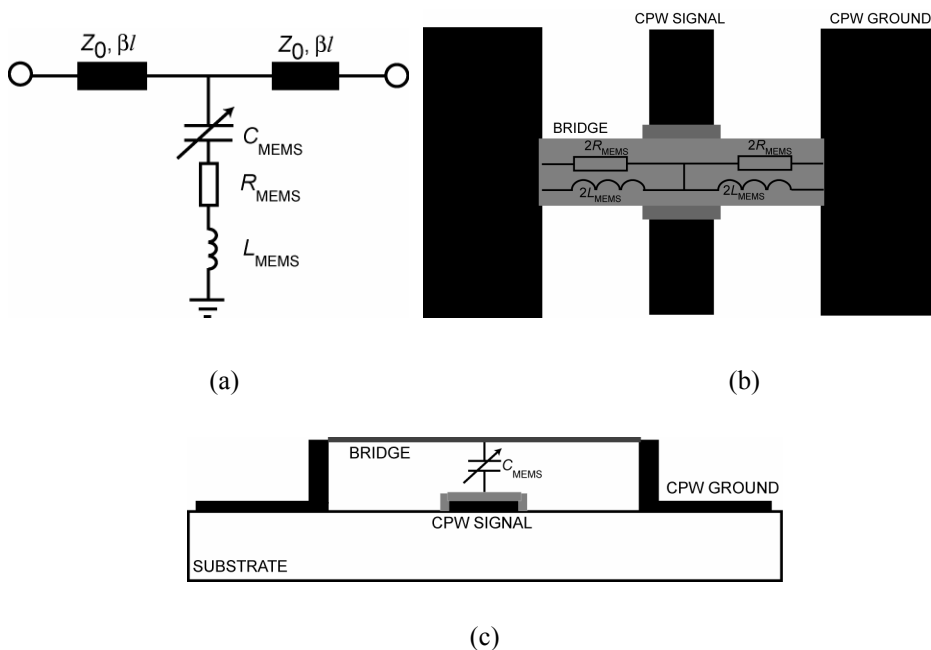


Figure 21. a) Equivalent circuit of capacitive shunt switch or varactor. Schematical drawing of a shunt switch showing the physical meaning of the equivalent circuit. b) Top view and c) side view.

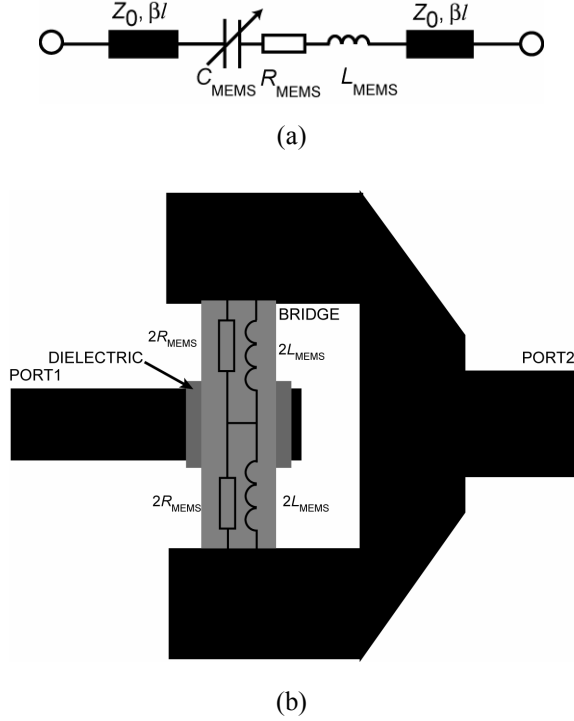


Figure 22. a) Equivalent circuit of a capacitive series switch and b) its possible layout.

The bridge can be used also as an analog varactor because the gap between the electrodes can be changed about 1/3 before the bridge pulls down. This method has been applied successfully to many tunable circuits like phase shifters [25] and filters [99], but has a limited capacitance ratio of only 1.4.

### Switched capacitors

The capacitance ratio (20–100) and down-state capacitance of a MEMS switch is too high for many tunable and reconfigurable circuits. The capacitance ratio and down-state capacitance can be lowered by using fixed capacitors with smaller capacitance in series with the MEMS switch (Figure 23). The total capacitance of the switched capacitor is a series combination of the fixed capacitor and the capacitance of the MEMS switch:

$$C_{\text{TOT}} = \frac{C_{\text{MEMS}} C_{\text{FIXED}}}{C_{\text{MEMS}} + C_{\text{FIXED}}} \quad (4)$$

In this case, the up-state capacitance is mostly defined by the up-state capacitance of a MEMS switch and the down-state capacitance by the fixed capacitor. Depending on the needed capacitances, fabrication process, and frequency, the fixed capacitors can be realized with stubs [100], metal-air-metal (MAM) [101], or metal-insulator-metal (MIM) capacitors [102]. If microstrip transmission lines are used, then stubs can be more easily implemented than MAM or MIM capacitors (all of these can also be applied to CPW circuits). The capacitance of MAM or MIM capacitors can be calculated easily with the parallel-plate capacitor equation. An additional advantage is that MEMS switches can be DC separated from other parts of circuits with the fixed capacitors.

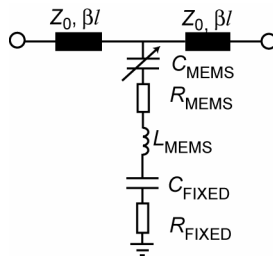


Figure 23. Equivalent circuit of a MEMS switch in series with a fixed capacitor.

The work in this thesis is primarily based on switch capacitors. These were realized with MEMS switches in series with MAM capacitors [P3–P8]. Figures 24 and 25 show the equivalent circuit and photograph with a cross-sectional view of a switched capacitor used as a tuning element in [P4]. Similar switched capacitors with different dimensions were also used in this work up to 80 GHz [P3, P6, P7, P8]. The fixed metal-air-metal capacitor is formed the following way: the bottom electrode of the MAM capacitor is the continuation of the MEMS switch and the top electrode is realized with the thick electroplated CPW ground. This can be made easily from the fabrication point of view. The same sacrificial layer is used under the MEMS switch and MAM capacitors, and it is removed later on. The capacitance of the MAM capacitors can be controlled accurately since the sacrificial layer thickness is controlled within  $\pm 0.1 \mu\text{m}$ . By changing the area of the MAM capacitor, the capacitance ratio and down-state capacitance of the switched capacitor can be chosen to be any value as long as it is less than the capacitance ratio and the down-state capacitance of the MEMS switch itself. In this particular case, the capacitance ratio of the switched capacitor was chosen to be 2.5 [P4].

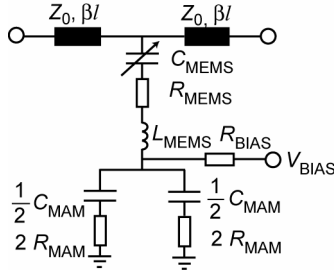


Figure 24. Equivalent circuit for the switched capacitors used in this work [P3–P8].

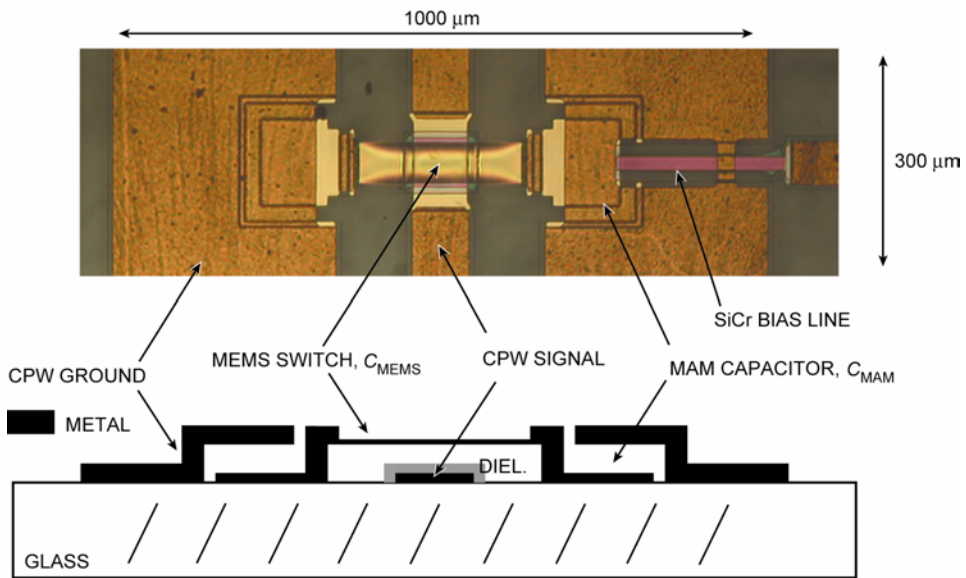


Figure 25. Photograph and cross-sectional view of a switched capacitor used in [P4].

Switched capacitors as in Figure 25 are difficult to use in compact reconfigurable circuits operating above 75 GHz due to their relatively large size. The reason is that the required capacitances and circuit dimensions are quite small at W-band frequencies. Figure 26 presents a novel realization of a W-band switched capacitor developed in this work [P6]. In this case, the anchors are floating and the signal line is connected to the ground using the  $C_{MEMS}$  in series with the two  $C_{MAM}$ . The anchor area is electroplated to 3–5  $\mu\text{m}$  thickness in order to make it stiff and not flexible.

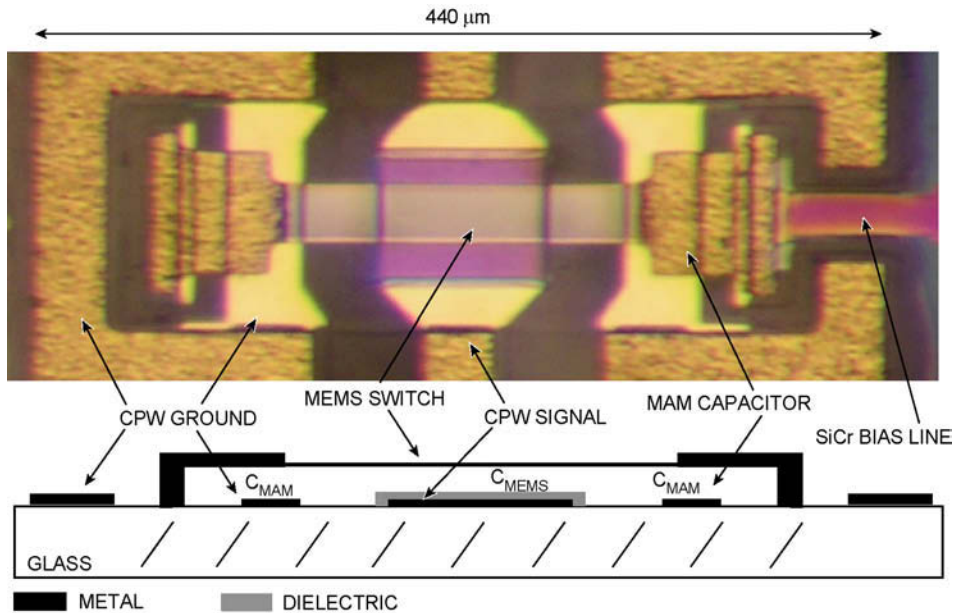


Figure 26. Photograph and schematical cross-sectional view of a W-band switched capacitor developed in this work [P6].

### ***Fabrication process***

The fabrication process for switched MEMS capacitors and circuits developed in this work is shown schematically in Figure 27. The process flow is related to Figures 25 and 26, presenting photographs of the fabricated switched capacitors. The fabrication process is a modified six masks version from the surface MEMS process developed before this work at the University of Michigan [103, 104]. The main steps of the process are presented here and detailed process is shown in Appendix A. Corning 7040 glass wafers with  $\epsilon_r = 4.6$  are used as substrates in this work, but the fabrication process is also suitable for other substrates. Only the exposing time of the photoresist in lithography should be adjusted according to the substrate material. High resistivity silicon chrome (SiCr) bias lines are deposited with a sputtering tool and patterned with the lift-off process as the first fabrication step. The second step is the deposition of the bottom electrodes of the MAM capacitors and MEMS switches with an evaporator (Figure 27b). This layer is also patterned with the lift-off process. After that, silicon nitride ( $\text{Si}_x\text{N}_y$ ) dielectric layer is deposited with plasma enhanced chemical vapor deposition

(PECVD) followed by reactive ion etch (RIE) patterning (Figure 27c). Polymethylmethacrylate (PMMA) is used as a sacrificial layer under the switches and MAM capacitors, and is patterned using oxygen plasma in the RIE (Figure 27d). A sputtered titanium/gold/titanium (Ti/Au/Ti) layer is used both as the structural layer and seed layer for gold electroplating, which is done after sputtering (Figure 27e). As a final step, MEMS switches are formed with Ti/Au/Ti etching and the sacrificial layer is removed in acetone followed by critical point drying (Figure 27f).

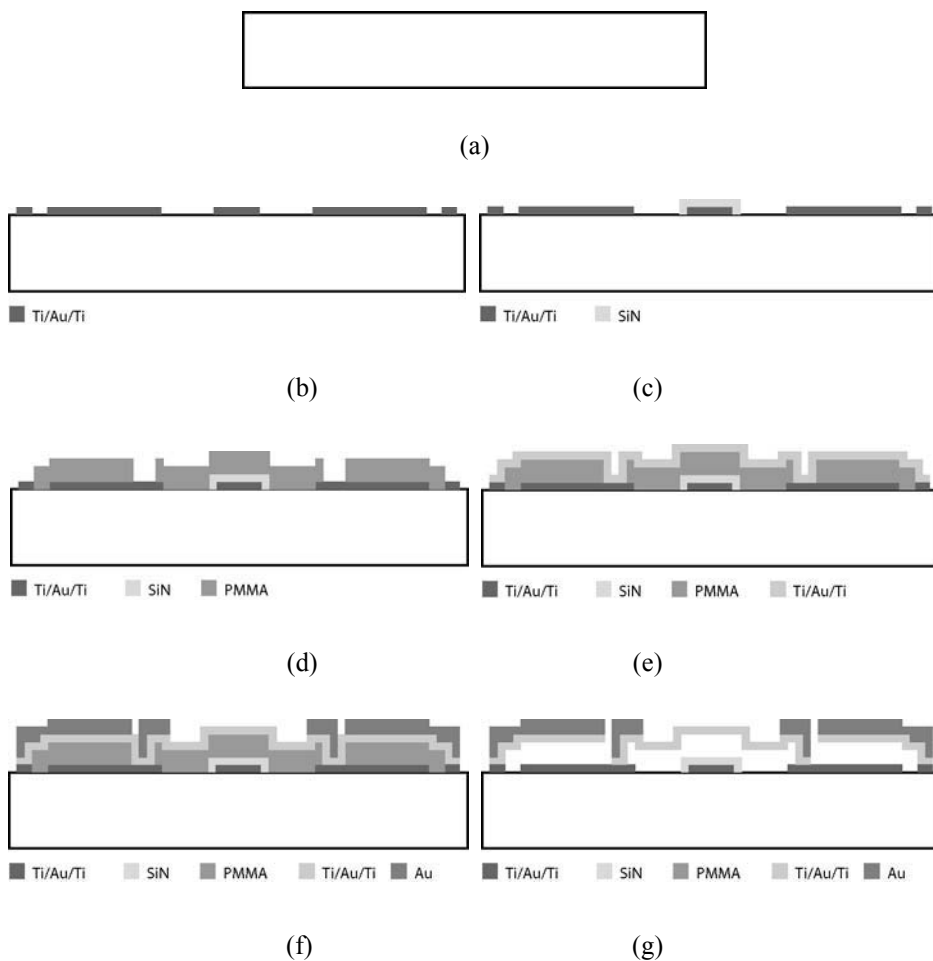
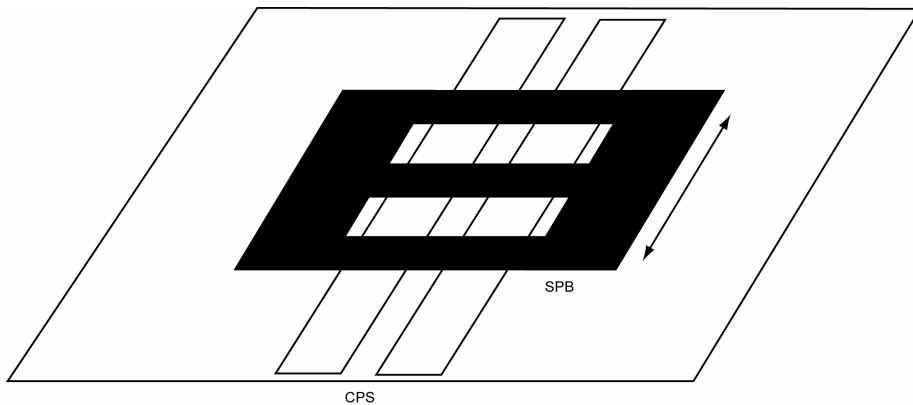


Figure 27. Surface MEMS fabrication process used in this work. The detailed fabrication process is described in Appendix A.

### 3.2.3 Sliding planar backshorts

In addition to MEMS switches, MEMS technology can be used for other tuning elements. Lubecke et al. realized sliding planar backshorts (SPB) with MEMS technology [35, 105, 106]. The schematical illustration of the SPB in coplanar stripline (CPS) configuration is shown in Figure 28. The metal transmission lines are covered with a dielectric layer and the sliding metal element is on top of these. The sliding element result in a short circuit along the transmission line (capacitively). If the element can be moved, then the position of the short circuit can be changed. Lubecke's sliding planar backshorts were not electrically controllable, and needles were used in on-wafer measurements for changing the place of the SPB on transmission line. However, Lubecke et al. demonstrated successfully that surface micromachining technology is beneficial for millimeter wave applications. Chiao et al. further developed sliding planar backshorts. They used scratch drive actuators (SDA) for the electrical position control of sliding planar backshorts [107, 108].



*Figure 28. Schematical illustration of a sliding planar backshort (SPB) on CPS configuration.*

### 3.3 Realized impedance tuners

#### 3.3.1 Active device based impedance tuners and matching networks

Bishoff presented the first electronically controllable impedance tuners for measurement purposes [109]. However, the VSWR of the tuner was limited to 6 at 27 GHz. McIntosh et al. showed MMIC designs with improved performance having VSWR of 12.3 and better Smith chart coverage [110]. The simplest impedance tuners or matching networks can be realized with LC networks in T- or  $\pi$ -type configuration [87]. These are suitable to be used as matching networks with power amplifiers or antennas. Matching networks based on *pin* diodes have been realized for applications below 0.4 GHz showing improved matching capability [111]. However, the impedance coverage and  $|\Gamma_{\text{MAX}}|$  of the impedance tuners and matching network are quite limited due to the resistance of the diodes, varactors, and transistor in all of these active device based impedance tuners.

#### 3.3.2 Impedance tuners based on sliding planar backshorts

The first impedance tuner based on micromachining techniques was published by Lubecke et al. in 1993 for 100 GHz [35], and extended it to 600 GHz later on [106]. These tuners were based on sliding planar backshorts. As described in Section 3.2.3, these were controlled with needles and Chiao et al. developed electrical control for these. They used the tuners for a Vee antenna matching and impedance generation [107, 108]. Measurement results for the antenna were presented demonstrating reconfigurability, but no results for the impedance tuner itself were shown.

#### 3.3.3 Stub-based impedance tuners and matching networks realized with MEMS switches

Kim et al. developed the first impedance tuners based on MEMS switches and varactors, and using the double-stub topology [112]. These tuners were realized with integrated circuit technologies and neither flip-chip nor wire bonding were

in the tuner realizations. Both analog and digital type impedance tuners were presented. The schematics of the tuners are shown in Figure 29. The analog tuner consists of two MEMS varactors, one in each stub. The capacitance of the varactors can be tuned 30 % from their initial value. This method results on fixed frequency impedance tuning at 29 GHz covering two quadrants of the Smith chart. The tuner was targeted for transistor noise matching applications. The digital tuner was realized with 12 MEMS switches having 10.9:1 capacitance ratio, and each switch was controlled separately. The tuner was optimized for optimum load matching of power transistors. The measured results for the tuner showed good impedance coverage for power transistor matching purposes at 29–32 GHz. However, only one quadrant of the Smith chart can be covered. Bandwidths of the tuners developed by Kim et al. were quite narrow (maximum 29–32 GHz), which was the drawback of using short-circuiting switches or low tuning-range analog varactors. The biggest advantage of these tuners compared to MMIC impedance tuners is that they can provide high reflection coefficients. Presented measurement results showed that the digital tuner produces maximum VSWR of 32.3, which is much better than obtained with MMIC impedance tuners.

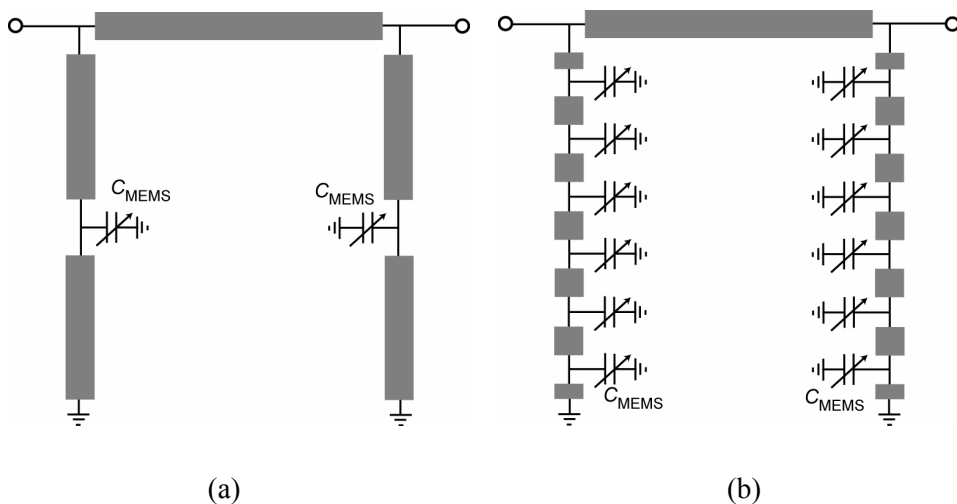


Figure 29. a) Analog and b) digital double-stub impedance tuners realized with MEMS varactors and switches [112].

Papapolymerou et al. [113] presented 2 bit  $\times$  2 bit, 3 bit  $\times$  3 bit, and 4 bit  $\times$  4 bit double-stub tuners. The electrical lengths of the stubs were changed with capacitor banks in the ends of the stubs. They realized capacitor banks with capacitive MEMS switches and fixed capacitors (open-ended microstrip stubs) in series with the switches. Microstrip transmission lines were fabricated on an alumina substrate and MEMS switches with fixed capacitors were wire bonded to the end of the stubs. In addition, biasing networks for the MEMS switches were wire-bonded. The 2 bit  $\times$  2 bit tuner provides 16 ( $2^4$ ) different impedances, 3 bit  $\times$  3 bit 64 ( $2^6$ ), and 4 bit  $\times$  4 bit 256 ( $2^8$ ). The schematic of the 4 bit  $\times$  4 bit double-stub impedance tuner is shown in Figure 30. The distance between the stubs is  $\lambda/10$  at 20 GHz.

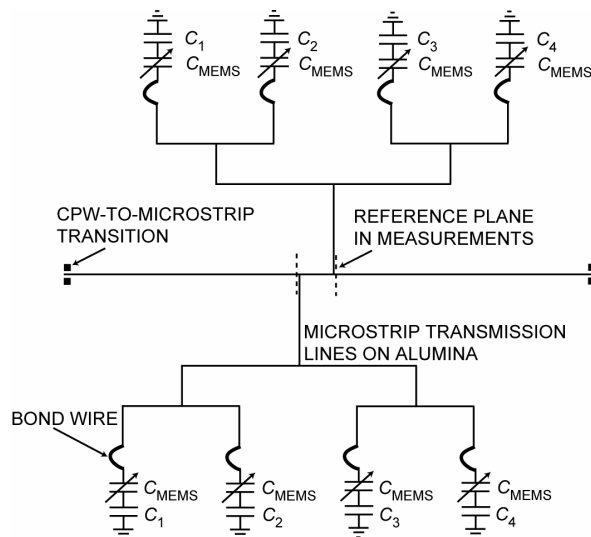
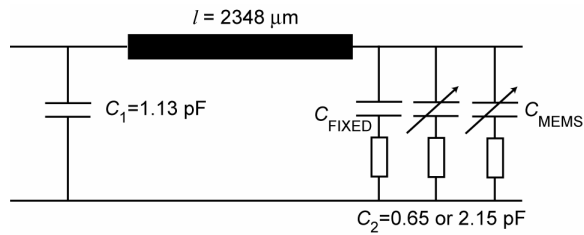


Figure 30. Schematics of the 4 bit  $\times$  4 bit double-stub impedance tuner [113].

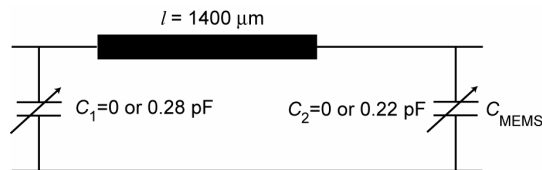
The 4 bit  $\times$  4 bit double-stub impedance tuner had 8 switched capacitor providing 256 different impedances. However, 142 different combinations were measured because of stiction problems of the MEMS switches. Reference planes were transformed to the intersection points of the two stubs. The impedance tuner had moderate impedance coverage at 20 GHz (design frequency) but lower performance was achieved at other frequencies. From two to three quadrants of the Smith chart could be covered with the tuner depending on frequency. The tuner also provided very high reflection coefficients ( $V_{SWR} = 99$ ), which were possible because both the microstrip lines on alumina and MEMS switches had

very low loss. It should be also noted that the reference planes were transformed mathematically next to the stubs avoiding the loss coming from the CPW to microstrip transitions, input and output transmission line sections, and contact resistance from a probe tip to the contact pads. However, these results were better than results showed for other integrated impedance tuners at the time they were published. Simulations and measurement results also showed a drawback of this realization. Modeling of the tuner was rather difficult because the bond wires were needed to connect the switched capacitors to the stubs. The 4 bit  $\times$  4 bit impedance tuner consists of ten chips (transmission lines on alumina, 8 switched capacitor chips, 2 bias network chips) which all should be connected with bond wires. The circuit could be further improved by integrating all parts on the same chip.

A reconfigurable power amplifier was presented by Lu et al. [114]. Reconfigurable input and output matching networks were connected to an RF power transistor in order to use the transistor in 6 and 8 GHz frequency bands. The double-stub tuner topology was used in the matching networks in their work (Figure 31). In this case, the stubs were realized with fixed MIM capacitors and MEMS switches parallel with them. Transmission lines were used only in the section between stubs. The matching networks were designed to be used only with this certain power transistor and need to be redesigned if used with other components. The advantage is that the number of MEMS switches can be minimized as well as the size of the circuit. Lu et al. presented the first results, where a matching network was connected to a power transistor. Also, power amplifier band switching was demonstrated in their work. The amplifier with the reconfigurable input and output matching networks demonstrated 7.2 dB gain with 26.4 % power added efficiency at 6 GHz and 6.1 dB gain with 16.7 % power added efficiency at 8 GHz when the input power was 8 dBm.



(a)



(b)

Figure 31. a) Reconfigurable double-stub input and b) output matching network used for power amplifier band switching [114].

Qiao et al. [115] also published an 8–12 GHz reconfigurable power amplifier with an RF MEMS output impedance tuner based on the double-stub topology. Figure 32 shows the schematics of the 4-bit double-stub output matching network with the varactor ( $C_{\text{MEMS}}$ ), four MEMS switches ( $C_{\text{MEMS1}}-C_{\text{MEMS4}}$ ), and eight fixed capacitors ( $C_1-C_8$ ). The matching network is more advanced version from the double-stub tuners presented Lu et al. in [114]. The varactor can be used for fine tuning of generated impedances. The simulated impedance coverage of the output matching network was presented at 9.6 GHz covering the second quadrant of the Smith chart, which is the optimum load impedance area for the power amplifier. No measurement results for the matching network itself was presented, but the power amplifier reconfigurability was demonstrated over 7–11 GHz frequency band.

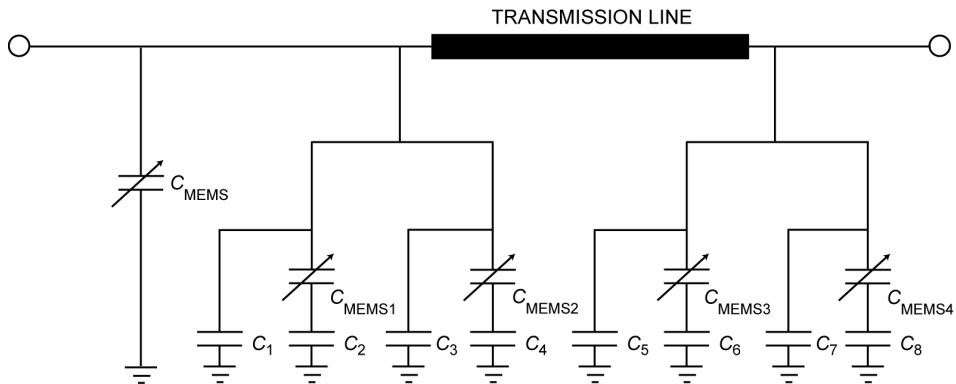


Figure 32. Schematics of a double-stub matching network developed by Qiao et al. [115].

MEMS varactors were developed at Nokia by Nieminen et al. [116, 117]. A simple 1-bit LC-matching network was demonstrated for 880–915 MHz cellular phone applications by combining a high-Q inductor and MEMS capacitor [118]. The power consumption of a power amplifier was lowered by 42 % at 23 dBm power level with the matching network. This matching network is the only published packaged RF MEMS matching network circuit. The drawbacks of the matching network are that it has to be redesigned for different amplifiers and it is quite sensitive for parasitics like bond wires. The main reason for this is that only one bit can be used. However, only one switch is needed reducing the cost, control logic, and size, which are very important factors in cellular phone applications.

In all stub-based tuners described here [112–115], the electrical length and/or impedance of stubs are changed but the electrical distance between the stubs is fixed. This limits both the impedance coverage and bandwidth of the impedance tuners and matching networks. Switched capacitors were applied to stub topologies in this work [P3–P6]. A single switched capacitor has mainly two effects between its two states: the delay and impedance of a transmission line can be changed. Figure 33 shows the schematics of the single, double, and triple-stub topologies with switched capacitors. In this work, the switched capacitors are distributed along to the stubs and also to the sections between the stubs. Because the switched capacitors are distributed along the stubs, more impedances can be generated compared to the situation where the switched capacitors are just at the end of the stubs. Figure 34 shows the fabricated triple-stub tuners that have been developed for 6–24 GHz and 75–115 GHz.

In this work, the stub-based impedance tuners were optimized for noise parameter measurement applications. Publication [P3] presents triple-stub tuners with 11 and 13 switched capacitors, a double-stub tuner with 11 switched capacitors, and a single-stub impedance tuner with 10 switched capacitors. All of the tuners are for 6–24 GHz, and have better and more wideband impedance coverage than any other published integrated impedance tuner in this frequency range. Also, the measured maximum available reflection coefficient  $|\Gamma_{MAX}|$  is comparable to other published integrated impedance tuners being 0.99 (equal to VSWR of 199) at 30 GHz for the double-stub tuner. Comparison of published integrated impedance tuners for frequencies below 30 GHz is shown in Table 1 also shows the advantage of using MEMS technology in integrated impedance tuners because they can produce very high reflection coefficients.

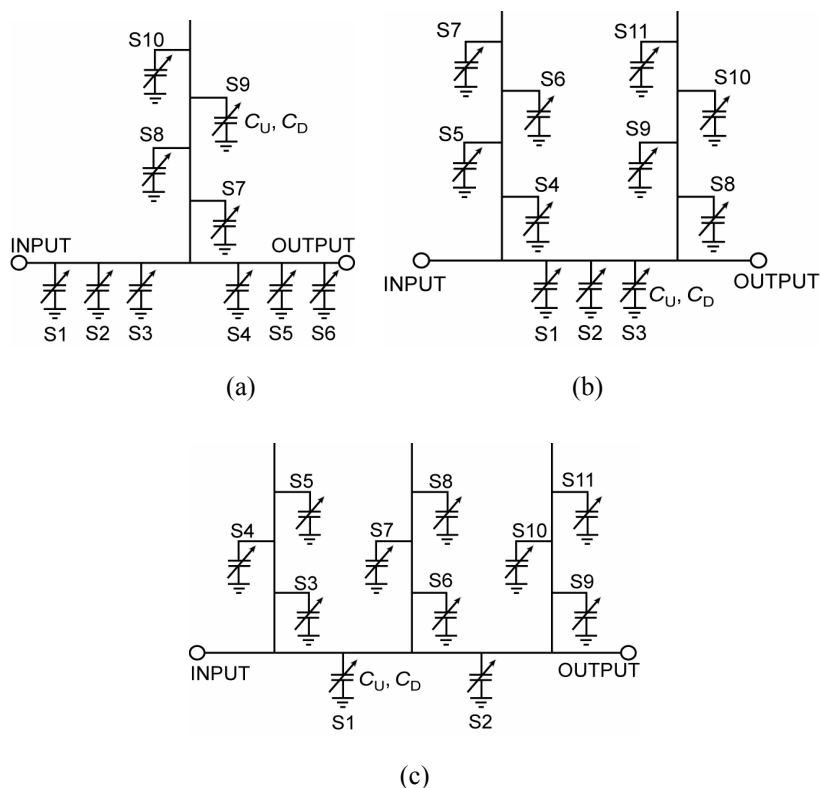


Figure 33. Schematics of the stub-based impedance tuners where the impedance tuning is realized with switched capacitors (S1–S11). a) The single-stub tuner, b) double-stub tuner, and c) triple-stub tuner [P3–P6]. Notice that both the stubs and the transmission line between the stubs (or before and after as in (a)) are tuned.

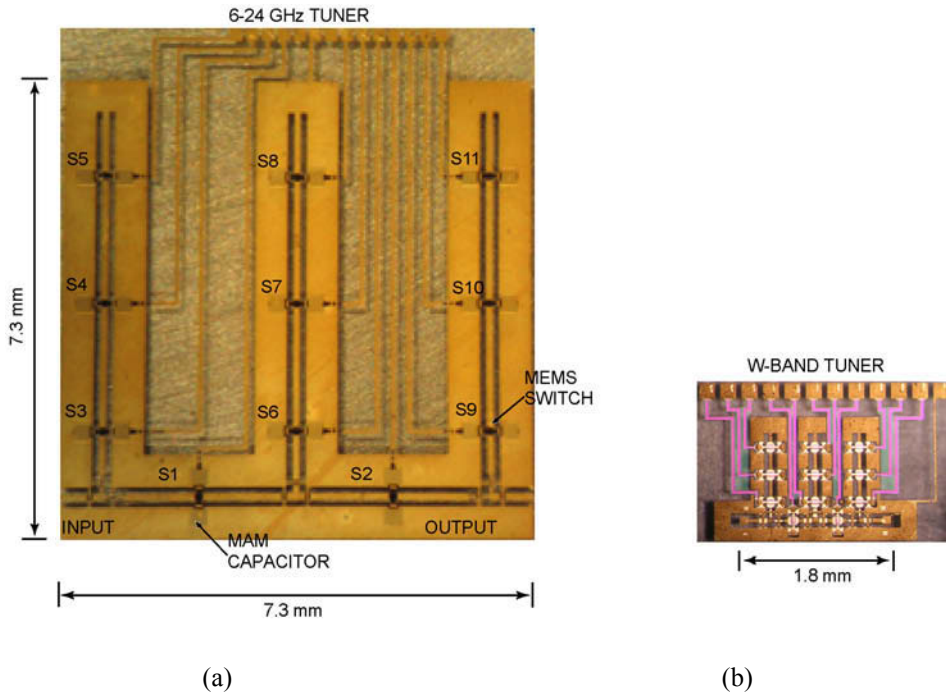


Figure 34. a) Photograph of the fabricated 6–24 GHz 3-stub impedance tuner [P3] and b) W-band 3-stub impedance tuner [P6].

The single-stub tuner was extended to 20–50 GHz, and a V-band design (50–80 GHz) was also realized with 10 switched MEMS capacitors [P4, P5]. Both tuners can generate 1024 ( $2^{10}$ ) different impedances. The 20–50 GHz single-stub impedance tuner has more wideband operation than other integrated tuners operating at the lower part of the frequency band [112, 113]. Measured  $|\Gamma_{MAX}|$  is 0.86, 0.88, 0.94 at 20, 30, and 40 GHz from 160 measurement points out of 1024 possible combinations for the 20–50 GHz impedance tuner. The results for the V-band single-stub impedance tuner are unique being the only published results for integrated impedance tuners at this frequency range [P5]. Measured  $|\Gamma_{MAX}|$  is 0.90 at 60 GHz and 0.99 at 78 GHz (equal to VSWR of 199) from 90 measurements out of 1024 possible combinations. Also, the results for W-band double and triple-stub impedance tuners presented in [P6] are the only published results for integrated impedance tuners at W-band.

Table 1. VSWR comparison of published integrated impedance tuners for frequencies 5–30 GHz.

Reference	Technology	VSWR	Freq. (GHz)
[109]	HEMT	6	27
[110]	HEMT	12.3	18
[112]	MEMS	32.3	30
[113]	MEMS	99	20
[P3]	MEMS	199	30

### 3.3.4 Distributed impedance tuners and matching networks realized with MEMS switches

The phase velocity and impedance of a transmission line can be changed by loading it capacitively. This idea has been used successfully in distributed MEMS transmission-line (DMTL) phase-shifters [25] and filters [119]. Distributed type phase shifters can be easily modified to be used as tunable quarter-wave impedance transformers. Both the electrical length and impedance of the transmission line can be changed and controlled very accurately [25, 27, 30, 100–102]. Because the impedance and electrical length of the transmission line are changed in a distributed manner, low loss and high power handling capability can be achieved.

Distributed type matching networks were developed for amplifier and antenna matching applications as well as for noise parameter and load-pull measurement applications in this work [P7–P8]. A transmission line is loaded with switched capacitors in this approach (Figure 35). Each switched capacitor has two states having two different capacitances, namely  $C_1$  and  $C_2$ . In this work, the switched capacitors were realized with MEMS switches ( $C_{MEMS}$ ) in series with fixed metal-air-metal capacitors ( $C_{MAM}$ ). The capacitance of the MEMS switches was matched with a high impedance transmission line so that the impedance of the loaded transmission line was close to 50- $\Omega$  in the up-state position of the MEMS switches. The high impedance unloaded transmission line at microwave

frequencies is effectively the same as an inductor-based matching at lower frequencies. By switching down more and more MEMS switches, the loading capacitance increases, transmission line impedance decreases, and the electrical length of the transmission line increases. Both 4 and 8-switch versions of distributed reconfigurable matching networks were realized for 4–18 GHz and an 8-switch version for 20–50 GHz amplifiers.

Publication [P7] describes the development of a novel reconfigurable matching network based on the loaded-line technique. The network is composed of N-switched capacitors ( $N = 4..8$ ) with a capacitance ratio of 4:1 to 5:1, and is suitable for power amplifiers at 4–18 GHz, or as an impedance tuner for noise parameter and load-pull measurements at 10–28 GHz. The networks are very small, and offer better performance than double or triple stub matching networks. Extensive loss analysis indicates that the 8-element network has a loss of 0.5 dB at 4–12 GHz, and less than 1.5 dB at 18 GHz, even when matching a 10  $\Omega$  output impedance to a 50  $\Omega$  load. As expected, the 4-element matching network has about half the loss of the 8-element network but with much less impedance coverage. Both networks were simulated and measured in high VSWR conditions and can handle at least 500 mW of RF power at 4–18 GHz. The application areas are in phased array antennas and reconfigurable power amplifiers.

Publication [P8] presents extension of the distributed reconfigurable matching networks to 20–50 GHz power amplifier applications (see Figure 35). The matching network consists of 8 switched MEMS capacitors producing 256 ( $2^8$ ) different impedances and is only  $1 \times 2.5 \text{ mm}^2$  in size on a glass substrate. The network is ideally suited to match power amplifiers with 10–20  $\Omega$  output impedance to 50–60  $\Omega$  systems at 20–50 GHz. The estimated loss of the network is only 1–1.5 dB at 40 GHz while matching a 10–20  $\Omega$  load to a 50  $\Omega$  load. The reconfigurable network can also be used as an impedance tuner in noise parameter and load-pull measurements of active devices at 30–65 GHz.

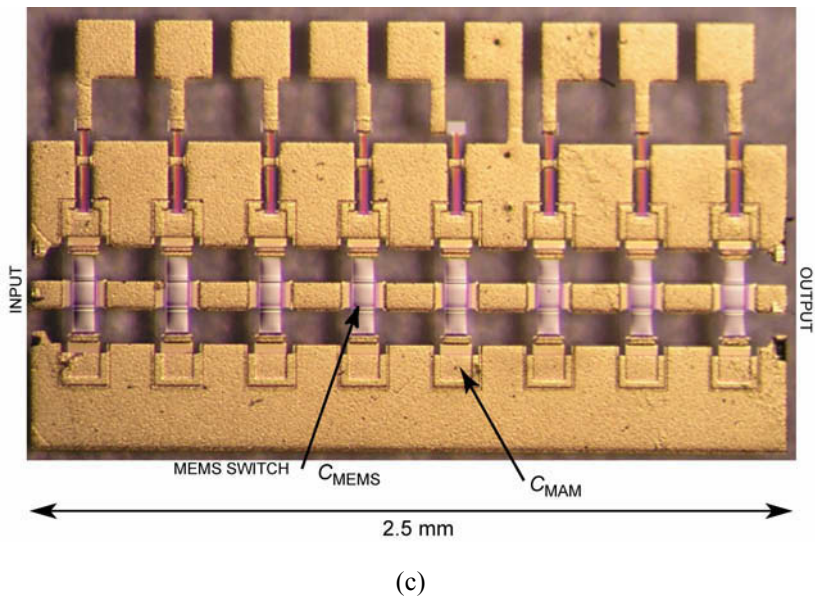
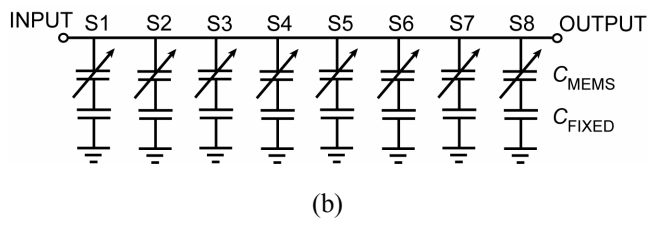
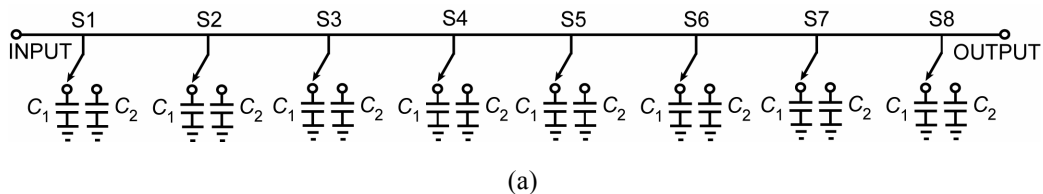


Figure 35. a) Schematics of a transmission line loaded with switched capacitors and b) switched capacitors realized with MEMS switches in series with switched capacitors. c) Photograph of a fabricated 20–50 GHz reconfigurable matching network [P8].

Shen and Barker have presented a distributed type impedance tuner based on the double-slug topology [120]. The schematic of a double-slug impedance tuner is shown in Figure 36. It has two 90° low impedance sections, the length of which determines the center frequency of the tuner, and the lengths  $L_1$  and  $L_2$  define the

impedance point being matched. Shen and Barker realized the double-slug tuner based on a DMTL, and having an individual bias control in each MEMS switched capacitor (totally 80 MEMS switched capacitors). The maximum VSWR generated by the tuner is  $VSWR = (Z_0/Z_L)^4$ , and was 4 in this case. This realization allows low loss and wideband operation with good impedance coverage inside the VSWR circle limited by  $(Z_0/Z_L)^4$ . The drawbacks of this realization are large number of control signals (80 in this case) and quite low maximum VSWR.

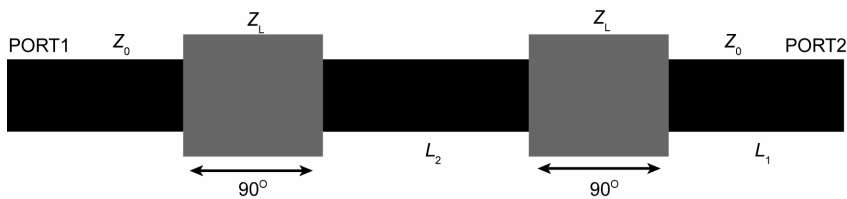


Figure 36. Schematic of the double-slug tuner [120].

## 4. Summary of publications

Publication [P1] presents an on-wafer noise parameter measurement set-up for W-band device characterization. Detailed description of the developed measurement system and procedures has been given. The noise parameters of an InP HEMT (DaimlerChrysler  $2 \times 40 \mu\text{m}$ ) have been measured, and measurement results have been presented in the 79–94 GHz frequency band. These are the first and only published on-wafer noise parameter measurement results for an active device above 75 GHz.

Publication [P2] presents on-wafer measurement system for wideband cryogenic device characterization. A V-band waveguide based measurement system has been extended to W-band. The S-parameters of HEMTs (DaimlerChrysler and HRL) has been measured at W-band and also in the 50–110 GHz frequency band and at 20–295 K. These are the first and only published cryogenic measurement results at this frequency range.

Publication [P3] introduces integrated triple, double, and single-stub impedance tuners for 6–24 GHz applications. Novel method for impedance tuning based on switched MEMS capacitors has been used in the tuners. The tuners have 10–13 switched capacitors producing 1024–8192 ( $2^{10}$ – $2^{13}$ ) different impedances. The impedance coverage of the tuners is the widest measured to-date from any integrated tuner at this frequency range. Also, the tuners can produce high reflection coefficients. The maximum measured  $|\Gamma_{\text{MAX}}|$  has been 0.99 (equal to VSWR 199) for the double-stub tuner at 30 GHz.

Publication [P4] describes the design, fabrication, and measurement results for a 20–50 GHz single-stub RF MEMS impedance tuner. The design is based on combining the loaded line technique with the single-stub topology to obtain wide impedance coverage with high  $|\Gamma_{\text{MAX}}|$ . The tuner consists of ten switched MEMS capacitors producing 1024 ( $2^{10}$ ) different impedances. The design has been optimized for noise parameter and load-pull measurements of active devices and shows excellent measured impedance coverage over the 20–50 GHz frequency range. Measured  $|\Gamma_{\text{MAX}}|$  is 0.86, 0.88, 0.94 at 20, 30, and 40 GHz from 160 measurements out of 1024 possible combinations, respectively.

Publication [P5] presents a single-stub RF MEMS impedance tuner optimized for 50–80 GHz noise parameter and load-pull measurement applications. This is the first and only published integrated impedance tuner operating at V-band (50–75 GHz). The tuner is small enough to be integrated inside an RF measurement probe. Measured (90 measurements out of 1024 possible combinations)  $|\Gamma_{\text{MAX}}|$  is 0.81, 0.80, 0.90, 0.94, 0.97, 0.99, and 0.99 at 50, 55, 60, 65, 70, 75, and 78 GHz, respectively. The tuner can be used as a reflection type impedance tuner over 40–80 GHz frequency band, when the output of the tuner is terminated with an open circuit.

Publication [P6] shows reconfigurable integrated double and triple-stub impedance tuners operating at W-band. The impedance tuners are based on 11 switched MEMS capacitors producing 2048 ( $2^{11}$ ) different impedances. Also, novel realization for switched capacitors is presented allowing compact size and accurate capacitance control. Measured  $|\Gamma_{\text{MAX}}|$  is 0.93, 0.87 and 0.87 at 75, 90, and 105 GHz for the double-stub tuner from 110 measurements and 0.92, 0.87, and 0.83 for the triple-stub tuner from 90 measurements out 2048 combinations.

Publication [P7] describes the development of a novel reconfigurable matching network based on the loaded-line technique. The network is composed of N-switched capacitors ( $N = 4 \dots 8$ ) with a capacitance ratio of 4:1 to 5:1 and is suitable for power amplifiers at 4–18 GHz, or as an impedance tuner for noise parameter and load-pull measurements at 10–28 GHz. The networks are very small, and offer better performance than double or triple stub matching networks. Extensive loss analysis indicates that the 8-element network has a loss of 0.5 dB at 4–12 GHz, and less than 1.5 dB at 18 GHz, even when matching a  $10 \Omega$  output impedance to a  $50\text{-}\Omega$  load. As expected, the 4-element matching network has about half the loss of the 8-element network but with much less impedance coverage. Both networks were simulated and measured in high VSWR conditions and can handle at least 500 mW of RF power at 4–18 GHz. The application areas are in phased array antennas, reconfigurable power amplifiers, and wideband noise parameter and load-pull measurement systems.

Publication [P8] presents extension of the distributed reconfigurable matching networks to 20–50 GHz power amplifier applications. The matching network consists of 8 switched MEMS capacitors producing 256 ( $2^8$ ) different impedances and is only  $1 \times 2.5$  mm in size on a glass substrate. The network is

ideally suited to match power amplifiers with 10–20  $\Omega$  output impedance to 50–60  $\Omega$  systems at 20–50 GHz. The estimated loss of the network is only 1–1.5 dB at 40 GHz while matching a 10–20  $\Omega$  load to a 50- $\Omega$  load. The reconfigurable network can also be used as an impedance tuner in noise parameter and load-pull measurements of active devices at 30–65 GHz.

## 5. Conclusion

This thesis extended both on-wafer cryogenic and noise parameter measurements to W-band frequencies. For the first time, noise parameters of an active device were measured at W-band. Also, wideband cryogenic on-wafer measurements have been carried out for transistors between 50 and 110 GHz and 20–295 K.

In order to further develop on-wafer noise parameter measurement methods, novel RF MEMS impedance tuners were designed, fabricated, and characterized in this thesis work. The integrated tuners were based on single, double, and triple-stub topologies and CPW transmission lines on glass substrate. The electrical tuning of the electrical length and transmission line impedance were realized innovatively with switched MEMS capacitors. By using  $N$  (number of switched capacitors) switched capacitors,  $2^N$  different impedances could be generated. The stub-based impedance tuners were realized with 10, 11, or 13 switched capacitors producing 1024, 2048, or 8192 different impedances. Several tuners were developed to cover 6–120 GHz frequency band. Single, double, and triple-stub tuners were developed for the 6–24 GHz band, a single-stub tuner for 20–50 GHz, a single stub tuner for 40–80 GHz, and both double and triple-stub tuners for 75–120 GHz. The highest reflection coefficients were measured from the 6–30 GHz double-stub tuner at 30 GHz and from the 40–80 GHz single-stub impedance tuner at 78 GHz having  $|\Gamma_{\text{MAX}}|$  of 0.99 which is equal to VSWR 199. The developed stub-based impedance tuners have the state-of-the-art performance compared to any other published integrated impedance tuners having the widest impedance and frequency coverage with highest measured  $|\Gamma_{\text{MAX}}|$ .

In addition to the stub-based impedance tuners, novel distributed reconfigurable matching networks were developed for 4–18 GHz and 20–50 GHz applications. The switched capacitor tuning was also applied to the distributed topology. These matching networks are most suitable for multi-band and reconfigurable applications, where systems need to operate at several frequencies over a wide frequency range and must tolerate changing impedance conditions. The distributed matching networks have lower loss and better RF power handling capabilities compared to the stub-tuners.

Future work includes further development of on-wafer measurement methods and especially characterization of RF MEMS components and circuits. Also, research will focus to the improvement of reconfigurable matching networks and impedance tuners, realization of RF MEMS circuits above 140 GHz, investigation of CMOS compatible fabrication methods for MEMS components and circuits for millimeter wave applications, and development of electrically steerable antenna arrays based on MEMS technology.

## References

1. T. Vähä-Heikkilä, J. Varis, H. Hakojärvi, and J. Tuovinen, "Cryogenic on-wafer measurements at W-band and at 20–295 K." *The 3rd ESA Workshop Millimetre Wave Technology and Applications: Antennas, Circuits, and Systems*, Espoo, Finland, 2003. Pp. 435–439.
2. T. Vähä-Heikkilä, M. Lahdes, M. Kantanen, T. Karttaavi, and J. Tuovinen, "Very wideband automated on-wafer noise figure and gain measurements at 50–110 GHz." *Proceedings of GAAS 2002, The European Gallium Arsenide & related III–V Compounds Applications Symposium*, Milan, Italy, 2002. Pp. 233–236.
3. T. Vähä-Heikkilä, M. Kantanen, M. Lahdes, and J. Tuovinen, "Practical methods for millimeter wave on-wafer measurements of active devices at 50–110 GHz." *Proceedings of the International Joint Conference of the Sixth Topical Symposium on Millimeter Waves (TSMMW2004) and the Fifth MINT Millimeter-Wave International Symposium (MINT-MIS)*, Yokosuka, Japan, 2004. Pp. 118–121.
4. M. Kantanen, M. Lahdes, T. Vähä-Heikkilä, J. Tuovinen, "A wideband automated measurement system for on-wafer noise parameter measurements at 50–75 GHz." *IEEE Transactions on Microwave Theory and Techniques*, Vol. 51, No. 5, pp. 1489–1495, 2003.
5. T. Vähä-Heikkilä, "Wideband Cryogenic and Room Temperature On-Wafer Measurements at 50–110 GHz." Licentiate thesis, University of Turku, 2005.
6. T. Vähä-Heikkilä, J. Varis, J. Tuovinen, G.M. Rebeiz, "Reconfigurable RF MEMS impedance tuners and matching networks." *The 34th European Microwave Conference, Proceedings of Workshop on Smart MEMS for RF and Millimeter Wave Communications*, Amsterdam, Netherlands, 2004. Pp. 123–136.

7. M.W. Pospieszalski, E.J. Wollack, N. Bailey, D. Thacker, J. Webber, L.D. Nguyen, N. Le, and M. Lui, "Design and performance of wideband, low-noise, millimeter-wave amplifiers for Microwave Anisotropy Probe radiometers." *2000 IEEE MTT-S International Microwave Symposium Digest*, Boston, MA, 2000. Pp. 25–28.
8. J. Tuovinen, P. Kangaslahti, P. Haapanen, N. Hughes, P. Jukkala, T. Karttaavi, O. Koistinen, M. Lahdes, H. Salminen, and J. Tanskanen, S. Urpo, "Development of 70 GHz receivers for the Planck LFI." *Astrophysics Letters and Communications*, Vol. 37, pp. 181–187, 2000.
9. P. J. Napier, D. S. Bagri, B.G. Clark, A.E.E. Rogers, J.D. Romney, A.R. Thompson, and R.C. Walker, "The Very Long Baseline Array." *Proceedings of the IEEE*, Vol. 82, No. 5, pp. 656–672, 1994.
10. A. Wootten, ed., *Science with the Atacama Large Millimeter Array*, San Francisco, CA, ASP, Vol. 253, 2001.
11. L.H. Eriksson and B. As, "A high performance automotive radar for automatic AICC." *IEEE Aerospace and Electronic Systems Magazine*, Vol. 10, No. 12, pp. 13–18, 1995.
12. H. Meinel, J. Wenger, H. Hentling, G. Rollmann, and H. Dominik, "Automotive radar: from long range collision warning to short range urban employment." *Proceedings of the International Joint Conference of the Seventh Topical Symposium on Millimeter Waves (TSMMW2004) and the Sixth MINT Millimeter-Wave International Symposium (MINT-MIS)*, Seoul, Korea, 2005. Pp. 244–247.
13. P. Mikkonen, "Modern 60 GHz radio link." *Proceedings of the 29th European Microwave Conference*, Munich, Germany, Vol. 3, 1999. Pp. 83–86.
14. M. Kärkkäinen, M. Varonen, J. Riska, P. Kangaslahti, and V. Porra, "A set of integrated circuits for 60 GHz radio front-end." *2002 IEEE MTT-S International Microwave Symposium Digest*, Seattle, WA, Vol. 2, 2002. Pp. 1273–1276.

15. M. Varonen, M. Kärkkäinen, P. Kangaslahti, and V. Porra, "Integrated power amplifier for 60 GHz wireless applications." *2003 IEEE MTT-S International Microwave Symposium Digest*, Philadelphia, PA, Vol. 2, 2003. Pp. 915–918.
16. K. Hmaguchi, Y. Shoji, H. Ogawa, Y.H. Kim, and S. Shimizu, "Millimeter-wave vertically connected wireless link system – system overview." *Proceedings of the International Joint Conference of the Seventh Topical Symposium on Millimeter Waves (TSMMW2004) and the Sixth MINT Millimeter-Wave International Symposium (MINT-MIS)*, Seoul, Korea, 2005. Pp. 255–258.
17. L. Yujiri, M. Shoucri, and P. Moffa, "Passive millimeter wave imaging." *IEEE Microwave Magazine*, Vol. 4, No. 3, pp. 39–50, 2003.
18. R.M. Smith, K.D. Trott, B.M. Sundstrom, and D. Ewen, "The passive mm-wave scenario." *Microwave Journal*, Vol. 39, No. 3, pp. 22–34, 1996.
19. M. Kantanen, M. Lahdes, and J. Tuovinen, "A millimeter wave imager." *Proceedings of the International Joint Conference of the Seventh Topical Symposium on Millimeter Waves (TSMMW2004) and the Sixth MINT Millimeter-Wave International Symposium (MINT-MIS)*, Seoul, Korea, 2005. Pp. 240–243.
20. J. Rizk, G.-L. Tang, J.B. Muldavin, and G.M. Rebeiz, "High-isolation W-band MEMS switches." *IEEE Microwave and Wireless Components Letters*, Vol. 11, No. 1, pp. 10–12, 2001.
21. J. Rizk and G.M. Rebeiz, "W-band microstrip RF-MEMS switches and phase shifters." *2003 IEEE MTT-S International Microwave Symposium Digest*, Philadelphia, PA, 2003. Pp. 1485–1488.
22. J. Rizk and G.M. Rebeiz, "W-band CPW RF MEMS circuits on quartz substrates." *IEEE Transactions on Microwave Theory and Techniques*, Vol. 51, No. 7, pp. 1857–1862, 2003.

23. D. Mercier, P.L. Charvet, P. Berruyer, C. Zanchi, L. Lapierre, O. Vendier, J.L. Cazaux, and P. Blondy, "A DC to 100 GHz high performance ohmic shunt switch." *2004 IEEE MTT-S International Microwave Symposium Digest*, Fort Worth, TX, 2004. Pp. 1931–1934.
24. J. Schobel, T. Buck, M. Reimann, M. Ulm, and M. Schneider, "W-band RF-MEMS subsystems for smart antennas in automotive radar sensors." *Proceedings of the 34th European Microwave Conference 2004*, Amsterdam, Netherlands, 2004. Pp. 1305–1308.
25. N.S. Barker and G.M. Rebeiz, "Optimization of distributed MEMS transmission line phase shifters – U-band and W-band designs." *IEEE Transactions on Microwave Theory and Techniques*, Vol. 48, No. 11, pp. 1957–1966, 2000.
26. H.-T. Kim, J.-H. Park, J. Yim, Y.-K. Kim, and Y. Kwon, "A compact V-band 2-bit reflection-type MEMS phase shifter." *IEEE Microwave and Wireless Components Letters*, Vol. 12, No. 9, pp. 324–326, 2002.
27. H.-T. Kim, J.-H. Park, S. Lee, S. Kim, J.-M. Kim, Y.-K. Kim, and Y. Kwon, "V-band 2-b and 4-b low-loss and low-voltage distributed MEMS digital phase shifter using metal-air-metal capacitors." *IEEE Transactions on Microwave Theory and Techniques*, Vol. 50, No. 12, pp. 2918–2923, 2002.
28. H.-T. Kim, S. Lee, J.-M. Kim, J.-H. Park, Y.-K. Kim, and Y. Kwon, "A V-band CPS distributed analog MEMS phase shifter." *2003 IEEE MTT-S International Microwave Symposium Digest*, Philadelphia, PA, 2003. Pp. 1481–1484.
29. J.-J. Hung, L. Dussopt, and G.M. Rebeiz, "Distributed 2- and 3-bit W-band MEMS phase shifters on glass substrates." *IEEE Transactions on Microwave Theory and Techniques*, Vol. 52, No. 2, pp. 600–606, 2004.

30. B. Lakshminarayanan and T. Weller, "MEMS phase shifters using cascaded slow-wave structures for improved impedance matching and/or phase shift." *2004 IEEE MTT-S International Microwave Symposium Digest*, Fort Worth, TX, 2004. Pp. 725–728.
31. H.-T. Kim, J.-H. Park, Y.-K. Kim, and Y. Kwon, "Low-loss and compact V-band MEMS-based analog tunable bandpass filters." *IEEE Microwave and Wireless Components Letters*, Vol. 12, No. 11, pp. 432–434, 2002.
32. E. Fourn, C. Quendo, E. Rius, A. Pothier, P. Blondy, C. Champeaux, J.C. Orlianges, A. Catherinot, G. Tanne, C. Person, and F. Huret, "Bandwidth and central frequency control on tunable bandpass filter by using MEMS cantilevers." *2003 IEEE MTT-S International Microwave Symposium Digest*, Philadelphia, PA, 2003. Pp. 523–526.
33. S. Lee, J.-H. Park, J.-M. Kim, H.-T. Kim, Y.-K. Kim, and Y. Kwon, "A compact low-loss reconfigurable monolithic low-pass filter using multiple-contact MEMS switches." *IEEE Microwave and Wireless Components Letters*, Vol. 14, No. 1, pp. 37–39, 2004.
34. B. Schoenlinner, A. Abbaspour-Tamijani, L.C. Kempel, and G.M. Rebeiz, "Switchable low-loss RF MEMS Ka-band frequency-selective surface." *IEEE Transactions on Microwave Theory and Techniques*, Vol. 52, No. 11, pp. 2474–2481, 2004.
35. V.M. Lubecke, W.R. McGrath, and D.B. Rutledge, "A 100-GHz coplanar strip circuit tuned with a sliding planar backshort." *IEEE Microwave Guided Wave Letters*, Vol. 3, No. 12, pp. 441–443, 1993.
36. C.-W. Baek, S. Song, C. Cheon, Y.-K. Kim, and Y. Kwon, "2-D mechanical beam steering antenna fabricated using MEMS technology." *2001 IEEE MTT-S International Microwave Symposium Digest*, Phoenix, AZ, 2001. Pp. 211–214.

37. B. Lakshminarayanan and T. Weller, "Electronically tunable multi-line TRL using an impedance matched multi-Bit MEMS phase shifter." *IEEE Microwave and Wireless Components Letters*, Vol. 15, No. 2, pp. 137–139, 2005.
38. F. Ulaby, R. Moore, and A. Fung, *Microwave Remote Sensing, Active and Passive*, Vol. 1. Addison–Wesley Publishing Company, Reading, MA, 1981.
39. L.A. Klein, *Millimeter-Wave and Infrared Multisensor Design and Signal Processing*, Artec House, Norwood, MA, 1997.
40. E.H. Armstrong, "The super-heterodyne – its origin, development, and some recent improvements." *Proceedings of the IRE*, Vol. 50, pp. 539–552, 1924.
41. A.R. Barnes, P. Munday, R. Jennings, M. Moore, M. Black, R. Appleby, R. Anderton, G. Sinclair, and P. Coward, "MMIC Technology and its application in passive mm-wave imaging systems." *The 3rd ESA Workshop Millimetre Wave Technology and Applications: Antennas, Circuits, and Systems*, Espoo, Finland, 2003. Pp. 543–547.
42. J. Tuovinen, N. Hughes, P. Jukkala, P. Kangaslahti, T. Karttaavi, P. Sjöman, and J. Varis, "Technology for millimetre wave radiometers." *Proceedings of the 33rd European Microwave Conference*, Munich, Germany, 2003. Pp. 883–886.
43. S.Y. Liao, *Microwave Circuit Analysis and Amplifier Design*. Prentice–Hall, Englewood Cliffs, NJ, 1987.
44. E.W. Strid and K.R. Gleason: "A DC–12 GHz monolithic GaAsFET distributed amplifier." *IEEE Transactions on Microwave Theory and Techniques*, Vol. 82, No. 7, pp. 969–975, 1982.
45. E.W. Strid and K.R. Gleason, "Calibration methods for microwave wafer probing." *Microwave and Millimeter-Wave Monolithic Circuits*, Vol. 84, No. 1, pp. 78–82, 1984.

46. M. Matloubian, S.E. Rosenbaum, H.R. Fetterman, and P.T. Greiling, "Wide-band millimeter wave characterization of sub-0.2 micrometer gate-length AlInAs/GaInAs HEMTs." *IEEE Microwave and Guided Wave Letters*, Vol. 1, No. 2, pp. 32–34, 1991.
47. R.Y. Yu, J. Pysl, Y. Konishi, M. Case, M. Kamegawa, and M. Rodwell, "8–96 GHz on-wafer network analysis." *Technical Digest of 14th Annual Gallium Arsenide Integrated Circuit (GaAs IC) Symposium 1992*, 1992. Pp. 75–77.
48. R. Anholt, J. Pence, and E. Godshalk, "On-wafer HEMT characterization to 110 GHz." *Technical Digest of the 16th Annual Gallium Arsenide Integrated Circuit (GaAs IC) Symposium 1994*, 1994. Pp. 108–111.
49. R. Lai, M. Barsky, T. Huang, M. Sholley, H. Wang, Y.L. Kok, D.C. Streit, T. Block, and P.H. Liu, "An InP HEMT MMIC LNA with 7.2-dB gain at 190 GHz." *IEEE Microwave and Guided Wave Letters*, Vol. 8, No. 11, pp. 393–395, 1998.
50. C.W. Pobanz, M. Matloubian, M. Lui, H.-C. Sun, M. Case, C.M. Ngo, P. Janke, T. Gaier, and L. Samoska, "A high-gain monolithic D-band InP HEMT amplifier." *IEEE Journal of Solid-State Circuits*, Vol. 34, No. 9, pp. 1219–1224, 1999.
51. A. Tessmann, O. Wohlgemuth, R. Reuter, W. Haydl, H. Massler, and A. Hulsmann, "A coplanar 148 GHz cascode amplifier MMIC using 0.15  $\mu\text{m}$  GaAs PHEMTs." *2000 IEEE MTT-S International Microwave Symposium Digest*, Boston, MA, Vol. 2, 2000. Pp. 991–994.
52. T.-N. Ton, H. Wang, S. Chen, K.L. Tan, G.S. Dow, B.R. Allen, and J. Berenz, "W-band monolithic pseudomorphic AlGaAs/InGaAs/GaAs HEMT CBCPW LNA." *Electronics Letters*, Vol. 29, No. 20, pp. 1804–1805, 1993.
53. T. Katoh, T. Kashiwa, H. Koski, A. Inoue, and T. Ishikawa, "Automated millimeter-wave on-wafer testing system." *IEICE Transaction on Electron.*, Vol. E82-C, pp. 1312–1317, 1999.

54. M.G. Case, C. Pobanz, S. Weinreb, M. Matloubian, M. Hu, M. Wetzel, P. Janke, and C. Ngo, "Low-cost, high-performance W-band LNA MMICs for millimeter-wave imaging." *Proceedings of Spie, Passive Millimeter-Wave Imaging Technology IV*, Vol. 4032, pp. 89–96, 2000.
55. A. Rodrigue, L.P. Dunleavy, and P. Kirby, "Best practice for on-wafer millimeter wave noise figure measurements." *57th ARFTG Conference Digest*, Phoenix, AZ, 2001.
56. H. Meschede, R. Reuter, J. Albers, J. Kraus, D. Peters, W. Brockerhoff, F.-J. Tegude, M. Bode, J. Schubert, and W. Zander, "On-wafer microwave measurement setup for investigations on HEMTs and high- $T_c$  superconductors at cryogenic temperatures down to 20 K." *IEEE Transactions on Microwave Theory and Techniques*, Vol. 40, No. 12, pp. 2325–2331, 1992.
57. J. Laskar, M.R. Murti, S.Y. Yoo, E. Gebara, and H.M. Harris, "Development of complete on-wafer cryogenic characterization: S-parameters, noise-parameters and load-pull." *1998 European GaAs and Related III–V Compounds, Application Symposium Digest*, Amsterdam, Netherlands, 1998. Pp. 33–38.
58. A. Caddemi, N. Donato, and M. Sannino, "Characterization techniques for temperature-dependent analysis of microwave transistors." *Proceedings of the 18th IEEE Instrumentation and Measurement Technology Conference 2001*, Vol. 3, 2001, Pp. 1893–1896.
59. J. Tuovinen, J. Varis, M. Lahdes, T. Karttaavi, and H. Hakojärvi, "Methods for on-wafer testing of cryogenic integrated circuits at millimetre waves." *Proceedings of the Fourth European Workshop on Low Temperature Electronics (WOLTE 4)*, Noordwijk, Netherlands, 2000. Pp. 157–162.
60. H. Rothe and W. Dahlke, "Theory of noisy four poles." *Proceedings of IRE*, Vol. 44, pp. 687–691, 1956.

61. "IRE standards on methods of measuring noise in linear twoports, 1959." *Proceedings of IRE*, Vol. 48, pp. 60–68, 1960.
62. R.Q. Lane, "The determination of device noise parameters." *Proceedings of the IEEE*, Vol. 57, No. 8, pp. 1461–1462, 1962.
63. M. Mitama and H. Katoh, "An improved computational method for noise parameter measurement." *IEEE Transactions on Microwave Theory and Techniques*, Vol. 27, No. 6, pp. 612–615, 1979.
64. G.I. Vasilescu, G. Alquie, and M. Krim, "Exact computation of two-port noise parameters." *Electronic Letters*, Vol. 25, No. 4, pp. 292–293, 1989.
65. A. Boudiaf, M. Laporte, J. Dangla, and G. Vernet, "Accuracy improvements in two-port noise parameter extraction method." *1992 IEEE MTT-S International Microwave Symposium Digest*, Albuquerque, NM, 1992, pp. 1569–1572.
66. L. Escotte, R. Plana, and J. Graffeuil, "Evaluation of noise parameter extraction methods." *IEEE Transactions on Microwave Theory and Techniques*, Vol. 41, No. 3, pp. 382–387, 1993.
67. M.W. Pospiezalski, "Modeling of noise parameters of MESFET's and MODFET's and their frequency and temperature dependence." *IEEE Transactions on Microwave Theory and Techniques*, Vol. 37, No. 9, pp. 1340–1350, 1989.
68. P.J. Tasker, W. Reinert, J. Braunstein, and M. Schlechtweg, "Direct extraction of all four transistor noise parameters from a single noise figure measurement." *Proceedings of the 22nd European Microwave Conference*, Helsinki, Finland, 1992. Pp. 157–162.
69. A. Lazaro, L. Pradell, A. Beltran, and J.M. O'Callaghan, "Direct extraction of all four transistor noise parameters from 50  $\Omega$  noise figure measurements." *Electronics Letters*, Vol. 34, No. 3, pp. 289–291, 1998.

70. T. Karttaavi, *Transistor Modeling for a Millimeter Wave Low-Noise Amplifier*, Licentiate thesis, TKK Helsinki University of Technology, 2000.
71. V. Adamian and A. Uhlir, "A novel procedure for receiver noise characterisation." *IEEE Transactions on Instrumentation and Measurements*, Vol. 22, No. 6, pp. 181–182, 1973.
72. C.A. Davidson, B.W. Leake, and E. Strid, "Accuracy improvements in microwave noise parameter measurements." *IEEE Transactions on Microwave Theory and Techniques*, Vol. 37, No. 12, pp. 1973–1977, 1989.
73. R. Meierer and C. Tsironis, "An on-wafer noise parameter measurement technique with automatic receiver calibration." *Microwave Journal*, Vol. 38, No. 3, pp. 80–88, 1995.
74. A. Davidson, K. Jones, and E. Strid, "LRM and LRRM calibrations with automatic determination of load inductance", *36th ARFTG Conference Digest*, Monterey, 1990. Pp. 57–62.
75. Y.-L. Kok, M. DuFault, T.-W. Huang, and H. Wang, "A calibration procedure for W-band on-wafer testing." *1997 IEEE MTT-S International Microwave Symposium Digest*, Denver, CO, Vol. 3, 1997. Pp. 1663–1666.
76. R.B. Mark, "A multi-line method of network analyzer calibration." *IEEE Transactions on Microwave Theory and Techniques*, Vol. 39, No. 7, pp. 1205–1215, 1991.
77. R.T. Webster, A.J. Slobodnik Jr., and G.A. Roberts, "Determination of InP HEMT noise parameters and S-parameters to 60 GHz." *IEEE Transactions on Microwave Theory and Techniques*, Vol. 43, No. 6, pp. 1216–1225, 1995.
78. M. Lahdes, M. Sipilä, and J. Tuovinen, "60 GHz noise parameter measurements using cold-source method." *49th ARFTG Conference Digest*, Denver, 1997. Pp. 146–154.

79. M. Lahdes and J. Tuovinen, "V-band on-wafer noise parameter measurements." *Proceedings of GaAs 1998, The European Gallium Arsenide & Related III-V Compounds Applications Symposium*, Amsterdam, 1998. Pp. 39–44.
80. M. Lahdes, "Uncertainty analysis of V-band on-wafer noise parameter measurement system." *Proceedings of the 28th European Microwave Conference*, Amsterdam, Netherlands, 1998. Pp. 445–450.
81. T.A. Alam, R.D. Pollard, and C.M. Snowden, "The determination of on-wafer noise parameters at W-band." *Proceedings of the 27th European Microwave Conference*, Jerusalem, 1997. Pp. 687–691.
82. T.A. Alam, R.D. Pollard, and C.M. Snowden, "Determination of W-band noise parameters." *Electronic Letters*, Vol. 34, No. 3, pp. 288–289, 1998.
83. R. Drury, R.D. Pollard, and C.M. Snowden, "A 75–110 GHz automated tuner with exceptional range and repeatability." *IEEE Microwave Guided Wave Letters*, Vol. 6, No. 10, pp. 378–379, 1996.
84. R.E. Collin, *Foundations For Microwave Engineering*, New York, McGraw–Hill Book Company, 1966.
85. R. Ludwig, and P. Bretchko, *RF Circuit Design Theory and Applications*, Upper Saddle River, Prentice Hall, 2000.
86. D.M. Pozar, *Microwave Engineering*, New York, John Wiley & Sons, 1998.
87. G.M. Rebeiz, *RF MEMS: Theory, Design, and Technology*, New York, John Wiley & Sons, 2003.
88. G.E. Ponchak and L.P.B. Katehi, "Open- and short-circuit terminated series stubs in finite-width coplanar waveguide on silicon." *IEEE Transactions on Microwave Theory and Techniques*, Vol. 45, No. 6, pp. 970–976, 1997.

89. K. Hettak, N. Dib, A. Omar, G.Y. Delisle, M. Stubbs, and S. Toutain, "A useful new class of miniature CPW shunt stubs and its impact on millimeter-wave integrated circuits." *IEEE Transactions on Microwave Theory and Techniques*, Vol. 47, No. 12, pp. 2340–2349, 1999.
90. K. Hettak, C.J. Verver, and M.G. Stubbs, "Overlapping, multiple CPW stub structures for high density MMICs." *2001 IEEE MTT-S International Microwave Symposium Digest*, Phoenix, AZ, Vol. 1, 2001. Pp. 311–314.
91. V.S. Möttönen, J. Mallat, and A.V. Räisänen, "Characterisation of European millimetre wave planar diodes." *Proceedings of the 34th European Microwave Conference*, Amsterdam, Netherlands, 2004. Pp. 921–924.
92. L.E. Larson, R.H. Hackett, M.A. Melendes, and R.F. Lohr, "Micromachined microwave actuator (MIMAC) technology – a new tuning approach for microwave integrated circuits." *Microwave and Millimeter-Wave Monolithic Circuits Symposium Digest*, Boston, MA, 1991. Pp. 27–30.
93. C. Goldsmith, J. Randall, S. Eshelman, T.H. Lin, D. Dennistor, S. Chen, and B. Norvell, "Characteristics of micromachined switches at microwave frequencies." *1996 IEEE MTT-S International Microwave Symposium Digest*, San Francisco, CA, 1996. Pp. 1141–1144.
94. C. Goldsmith, S. Eshelman, and D. Dennistor, "Performance of low-loss RF MEMS capacitive switches." *IEEE Microwave and Guided Wave Letters*, Vol. 8, No. 8, pp. 269–271, 1998.
95. J.Y. Park, G.H. Kim, K.W. Chung, and J.U. Bong, "Fully integrated micromachined capacitive switches for RF applications." *2000 IEEE MTT-S International Microwave Symposium Digest*, Boston, MA, 2000. Pp. 283–286.
96. J.B. Muldavin and G.M. Rebeiz, "High isolation MEMS shunt switches; Part 1: Modeling." *IEEE Transactions on Microwave Theory and Techniques*, Vol. 48, No. 6, pp. 1045–1052, 2000.

97. J.B. Muldavin and G.M. Rebeiz, "High isolation MEMS shunt switches; Part 2: Design." *IEEE Transactions on Microwave Theory and Techniques*, Vol. 48, No. 6, pp. 1053–1056, 2000.
98. H.A.C. Tilmans, H. Ziad, H. Jansen, O. Di Monaco, A. Jourdain, W. De Raedth, X. Rottenburg, E. De Backerand, A. Decaussemaeker, and K. Baert, "Wafer-level packaged RF-MEMS switches fabricated in a CMOS fab." *Proceedings of International Electron Devices Meeting*, Washington DC, 2001. Pp. 41.4.1–41.4.4.
99. A. Abbaspour-Tamijani, L. Dussopt, and G.M. Rebeiz, "Miniature and tunable filters using MEMS capacitors." *IEEE Transactions on Microwave Theory and Techniques*, Vol. 51, No. 7, pp. 1878–1885, 2003.
100. J.S. Hayden, A. Malczewski, J. Kleber, C.L. Goldsmith, and G.M. Rebeiz, "2 and 4-bit DC-18 GHz microstrip MEMS distributed phase shifters." *2001 IEEE MTT-S International Microwave Symposium Digest*, Phoenix, AZ, 2001. Pp. 219–222.
101. J.S. Hayden and G.M. Rebeiz, "A low-loss Ka-band distributed MEMS 2-bit phase shifters using metal-air-metal capacitors." *2002 IEEE MTT-S International Microwave Symposium Digest*, Seattle, WA, 2002. Pp. 337–340.
102. J.S. Hayden and G.M. Rebeiz, "2-bit MEMS distributed X-band phase shifters." *IEEE Microwave and Guided Wave Letters*, Vol. 10, No. 12, pp. 540–542, 2000.
103. J.B. Rizk, *W-band RF MEMS Switches, Phase Shifters and Antennas*, Ph.D. dissertation, Department of Electrical Engineering, University of Michigan, Ann Arbor, MI, 2003.
104. J.S. Hayden, *High-Performance Digital X-Band and Ka-Band Distributed MEMS Phase Shifters*, Ph.D. dissertation, Department of Electrical Engineering, University of Michigan, Ann Arbor, MI, 2002.

105. V.M. Lubecke, W.R. McGrath, P.A. Stimson, and D.B. Rutledge, "Micromechanical tuning elements in a 620 GHz integrated circuit." *IEEE Transactions on Microwave Theory and Techniques*, Vol. 46, No. 8, pp. 2098–2103, 1998.
106. V.M. Lubecke, K. Mizuno, and G.M. Rebeiz, "Micromachining for Terahertz applications." *IEEE Transactions on Microwave Theory and Techniques*, Vol. 46, No. 11, pp. 1821–1831, 1998.
107. J.-C. Chiao, Y. Fu, I. Chio, M. DeLisio, and L.-Y. Lin, "MEMS reconfigurable Vee antenna." *1999 IEEE MTT-S International Microwave Symposium Digest*, Anaheim, CA, 1999. Pp. 1515–1518.
108. J.-C. Chiao, S.-Y. Cheng, J.J.L. Chang, I.M. Chio, Y. Kang, and J. Hayasaka, "MEMS reconfigurable antennas." *International Journal of RF and Microwave Computer Aided Engineering*, Vol. 11, No. 5, pp. 301–309, 2001.
109. W. Bischof, "Variable impedance tuner for MMIC's." *IEEE Microwave and Guided Wave Letters*, Vol. 4, No. 6, pp. 172–174, 1994.
110. C.E. McIntosh, R.D. Pollard, and R.E. Miles, "Novel MMIC source-impedance tuners for on-wafer microwave noise-parameter measurements." *IEEE Transactions on Microwave Theory and Techniques*, Vol. 47, No. 2, pp. 125–131, 1999.
111. J. de Mingo, A. Valdovinos, A. Crespo, D. Navarro, and P. García, "An RF electronically controlled impedance tuning network design and its application to an antenna input impedance automatic matching system." *IEEE Transactions on Microwave Theory and Techniques*, Vol. 52, No. 2, pp. 489–497, 2004.
112. H.-T. Kim, S. Jung, K. Kang, J.-H. Park, Y.-K. Kim, and Y. Kwon, "Low-Loss analog and digital micromachined impedance tuners at the Ka-band." *IEEE Transactions on Microwave Theory and Techniques*, Vol. 49, pp. 2394–2400, 2001.

113. J. Papapolymerou, K.L. Lange, C.L. Goldsmith, A. Malczewski, and J. Kleber, "Reconfigurable double-stub tuners using MEMS switches for intelligent RF front-ends." *IEEE Transactions on Microwave Theory and Techniques*, Vol. 51, No.1, pp. 271–278, 2003.
114. Y. Lu, D. Peroulis, S. Mohammadi, and L.P.B. Katehi, "A MEMS reconfigurable matching network for a class AB amplifier." *IEEE Microwave Wireless Components Letters*, Vol. 13, No. 10, pp. 437–439, 2003.
115. D. Qiao, R. Molfino, S.M. Lardizabal, B. Pillans, P.M. Asbeck, and G. Jerinic, "An intelligently controlled RF power amplifier with a reconfigurable MEMS-varactor tuner." *IEEE Transactions on Microwave Theory and Techniques*, Vol. 53, No. 3, pp. 1089–1095, 2005.
116. H. Nieminen, V. Ermolov, K. Nybergh, S. Silanto, and T. Ryhänen, "Microelectromechanical capacitors for RF applications." *Journal of Micromechanics and Microengineering*, Vol. 12, No. 2, pp. 177–186, 2002.
117. H. Nieminen, V. Ermolov, S. Silanto, K. Nybergh, and T. Ryhänen, "Design of a temperature-stable RF MEM capacitor." *IEEE Journal of Microelectromechanical Systems*, Vol. 13, No. 5, pp. 705–714, 2004.
118. H. Nieminen, J. Kankaanpää, V. Ermolov, S. Silanto, and T. Ryhänen, "RF MEMS for 0.8–2.5 GHz applications in mobile terminals." *MEMSWAVE 5th Workshop on MEMS for Millimeter Wave Communications*, Uppsala, Sweden, 2004. Pp. A42–A48.
119. K. Entesari and G.M. Rebeiz, "A 12–18 GHz three-pole RF MEMS tunable filter." *IEEE Transactions on Microwave Theory and Techniques*, Vol. 53, No. 8, pp. 2566–2571, 2005.
120. Q. Shen and N.S. Barker, "A reconfigurable RF MEMS double slug impedance tuner." *Proceedings of the 35th European Microwave Conference*, Paris, France, 2005. Pp. 537–540.

# Appendix A: Detailed surface MEMS fabrication procedure used in this thesis

The fabrication process used in this thesis work is a modified six masks version from the surface MEMS process developed at the University of Michigan [103, 104]. Corning 7040 glass wafers with  $\epsilon_r = 4.6$  are used as substrates in this work, but the fabrication process is also suitable for other substrates. Only the exposing time of the photoresist in lithography should be adjusted according to the substrate material.

## Fabrication steps

### Resistive bias lines

- 1) Clean wafer with acetone and IPA. Blow dry with  $N_2$ .
- 2) Softbake at 80 °C for 2 min. to remove all humidity.
- 3) Spin negative photoresist 5214 at 2000 rpm for 30 sec. Soft-bake at 105 °C for 2 min. Align and expose 1.7 sec for quartz or glass wafers, 4.5 sec for silicon. Use Mask1. Hard-bake at 130 °C for 90 sec. Flood expose 45 sec. Develop in AZ327 developer for 80 sec. Rinse in cascade DI water 2 min + 2 min. Blow dry with  $N_2$ . Use the microstripper ( $O_2$  plasma) at 80 W and 250 mT for 2 min.
- 4) Sputter SiCr, 1200 Å. Parameters used in RF sputtering: Target number 2. 7 mT, 700 W, 18 min. Gas: Ar and  $N_2$  (10 %).
- 5) Lift off in hot PRS1000 or PRS2000. Overnight soak is preferred. Rinse in DI water at least 15 min. Clean with acetone and IPA. Blow dry with  $N_2$ . Use the microstripper ( $O_2$  plasma) at 150 W and 250 mT for 3 min to remove photoresist and other organic scums.

### **First metal layer**

- 1) Softbake at 80 °C for 2 min. to remove all humidity.
- 2) Spin negative photoresist 5214 at 2000 rpm for 30 sec. Soft-bake at 105 °C for 2 min. Align and expose 1.7 sec for quartz or glass wafers, 4.5 sec for silicon. Use Mask1. Hard-bake at 130 °C for 90 sec. Flood expose 45 sec. Develop in AZ327 developer for 80 sec. Rinse in cascade DI water 2 min + 2 min. Blow dry with N<sub>2</sub>. Use the microstripper (O<sub>2</sub> plasma) at 80 W and 250 mT for 2 min.
- 3) Blow the wafer with N<sub>2</sub> just before putting it to the evaporator. Evaporate Ti/Au/Ti, 500 Å/5000 Å/500 Å.
- 4) Lift off in hot PRS1000 or PRS2000. Overnight soak is preferred. Rinse in DI water at least 15 min. Clean with acetone and IPA. Blow dry with N<sub>2</sub>. Use the microstripper (O<sub>2</sub> plasma) at 150 W and 250 mT for 3 min to remove photoresist and other organic scums.

### **Silicon nitride dielectric layer**

- 1) Deposit Si<sub>3</sub>N<sub>4</sub>, 2000 Å, with the PECVD. Use the following parameters: SiH<sub>4</sub> = 100 sccm, NH<sub>3</sub> = 10 sccm, He = 900 sccm, N<sub>2</sub> = 990 sccm, pressure = 700 mT, power = 100 W, temperature = 400 °C, time = 12 min.
- 2) Softbake at 80 °C for 2 min. Spin HMDS adhesion promoter at 3000 rpm for 30 sec. Spin photoresist 1813 or 1827 at 3000 rpm for 30 sec. Soft-bake at 105 °C for 2 min. Align and expose 7 sec for 1813 and 15 sec for 1827. Use Mask3. Develop in diluted MF 351 developer for 45 sec. Rinse in cascade DI water 2 min + 2 min. Blow dry with N<sub>2</sub>. Hard-bake at 130 °C for 2 min. Clean the wafer with the microstripper (O<sub>2</sub> plasma) at 150 W and 250 mT for 2 min.
- 3) Pattern the Si<sub>3</sub>N<sub>4</sub> with RIE using next parameters: CF<sub>4</sub> = 40 sccm, O<sub>2</sub> = 1 sccm, pressure = 100 mT, power = 100 W, time = 12 min (includes some over etching).
- 4) Flood expose 90 sec. Develop in diluted MF351 90 sec. Rinse in cascade DI water 1 min + 1 min. Blow dry with N<sub>2</sub>. Strip the remaining

photoresist in hot PRS1000 or PRS2000 at least 3 hours. Rinse in DI water at least 15 min. Clean with acetone and IPA. Blow dry with N<sub>2</sub>. Clean with the microstripper (O<sub>2</sub> plasma) at 150 W and 250 mT for 3 min.

### **Sacrificial layer**

- 1) Softbake at 80 °C for 2 min. Spin HMDS at 3000 rpm for 30 sec.
- 2) Spin PMMA 950K 9 % at 2300 RPM for 45 sec. to get about 1.3–1.5 um.
- 3) Bake in an oven at 170 °C for 30 min.
- 4) Evaporate or sputter Ti, 2000 Å, to be used as a mask for the PMMA patterning.
- 5) Soft-bake at 80 °C for 2 min. Spin HMDS at 3000 rpm for 30 sec. Spin positive photoresist 1827 at 3000 rpm for 30 sec. Softbake at 105 °C for 30 sec. Align and expose 15 sec with Mask4. Develop in diluted MF351 45 sec. Rinse in cascade DI water 2 min + 2 min. Blow dry with N<sub>2</sub>. Softbake at 80 °C for 30 sec, softbake at 105 °C for 30 sec, hardbake at 130 °C for 90 sec.
- 6) Etch Ti with HF:DI (1:20). Ti etch takes just a few seconds. Watch for bubble coming out. Rinse in DI water for 3 min. Blow dry with N<sub>2</sub>.
- 7) Flood expose 90 sec and develop in diluted MF351 2 min. Rinse in cascade DI water 2 min + 2 min. Blow dry with N<sub>2</sub>. Do not clean with the microstripper (O<sub>2</sub> plasma) because it etches the PMMA sacrificial layer.
- 8) Etch PMMA in RIE. Recipe 1: O<sub>2</sub> = 100 sccm, pressure = 50 mT, power = 250 W, time = 21 min (etch 90 sec, RF off 60 sec). An other possibility is to use O<sub>2</sub> = 20 sccm, pressure = 20 mT, power = 50 W, time = 30 min (this is continuous etch).
- 9) Etch the Ti mask with HF:DI (1:20). Rinse in DI water for 3 min. Blow dry with N<sub>2</sub>.

## **Structural layer deposition**

Sputter Ti/Au/Ti, 100 Å/8000 Å/100 Å. Sputtering parameters: Ti: 7 mT, target 1, 650 W, deposition rate 50 Å/min (20 rpm). Au: 10 mT, target 3, 0.5 A, time = 30 min, (20 rpm).

## **Gold electroplating**

- 1) Soft-bake at 80 °C for 2 min. Spin HMDS at 3000 rpm for 30 sec. Spin positive photoresist 1827 at 3000 rpm for 30 sec. Softbake at 105 °C for 30 sec. Align and expose 15 sec with Mask5. Develop in diluted MF351 45 sec. Rinse in cascade DI water 2 min + 2 min. Blow dry with N<sub>2</sub>. Softbake at 105 °C for 2 min to improve photoresist adhesion.
- 2) Etch Ti with HF:DI (1:20). Rinse in DI water for 3 min. Blow dry with N<sub>2</sub>. Softbake at 105 °C for 1 min.
- 3) Electroplate 3–5 μm of Au. Parameters for the gold plating: Plating solution either Arotemp 24 (K<sub>2</sub>CN<sub>2</sub>) and DI water or BDT 510. Temperature of the solution = 50–55 °C. Current density = 10 mA, stirrer speed = 200 rpm (increases plating uniformity). Rinse in DI water 2 min and blow with N<sub>2</sub>.
- 4) Flood expose 90 sec. Develop in diluted MF351 2 min. Rinse in cascade DI water 2 min + 2 min. Blow dry with N<sub>2</sub>.

## **Structural layer annealing**

- 1) Softbake at 80 °C for 2 min on a hot plate.
- 2) Softbake at 105 °C for 2 min on a hot plate.
- 3) Hardbake at 130 °C for 2 min on a hot plate.
- 4) Hardbake at 150 °C for 2 min on a hot plate.
- 5) Bake in an oven at 170 °C for 3 min.

The wafer needs to be transferred quickly between the hot plates.

Other possibility is to use just one hot plate and temperature ramp from 80 °C to 150 °C totally 8 min and then to the oven for 3 min and 170 °C.

### **Structural layer patterning and release**

- 1) Softbake at 80 °C for 2 min. Spin HMDS at 3000 rpm for 30 sec. Spin positive photoresist 1827 at 3000 rpm for 30 sec. Softbake at 105 °C for 1 min. Align and expose 15 sec with Mask6. Develop in diluted MF351 45 sec. Rinse in cascade DI water 2 min + 2 min. Blow dry with N<sub>2</sub>. Softbake at 105 °C for 2 min to improve photoresist adhesion.
- 2) Etch Ti with HF:DI (1:20). Rinse in DI water for 3 min. Blow dry with N<sub>2</sub>.
- 3) Etch Au with TFA gold etchant. Rinse in DI water for 3 min. Blow dry with N<sub>2</sub>.
- 4) Flood expose 90 sec and develop in diluted MF351 90 sec. Rinse in cascade DI water 2 min + 2 min. Blow dry with N<sub>2</sub>.
- 5) Etch remaining Ti with HF:DI (1:20). Rinse in DI water for 3 min. Blow dry with N<sub>2</sub>.
- 6) Remove sacrificial layer by soaking in PRS2000 at least 3 hours, preferably overnight.
- 7) Rinse in DI water 15 min, without bubbles. Do not blow dry.
- 8) Soak in acetone 3 hours. This is optional but ensures that all PMMA and PRS2000 is removed.
- 9) Soak in IPA 15 min + 15 min.
- 10) Transfer to ethanol.
- 11) Transfer to the critical point dryer. Try the wafer in the critical point dryer.

PUBLICATION P1

# **On-Wafer Noise-Parameter Measurements at *W*-band**

In: IEEE Transactions on Microwave Theory and Techniques  
2003. Vol. 51, No. 6, pp. 1621–1628.  
© 2003 IEEE. Reprinted with permission from the publisher.

# On-Wafer Noise-Parameter Measurements at $W$ -Band

Tauno Vähä-Heikkilä, *Student Member, IEEE*, Manu Lahdes, Mikko Kantanen, and Jussi Tuovinen, *Member, IEEE*

**Abstract**—A wide-band on-wafer noise-parameter measurement setup has been developed for  $W$ -band. The system is based on a cold-source method and uses a simple manual impedance tuner. In addition to noise parameters,  $S$ -parameters can be measured with the same setup. Using the developed system, noise parameters of an InP high electron-mobility transistor have been measured and results are shown in the 79–94-GHz frequency band. This is the first comprehensive report of noise-parameter measurements made on active devices at  $W$ -band.

**Index Terms**—High electron-mobility transistor (HEMT), noise measurement, noise parameter, on-wafer characterization.

## I. INTRODUCTION

SEVERAL current and planned space missions for earth observation and astronomy applications require very low-noise receivers at  $W$ -band (75–110 GHz). A key component in this kind of low-noise receiver is a low-noise amplifier (LNA). The design of LNAs is greatly dependent on the availability of good noise models for devices used in the LNAs. Therefore, to design an optimum amplifier both noise and scattering ( $S$ )-parameters are needed. The noise parameters cannot be measured directly. The determination of the noise parameters involves scattering parameter and noise-figure measurements and data processing. The  $S$ -parameters of a two-port can be measured using a standard commercial vector network analyzer (VNA). However, the noise-parameter measurements are very challenging. Commercial measurement systems are available only up to 40 GHz. A good description of measurements below 40 GHz is given in [1]. Measured  $W$ -band noise parameters have been presented earlier only for passive devices and at a single frequency [5], [6]. We have recently been working with noise-parameter measurements at  $V$ - and  $W$ -bands. Our  $V$ -band (50–75 GHz) noise-parameter measurement setup and results were reported in [2]–[4] and the first results with an active device at  $W$ -band were published in [7]. This paper presents a full report on the measurement system that allows simultaneous on-wafer noise and scattering parameter measurements at  $W$ -band.

To determine the noise parameters, the noise figure of a device-under-test (DUT) is measured with different values of the

input reflection coefficients. The noise figure of a two-port as a function of source reflection coefficient  $\Gamma_i$  is given by [8]

$$F = F_{\min} + \frac{4r_n}{1 - |\Gamma_i|^2} \left| \frac{\Gamma_i - \Gamma_{\text{opt}}}{1 + \Gamma_{\text{opt}}} \right|^2 \quad (1)$$

where  $F_{\min}$  is the minimum noise figure of the two-port,  $r_n$  is the normalized noise resistance, and  $\Gamma_{\text{opt}}$  is the optimum reflection coefficient. Variables  $F_{\min}$ ,  $r_n$ , and  $\Gamma_{\text{opt}}$  are called noise parameters. The noise parameters are obtained by fitting the above equation with the measured data.

## II. MEASUREMENT SETUP

The measurement system is shown schematically in Fig. 1, and the photograph of the measurement setup is shown in Fig. 2, respectively. The measurement setup is based on the cold-source method [9], [10]. The improved technique, described in [2], is used. This technique corrects the effects of reflection-coefficient changes between the cold and hot states of the noise source and takes into account the losses of the passive network between the DUT and noise receiver.

The DUT is connected to the measurement system using waveguide probes. By including two waveguide switches, both noise and  $S$ -parameter measurements can be done without breaking any connections. These are commercial switches with less than 1-dB loss, more than 60-dB isolation between ports, and repeatability better than 0.05 at  $W$ -band. Only a simple uncalibrated one-port impedance tuner is needed in the input side of the DUT. This is possible due to switch 1. The one-port tuner consists of an adjustable waveguide short and attenuator. System characterization and the  $S$ -parameter measurements of the DUT are done using the HP8510C VNA. The VNA is also needed during noise measurements of the DUT to measure the reflection coefficient of the impedance tuner. The noise source is used here only during the calibration of the noise receiver. The noise-receiver calibration can also be done during long measurement sessions without breaking any connections due to switch 2. An LNA is used to increase the sensitivity of the noise receiver. The LNA was obtained through the Planck surveyor collaboration [11]. The mixer is used to downconvert the noise power from  $W$ -band to the measurement region of the HP8970A noise-figure meter. The local oscillator (LO) chain consists of the HP83650A synthesized sweeper, HP 8349B microwave amplifier, and HP83558A millimeter-wave source module. All measurement instruments are controlled using a personal computer (PC) via general-purpose interface

Manuscript received January 4, 2002; revised November 19, 2002. This work was supported by the European Space Agency/European Space Research and Technology Centre under Contract 1655/95/NL/MV and by the Graduate School in Electronics, Telecommunications, and Automation.

The authors are with Millimeter Wave Laboratory of Finland–Millilab, VTT TECHNICAL RESEARCH CENTRE OF FINLAND, Espoo, FIN-02044 VTT, Finland (e-mail: tauno.vaha-heikkila@vtt.fi; mikko.kantanen@vtt.fi).

Digital Object Identifier 10.1109/TMTT.2003.812554

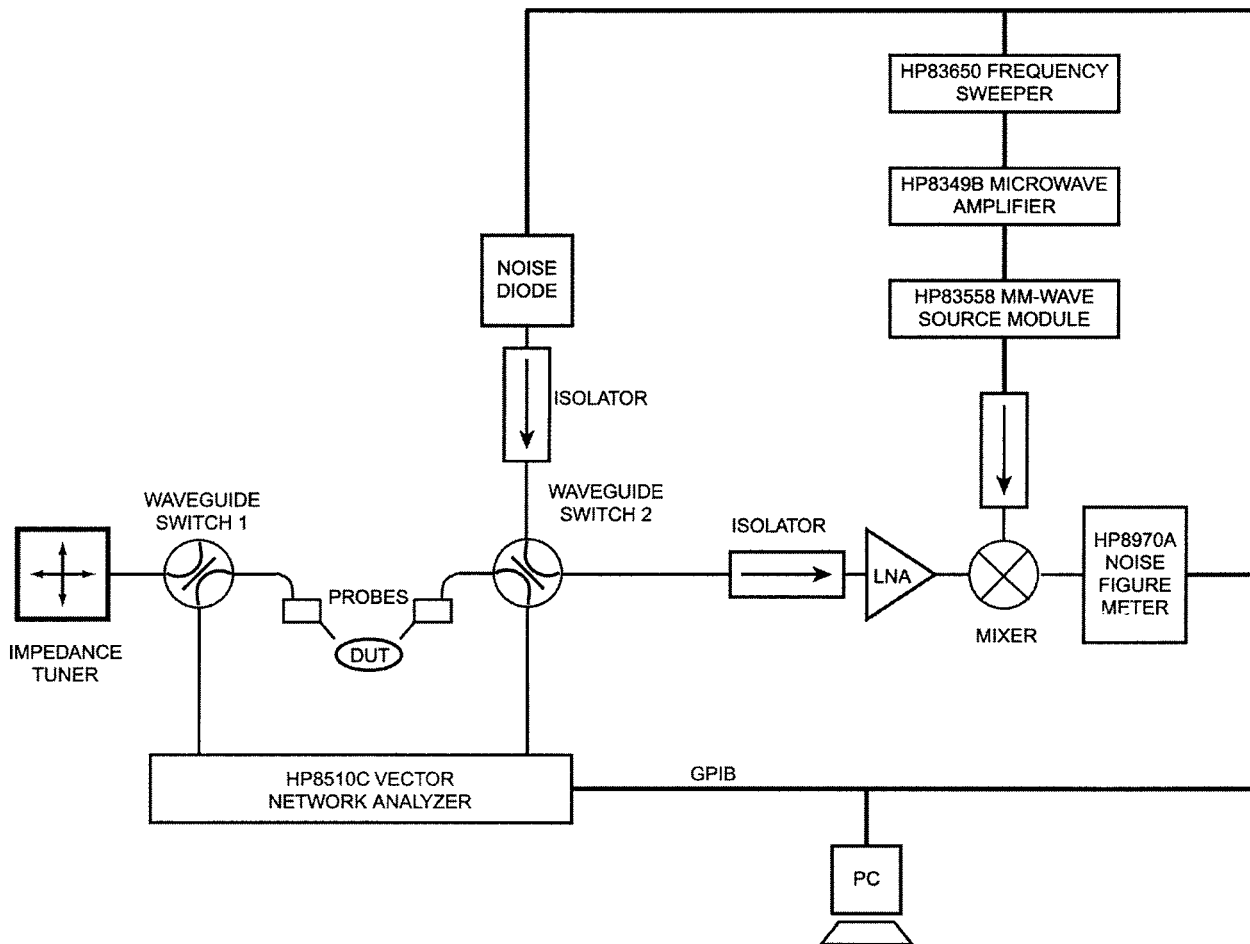


Fig. 1. Setup for noise-parameter measurements at 79–94 GHz.

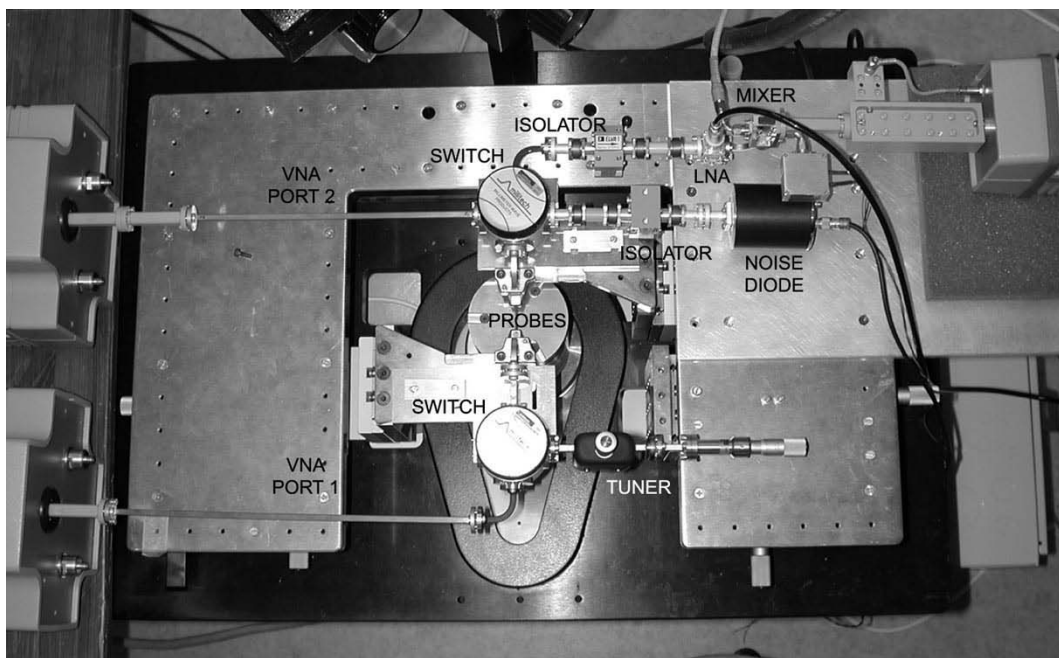


Fig. 2. Photograph of the measurement setup. All waveguide components are on top of a probe station.

bus (GPIB) line. The PC and in-house-made software make automatic data acquisition and complex calculations possible.

### III. MEASUREMENTS

Measurements can be divided into the following three parts:

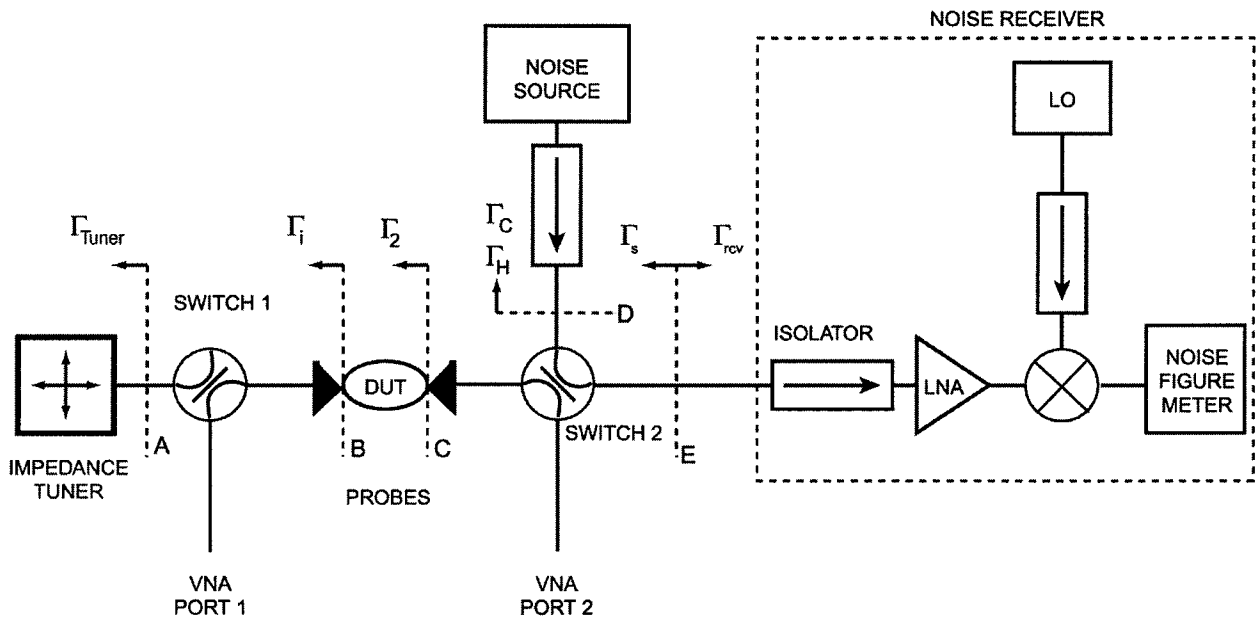


Fig. 3. Measurement system with reference planes and reflection coefficients.

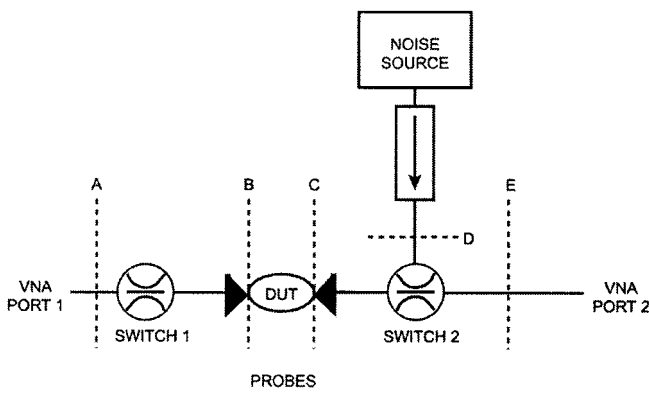


Fig. 4. Measurement setup for the characterization of the passive networks A–B and C–E.

- 1) system characterization;
- 2) noise-receiver calibration;
- 3) noise measurements of the DUT.

### A. System Characterization

The system characterization is done using the VNA. It consists of the *S*-parameter measurements of the passive networks A–B, C–E, and D–E and the reflection-coefficient measurements of the noise receiver  $\Gamma_{rcv}$  and the noise source  $\Gamma_C$ ,  $\Gamma_H$  (both cold and hot states). The meanings of these reference planes and reflection coefficients are shown in Fig. 3.

The passive networks A–B and C–E cannot be measured directly with the VNA because they are noninsertable. To characterize these networks, the VNA is first calibrated to the reference planes A and E using a one-port waveguide calibration. The configuration is shown in Fig. 4. An on-wafer two-port LRRM calibration [12] is then done to reference planes B and C. The *S*-parameters of these networks are calculated from the two sets of

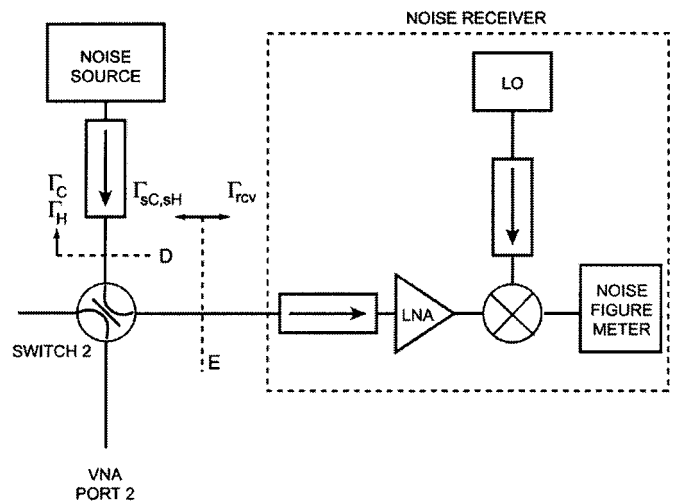


Fig. 5. Measurement setup for the noise-receiver calibration.

error coefficients. The passive network D–E and reflection coefficients are also measured with the VNA. Measured attenuation of the passive network A–B was from 1.6 to 1.8 dB and attenuation of the passive network C–E was between 0.8–1.4 dB. Attenuation of passive network A–B limits impedance range of the impedance tuner. The maximum amplitude of achievable source reflection coefficient  $\Gamma_i$  is approximately 0.72 at 90 GHz at reference plane B.

### B. Noise-Receiver Calibration

The noise-receiver calibration includes a determination of the *kBG* factor and the noise figure of the noise receiver. The noise source is connected to the noise receiver by switch 2. The noise power of the noise source is measured in the cold and hot states. This is done at all frequencies with the setup shown in Fig. 5. This figure also shows the notations of the reference planes D and E and reflection coefficients.

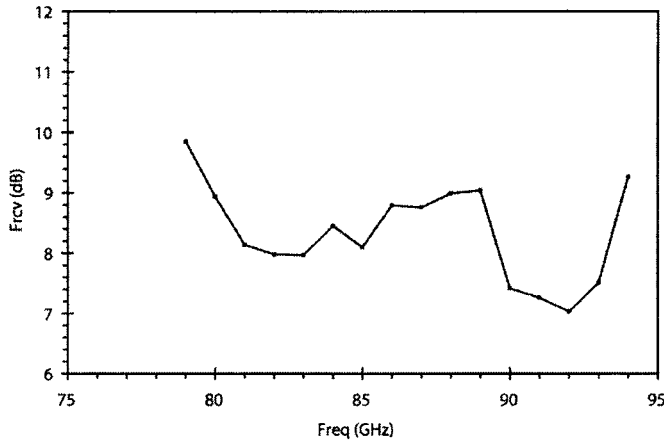


Fig. 6. Measured noise figure of the noise receiver.

The noise powers delivered to the noise receiver in the cold and hot states are calculated from

$$P_C = kBG T_{C\text{eff}} \quad (2)$$

$$P_H = kBG T_{H\text{eff}} \quad (3)$$

where  $T_{C\text{eff}}$  and  $T_{H\text{eff}}$  are the effective noise temperatures of the cold and hot states. Effective noise temperatures can be expressed in the form

$$T_{C\text{eff}} = [T_C G_{aC} + (1 - G_{aC}) T_a] \cdot M_C \quad (4)$$

$$T_{H\text{eff}} = [T_H G_{aH} + (1 - G_{aH}) T_a] \cdot M_H \quad (5)$$

where  $T_a$  is the ambient temperature,  $T_C$  and  $T_H$  are the cold and hot noise temperatures of the noise source,  $G_{aC}$  and  $G_{aH}$  are the available gains of the passive network between the reference planes D and E in the cold and hot states, and  $M_C$  and  $M_H$  are the mismatch factors of the cold and hot states [13]

$$M_{C,H}(\Gamma_{sC,sH}) = \frac{(1 - |\Gamma_{sC,sH}|^2)(1 - |\Gamma_{rcv}|^2)}{|1 - \Gamma_{sC,sH}\Gamma_{rcv}|^2} \quad (6)$$

The  $kBG$  factor is

$$kBG = \frac{P_{Hm} - P_{Cm}}{T_{H\text{eff}} - T_{C\text{eff}}} \quad (7)$$

where  $P_{Hm}$  and  $P_{Cm}$  are the measured noise powers in the hot and cold states.

When a noise diode is used as a noise source, then  $T_C = T_a$  and (4) reduces to

$$T_{C\text{eff}} = T_a M_C \quad (8)$$

The noise factor of the noise receiver  $F_{rcv}$ , which is independent of the source reflection coefficient  $\Gamma_i$ , can be expressed in the form

$$F_{rcv} = \frac{T_{H\text{eff}} - Y \cdot T_{C\text{eff}}}{T_0(Y - 1)} + 1 \quad (9)$$

where  $T_0$  is the standard temperature, and the  $Y$  coefficient is

$$Y = \frac{P_{Hm}}{P_{Cm}} \quad (10)$$

The measured noise figure of the noise receiver is presented as a function of frequency in Fig. 6.

### C. Noise Measurements of the DUT

After system characterization and noise-receiver calibration, the noise measurements of the DUT are carried out. The VNA is calibrated to the reference planes B and C using the line–reflect–reflect–match (LRRM) on-wafer calibration. The DUT is then placed between the probes and set to the operating point of interest. The  $S$ -parameters of the DUT are measured. Noise-figure measurements are done in two steps. The first step is to measure the reflection coefficient of the impedance tuner  $\Gamma_{\text{tuner}}$  using the VNA, and the second step is to measure the corresponding noise power of the entire system. The VNA port 1 is switched to the tuner. The tuner is set and its reflection coefficient  $\Gamma_{\text{tuner}}$  is measured. The tuner is then switched to the DUT and the corresponding noise power  $P_i$  is measured with the noise receiver. These steps are done for every selected value of the tuner and as a function of the frequency. Since the  $S$ -parameters of the passive network A–B are known, the source reflection coefficient  $\Gamma_i$  can be calculated. It is then possible to calculate the noise figure of the entire system as a function of the source reflection coefficient  $\Gamma_i$  [2]

$$F_{\text{tot},i} = \frac{P_i |1 - S_{11\text{DUT}}\Gamma_i|^2 |1 - \Gamma_s\Gamma_{rcv}|^2 |1 - S_{11\text{CE}}\Gamma_2|^2}{T_0 kBG |S_{21\text{DUT}}|^2 (1 - |\Gamma_i|^2) |S_{21\text{CE}}|^2} - \frac{T_a}{T_0} + 1 \quad (11)$$

where  $S_{11\text{DUT}}$  and  $S_{21\text{DUT}}$  are the  $S$ -parameters of the DUT and  $S_{11\text{CE}}$  and  $S_{21\text{CE}}$  are the  $S$ -parameters of the passive network between reference planes C and E, respectively.

The noise figure of the DUT as a function of the source reflection coefficient  $F_{\text{DUT}}(\Gamma_i)$  is calculated using the Friis formula [14]

$$F_{\text{DUT}}(\Gamma_i) = F_{\text{tot}} - \frac{F_{rcv}(\Gamma_i) - G_{aCE}}{G_{a\text{DUT}}G_{aCE}} \quad (12)$$

where  $G_{a\text{DUT}}$  and  $G_{aCE}$  are the available gain of the DUT and network between reference planes C and E,  $F_{rcv}(\Gamma_i)$  is the noise figure of the noise receiver that is dependent of source reflection coefficient  $\Gamma_i$

$$F_{rcv}(\Gamma_i) = F_{rcv} \cdot \frac{|1 - \Gamma_{rcv}\Gamma_s|^2}{1 - |\Gamma_s|^2} \quad (13)$$

where  $\Gamma_s$  is the reflection coefficient seen by the noise receiver. After solving  $F_{\text{DUT}}$  and  $\Gamma_i$  data pairs, noise parameters can be extracted with mathematical fitting methods.

## IV. RESULTS

As an example of  $W$ -band noise-parameter measurements, a DaimlerChrysler InP high electron-mobility transistor (HEMT) was measured. It has  $0.18\text{-}\mu\text{m}$  gate length and  $2 \times 40 \mu\text{m}$  gatewidth. During the measurements, the HEMT was set to the operating point with a drain voltage  $V_{ds} = 1.0 \text{ V}$  and a drain current  $I_{ds} = 10 \text{ mA}$ . The noise parameters of the HEMT are shown in Figs. 7–10. To show repeatability, three different measurements are presented ( $M1$ – $M3$  in Figs. 7–10). The noise parameters are extracted from measurement data using Lane's method [15]. Five different source impedances were used. One

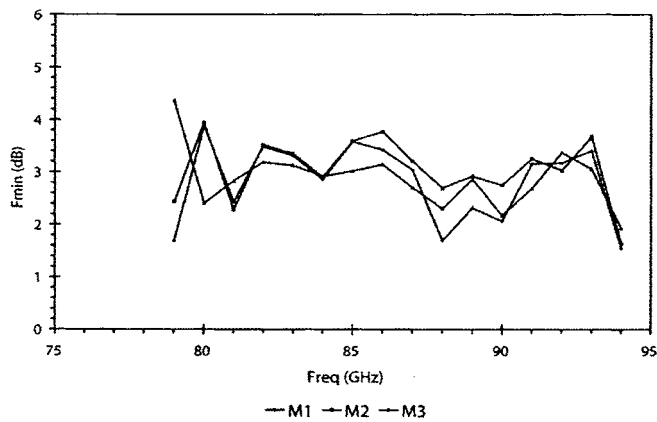


Fig. 7. Measured minimum noise figure as a function of frequency. Measurements were carried out three times.

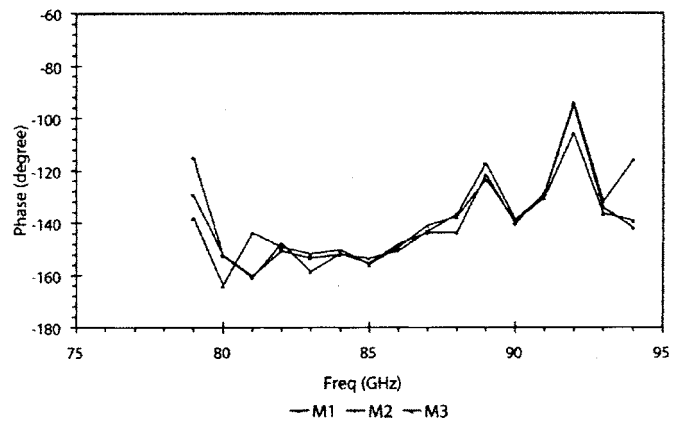


Fig. 10. Phase of the optimum reflection coefficients. Measurements were carried out three times.

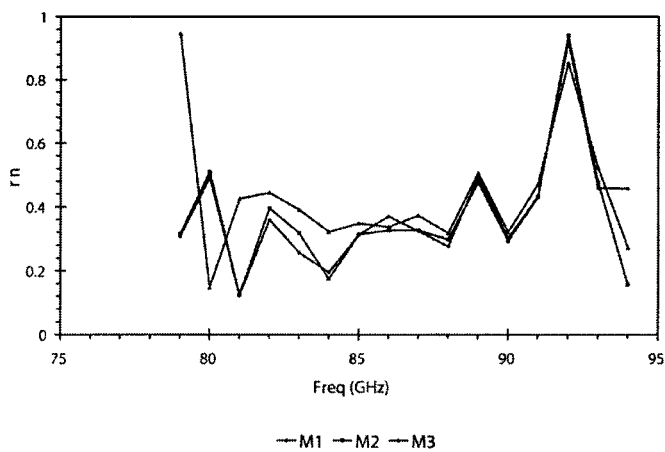


Fig. 8. Normalized noise resistance as a function of frequency. Measurements were carried out three times.

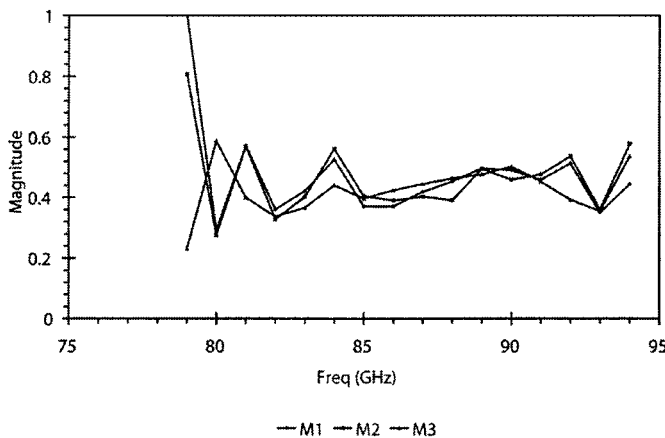


Fig. 9. Magnitude of the optimum reflection coefficients. Measurements were carried out three times.

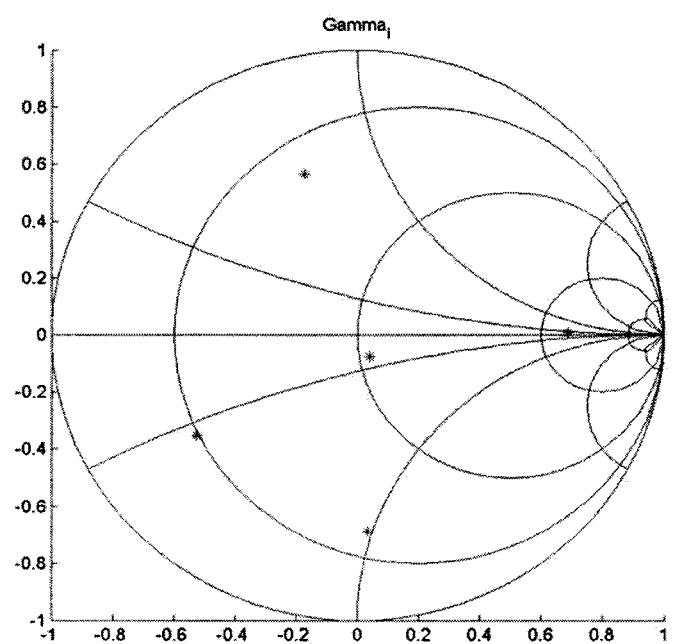


Fig. 11. Source reflection coefficients  $\Gamma_s$  at 90 GHz in measurement 2.

was set close to the center of the Smith chart and the others were set symmetrically around the center of the Smith chart. These are presented in Fig. 11 at 90 GHz. Noise parameters of similar HEMTs were presented in [4] at the V-band. V-band measurements were made on a different device from the same wafer. Peaks are seen in the normalized noise resistance and the phase of  $\Gamma_{opt}$  around 89–92 GHz. These are likely due to

the difficulties in the on-wafer calibrations and the sensitivity of the noise receiver at these frequencies.

### V. DISCUSSION AND ERROR ANALYSIS

Sensitivity and linearity of the noise receiver are important in noise-parameter measurements. The noise power  $P_i$  as a function of frequency is shown in Fig. 12. The source reflection coefficient  $\Gamma_s$  is the nearest value of the center of the Smith chart (see Fig. 11). The noise power is under 400 K below 88 GHz and increases rapidly toward higher frequencies reaching 13 600 K at 93 GHz. This is one possible explanation for the peaks in the normalized noise resistance and the phase of  $\Gamma_{opt}$ . The measurement system will be improved by obtaining a W-band LNA for the noise receiver with lower noise figure, higher gain, and wider bandwidth.

As can be seen from the measurement results, single-frequency measurements are not reliable at the W-band. Wide-band measurements are important for obtaining reliable

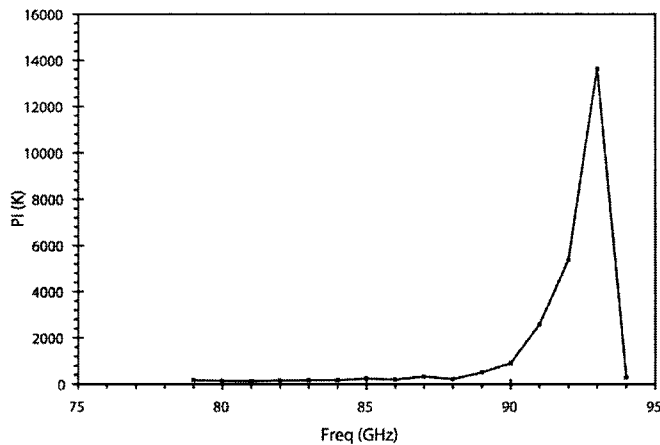


Fig. 12. Noise power  $P_i$  as a function of frequency. The corresponding source reflection coefficient  $\Gamma_i$  is the point closest to the center of the Smith chart.

results. All steps are critical in the noise-parameter measurements with characterization of the passive networks A–B and C–E needing careful attention. These include both waveguide and on-wafer calibrations. If system characterization is not done carefully, large systematic errors may remain undiscovered. These errors are usually caused by reflections in the setup, which are difficult to calibrate out.

Since there are no active on-wafer noise-parameter standards, which could be used directly to determine the uncertainty of the measurement system, the uncertainties have to be determined indirectly. The task is quite complex since the noise-parameter measurements involve a large number of variables and numerous different measurement steps and calibrations. Approximately 40 measured variables are used to calculate the noise parameters. Measurements consist of  $S$ -parameters and reflection coefficients (both magnitudes and phases), noise power measurements, and the excess noise ratio (ENR) calibration of the noise source.

A partial derivative method is usually used in uncertainty analysis, but when the number of variables is large or variables have complicated functional relations, it becomes impractical [16]. Instead, a statistical Monte Carlo method is applied in the analysis of the uncertainties of noise parameters [17]. In the Monte Carlo method, a large set of noise parameters are created by adding random fluctuations to the measured data. When the number of conducted runs is large (thousands), results can be studied statistically. Graphical presentation of the Monte Carlo method is shown in Fig. 13. Uncertainties with random distribution are added to measured values, and noise parameters are calculated. This is repeated many times and the new calculated noise parameters are stored after every run. Having many sets of noise parameters, results can be analyzed statistically.

Monte Carlo simulations were done at a single frequency. Uncertainties, presented in Table I, were used for each measured variable, and noise parameters were calculated. Uncertainties are divided in classes A and B [18]. The evaluation of type-A uncertainty was done by statistical method and type B was evaluated by other means, e.g., using approximation or manufacturer's specifications. Evaluation of uncertainty values of measured values is based mostly on [17], where similar work was

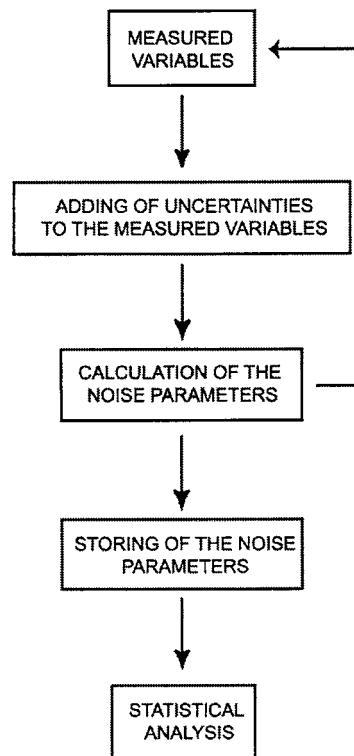


Fig. 13. Graphical presentation of Monte Carlo analysis used to analyze uncertainties of the noise parameters.

TABLE I  
UNCERTAINTIES FOR MEASURED PARAMETERS

Measured parameter	Uncertainty	Type
$\Gamma_{\text{tuner}}, \Gamma_{\text{rev}}, \Gamma_H, \Gamma_C$	0.005	B
$S_{11\_AB}, S_{11\_CE}$	0.036	A, B
$S_{22\_AB}, S_{22\_CE}$	0.036	A, B
$S_{12\_AB}, S_{21\_AB}, S_{12\_CE} \times S_{21\_CE}$	0.0013	A, B
$S_{11\_DE}, S_{22\_DE}$	0.005	B
$S_{12\_DE}, S_{21\_DE}$	0.006	B
$S_{11\_DUT}$	0.036	A
$S_{12\_DUT}, S_{21\_DUT}$	0.05	A
$S_{22\_DUT}$	0.024	A
ENR [dB]	0.1	B
$P_H, P_C, P_i$ [K]	1.01	A
$T_a$ [K]	1	A

TABLE II  
RESULTS OF MONTE CARLO SIMULATIONS AT 90 GHz

Parameter	Mean	$2\sigma$
$F_{\text{min}}$ [dB]	2.8	$\pm 0.7$
$r_n$	0.3	$\pm 0.09$
$ \Gamma_{\text{opt}} $	0.46	$\pm 0.09$
$\phi_{\text{opt}}$	-139	$\pm 10$

carried out for  $V$ -band cold-source noise-parameter setup. For the uncertainties of  $S$ -parameters, the magnitude is determined using a rectangular distribution and corresponding angle using a uniform distribution from  $-180^\circ$  to  $180^\circ$ . Calculated Monte Carlo simulation results for measurement 2 at 90 GHz are presented in Table II. The mean of each noise parameter and  $2\sigma$  (95.5% confidence level) of 10 000 simulation runs are shown in this table.

## VI. CONCLUSION

A *W*-band on-wafer noise-parameter measurement system has been designed and built. For the first time, to the author's knowledge, wide-band results for the *W*-band on-wafer noise parameters of an active device have been reported. The noise parameters of an InP HEMT (DaimlerChrysler  $2 \times 40 \mu\text{m}$ ) were measured using the cold-source method. Measurement results were presented between the 79–94-GHz frequency band.

## ACKNOWLEDGMENT

The help of T. Gaier, Jet Propulsion Laboratory, Pasadena, CA, and N. Hughes and P. Kangaslahti, both of Ylinen Electronics, Kauniainen, Finland, are greatly appreciated. The authors would also like recognize the invaluable comments and contribution of T. Närhi, European Space Agency (ESA), Noordwijk, The Netherlands, as well as colleagues T. Karttaavi, J. Varis, H. Hakojärvi and M. Jenu, all of the Millimeter Wave Laboratory of Finland–Millilab, VTT TECHNICAL RESEARCH CENTRE OF FINLAND, Espoo, Finland.

## REFERENCES

- [1] J. Laskar, M. R. Murti, S. Y. Yoo, E. Gebara, and H. M. Harris, "Development of complete on-wafer cryogenic characterization: *S*-parameters, noise-parameters and load-pull," in *Eur. GaAs and Related III–V Compounds, Application Symp. Dig.*, Amsterdam, The Netherlands, 1998, pp. 33–38.
- [2] M. Lahdes, M. Sipilä, and J. Tuovinen, "60 GHz noise parameter measurements using cold-source method," in *49th ARFTG Conf. Dig.*, Denver, CO, 1997, pp. 146–154.
- [3] M. Lahdes and J. Tuovinen, "*V*-band on-wafer noise parameter measurements," in *Eur. GaAs and Related III–V Compounds, Application Symp. Dig.*, Amsterdam, The Netherlands, 1998, pp. 39–44.
- [4] M. Kantanen, M. Lahdes, J. Tuovinen, T. Vähä-Heikkilä, P. Kangaslahti, P. Jukkala, and N. Hughes, "A wideband automated measurement system for on-wafer noise parameter measurements at 50–75 GHz," in *Eur. GaAs and Related III–V Compounds, Application Symp. Dig.*, 2001, pp. 255–258.
- [5] T. A. Alam, R. D. Pollard, and C. M. Snowden, "Determination of *W*-band noise parameters," *Electron. Lett.*, vol. 34, no. 3, pp. 288–289, 1998.
- [6] —, "The determination of on-wafer noise parameters at *W*-band," in *Proc. 27th Eur. Microwave Conf.*, Jerusalem, Israel, 1997, pp. 687–691.
- [7] T. Vähä-Heikkilä, M. Lahdes, J. Tuovinen, M. Kantanen, P. Kangaslahti, P. Jukkala, and N. Hughes, "*W*-band on-wafer noise parameter measurements," in *Proc. 31st Eur. Microwave Conf.*, London, U.K., 2001, pp. 355–358.
- [8] IRE Subcommittee on Noise, "Representation of noise in linear two-ports," *Proc. IRE*, vol. 48, pp. 69–74, Jan. 1960.
- [9] V. Adamian and A. Uhler, "A novel procedure for receiver noise characterization," *IEEE Trans. Instrum. Meas.*, vol. IM-22, pp. 181–182, 1973.
- [10] R. Meierer and C. Tsironis, "An on-wafer noise parameter measurement technique with automatic receiver calibration," *Microwave J.*, vol. 38, no. 3, pp. 80–88, 1995.
- [11] J. Tuovinen, P. Kangaslahti, P. Haapanen, N. Hughes, P. Jukkala, T. Karttaavi, O. Koistinen, M. Lahdes, H. Salminen, J. Tanskanen, and S. Urpo, "Development of 70 GHz receivers for the Planck LFI," *Astrophys. Lett. Commun.*, vol. 37, pp. 181–187, 2000.
- [12] A. Davidson, K. Jones, and E. Strid, "LRM and LRRM calibrations with automatic determination of load inductance," in *36th ARFTG Conf. Dig.*, Monterey, CA, 1990, pp. 57–62.
- [13] E. Strid, "Noise measurements for low-noise GaAs FET amplifiers," *Microwave Syst. News*, vol. 10, pp. 62–70, 1981.
- [14] H. T. Friis, "Noise figures of radio receivers," *Proc. IEEE*, vol. 57, pp. 1461–1462, Aug. 1969.
- [15] R. Q. Lane, "The determination of device noise parameters," *Proc. IEEE*, vol. 57, pp. 1461–1462, Aug. 1962.
- [16] V. Adamian, "Calibration, measurement and accuracy of the noise parameter measurements," in *IEEE MTT-S Int. Microwave Symp. Workshop*, San Francisco, CA, 1996, pp. 83–110.
- [17] M. Lahdes, "Uncertainty analysis of *V*-band on-wafer noise parameter measurement system," in *28th Eur. Microwave Conf.*, Amsterdam, The Netherlands, 1998, pp. 445–450.
- [18] B. N. Taylor and C. E. Kuyatt, "Guidelines for evaluating and expressing the uncertainty on NIST measurement results," NIST, Boulder, CO, Tech. Note 1297, 1994.



**Tauno Vähä-Heikkilä** (S'01) received the B.S. and M.S. degrees in physics from the University of Turku, Turku, Finland, in 2000 and 2001, respectively. His M.S. thesis concerned *W*-band on-wafer noise-parameter measurements.

He was a Trainee Research Scientist and, since 2001, he has been a Research Scientist with the Millimeter Wave Laboratory of Finland–MilliLab, VTT TECHNICAL RESEARCH CENTRE OF FINLAND, Espoo, Finland. He is also currently a Visiting Scholar with the Radiation Laboratory,

The University of Michigan at Ann Arbor. His research interests include RF microelectromechanical systems (MEMS) and millimeter-wave on-wafer measurements.

Mr. Vähä-Heikkilä has been a secretary for the IEEE Antennas and Propagation (AP)/Electron Devices (ED)/Microwave Theory and Techniques (MTT) Finland Chapter since 2001.



**Manu Lahdes** received the Master of Science degree in electrical engineering degree from the Helsinki University of Technology, Espoo, Finland, in 1996.

Since 1996, he has been with a Research Scientist the Millimeter Wave Laboratory of Finland–MilliLab, VTT TECHNICAL RESEARCH CENTRE OF FINLAND, Espoo, Finland. His research interests in the millimeter-wave area have been on-wafer noise-parameter measurements, cryogenic on-wafer measurements, active device modeling, and MMIC design and testing. He has

authored or coauthored several papers. His current activities also include passive millimeter imaging.



**Mikko Kantanen** received the Master of Science degree in electrical engineering degree from the Helsinki University of Technology (HUT), Espoo, Finland, in 2001.

Since 1999, he has been with the Millimeter Wave Laboratory of Finland–MilliLab, VTT TECHNICAL RESEARCH CENTRE OF FINLAND, Espoo, Finland, initially as a Trainee Research Scientist and, since 2001, as a Research Scientist involved with noise measurements at millimeter waves. He is also currently involved with other millimeter-wave activities including on-wafer measurement systems, monolithic microwave integrated circuit (MMIC) design, and passive imaging.



**Jussi Tuovinen** (S'86–M'91) received the Dipl.Eng., Lic.Tech., and Dr.Tech. degrees in electrical engineering from the Helsinki University of Technology (HUT), Espoo, Finland, in 1986, 1989, and 1991, respectively.

From 1986 to 1991, he was a Research Engineer with the HUT Radio Laboratory, where he was involved with millimeter-wave antenna testing for the European Space Agency (ESA), quasi-optical measurements, and Gaussian beam theory. From 1991 to 1994, he was a Senior Post-Doctoral

Fellow with the Five College Radio Astronomy Observatory, University of Massachusetts, Amherst, where he studied holographic testing methods and developed frequency multipliers up to 1 THz. From 1994 to 1995, he was a Project Manager with the HUT Radio Laboratory, where he was involved with hologram compact antenna test range (CATR) and 119-GHz receiver development for Odin-satellite. He is currently a co-investigator and heads development of 70-GHz receivers for the low-frequency instrument of the ESA Planck Surveyor. His research activities also includes development of methods for on-wafer testing of integrated circuits and components. He is currently a Research Professor with VTT TECHNICAL RESEARCH CENTRE OF FINLAND Information Technology and a Director of the Millimeter Wave Laboratory of Finland–MilliLab, ESA External Laboratory. From 2001 to 2002, he was a Visiting Researcher with the University of Hawaii at Manoa, where he developed communications methods using retrodirective antennas. He has authored or coauthored over 100 papers.

Dr. Tuovinen is a past secretary of the Finnish National Committee of the Committee on Space Research (COSPAR) and the IEEE Finland Section. He was also the executive secretary of the Local Organizing Committee of the 27th Plenary Meeting of COSPAR, held in 1988. In 1998, he was a co-chairman of the Second ESA Workshop on Millimeter Wave Technology and Applications. He has served as a chairman of the IEEE Microwave Theory and Techniques (MTT)/Antennas and Propagation (AP) Finland Chapter. He is the chairman of the Third ESA Workshop on Millimeter Wave Technology and Applications. He was the recipient of an ESA Fellowship for multiplier work at the University of Massachusetts in 1992 and again in 1993.

PUBLICATION P2

**Wideband Cryogenic On-Wafer  
Measurements at 20–295 K  
and 50–110 GHz**

In: Proceedings of the 33rd European Microwave Conference,  
Munich, Germany, 2003. Pp. 1167–1170.  
Reprinted with permission from the European Microwave  
Association.

# Wideband cryogenic on-wafer measurements at 20 – 295 K and 50-110 GHz

Tauno Vähä-Heikkilä, Jussi Varis, Hannu Hakojarvi, Jussi Tuovinen

MilliLab, VTT Information Technology, P.O. BOX 12021, 02044 VTT, Finland, tel. 358 9 4567219,  
fax. +358 9 453 7013, tauno.vaha-heikkila@vtt.fi

**Abstract** — A measurement system has been developed for cryogenic on-wafer characterization at 50–110 GHz. The measurement system allows on-wafer S-parameter measurements of active and passive devices at this frequency range. The S-parameters of active devices can be measured as function of frequency, temperature, and bias conditions. As an example of cryogenic on-wafer measurements, measured S-parameters of InP HEMTs are presented at temperatures of 20, 80, 160, and 295 K and in the frequency range of 50 –110 GHz.

## I. INTRODUCTION

S-parameter measurement is a basic tool in any linear microwave (3-30 GHz) and millimeter wave (30-300 GHz) circuit characterization. Impedance, VSWR, gain, and other similar quantities can be derived from the S-parameter data of a device under test (DUT). Reliable S-parameter measurements are also an important part of noise figure, available gain and noise parameter measurements [1-3]. Especially at millimeter waves and low temperatures, where simulations tools and models for components are not always accurate, the on-wafer measurements are an important part of the design chain from a prototype to a real product. For example, the design of low noise amplifiers (LNA) and high temperature superconductor (HTS) devices are greatly dependent on on-wafer measurements. Cryogenic on-wafer measurement systems have been developed mostly for frequency ranges below 50 GHz [2-4]. We have earlier presented a measurement system that allows cryogenic on-wafer S-parameter measurements at 50-75 GHz (V-band) and 20-295 K [5-6]. Here, we present a measurement set-up, which extends the cryogenic on-wafer measurements to include W-band.

## II. MEASUREMENT SYSTEM

The developed cryogenic measurement station is based on a commercial cryogenic on-wafer system by Nagase Co. originally designed for measurements below 50 GHz. The Nagase system consists of a stainless steel vacuum chamber, vacuum pump, closet cycle Helium cryo cooler, cold plate (chuck) for the test devices, and a temperature controller. All the installations necessary for waveguide based V- and W-bands measurements have been designed and built in-house. A schematic view of the V- and W-

bands measurement system is shown in Fig. 1 and a photograph of the W-band system in Fig. 2. Inside the vacuum chamber, special in-house built spiral-shape waveguides are used for connecting the two feed throughs to the RF probes. V- and W-bands have different waveguide setups.

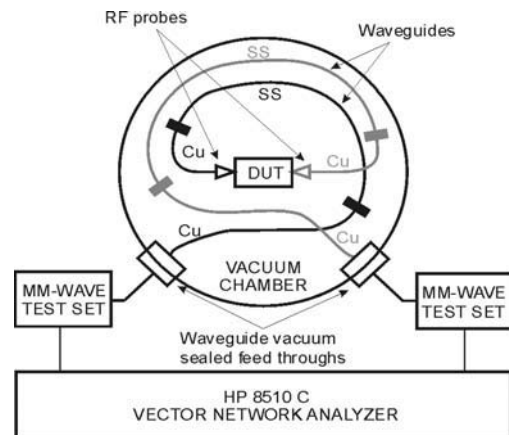


Fig. 1. Schematic view of cryogenic V- and W-bands on-wafer measurement set-ups.

Each of the waveguides is about 450 mm long and consists of three sections. Two of the sections are gold-plated copper, and the third one is gold-plated stainless steel. The steel section is about 200 mm long, and it provides a thermal isolation as well as mechanical flexibility. The feed throughs are in room temperature, whereas a device under test (DUT) can have a temperature as low as 15 K. The steel sections reduce heat flow to the DUT helping to maintain the wanted testing temperature. S-parameter measurements are carried out using a HP8510 C vector network analyzer (VNA) with V- and W-band extension units.

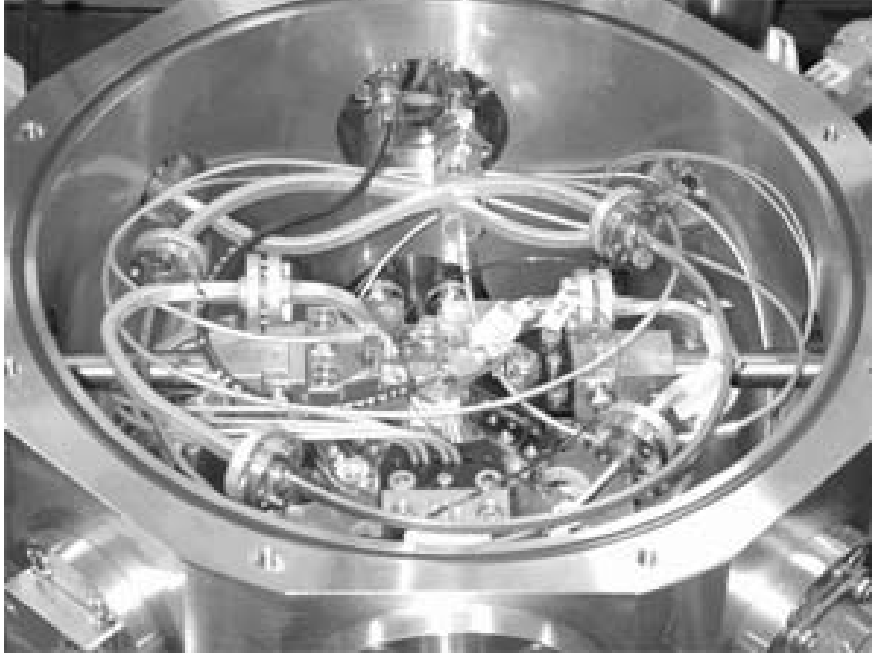


Fig. 2. A photograph showing the RF and bias probes with W-band waveguide installations inside the vacuum chamber.

### III. MEASUREMENTS

As an example of cryogenic on-wafer measurements at W-band, the S-parameters of a DaimlerChrysler InP HEMT are presented. The HEMT had a  $0.18 \mu\text{m}$  gate length and  $2 \times 40 \mu\text{m}$  gate width. Measurements were carried out at 20, 80, 160 and 295 K (Figs. 3-6). Operating point was  $V_{\text{ds}} = 1 \text{ V}$  and  $I_{\text{ds}} = 10 \text{ mA}$  in these measurements. The vector network analyzer was calibrated with LRRM or SOLT on-wafer calibrations. Also, wideband measurements (50-110 GHz) at 20 K, 80 K, 160 K, and 295 K were carried out. Two different waveguide set-ups were used with the results combined. Here, an HRL InP HEMT was used as the DUT. The HRL InP HEMT had a  $0.1 \mu\text{m}$  gate length and  $2 \times 25 \mu\text{m}$  gate width. The operating point was  $V_{\text{ds}}=1.0 \text{ V}$  and  $I_{\text{ds}}=6.25 \text{ mA}$ . The measured S-parameters of the HRL HEMT are shown in Figs. 7 - 8. In the cases of both HEMTs, the gain improves about 1 dB when temperature is lowered from 295 K to 20 K. The biggest change occurs from 295 K to 160 K, after which the effect of cooling is smaller.

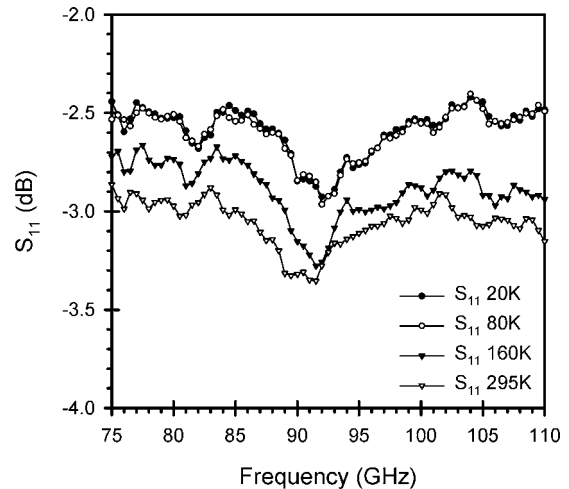


Fig. 3. Measured W-band S<sub>11</sub> of a DaimlerChrysler InP HEMT at different temperatures.

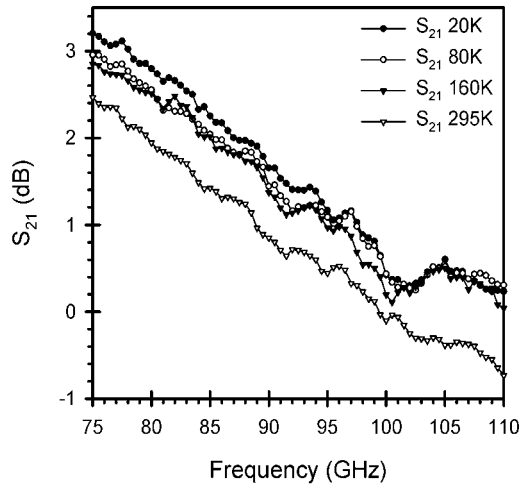


Fig. 4. Measured W-band  $S_{21}$  of a DaimlerChrysler InP HEMT at different temperatures.

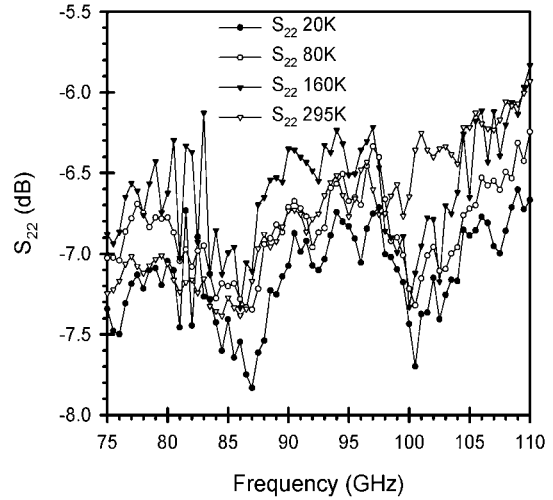


Fig. 6. Measured W-band  $S_{22}$  of a DaimlerChrysler InP HEMT at different temperatures..

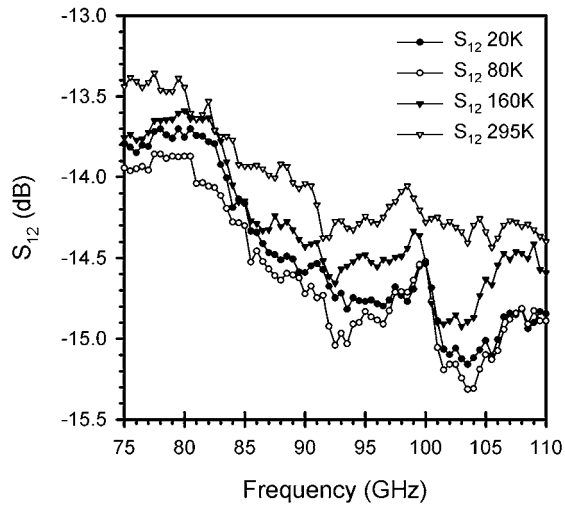


Fig. 5. Measured W-band  $S_{12}$  of a DaimlerChrysler InP HEMT at different temperatures..

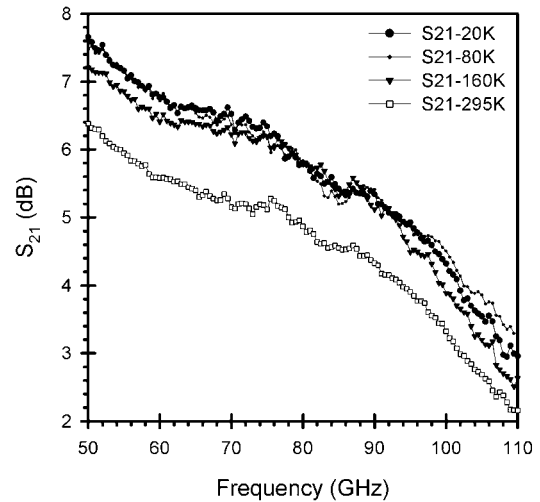
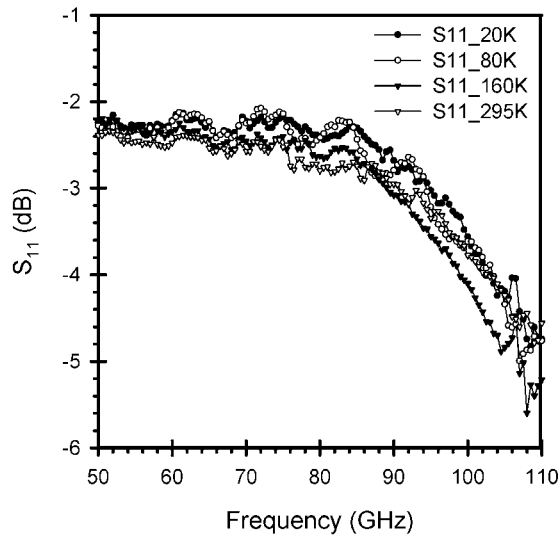
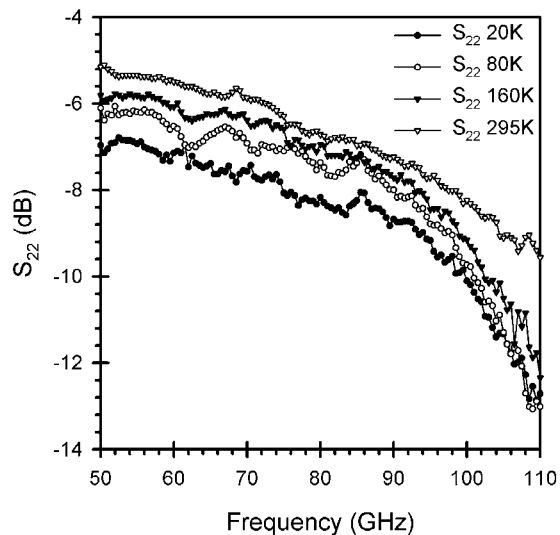


Fig. 7. Measured wideband  $S_{21}$  of a HRL InP HEMT at various temperatures.



(a)



(b)

Fig. 8. Measured wideband (a)  $S_{11}$  and (b)  $S_{22}$  of a HRL InP HEMT at various temperatures.

## V. CONCLUSIONS

A cryogenic on-wafer system has been demonstrated for measurements at 50-110 GHz and 20-295 K. Measured results have been presented for a DaimlerChrysler InP HEMT at W-band and for a HRL InP HEMT at 50-110 GHz with temperatures of 20, 80, 160, and 295 K. For both HEMTs, the gain improved about 1 dB when cooled from 295 K to 20 K.

## ACKNOWLEDGEMENT

This work has been supported by the ESA/ESTEC contract no. 1655/95/NL/MV and the Graduate School in Electronics, Telecommunications and Automation, GETA, Finland.

## REFERENCES

- [1] Vähä-Heikkilä T., Lahdes M., Tuovinen J., Kantanen M., Kangaslahti P., Jukkala P., Hughes N.: "W-band on-wafer noise parameter measurements", *IEEE Transactions on Microwave Theory and Techniques*, Vol. 51, Issue 6, pp. 1621-1628, 2003.
- [2] Caddemi A., Donato N., Sannino M.: "Characterization techniques for temperature-dependent analysis of microwave transistors", *Proceedings of the 18th IEEE Instrumentation and Measurement Technology Conference 2001 vol. 3*, pp. 1893-1896, 2001.
- [3] Laskar J., Murti M.R., Yoo S. Y., Gebara E., Harris H. M.: "Development of complete on-wafer cryogenic characterization: S-parameters, noise-parameters and load-pull", *Proceedings of GAAS'98*, pp. 33-38, 1998.
- [4] Meschede H., Reuter R., Albers J., Kraus J., Peters D., Brockerhoff W., Tegude F.-J., Bode M., Schubert J., Zander W.: "On-wafer microwave measurement setup for investigations on HEMTs and high- $T_c$  superconductors at cryogenic temperatures down to 20 K", *IEEE Transactions on Microwave Theory and Techniques*, Volume: 40 Issue: 12, pp. 2325-2331, 1992.
- [5] Tuovinen J., Varis J., Lahdes M., Karttaavi T., Hakojärvi H.: "Methods for on-wafer testing of cryogenic integrated circuits at millimetre waves", *Proceedings of WOLTE 4*, Noordwijk, pp. 157-162, 2000.
- [6] Tanskanen, J.M., Kangaslahti, P., Ahtola, H., Jukkala, P., Karttaavi T., Lahdes M., Varis J., Tuovinen J.: "Cryogenic indium-phosphide HEMT low-noise amplifiers at V-band", *IEEE Transactions on Microwave Theory and Techniques*, Volume: 48 Issue: 7 Part: 2, pp. 1283-1286, 2000.

PUBLICATION P3

# **RF MEMS Impedance Tuners for 6–24 GHz Applications**

Accepted for publication to International Journal  
of RF and Microwave Computer-Aided  
Engineering, February 2006.  
Reprinted with permission from the publisher.

## RF MEMS Impedance Tuners for 6-24 GHz Applications

Tauno Vähä-Heikkilä<sup>1,2</sup>, Koen Van Caekenberghe<sup>2</sup>, Jussi Varis<sup>1</sup>, Jussi Tuovinen<sup>1</sup> and Gabriel M. Rebeiz<sup>2,3</sup>

<sup>1</sup>MilliLab, VTT Technical Research Centre of Finland, P.O. BOX 1000, 02044 VTT, Finland, tauno.vaha-heikkila@vtt.fi

<sup>2</sup>The University of Michigan, Electrical Engineering and Computer Science Department, Ann Arbor, MI, 48109-2122, USA

<sup>3</sup>University of California at San Diego, Electrical and Computer Engineering Department, La Jolla, 92037, CA USA, rebeiz@ece.ucsd.edu

### ABSTRACT

RF MEMS tuners with wide impedance coverage have been developed for 6-24 GHz noise parameter and load-pull measurement systems. The tuners are based on triple-, double-, and single-stub topologies loaded with switched MEMS capacitors. Several designs are presented, and they use 10-13 switched MEMS capacitors to produce 1024 to 8192 ( $2^{10}$ - $2^{13}$ ) different impedances. The measured impedance coverage agrees well with simulations and it is the widest ever measured impedance coverage from any planar tuner to-date.

Keywords: RF MEMS, impedance tuner, noise parameters, load-pull, matching network, antenna tuner

### I. INTRODUCTION

Impedance tuners are commonly used in both load-pull and noise parameter measurements of transistors at microwave and mm-wave frequencies, e.g. [1-3]. Typically, these are mechanical devices with either coaxial or waveguide structures, and use motors for automatic control. Tuners are also made using diodes and transistors, but these designs are lossy and result in a limited impedance coverage [4,5]. Also, they add electronic noise which makes accurate noise measurements more challenging. RF MEMS impedance tuners with low loss and large impedance coverage are therefore desirable to increase measurement automation and accuracy. Also, MEMS-based impedance tuners are small enough to be mounted inside an on-wafer probe. An impedance tuner can either be of the transmission or reflection-type (Fig. 1) design, and typical impedance tuners are based either on double-stub [6,7] or triple-stub topologies [8,9]. The stub topologies are not ideal for power amplifier applications since they result in a higher loss compared to loaded-line tuners introduced by Vähä-Heikkilä and Rebeiz in [10,11]. Also, Shen and Barker have presented a distributed type double slug impedance tuner with low loss [12]. Still, the stub-based tuners result in excellent impedance coverage over a wide frequency range as well as high voltage standing wave ratios (VSWR), and are suitable to be used as noise parameter or load-pull impedance tuners.

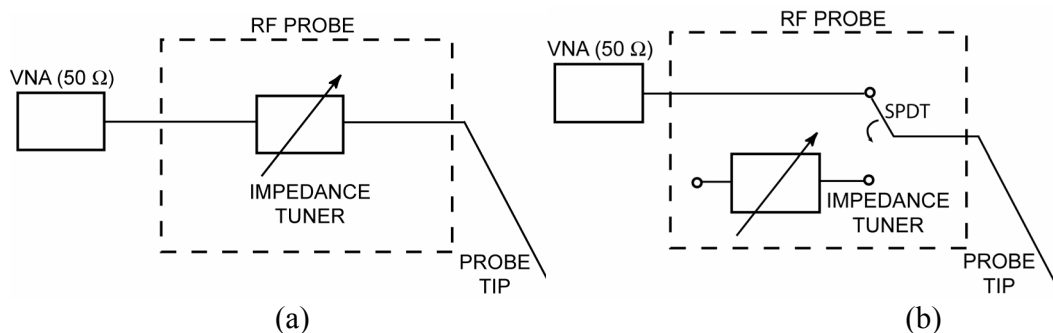


Figure 1. a) Transmission and b) reflection-type impedance tuner inside an RF probe used in on-wafer measurements.

In this work, impedance tuners based on switched MEMS capacitors are presented. The goal is not only to achieve a wide impedance coverage, but also to achieve this over a wide frequency range. This is done using a novel idea based on changing the electrical length *and* separation between the tuning stubs with the switched capacitor approach. The impedance and electrical length of the stub is also changed using MEMS switched capacitors. This method results in  $2^N$  different impedances over a wide frequency range for a stub circuit loaded with N different switched capacitors.

## II. TUNER DESIGN

An RF MEMS switch in series with a fixed metal-air-metal (MAM) capacitor is the basic building block of the stub-based tuners. There are several parameters which affect the impedance coverage of impedance tuners: the number and capacitance values of the switched MEMS capacitors have the most important effect on the tuning range and bandwidth. Other selectable parameters are the spacing of the switched capacitors, the transmission-line (t-line) properties ( $Z_0$ ,  $\epsilon_{\text{reff}}$ ), the distance between the stubs, and the lengths of the stubs.

The single-, double-, and triple-stub designs are optimized using Agilent ADS<sup>1</sup> to obtain as large a tuning range and bandwidth as possible with the minimum number of switched MEMS capacitors. We have not found a closed-form design technique since there are many design parameters for impedance tuners. Some design insights are given later in the paper. The equivalent circuit of the switched MEMS capacitor is shown in Fig. 2, and the component values are presented in Table 1. The up-state capacitance of the switched capacitor is determined mostly by the up-state capacitance of the MEMS switch, and the down-state capacitance is determined by the two MAM capacitors [11].

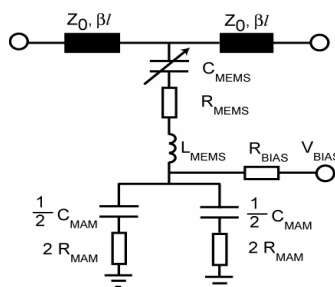


**Figure 2.** Equivalent circuit of a switched MEMS capacitor (unit cell in tuner design).

Fig. 3 shows a fabricated switched MEMS capacitor on a coplanar waveguide (CPW) t-line on a glass substrate (Corning 7040). The fabrication process is based on standard surface MEMS techniques and is described in [13]. The dimensions of the gold MEMS switch are  $280 \mu\text{m} \times 80 \mu\text{m} \times 0.8 \mu\text{m}$ , and it is suspended  $1.1 \mu\text{m}$  above the t-line. A  $3500 \text{ \AA}$  silicon nitride layer was used as a dielectric interlayer. The circuit is electroplated to  $3 \mu\text{m}$  thickness (except the MEMS bridges) to reduce the t-line and MAM capacitor loss. SiCr bias lines with resistance of  $700 \Omega/\text{square}$  are used for actuating the MEMS switches. The measured pull-down voltage is 15-17 V, and a bipolar actuation voltage of  $\pm 35 \text{ V}$  was used for obtaining an excellent metal-to-dielectric contact in the down-state position.

<sup>1</sup> Advanced Design System 2002, Agilent Technologies, Santa Clara, CA, USA, 2002.

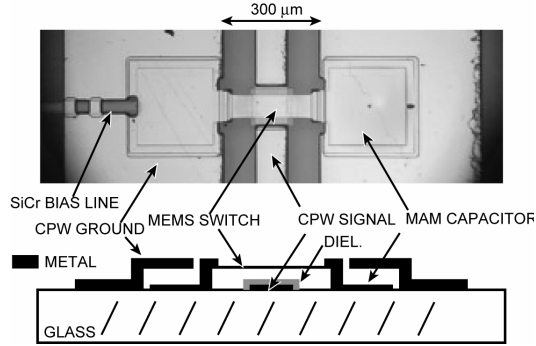


**Figure 3.** Picture and cross-sectional view of a switched MEMS capacitor unit cell.

**TABLE 1. Measured t-line properties from the trl calibration and fitted values for the switched MEMS capacitor.**

$\epsilon_r$	4.6
$Z_0(\Omega)$ (100/100/100 $\mu\text{m}$ )	86.2
$\epsilon_{\text{reff}}$	2.72
$\alpha$ (dB/cm), 10/20 GHz	0.35/0.52
$C_{\text{MEMS}}$ Up-State (fF)	91
$C_{\text{MEMS}}$ Down-State (fF)	750
$R_{\text{BIAS}}$ (k $\Omega$ )	> 3
$L_{\text{MEMS}}$ (pH)	9.5
$R_{\text{MEMS}} + R_{\text{MAM}}$ ( $\Omega$ )	0.6
$C_{\text{MAM}}$ (fF)	850

As seen in Table 1, the measured capacitance ratio of the RF MEMS switch is only 8:1 due to its low height and the thick silicon-nitride layer. The total up-state and down-state capacitances of the switched capacitor are  $C_U = 82.2$  fF and  $C_D = 398$  fF, respectively, resulting in a capacitance ratio of 4.9:1. The quality factor of the switched MEMS capacitor is calculated using  $Q = (2\pi f C (R_{\text{MEMS}} + R_{\text{MAM}}))^{-1}$  and at 12 GHz, results in an up and down-state values of  $Q_U = 269$  ( $C_U = 82.2$  fF,  $X = -j161 \Omega$ ) and  $Q_D = 55$  ( $C_D = 398$  fF,  $X = -j33.3 \Omega$ ), respectively. Table 2 summarizes the properties of the entire unit cell of Fig. 3. The unit cell has 31 degree phase change between its up and down-states at 12 GHz.

**TABLE 2. Properties of the unit cell.**

Length ( $\mu\text{m}$ )	480
$Z_0(\Omega)$	86.2
$Z_U(\Omega)$	45
$Z_D(\Omega)$	23
$\phi_U$ (degree) at 12 GHz	-22.3
$\phi_D$ (degree) at 12 GHz	-53.2
$Q_U$ at 12 GHz	269
$Q_D$ at 12 GHz	55

The reconfigurable triple-, double-, and single-stub impedance tuners were optimized to have 10-13 identical switched MEMS capacitors (S1-S13). The number of switched capacitors (N) has great effect to the impedance coverage of the tuners. By using a larger number of switched capacitors better impedance coverage can be achieved at the cost of a more complicated control system and higher circuit loss.

The switched capacitors were used for tuning the electrical lengths of the stubs and also the separation between them. Spacing between the stubs is 3.0 mm for the double- and triple-stub designs (Figs. 4-7). It should be noted that a small capacitance ratio does not result in a large tuning range at the lower frequencies, but on the other hand, a high capacitance ratio causes a short circuit at higher frequencies. Therefore, the circuits were optimized with a large number of simulations in ADS, and the best capacitance ratio was found to be between 4 and 10.

There is truly a large number of circuit combinations which can offer a wide frequency coverage and wide tuning range, and in this paper, we will present four representative circuits based on triple (Figs. 4 and 5), double (Fig. 6), and single-stub (Fig. 7) designs. Notice that the double-stub design is physically rather small, and owes its wide tuning range to the use of 3 switched capacitors between the stubs.

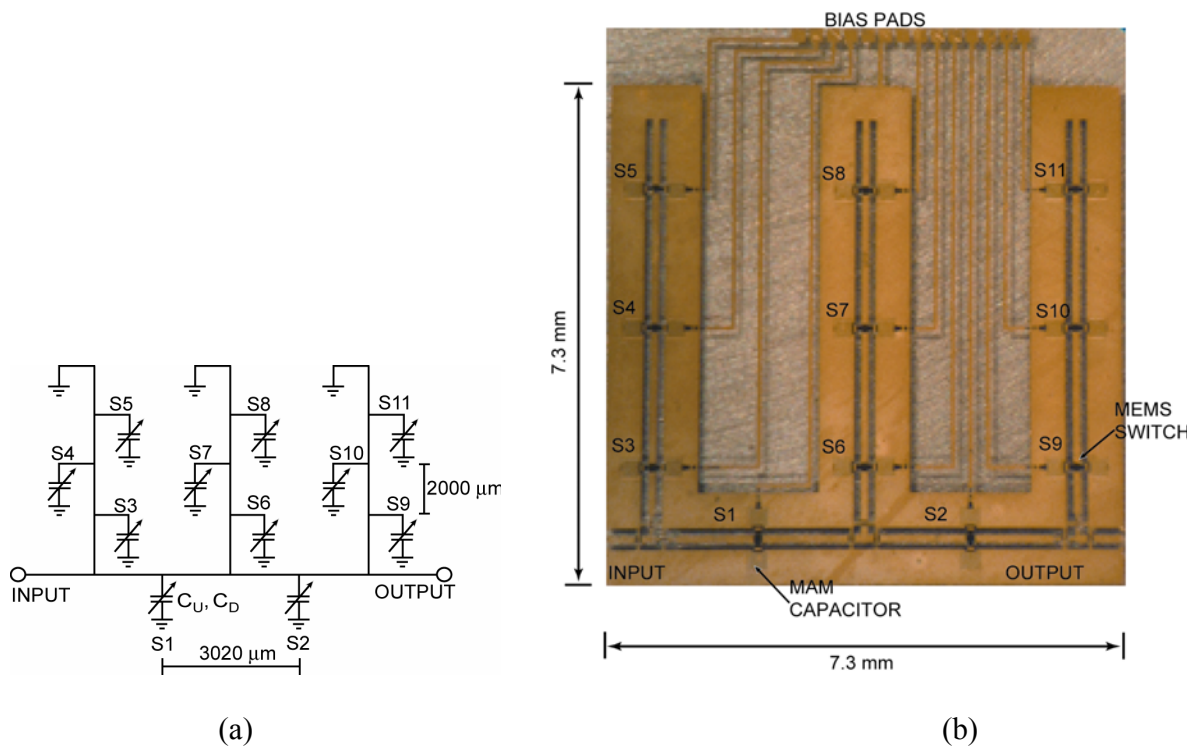


**Figure 4.** a) Circuit diagram and b) picture of the 6-20 GHz reconfigurable triple-stub RF MEMS impedance tuner with 11 switched MEMS capacitors (S1-S11). Notice that the stubs are short circuited.

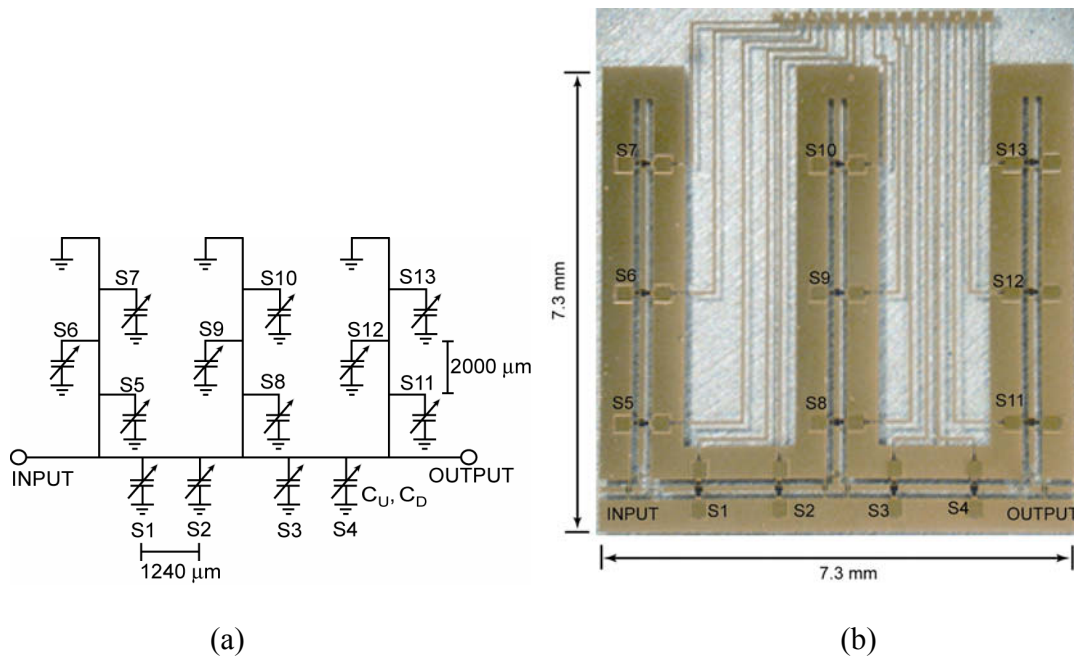


**Figure 5.** a) Circuit diagram and b) picture of the 6-20 GHz reconfigurable triple-stub RF MEMS impedance tuner with 13 switched MEMS capacitors (S1-S13). Note that 2 switched capacitors are used between the stubs and the stubs are short circuited.

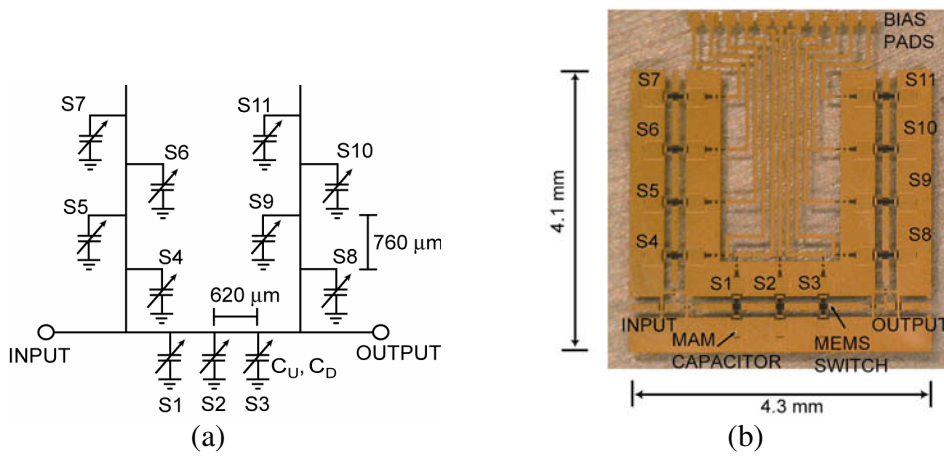


**Figure 6.** a) Circuit diagram and b) picture of the 4-30 GHz double-stub RF MEMS impedance tuner with 11 switched MEMS capacitors (S1-S11). Notice that three switched capacitors are used between the stubs, and that the stubs are open circuited.

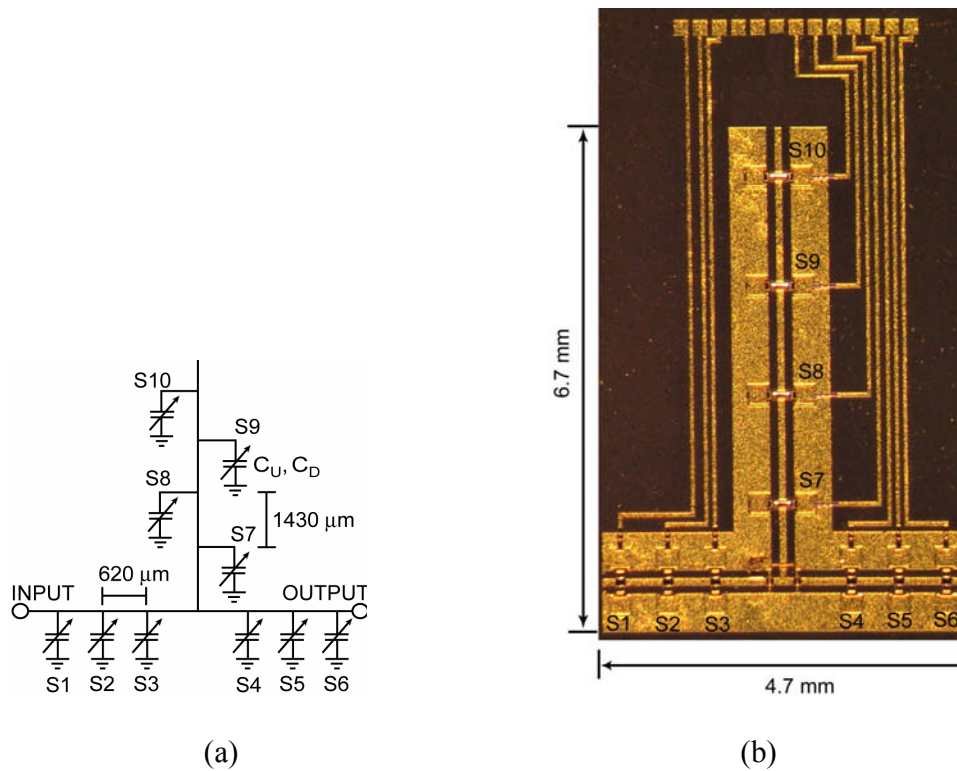


**Figure 7.** a) Circuit diagram and b) picture of the 6-25 GHz single-stub RF MEMS impedance tuner with 10 switched MEMS capacitors (S1-S10). Notice that three switched capacitors are placed both before and after the stub.

### III. CIRCUIT MODEL

An accurate circuit model of the tuner is very important in predicting the impedance coverage and behavior over a wide frequency range. Also, the tuners have 10 to 13 switched capacitors producing 1024-8192 different impedances making it time consuming to measure all the different combinations. The circuit models were developed by first measuring several switched MEMS capacitors both as single elements and as elements in a distributed (loaded-line) network as in [11], and deriving the equivalent circuit of the unit-cell switched capacitor (see Fig. 2 and Tables 1-2). To get accurate models for the T-junctions, they were simulated with the Sonnet2 full wave EM simulator as three port elements, and also having air bridges crossing each arm. The unit cell, the Sonnet models of the T junctions, and the t-line characteristics were all used in Agilent ADS for predicting the response of the whole network under different switch combinations. The accuracy of the model is clearly seen with a comparison between the simulated and measured S-parameters for the triple- and double-stub tuners in Figs. 8 and 9. The models agree for all switch combinations which were tested, but only two representative conditions are shown in Figs. 8 and 9.

<sup>2</sup> Sonnet, ver. 8.52, Sonnet Software Inc., Syracuse, NY, 1986-2001.

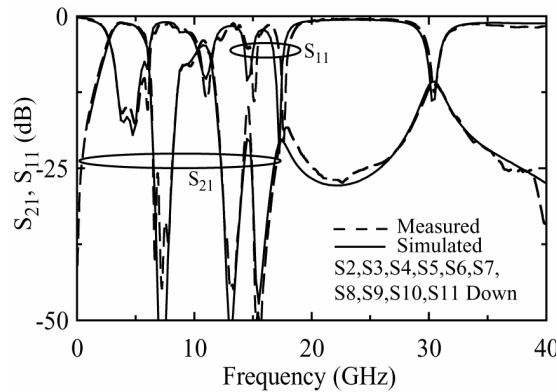


**Figure 8.** Measured and simulated S-parameters for the triple-stub tuner of Fig. 4 with 11 switches, when switches S2, S3, S4, S5, S6, S7, S8, S9, S10, and S11 are in the down-state.

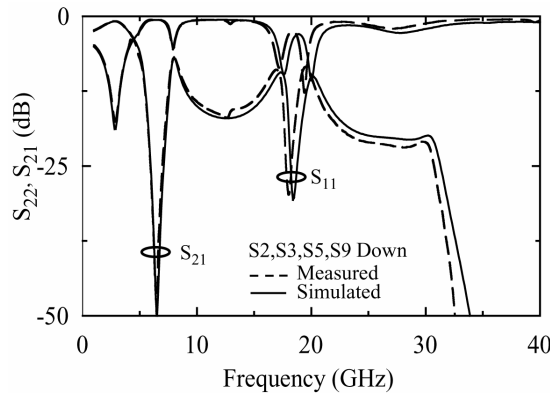


**Figure 9.** Measured and simulated S-parameters for the double-stub tuner of Fig. 6 with 11 switches, when switches S2, S3, S5, and S9 are in the down-state.

#### IV. IMPEDANCE COVERAGE

##### A. Triple-Stub Tuner with 11 Switched Capacitors

The measured (160) and simulated ( $2^{11} = 2048$ ) impedance points of the reconfigurable triple-stub tuner are presented in Fig. 10 at 6-20 GHz. In this case, a  $50 \Omega$  load was placed at the output port, and the input reflection coefficients were measured with different switches actuated into the down-state position. Due to the number of points in the measurement set-up, it is hard to show a 1:1 mapping between the measured and simulated data, but they agree quite well with each other (see also Figs. 8 and 9). It can be seen that the obtained impedance coverage is good for noise-parameter or load-pull measurements. There is some discrepancy at 20 GHz, and this is when the triple-stub network is quite large and the CPW lines are starting to radiate, which is not modeled by Agilent ADS.

The network can also be used for matching a low-impedance load ( $10 \Omega$ ) at virtually all frequencies between 6 and 20 GHz, but as will be seen in Section V, the triple stub tuner results in higher loss compared to other designs [9].

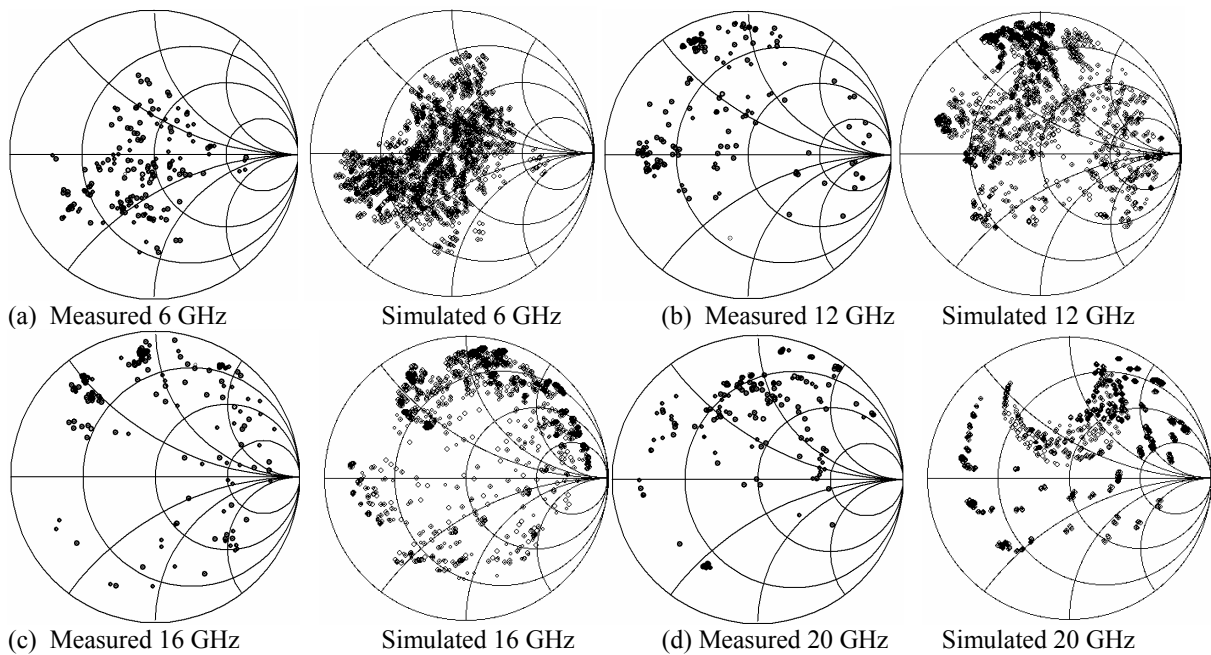


**Figure 10.** (a)-(d) Measured (160 points) and simulated (2048 points) impedance coverage of the triple-stub tuner with 11 switched capacitors.

The triple-stub tuner with 11 switches can also be used in a reflection-mode with open or short-circuit termination at the output port (see Fig. 1) for obtaining wide impedance coverage (Fig. 11). This is useful in noise parameter measurements, and in this case, an important characteristic is to get a near-circular impedance locus on the Smith chart [14].

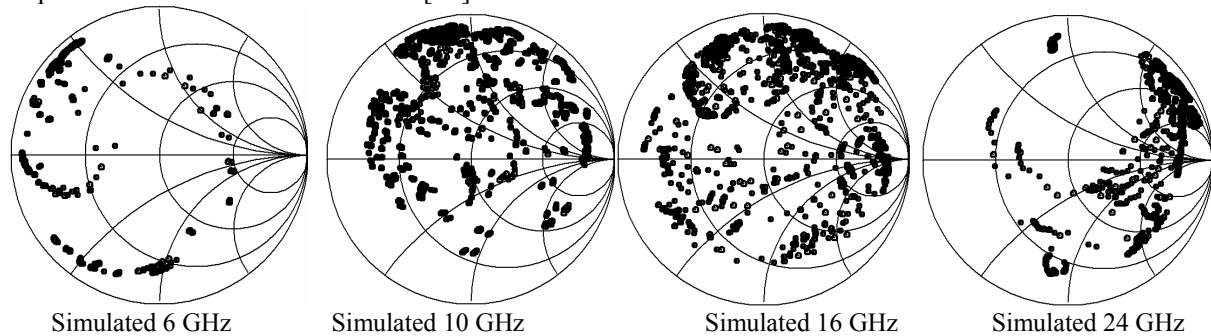


**Figure 11.** Simulated (2048 points) impedance coverage of the triple-stub tuner when the output terminated with an open circuit. Similar results are achieved for a short-circuit termination.

## B. Triple-Stub Tuner with 13 Switched Capacitors

The triple-stub tuner was also optimized for 13 switched capacitors. Two additional switched capacitors were placed between the stubs to result in a higher tuning (2 bit instead of 1-bit) range for the electrical distance between the stubs. This tuner results in 8192 ( $2^{13}$ ) different impedances, and its measured (160 points) and simulated impedance coverage with a  $50 \Omega$  load at the output port are shown in Fig. 12. Also, the simulated impedance coverage with the output terminated with an open circuit is shown in Fig. 13. It

is seen that the impedance coverage with the  $50\ \Omega$  load is not much wider compared to the design with 11 switched capacitors, but better impedance coverage can be achieved with the output terminated either with an open or a short circuit (reflection mode).

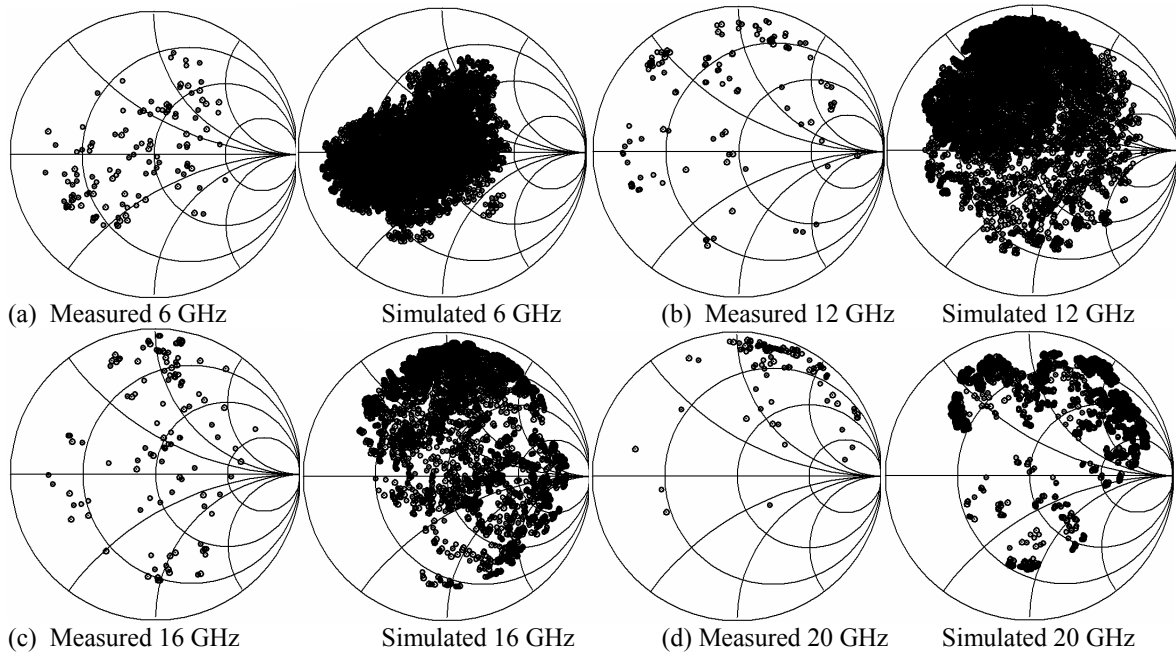


**Figure 12.** (a)-(d) Measured (160 points) and simulated (8192 points) impedance coverage of the triple-stub tuner with 13 switched capacitors with a  $50\ \Omega$  load.

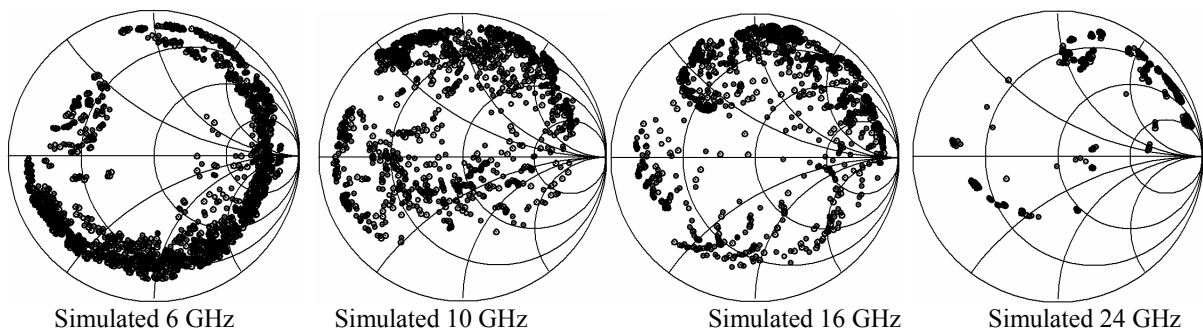


**Figure 13.** Simulated (8192 points) impedance coverage of the triple-stub tuner with 13 switched capacitors when the output is terminated with an open circuit (reflection mode). Similar results are achieved for a short-circuit termination.

### C. Double-Stub Tuner with 11 Switched Capacitors

The measured (160) and simulated (2048) impedance points for the double-stub tuner are shown in Fig. 14 at 4-30 GHz. The impedance coverage of the double-stub tuner is not as wide as the impedance coverage of the triple-stub tuners at 6-20 GHz, but on the other hand, it is much better above 20 GHz. Notice that the impedance coverage at 6 GHz is very small and this is due to the value of the switched capacitors and a resonant phenomena which is occurring at 6 GHz due to the size of the double-stub tuner (this is not

observed at 4 or at 8 GHz). Our simulations clearly indicate that this can be mitigated by changing the values of the switched capacitor to be  $C_U = 50$  fF and  $C_D = 750$  fF, but at the expense of a reduction in the tuning range to 18 GHz.

Fig. 15 shows that even with the double-stub topology and an open-circuit termination at the output (reflection mode), it is possible to achieve as good impedance coverage as with the triple-stub tuners over a wide frequency range.

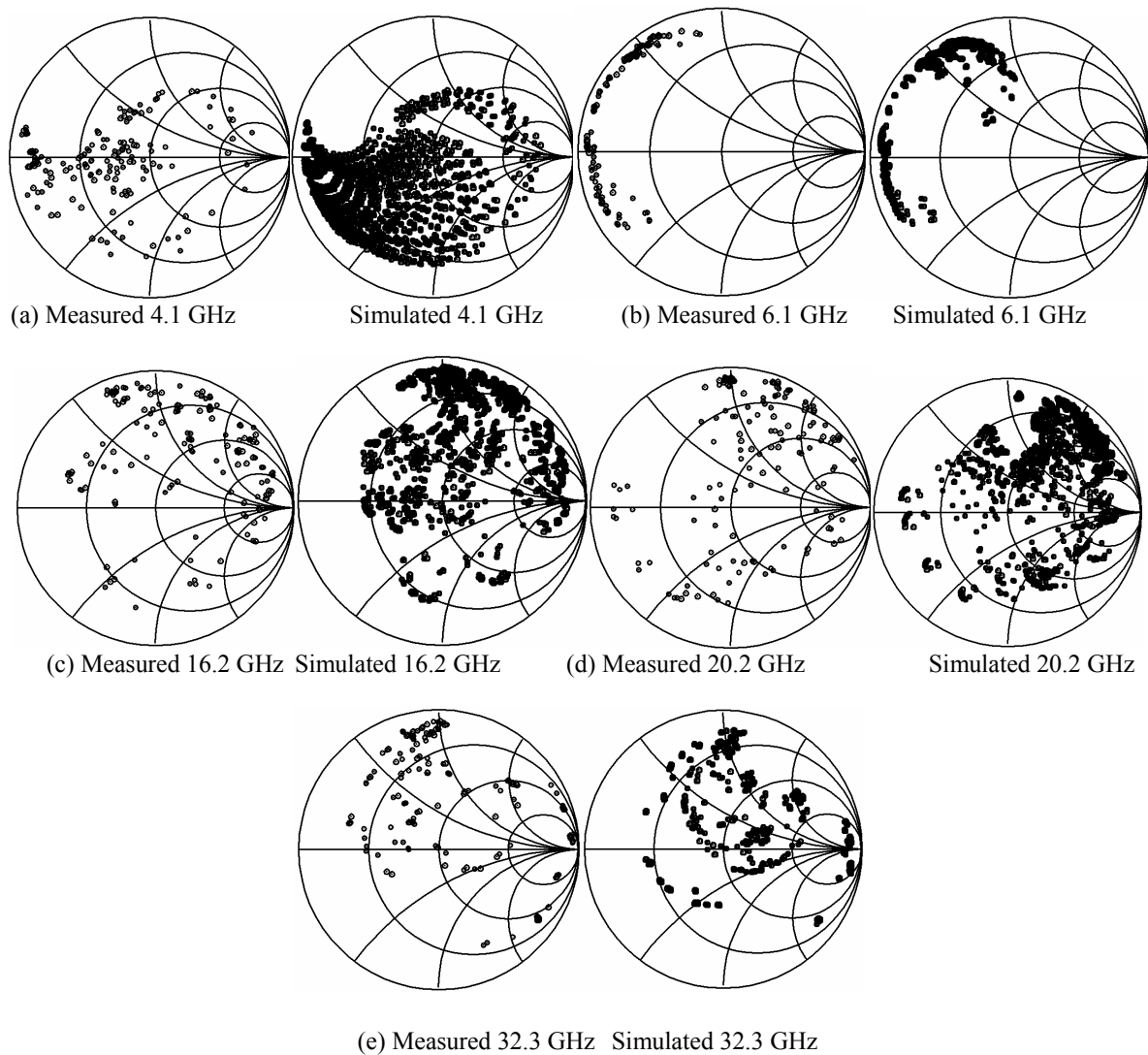


**Figure 14.** (a)-(f) Measured (160 points) and simulated (2048 points) impedance coverage of the double-stub tuner with 11 switched capacitors with a  $50 \Omega$  load.

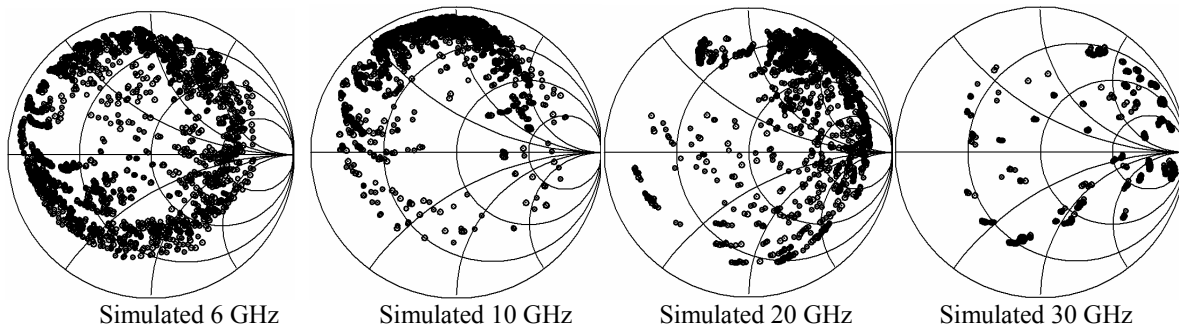


**Figure 15.** Simulated (2048 points) impedance coverage of the double-stub tuner when the output terminated with an open circuit (reflection mode). The impedance coverage is the same at 10-30 GHz for a short circuit termination and with a slightly reduced coverage at 6 GHz.

#### D. Single-Stub Tuner with 10 Switched Capacitors

Measured (90 points) and simulated (1024 points) impedance coverage of the single-stub tuner with an open circuited is presented in Fig. 16 at 6-20 GHz. The single-stub tuner does not have the frequency bandwidth of the triple-stub design showing only good impedance coverage between 10 and 20 GHz. Still, these are excellent results from a single-stub design, and is due to the variable impedance and electrical-length loading of the switched capacitors which are not only used in the stub, but also in the t-line before and after the stub. A single-stub tuner with a short circuited stub was also realized. It has as good impedance coverage as with the open circuited single-stub tuner. Our simulations indicate that the single-stub tuner with a  $50 \Omega$  load can be improved by using switched capacitors having a higher capacitance ratio with  $C_U = 50$  fF and  $C_D = 800$  f. It will be seen in Section V that the single stub tuner results in the lowest loss matching network out of all the cases presented above (for power amplifier applications).

Finally, if the network is terminated with an open or short circuit (reflection mode), one can obtain a very good impedance coverage at 6-24 GHz (Fig. 17).

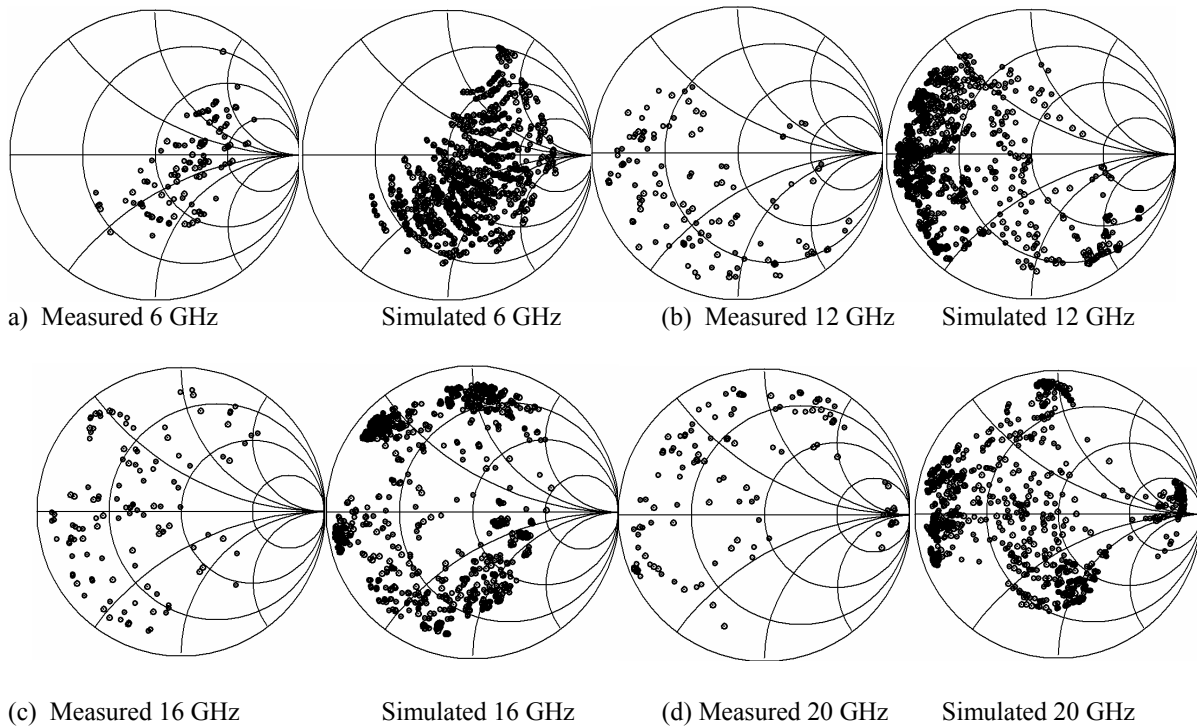


**Figure 16.** (a)-(d) Measured (90 points) and simulated (1024 points) impedance coverage of the single-stub tuner with a 50 Ω load.

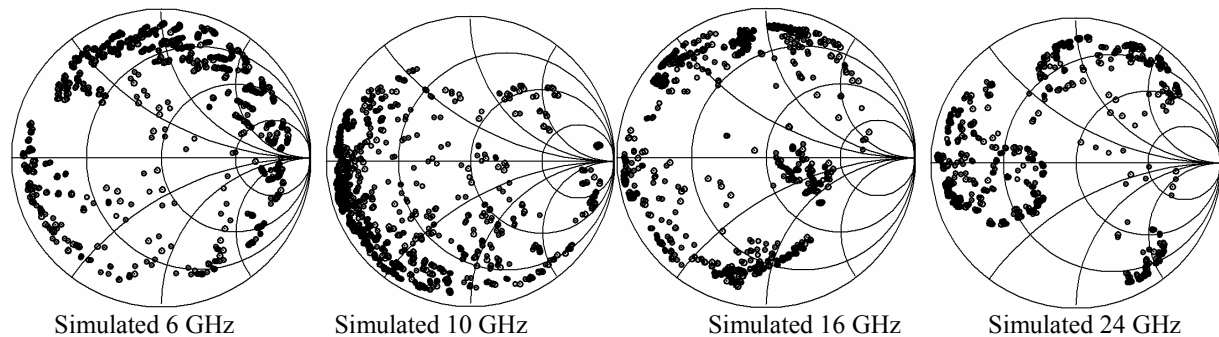


**Figure 17.** Simulated (1024 points) impedance coverage of the single-stub tuner when the output terminated with an open circuit (reflection mode). The impedance coverage is the same at 10-30 GHz for a short circuit termination but results in reduced coverage at 6 GHz.

## V. CASE STUDY: MATCHING OF A 20 Ω LOAD TO 50 Ω

The circuit model developed above can be used for analyzing different matching conditions. A 20 Ω load was matched to 50 Ω with the triple, double, and single-stub tuners at 4-20 GHz and different switch combinations were chosen to achieve an impedance match better than -19 dB at different frequencies. Fig. 18 shows the case of the single-stub tuner, where the loss is defined as  $1 - |S_{11}|^2 - |S_{21}|^2$  and includes the ohmic loss in the t-line and bridges, and radiation loss. The single-stub tuner is well suited for matching applications up to 16 GHz with a loss of 0.1-0.2 (90-80% efficient which is 0.5-1 dB of loss). However, the loss is quite high in the triple- and double stub tuners at 6-20 GHz (1-2 dB loss) and is not shown. The

reason is that these networks are quite large and include two or three T-junctions. Therefore, double and triple-stub tuners are better suited for noise parameter and load-pull measurement applications.

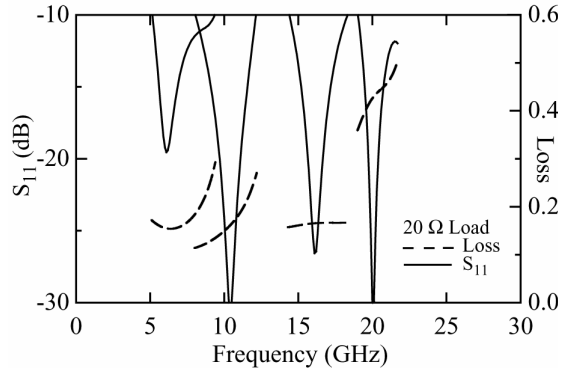


**Figure 18.** Simulated input reflection coefficient and loss of the single-stub tuner with 10 switched capacitors at 6, 10, 16, and 20 GHz with a 20 Ω load matched to 50 Ω. Simulations were done based on the circuit model (which agrees very well with measurements). Switches S3, S4, S5, S7, S9, and S10 were down when matching at 6 GHz, S5 and S10 at 10 GHz, S8 and S10 at 16 GHz, and S4, S5, and S8 at 20 GHz.

## VI. MEASURED $|\Gamma_{MAX}|$

A figure of merit for impedance tuners is the maximum achievable reflection coefficient,  $|\Gamma_{MAX}|$ , and the measured  $|\Gamma_{MAX}|$  values for the tuners are shown in Table 3 (for the 90-160 points out of 1024-8192 possible). These measurements show that the double-stub tuner design with three switched capacitors between the stubs results in a measured  $|\Gamma_{MAX}| > 0.9$  for the whole frequency band, and the best measured  $|\Gamma_{MAX}|$  is 0.99 at 30 GHz, which is equal to VSWR of 199. The measured  $|\Gamma_{MAX}|$  values are comparable to previously published integrated impedance tuners. Some notable results were: A VSWR of 6 at 27 GHz [4], a VSWR of 12.3 at 27 GHz [5], a VSWR of 32.3 at 30 GHz [6], and a VSWR of 99 at 20 GHz [7]. However, all of the tuners in [4-7] were quite narrowband as opposed to the wideband designs presented here.

**TABLE 3. Measured  $|\Gamma_{MAX}|$  for the difference tuners for 90-160 points with 50 Ω terminations. Higher  $|\Gamma_{MAX}|$  could be achieved if more measurements points were taken.**

Frequency (GHz)	$ \Gamma_{MAX} $ 3-stub 11 switches	$ \Gamma_{MAX} $ 3-stub 13 switches	$ \Gamma_{MAX} $ 2-stub 11 switches	$ \Gamma_{MAX} $ 1-stub 10 switches
6	0.77	0.77	0.95	0.86
8	0.92	0.92	0.94	0.69
12	0.92	0.92	0.91	0.93
16	0.95	0.95	0.93	0.91
20	0.96	0.97	0.96	0.97
30	0.95	0.97	0.99	0.98

## VII. INTERMODULATION MEASUREMENTS

The intermodulation analysis of MEMS switches, and varactors is presented in [15] and show that MEMS-based circuits generate insignificant amount of intermodulation products, especially if the frequency difference between the two RF signals ( $\Delta f$ ) is higher than the mechanical resonant frequency of the bridge. The intermodulation measurements of the impedance tuners were carried out with the measurement set-up shown in Fig. 19, and the circuits were terminated with either a  $50\ \Omega$  load or with a short circuit. In the case of the short circuit condition, the generated intermodulation signals (IM3 products) were measured at the input port using a circulator.

The triple-stub tuner with 11 switched-capacitors was measured at 8 and 17 GHz, and the measurement IIP3 is  $> 35\ \text{dBm}$  for a 5 kHz separation frequency, even under short circuit conditions (Fig. 20). Fig. 20 also shows that the intermodulation products are higher at 17 GHz than at 8 GHz as predicted in [15]. Also, the IIP3 increases as  $(\Delta f)^4$  and therefore it can be expected to be  $> +60\ \text{dBm}$  for a  $\Delta f$  of 1 MHz. This is so low that it is simply un-measurable in most experimental set-ups. These findings confirm the results of [15].

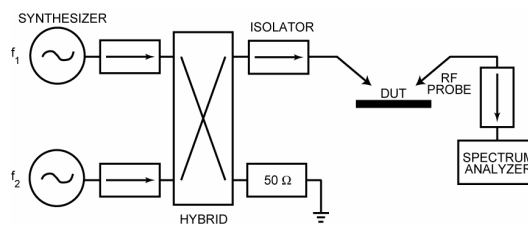


**Figure 19.** Schematic of the intermodulation measurement set-up.

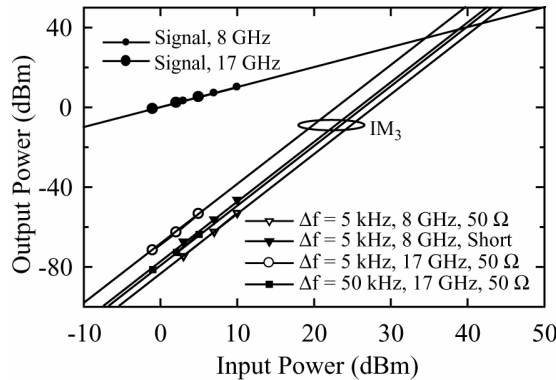


**Figure 20.** Measured third-order intermodulation of the triple-stub tuner with 11 switched capacitors at 8 and 17 GHz, when all the switches were in the up-state.

## VIII. POWER HANDLING

Power handling is not a critical issue if the tuners are used in noise parameter measurements. However, in load-pull measurements, power handling can be important especially if the tuners are used at the output port. As is well known [14], if a DC or an RF voltage is applied between the electrodes of a MEMS switch, the position of the switch changes since the electrostatic force is dependent on  $V^2$ , and this translates to  $V_{\text{rms}}^2$  for RF voltages. The MEMS switch is pulled down if  $|V_{\text{rms}}|$  is equal or greater than the DC pull-down voltage of the switch. Another problem related to high RF power is the hold-down voltage in the down-state position [15].

The power handling measurement set-up is shown schematically in Fig. 21, where isolators were used for achieving a  $50\ \Omega$  system at the source and the power meter. The power handling of the triple-stub tuner with 11 switched capacitors was measured at 8 and 17.6 GHz (Fig. 22). The triple-stub tuner circuits can handle up to 23-24 dBm RF power at 8-17 GHz depending on the switch combination. This is enough for most transistors operating at this frequency band at the input port or as a tuner in noise parameter measurements, but this is not enough for an output port matching network.

The voltages and currents across the switched capacitors were simulated using Agilent ADS with 24 dBm RF power (Fig. 23). The simulation predicts that switches S1 and S2 have the highest rms voltage (5 V). In this case, the pull-down voltage of the switches was closer to 10 V and a 5-6 V RF rms voltage will start to change the switch capacitance. However, this is not a complete solution, since it is assumed that the circuit is not changing, but as the bridge position and capacitance changes, the voltage distribution on the circuit changes, and may result in a higher voltage across S1 and S2. This means that a coupled microwave-circuit/mechanical-analysis solution is needed to find the behavior of the reconfigurable circuit in a dynamic fashion, and this is not done here.

For higher power handling, it is recommended that the MEMS switches are fabricated with a high pull-down voltage (30 V instead of 10-15 V). This will increase the power handling by a factor of 4 to around 30 dBm. A potential problem which may arise from using 30-40 V bias voltages is the charging of the dielectric layer in the MEMS switch, but this is mitigated by the use of a thick SiN dielectric layer (3500 Å instead of the standard 1000 Å) since the design does not necessitate a large capacitance ratio. The currents in the switches are quite low, in the both the up-state and down-state positions, and remain lower than 150 mA rms for virtually all switch combinations up to 30 dBm.

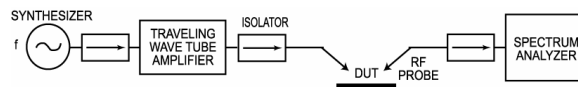


**Figure 21.** Schematic drawing of the power handling measurement set-up.

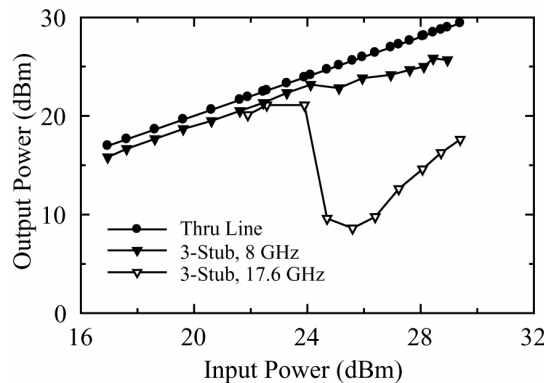


**Figure 22.** Measured power handling of the triple-stub tuner with 11 switched capacitors at 8 and 17.6 GHz, when all of the switches were in the up-state position. In this case, a 24 dBm power handling is observed.

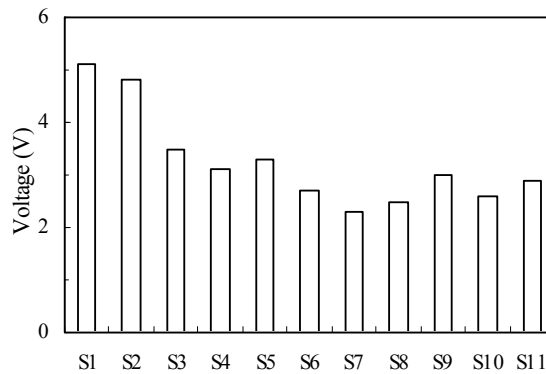


**Figure 23.** Simulated rms voltage across the switched capacitors in the triple-stub tuner with 11 switched capacitors at 17.6 GHz with 24 dBm input RF power. All switches were in the up-state in the simulations.

## IX. CONCLUSIONS

This paper presented a whole set of impedance tuners for 6-24 GHz applications using single-, double-, and triple-stub topologies. The essential idea of the design is that switched capacitors with a relatively low capacitance ratio are used (and not switches), which results in a very large number of impedance combinations (1024-8192 different impedances for 10-13 switched capacitors). The switched capacitors were used for changing the electrical lengths and impedance of stubs and sections between the stubs. The measured impedance and frequency coverage of these tuners is the widest to-date from any integrated tuner at this frequency range. Also, these tuners can achieve a very high VSWR over a wide frequency range, and the double-stub tuner resulted in a measured VSWR of 199 at 30 GHz. The areas of the single and double-stub tuners are small enough to be integrated inside on-wafer measurement probes to increase the measurement accuracy and automation in noise parameter or load-pull measurements systems. If the stub-based tuners are used as matching networks with amplifiers, the single-stub topology should be used to get the lowest loss. The tuners can be scaled up to 120 GHz and this work has been presented in [17-19].

## ACKNOWLEDGEMENTS

This work has been supported by the ESA/ESTEC contract no. 1655/95/NL/MV at MilliLab, VTT, and the DARPA IRFFE program at the University of Michigan.

## REFERENCES

1. M. Kantanen, M. Lahdes, T. Vähä-Heikkilä, and J. Tuovinen, A wideband automated measurement system for on-wafer noise parameter measurements at 50-75 GHz, *IEEE Transactions on Microwave Theory and Techniques*, vol. 51, no. 5, 2003, pp. 1489-1495.
2. T. Vähä-Heikkilä, M. Lahdes, M. Kantanen, and J. Tuovinen, On-wafer noise parameter measurements at W-band, *IEEE Transactions on Microwave Theory and Techniques*, vol. 51, no. 6, 2003, pp. 1621-1628.
3. M. Pierpoint, R.D. Pollard, and J.R. Richardson, An automated measurement technique for measuring amplifier load-pull and verifying large-signal device models, *IEEE MTT-S International Microwave Symposium Digest*, vol. 86, Baltimore, Maryland, 1986, pp. 625 - 628.

4. W. Bischof, Variable impedance tuner for MMIC's, *IEEE Microwave and Guided Wave Lett.*, vol. 4, no. 6, pp. 172-174, 1994.
5. C.E. McIntosh, R.D. Pollard, and R.E. Miles, Novel MMIC source-impedance tuners for on-wafer microwave noise-parameter measurements, *IEEE Transactions on Microwave Theory and Techniques*, vol. 47, no. 2, 1999, pp. 125-131.
6. H.-T. Kim, S. Jung, K. Kang, J.-H. Park, Y.-K. Kim, and Y. Kwon, Low-loss analog and digital micromachined impedance tuners at the Ka-band, *IEEE Transactions on Microwave Theory and Techniques*, vol. 49, no. 11, 2001, pp. 2394-2400.
7. J. Papapolymerou, K. L. Lange, C. L. Goldsmith, A. Malczewski, and J. Kleber, Reconfigurable double-stub tuners using MEMS switches for intelligent RF front-ends, *IEEE Transactions on Microwave Theory and Techniques*, vol. 51, 2003, pp. 271-278.
8. R. E. Collin, *Foundations for Microwave Engineering*, 2<sup>nd</sup> edition, New York, McGraw-Hill, 1992.
9. T. Vähä-Heikkilä, J. Varis, J. Tuovinen, and G.M. Rebeiz, A reconfigurable 6-20 GHz RF MEMS impedance tuner, *IEEE MTT-S International Microwave Symposium digest*, Forth Worth, TX, USA, 2004, pp. 729-732.
10. T. Vähä-Heikkilä, and G.M. Rebeiz, A 20-50 GHz reconfigurable matching network for power amplifier applications, *IEEE MTT-S International Microwave Symposium digest*, Forth Worth, TX, USA, 2004, pp. 717-721.
11. T. Vähä-Heikkilä and G.M. Rebeiz, A 4-18 GHz reconfigurable RF MEMS matching network for power amplifier applications, *International Journal of RF and Microwave Computer-Aided Engineering*, " vol. 14, no. 6, 2004, pp. 356-372.
12. Q. Shen and N.S. Barker, A reconfigurable RF MEMS based double slug impedance tuner, *Proceedings of the 35th European Microwave Conference*, Paris, France, 2005, pp. 537-540.
13. J. B. Rizk, W-band RF MEMS Switches, Phase Shifters and Antennas, Ph.D. dissertation, Dept. Elect. Eng. Univ. of Michigan at Ann Arbor, MI, 2003.
14. S. Van den Bosch and L. Martens, Improved impedance-Pattern Generation for Automatic Noise-Parameter Determination, *IEEE Transactions on Microwave Theory and Techniques*, vol. 46, no. 11, 1998, pp. 1673-1678.
15. L. Dussopt and G.M. Rebeiz, Intermodulation distortion and power handling in RF MEMS switches, varactors and tunable filters, *IEEE Transactions on Microwave Theory and Techniques*, vol. 51, no. 4, 2003, pp. 1247-1256.
16. G.M. Rebeiz, *RF MEMS: Theory, Design, and Technology*, John Wiley & Sons, New York, 2003.
17. T. Vähä-Heikkilä, J. Varis, J. Tuovinen, and G.M. Rebeiz, A 20-50 GHz RF MEMS single-stub impedance tuner, *IEEE Microwave and Wireless Components Letters*, vol. 15, no. 4, 2005, pp. 205-207.
18. T. Vähä-Heikkilä, J. Varis, J. Tuovinen, and G.M. Rebeiz, A V-band single-stub RF MEMS impedance tuner, *Proceedings of the 34th European Microwave Conference*, Amsterdam, Netherlands, 2004, pp. 1301-1304.
19. T. Vähä-Heikkilä, J. Varis, J. Tuovinen, and G.M. Rebeiz, W-band RF MEMS double- and triple-stub impedance tuners, *IEEE MTT-S International Microwave Symposium 2005*, Long Beach, CA, June 2005, pp. 923-926.

PUBLICATION P4

**A 20–50 GHz RF MEMS  
Single-Stub Impedance tuner**

In: IEEE Microwave and Wireless Components Letters 2005.  
Vol. 15, No. 4, pp. 205–207.

© 2005 IEEE. Reprinted with permission from the publisher.

# A 20–50 GHz RF MEMS Single-Stub Impedance Tuner

T. Vähä-Heikkilä, J. Varis, J. Tuovinen, and G. M. Rebeiz

**Abstract**—A novel radio-frequency (RF) microelectromechanical system (MEMS) single-stub impedance tuner has been developed. The design is based on combining the loaded line technique with the single-stub topology to obtain wide impedance coverage with high  $|\Gamma_{MAX}|$ . The tuner consists of ten switched MEMS capacitors producing 1024 ( $2^{10}$ ) different impedances. The design has been optimized for noise parameter and load-pull measurements of active devices and shows excellent measured impedance coverage over the 20–50 GHz frequency range.

**Index Terms**—Impedance tuner, load-pull, matching network, multiband, noise parameters, radio-frequency (RF) microelectromechanical system (MEMS).

## I. INTRODUCTION

IMPEDANCE tuners are needed in noise parameter (NP) and load-pull measurements of active devices and are currently built using coaxial or waveguide structures [1]. However, integrated tuners can be assembled inside an radio-frequency (RF) probe minimizing the loss between the tuner and a device under test. Integrated tuners are based on the double-stub [2] or triple-stub topologies [3], and can be made using GaAs or RF microelectromechanical system (MEMS) devices. A problem related to GaAs tuners is limited impedance coverage because of the resistance of active devices. In [4], we presented a distributed-type 20–50 GHz matching network which was optimized for power (PA) amplifier applications. In this case, the loss is minimized and the impedance coverage is designed to address the low impedance of PAs. In contrast, tuners in NP measurements must have wide impedance coverage with high reflection coefficients, and the loss of a tuner is not critical. This letter presents a tuner optimized for NP measurement purposes. The tuner is built using a combination of loaded-line techniques and a single-stub providing high reflection coefficients, and results in a wide impedance coverage area from 20 to 50 GHz.

## II. DESIGN OF THE SINGLE-STUB IMPEDANCE TUNER

Standard single-stub tuners result in a limited impedance coverage area and are not useful, but on the other hand, the stub-topology is beneficial since it can provide high reflection coefficients. The design presented here is based on variable loaded-

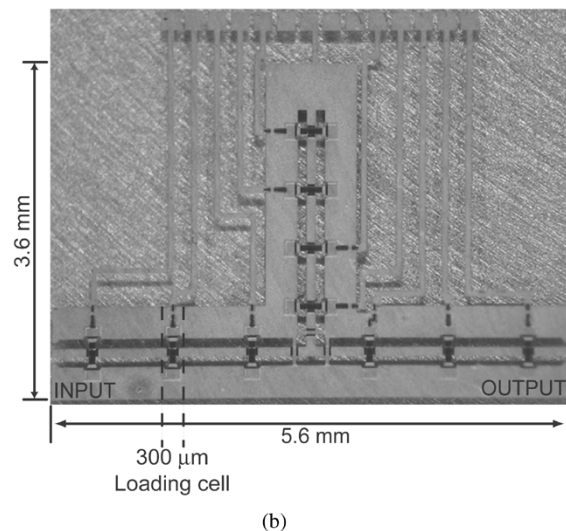
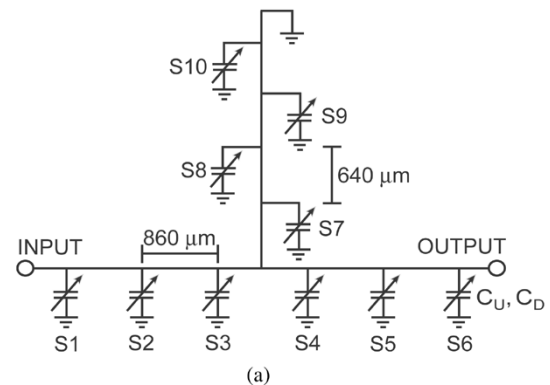


Fig. 1. (a) Circuit diagram and (b) photograph of the fabricated 20–50 GHz single-stub impedance tuner based on ten switched capacitors.

lines which are added before and after the single stub (Fig. 1). The impedance and electrical length of the loaded lines and of the single stub are controlled at discrete positions by digital-type RF MEMS capacitors.

The single-stub tuner can be designed by optimizing several key parameters. The number of the switched capacitors ( $N$ ) and their capacitance values ( $C_U, C_D$ ) have the most important effect on the tuning range and bandwidth. In general, a larger  $N$  yields more wide-band operation and better impedance coverage but results in an increased component size and loss. Other parameters that need to be optimized are the spacing of the switched capacitors ( $s$ ) and the length of the stub. There are many variables and different acceptable solutions, and Agilent ADS<sup>1</sup> is used to for the optimization procedure.

<sup>1</sup>Advanced Design System 2002, Agilent Technologies, Santa Clara, CA, 2002.

Manuscript received July 12, 2004; revised November 17, 2004. This work was supported by MilliLab under ESA/ESTEC Contract 1655/95/NL/MV, and by the DARPA IRFFE Program, University of Michigan. The review of this letter was arranged by Associate Editor A. Weisshaar.

T. Vähä-Heikkilä and G. M. Rebeiz are with The University of Michigan, Ann Arbor, MI 48109-2122 USA.

J. Varis and J. Tuovinen are with VTT Information Technology, MilliLab, VTT FIN-02044, Finland.

Digital Object Identifier 10.1109/LMWC.2005.845690

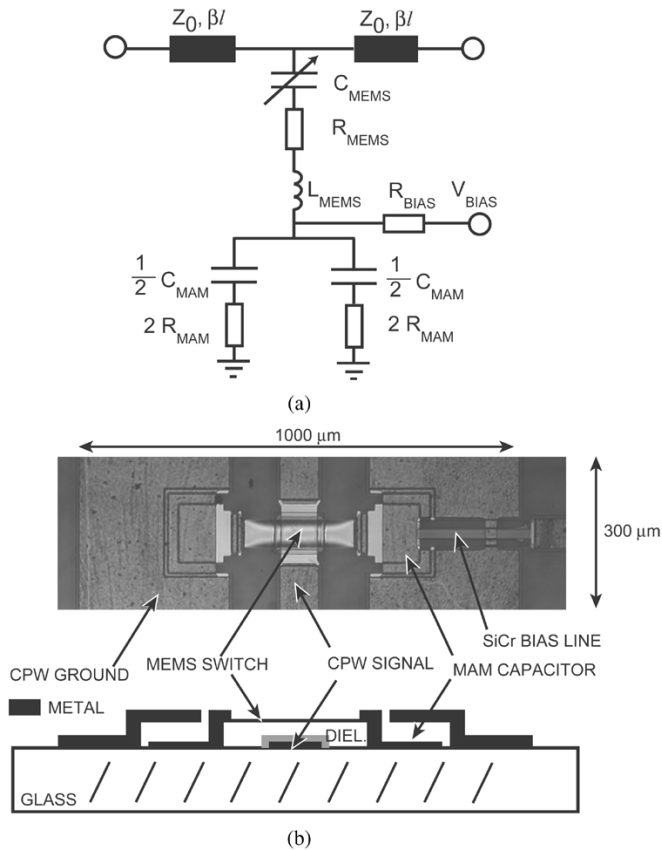


Fig. 2. (a) Equivalent circuit and (b) picture with cross-sectional view of a switched MEMS capacitor (unit cell in tuner design).

In general, it is found that for a glass substrate ( $\epsilon_r = 4.6$ ,  $\epsilon_{\text{reff}} = (1 + \epsilon_r)/2 = 2.8$ ) with  $Z_0 = 87 \Omega$  (100/100/100 CPW line), a capacitance ratio around 2.5 is best for wide impedance coverage ( $C_U = 52$  fF,  $X_U = -j100 \Omega$ , and  $C_D = 138$  fF,  $X = -j38 \Omega$ , at 30 GHz). The loading cell dimension ( $lc$ ) is around  $300 \mu\text{m}$ , and the localized impedance and effective dielectric constant of each cell are  $Z_U = 45 \Omega$ ,  $\epsilon_{\text{reff}U} = 10.1$ , and  $Z_D = 30 \Omega$ ,  $\epsilon_{\text{reff}D} = 22.3$  [5] in the up- and down-state positions of the capacitors. The loading cells are placed  $s_1 = 860 \mu\text{m}$  and  $s_2 = 640 \mu\text{m}$  apart in the t-line and stub, respectively. It is important to note that there are many different values of  $C_U$ ,  $C_D$ ,  $lc$ ,  $s_1$ , and  $s_2$ , which yield excellent impedance coverage due to flexible nature of this design. The values chosen above are a compromise between 20 GHz (high capacitance values, large  $s$ ), and 50 GHz (low capacitance values, small  $s$ ). The quality factor of the switched MEMS capacitor is calculated with  $Q = (2\pi f C (R_{\text{MEMS}} + R_{\text{MAM}}))^{-1}$  resulting  $Q_U = 146$  and  $Q_D = 55$  at 30 GHz in up and down states. This means that the switched capacitors do not contribute a lot of loss to the tuner circuit.

### III. FABRICATION AND MEASUREMENT

The switched capacitor ( $C_U, C_D$ ) is a combination of a capacitive MEMS switch ( $C_{\text{MEMS}}$ ) attached to fixed metal-air-metal (MAM) capacitors ( $C_{\text{MAM}}$ ) (Fig. 2) and the fabrication process is well described in [5]. Note that in this design, the dielectric thickness is  $3000 \text{ \AA}$ , and the capacitance

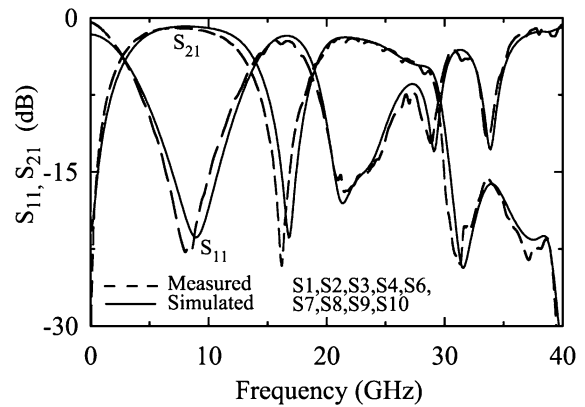


Fig. 3. Measured and simulated  $S$ -parameters for the reconfigurable single-stub impedance tuner when switches S1, S2, S3, S9, and S10 are in the down-state position.

TABLE I  
MEASURED T-LINE PROPERTIES FROM THE TRL CALIBRATION AND FITTED VALUES FOR THE SWITCHED MEMS CAPACITOR

$Z_0 (\Omega)$ ,	87
$\epsilon_{\text{reff}}$	2.72
$\alpha$ (dB/cm), 20/30/40 GHz	0.52/0.78/1.1
$C_{\text{MEMS}}$ Up State (fF)	74
$C_{\text{MEMS}}$ Down State (fF)	683
$C_{\text{MAM}}$ (fF)	173
$R_{\text{BIAS}}$ (k $\Omega$ )	> 3
$L_{\text{MEMS}}$ (pH)	13.5
$R_{\text{MEMS}} + R_{\text{MAM}}$ ( $\Omega$ )	0.7

ratio of the MEMS switch is only 9.3. This is acceptable since the final capacitance ratio is 2.5.

The measured and simulated (with Agilent ADS)  $S$ -parameters with half of the switches in the down-state and half in the up-state are shown in Fig. 3 (see also Table I). This shows that the t-line model predicts very accurately the behavior of the circuit over a wide frequency range.

### IV. IMPEDANCE COVERAGE

The single-stub tuner has ten switched capacitors producing 1024 ( $2^{10}$ ) different impedances. Measured (160 points) and simulated (1024 points) impedance coverage at different frequencies are shown in Fig. 4 with  $50 \Omega$  input and output terminations. There is a good one-to-one correspondence in the measured and simulated data, but this is not shown due to the number of points on the Smith chart. From the 160 measured points, the measured  $|\Gamma_{\text{MAX}}|$  is 0.86, 0.88, 0.94 at 20, 30, and 40 GHz.

The single-stub tuner can be used as a reflection type tuner with an open or short-circuited output port. The simulated impedance coverage of the tuner with open circuit termination at the output port is shown in Fig. 5. Notice the near circular and complete coverage of the Smith chart from 15 to 45 GHz. This is excellent for transistor and low noise amplifier characterization.

The single-stub impedance tuner can also be used as a matching network. However, for this application, the authors recommend the distributed-type matching networks due to their smaller size and lower loss [4], [5].

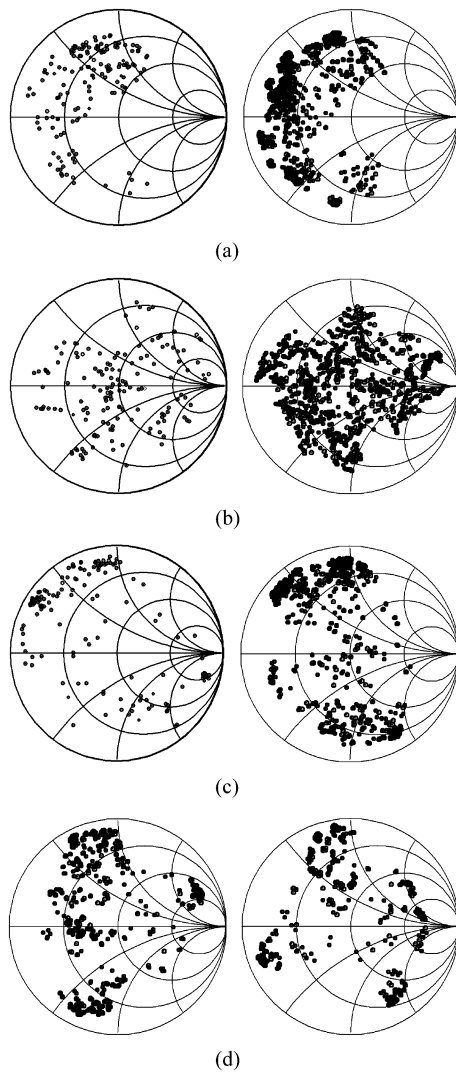


Fig. 4. Measured (160 points) and simulated (1024 points) impedance coverage of the single-stub impedance tuner. (a) Measured 20 GHz, simulated 20 GHz. (b) Measured 30 GHz, simulated 30 GHz. (c) Measured 40 GHz, simulated 40 GHz. (d) Measured 44 GHz, simulated 48 GHz.

## V. CONCLUSION

This letter presented a novel impedance tuner for 20–50 GHz noise parameter and load pull measurements of active devices. The tuner is based on a single stub and two loaded-lines. The tuner has better impedance coverage than any previously published integrated impedance tuner at this frequency range. The results indicated that this design is quite competitive with

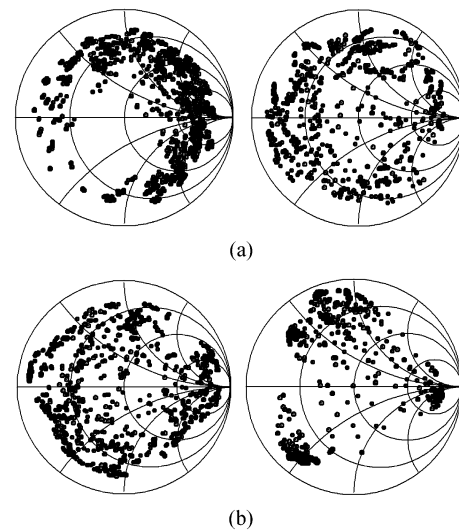


Fig. 5. Simulated (1024 points) impedance coverage of the tuner when the output is terminated with an open circuit. (a) Simulated 15 GHz, simulated 25 GHz. (b) Simulated 35 GHz, simulated 45 GHz.

coaxial and waveguide based tuners and can be integrated inside an RF probe.

## ACKNOWLEDGMENT

The authors wish to thank K. Van Caekenberghe, University of Michigan, for developing the multiport high-voltage bias network.

## REFERENCES

- [1] M. Kantanen, M. Lahdes, T. Vähä-Heikkilä, and J. Tuovinen, "A wide-band automated measurement system for on-wafer noise parameter measurements at 50–75 GHz," *IEEE Trans. Microw. Theory Technol.*, vol. 51, no. 5, pp. 1489–1495, May 2003.
- [2] H.-T. Kim, S. Jung, K. Kang, J.-H. Park, Y.-K. Kim, and Y. Kwon, "Low-loss analog and digital micromachined impedance tuners at the Ka-Band," *IEEE Trans. Microw. Theory Technol.*, vol. 49, no. 12, pp. 2394–2400, Dec. 2001.
- [3] T. Vähä-Heikkilä, J. Varis, J. Tuovinen, and G. M. Rebeiz, "A 6–20 GHz reconfigurable RF MEMS impedance tuner," in *IEEE MTT-S Int. Dig.*, Forth Worth, TX, 2004, pp. 729–732.
- [4] T. Vähä-Heikkilä and G. M. Rebeiz, "A 20–50 GHz reconfigurable matching network for power amplifier applications," in *IEEE MTT-S Int. Dig.*, Forth Worth, TX, 2004, pp. 717–721.
- [5] —, "A 4–18 GHz reconfigurable RF MEMS matching network for power amplifier applications," *Int. J. RF Microw. Comput.-Aided Eng.*, vol. 14, pp. 356–372, Jul. 2004.

PUBLICATION P5

# **A V-Band Single-Stub RF MEMS Impedance Tuner**

In: Proceedings of the 34th European Microwave Conference,  
Amsterdam, Netherlands, 2004.

Pp. 1301–1304.

Reprinted with permission from the European Microwave  
Association.

# A V-Band Single-Stub RF MEMS Impedance Tuner

Tauno Vähä-Heikkilä<sup>1,2</sup>, Jussi Varis<sup>2</sup>, Jussi Tuovinen<sup>2</sup> and Gabriel M. Rebeiz<sup>1</sup>

<sup>1</sup>University of Michigan, Ann Arbor, USA, Tel. +1 734 647 1793

<sup>2</sup>MilliLab, VTT Information Technology, Espoo, Finland, Tel. +358 9 456 7219

**Abstract** — A V-Band reconfigurable single-stub impedance tuner has been developed which is suitable to be integrated inside an RF probe. The tuner has 10 RF MEMS switched capacitors producing 1024 ( $2^{10}$ ) different impedances. The tuner is the first published integrated V-Band impedance tuner having good impedance coverage for the whole 50 to 75 GHz frequency range with a measured of  $|\Gamma_{\text{MAX}}| = 0.90$  at 60 GHz. Measurement results verifying the tuner performance are presented.

## I. INTRODUCTION

Impedance tuners are used in noise parameter and load-pull measurements of transistors and amplifiers. Tuners are typically waveguide components at V-Band (50-75 GHz) or W-Band (75-110 GHz) and they are tuned either with motorized [1] or manual [2] methods. Usually in on-wafer measurement, mechanical tuners have to be placed electrically far away from a device under test (DUT) in measurement set-ups because they are large in size. This limits the maximum achievable reflection coefficient and the accuracy of the measurements. In addition to measurement applications, impedance tuners can be used as reconfigurable matching networks for power amplifiers (PA) and antennas.

Both MMIC [3] and RF MEMS [4,5] based integrated matching networks and impedance tuners have been published previously for lower frequencies. We have presented a novel capacitive loading based tuning method for impedance tuners and applied it to X-Band triple-stub impedance tuners [5]. The electrical length of stubs and distance between them were tuned with switched RF MEMS capacitors. Using  $N$  (number of switched capacitors) switched capacitors it is possible to get  $2^N$  different impedances. This method was applied for the designing of a reconfigurable V-Band single-stub tuner. In this work, we show that it is possible to achieve wideband good Smith chart coverage with the single-stub topology.

## II. TUNER DESIGN AND FABRICATION

Impedance coverage and maximum achievable reflection coefficient are important design issues in impedance tuner design. A switched capacitor is used as a unit cell for the designing of the single-stub tuner. Several parameters affect to the design of impedance tuners. The number and capacitance values of the switched capacitors have the most important effect to the tuning range and bandwidth of the tuner. Other selectable parameters are the spacing of the switched capacitors ( $s$ ), transmission

line properties ( $Z_0$ ,  $\epsilon_{\text{reff}}$ ), and the lengths of the stubs. The switched MEMS capacitor is a series combination of a capacitive RF MEMS switch and fixed MAM (metal-air-metal) capacitors. Fig. 1 shows a fabricated MEMS switched capacitor with cross-sectional view and the equivalent circuit. It is based on a coplanar waveguide (CPW) transmission line having dimensions of 60/60/60  $\mu\text{m}$  on a glass substrate. The component values are presented in Table 1. The switched capacitors has up and down-state capacitances  $C_U = 31$  fF and  $C_D = 101$  fF resulting  $X_U = -j86 \Omega$  and  $X_D = -j26 \Omega$  at 60 GHz. The quality factor of the switched MEMS capacitor is calculated with  $Q = (2\pi f C (R_{\text{MEMS}} + R_{\text{MAM}}))^{-1}$ , and results in up and down states values of  $Q_U = 144$  and  $Q_D = 44$  at 60 GHz, respectively.

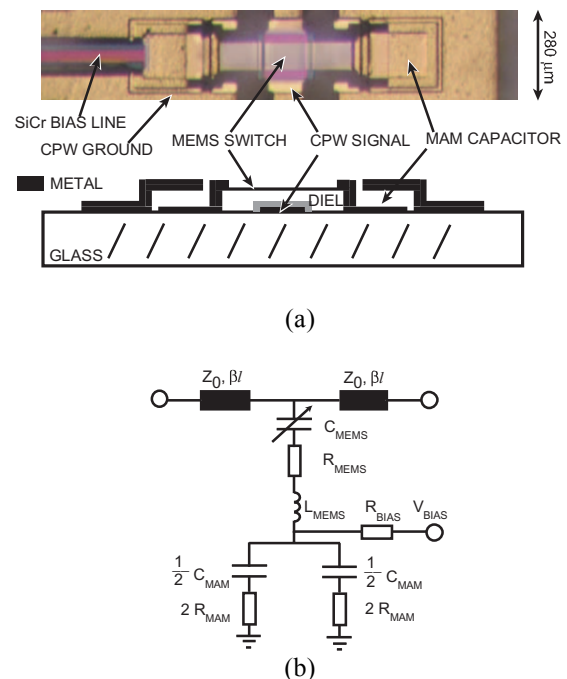


Fig. 1. a) A photograph and a cross-sectional view of the V-Band switched capacitor. b) Equivalent circuit of the switched capacitors.

Dimensions of the titanium/gold/titanium ( $100\text{\AA}/8000\text{\AA}/300\text{\AA}$ ) MEMS switch are  $250 \mu\text{m} \times 60 \mu\text{m} \times 0.84 \mu\text{m}$ , and it is suspended  $1.3 \mu\text{m}$  above the transmission line. A  $2000 \text{\AA}$  silicon nitride layer was used as a dielectric interlayer. The fabrication process is based on standard techniques and is described in [4]. The circuit is electroplated to  $3 \mu\text{m}$  thickness (except the MEMS bridges) to reduce the t-line and MAM capacitor loss.

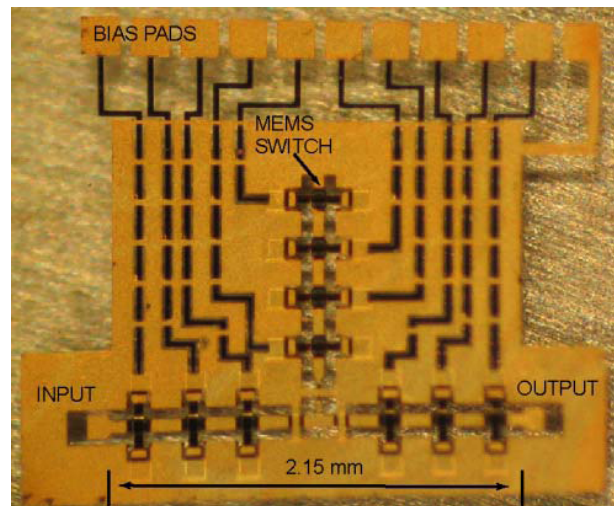
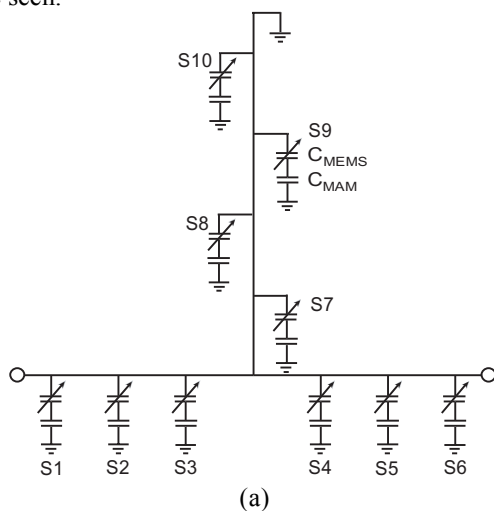
SiCr bias lines with resistance of  $700 \Omega/\text{square}$  are used for actuating the MEMS switches. The measured pull-down voltage was  $22 \text{ V}$ , and a bipolar actuation voltage of  $\pm 35 \text{ V}$  was used for obtaining an excellent metal-to-dielectric contact in the down-state position, and to avoid charging of the dielectric layer.

$\epsilon_r$	4.6
$Z_0 (\Omega)$	86
$\epsilon_{\text{reff}}$	2.72
$\alpha (\text{dB/cm})$ at 60 GHz	1.5
$C_{\text{MEMS}}$ Up-State (fF)	42
$C_{\text{MEMS}}$ Down-State (fF)	800
$C_{\text{MAM}}$ (fF)	116
$R_{\text{BIAS}}$ (k $\Omega$ )	> 3
$L_{\text{MEMS}}$ (pH)	9.5
$R_{\text{MEMS}} + R_{\text{MAM}}$ ( $\Omega$ )	0.6

TABLE I

FITTED VALUES FOR THE SWITCHED MEMS CAPACITOR

The T-junction in the tuner was simulated with Sonnet EM Suite [6]. Its S-parameters with the equivalent circuits of the switched capacitors were used in Agilent ADS [7] for simulating the S-parameters of the tuner. The single-stub design was optimised using Agilent ADS to get as large tuning range and bandwidth as possible with the minimum number of switched MEMS capacitors. Larger amount of switched capacitors yields better Smith chart coverage and more possible impedances since  $N$  switched capacitors produce  $2^N$  different impedances. On the other hand, control system for the tuner comes more complicated and characterization of the tuner is more time consuming. The single-stub tuner was optimized to have 10 switched capacitors producing 1024 ( $2^{10}$ ) different impedances. Spacing between the switched capacitors,  $s$ , is  $280 \mu\text{m}$  in the sections before and after the stub (S1,S2,S3,S4,S5,S6) and  $260 \mu\text{m}$  in the stub (S7,S8,S9,S10). The schematic and photograph of the fabricated tuner are shown in Fig. 2. Measured and simulated S-parameters of the tuner with two different switch setting are presented in Fig. 3. Good agreement can be seen.



(b)

Fig. 2. a) Schematics of the V-Band single-stub tuner. Switched capacitors S1-S10 are used for producing 1024 ( $2^{10}$ ) different impedances. b) Photograph of the fabricated V-Band single-stub tuner.

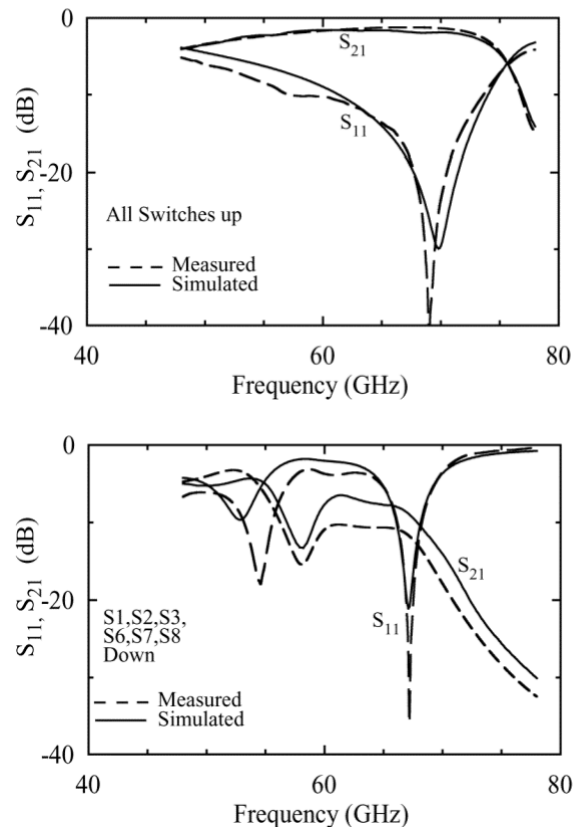


Fig. 3. Measured and simulated S-parameters of the single-stub tuner when all of the MEMS switches are in the up-state and when S1, S2, S3, S6, S7, and S8 are in the down-state.

### III. IMPEDANCE COVERAGE

The measured (90) and simulated (1024) impedance points of the single-stub tuner are presented in Fig. 4 at V-Band. In this case, a  $50 \Omega$  load was placed at the output port, and the input reflection coefficient was measured with different switches actuated into the down-state position. The circuit model was used for simulating

all possible switch combinations. The tuner can be used as a reflection type impedance tuner when the output is terminated with an open circuit, and simulated impedance coverage for the single-stub tuner is shown in Fig. 5. The tuner has good impedance coverage over the whole V-Band with 50  $\Omega$  terminations and can be used in noise parameter measurements at 40-80 GHz when the output is terminated with an open circuit.

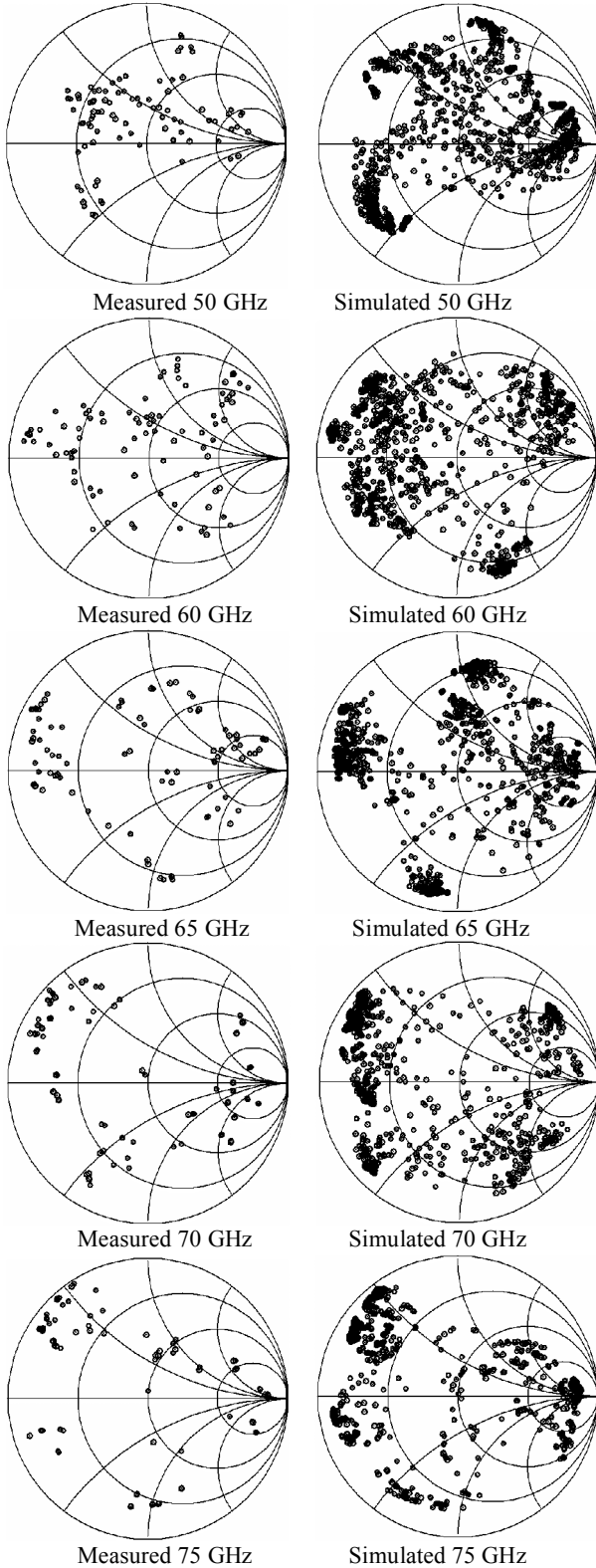


Fig. 4. Measured (90 points) and simulated (1024) impedance coverage of the V-Band single-stub impedance tuner.

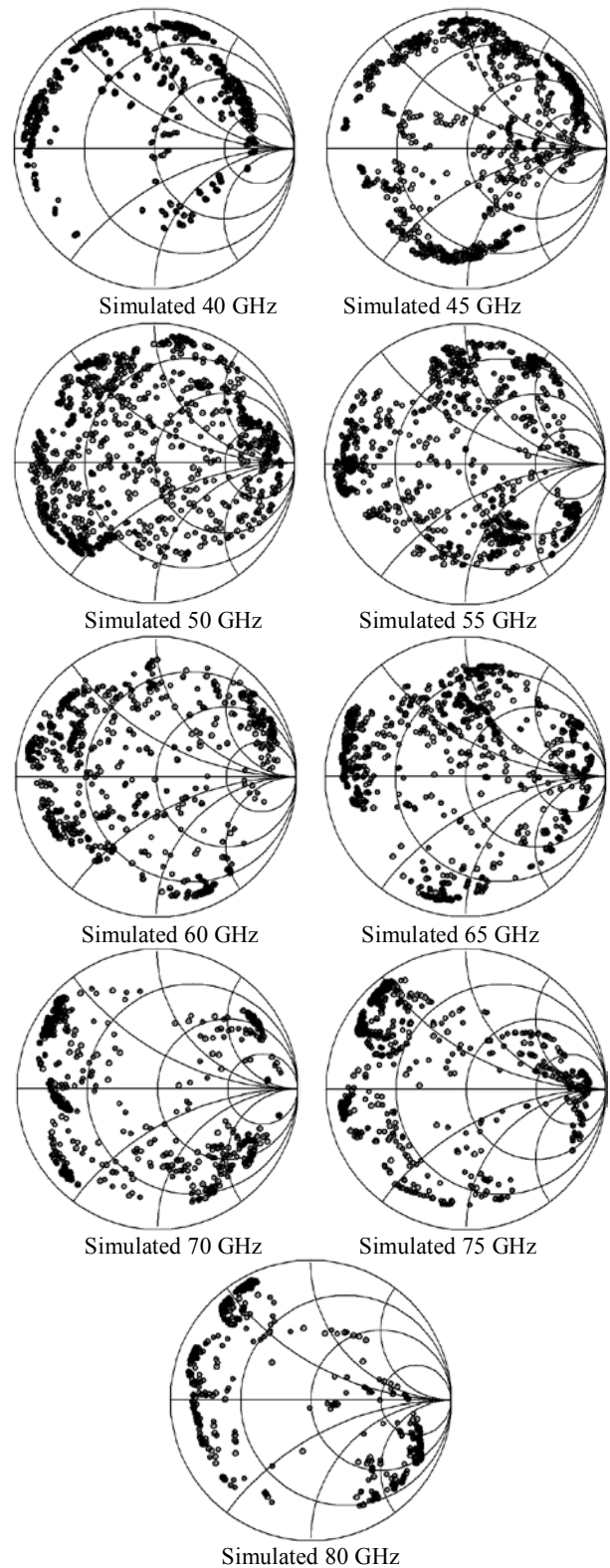


Fig. 5. Simulated (1024 points) impedance coverage of the V-Band single-stub impedance tuner when the output is terminated with an open circuit.

In addition to good impedance coverage, it is beneficial to have reflection coefficients with high amplitude. The highest measured reflection coefficients  $|\Gamma_{MAX}|$  (from 90 measurements) at different frequencies are shown in Table 2. Measured  $|\Gamma_{MAX}|$  was better than 0.9 at 60 GHz and above. It should be noted that less than 10 % of all impedances were measured, and it is expected to have

higher reflection coefficients especially at the lower frequency part of the V-Band. Highest achievable reflection coefficient at the probe tip with mechanical waveguide based impedance tuner is about 0.8 at V-Band [1] and 0.7 at W-Band [2]. If the single-stub tuner is integrated inside an RF probe the loss between the tuner and probe tip can be minimized. Based on the measured  $|\Gamma_{MAX}|$  values of the single-stub tuner, higher reflection coefficients are expected to get at the probe tip compared to the waveguide tuners.

f (GHz)	$ \Gamma_{MAX} $
50	0.81
55	0.80
60	0.90
65	0.94
70	0.97
75	0.97
78	0.99

TABLE II  
MEASURED (90 IMPEDANCES OUT OF TOTAL 1024 POSSIBLE) MAXIMUM REFLECTION COEFFICIENTS  $|\Gamma_{MAX}|$  OF THE SINGLE-STUB IMPEDANCE TUNER.

## VI. CONCLUSION

A novel impedance tuner for V-Band noise parameter and load-pull measurement applications was presented. The tuner is based on a single-stub topology and 10 switched RF MEMS capacitors producing 1024 ( $2^{10}$ ) different impedances. The tuner is the first integrated V-Band impedance tuner. Measured and simulated performance over the 50 to 75 GHz range were presented showing excellent impedance coverage over the whole band and  $|\Gamma_{MAX}|$  better than 0.90 at 60 GHz and above.

## ACKNOWLEDGEMENT

This work has been supported by the ESA/ESTEC contract no. 1655/95/NL/MV at MilliLab, VTT, and by the DARPA IRFFE program at the University of Michigan.

## REFERENCES

- [1] M. Kantanen, M. Lahdes, T. Vähä-Heikkilä, J. Tuovinen, "A wideband automated measurement system for on-wafer noise parameter measurements at 50-75 GHz", *IEEE Transactions on Microwave Theory and Techniques*, vol. 51, pp. 1489-1495, June 2003.
- [2] T. Vähä-Heikkilä, M. Lahdes, M. Kantanen, J. Tuovinen, "On-wafer noise parameter measurements at W-band", *IEEE Transactions on Microwave Theory and Techniques*, vol. 51, pp. 1621-1628, June, 2003.
- [3] M. Pierpoint, Roger. D. Pollard, J.R. Richardson, "An Automated Measurement Technique for Measuring Amplifier Load-Pull and Verifying Large-Signal Device Models", *IEEE MTT-S International Microwave Symposium digest*, Volume: 86, Baltimore Maryland, pp. 625 - 628 June 1986.
- [4] T. Vähä-Heikkilä, G. M. Rebeiz, "A 4-18 GHz reconfigurable RF MEMS matching network for power amplifier applications," RF MEMS special issue in *International Journal of RF and Microwave Computer-Aided Engineering*, " vol. 14, pp. 356-372, July, 2004.
- [5] T. Vähä-Heikkilä, J. Varis, J. Tuovinen, G. M. Rebeiz, "A 6-20 GHz Reconfigurable RF MEMS Impedance Tuner," *IEEE MTT-S International Microwave Symposium digest*, Forth Worth, TX, pp. 729-732, 2004.
- [6] Sonnet EM Suite, Sonnet Software Inc., Liverpool, NY, USA, Release 6.0a, 1998.
- [7] Advanced Design System 2002, Agilent Technologies, Santa Clara, CA, USA, 2002.

PUBLICATION P6

## **W-Band RF MEMS Double and Triple-Stub Impedance Tuners**

In: 2005 IEEE MTT-S International Microwave Symposium  
Digest, Long Beach, CA, USA, 2005.  
Pp. 923–926.

© 2005 IEEE. Reprinted with permission from the publisher.

# W-Band RF MEMS Double and Triple-Stub Impedance Tuners

T. Vähä-Heikkilä<sup>1,2</sup>, J. Varis<sup>2</sup>, J. Tuovinen<sup>2</sup> and G. M. Rebeiz<sup>1</sup>

<sup>1</sup>The University of Michigan, Ann Arbor, MI, 48109-2122, USA

<sup>2</sup>MilliLab, VTT Information Technology, P.O. Box 12021, 02044 VTT, Finland

**Abstract** — Reconfigurable integrated impedance tuners have been developed for W-Band on-wafer noise parameter and load-pull measurement applications. The impedance tuners are based on double and triple-stub topologies and employ 11 switched MEMS capacitors producing 2048 ( $2^{11}$ ) different impedances. Measured  $|\Gamma_{\text{MAX}}|$  for the double-stub tuner is 0.92 and 0.82 at 75 and 100 GHz from 110 measurements out of 2048 possible impedances, and 0.92 and 0.83 for the triple-stub tuner. To our knowledge, this represents the first W-band integrated impedance tuner to date.

**Index Terms** — RF MEMS, impedance tuner, matching network, noise parameter, load-pull, on-wafer.

## I. INTRODUCTION

Impedance tuners based on waveguides are used at frequencies above 50 GHz in noise parameter and load-pull measurements of active devices. In practice, these are large in size and expensive. The maximum achievable reflection coefficient,  $|\Gamma_{\text{MAX}}|$ , which can be generated using waveguide tuners is very high (about 0.97) but this is referred to the waveguide flange. For on-wafer measurements, the loss of the connecting waveguide sections and W-band-to-CPW probe can limit  $|\Gamma_{\text{MAX}}|$  to about 0.7-0.8 at 50-110 GHz [1,2]. If a tuner can be integrated inside an RF probe, the loss between the tuner and the DUT can be minimized. Also, measurement automation can be increased with electrically controllable tuners.

In this work, we present the first integrated impedance tuners operating at W-Band (75-110 GHz). The impedance tuners are based on double- and triple-stub topologies and switched MEMS capacitors. The MEMS switches are used since they provide excellent performance compared to mm-wave transistors or varactor diodes [3].

## II. IMPEDANCE TUNER DESIGN

The impedance and electrical length of the stubs and connecting t-line are controlled at discrete positions by digital-type RF MEMS capacitors (Fig. 1) as done previously in [4-6]. This method results in more wideband tuning and better impedance coverage compared to standard reconfigurable impedance tuners [7,8]. In the switched capacitor-based tuner, the number of the switched capacitors ( $N$ ) and their capacitance values ( $C_U$ ,  $C_D$ ) have the most important effect on the tuning range and bandwidth. In general, a larger  $N$  yields

more wideband operation and better impedance coverage but results in an increased component size and loss. Other parameters that need to be optimized are the spacing of the switched capacitors and the lengths of the stubs. There are many variables and several acceptable solutions. The tuners were optimized to have 11 switched capacitors producing 2048 ( $2^{11}$ ) different impedances, and Agilent ADS,<sup>1</sup> was used to for the optimization procedure. The fabricated impedance tuners are shown in Fig. 2, and the process is similar to [4-6] having the same materials and layer thicknesses.

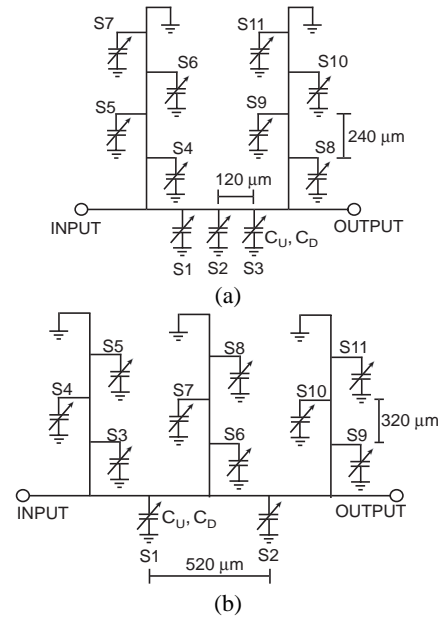


Fig. 1. a) Schematic a of the reconfigurable W-Band double-stub and b) triple-stub impedance tuners.

The switched capacitor is a series combination of a MEMS switch and metal-air-metal (MAM) capacitors (Fig. 3). The size of the MEMS switch is  $200 \mu\text{m} \times 40 \mu\text{m} \times 0.9 \mu\text{m}$  and the area of the fixed MAM capacitor is  $280 \mu\text{m}^2$ , respectively. The MAM capacitors are realized as a part of the anchor area of the MEMS switch. These are electroplated to  $3 \mu\text{m}$ , and being very stiff, they are not actuated with the bias voltage. The CPW dimensions are  $50/50/50 \mu\text{m}$  (G/W/G) and under the MEMS switches  $45/90/45 \mu\text{m}$  in both designs. The center

<sup>1</sup> Advanced Design System 2002, Agilent Technologies, Santa Clara, CA, USA, 2002.

conductor was widened under the MEMS switches for a lower pull-down voltage. Measured pull-down voltage was 28 V, and a 36 V bipolar actuation was used for getting a firm down-state contact and avoiding charging in the dielectric layer.

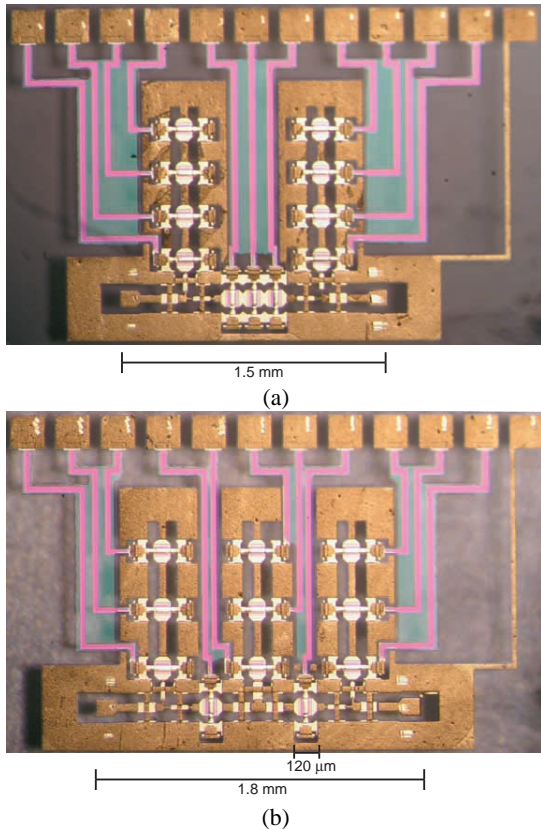


Fig. 2. a) Photograph of the fabricated W-Band double-stub and b) triple-stub impedance tuners.

TABLE I

FITTED VALUES FOR THE SWITCHED MEMS CAPACITOR.

$C_{MEMS}$ Up-State (fF)	24
$C_{MEMS}$ Down-State (fF)	410
$C_{MAM}$ (fF)	52
$R_{BIAS}$ (k $\Omega$ )	> 3
$L_{MEMS}$ (pH)	6
$R_{MEMS} + R_{MAM}$ ( $\Omega$ )	0.7

The switched MEMS capacitor total up and down-state capacitances are  $C_U = 23$  fF and  $C_D = 46$  fF ( $X_U = -j78 \Omega$  and  $X_D = -j39 \Omega$  at 90 GHz), which results in total capacitance ratio of 2.0. Previous lower frequency designs employed a capacitance ratio of 3.5-4.5 for the entire coverage of the Smith Chart [4-6]. The quality factor of the switched MEMS capacitor is calculated using  $Q = (2\pi f C (R_{MEMS} + R_{MAM}))^{-1}$  and results in  $Q_U = 111$  and  $Q_D = 54$  at 90 GHz. This means that the switched capacitors do not contribute a lot to the loss of the tuner circuit. Measured and simulated S-parameters for the tuners are shown in Fig. 4. The T-junctions were simulated

with Sonnet<sup>2</sup>, and the S-parameters for the tuners with Agilent ADS using the equivalent circuits of the switched capacitors (Figs. 3 and 4, and Table I).

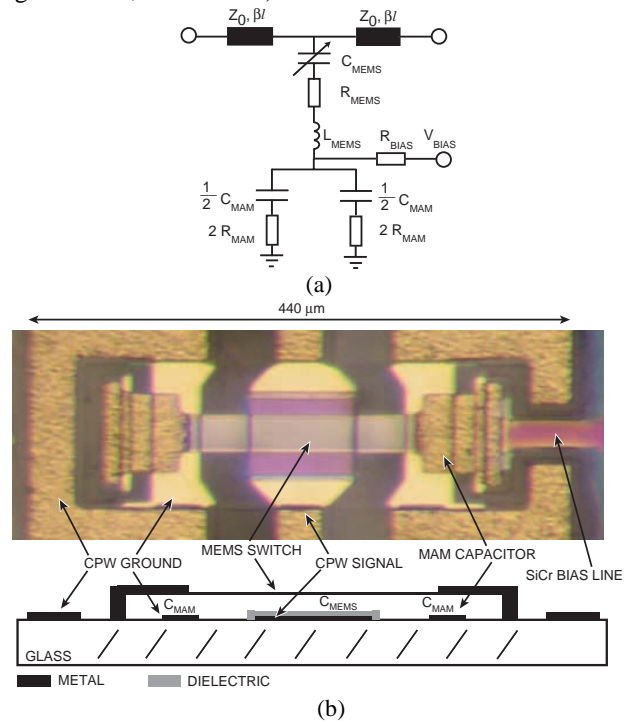


Fig. 3. a) Circuit model and b) photograph with schematic side-view of the W-Band switched capacitors.

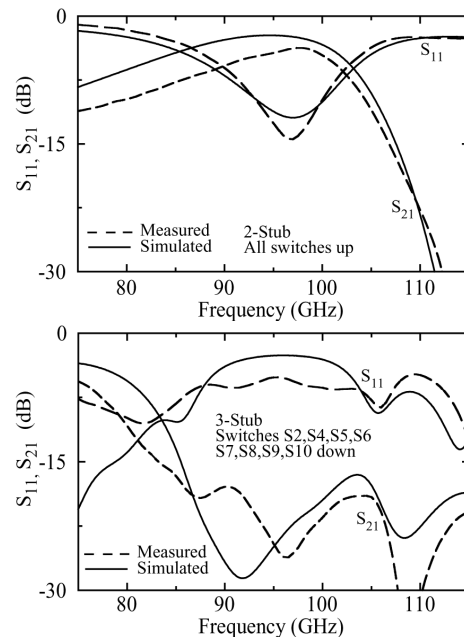


Fig. 4. Measured and simulated S-parameters for the double-stub tuner when all of the switches are in the up-state position and for the triple-stub tuner when switches S2, S4, S5, S6, S7, S8, S9, S10 are in the down-state position.

<sup>2</sup> Sonnet, ver. 8.52, Sonner Software Inc., Syracuse, NY, 1986-2001.

### III. IMPEDANCE COVERAGE

The tuners can produce 2048 ( $2^{11}$ ) different impedances. Measured (110 points for the 2-stub tuner, and 90 for the 3-stub) and simulated (all 2048 points) impedance coverage for the tuners are shown in Figs. 5 and 6. Measured  $|\Gamma_{MAX}|$  was 0.93, 0.87 and 0.87 at 75, 90, and 105 GHz for the double-stub tuner from 110 measurements and 0.92, 0.87, and 0.83 for the triple-stub tuner from 90 measurements. The tuners have reasonably good impedance coverage with high reflection coefficients at W-Band frequencies, and demonstrate that stub tuners can be employed at 110 GHz and above.

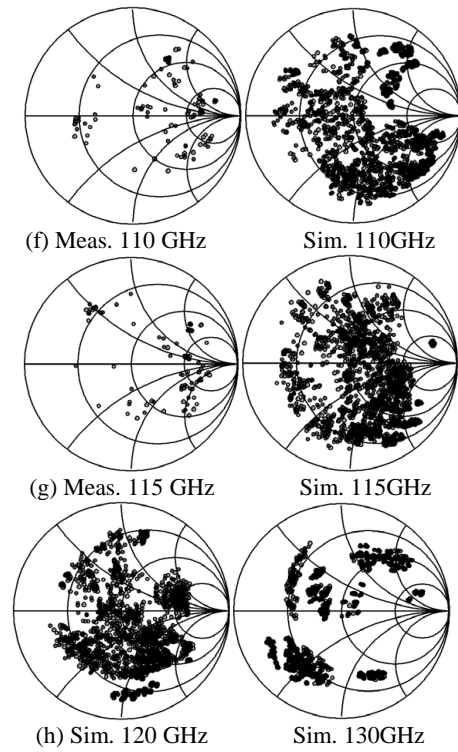
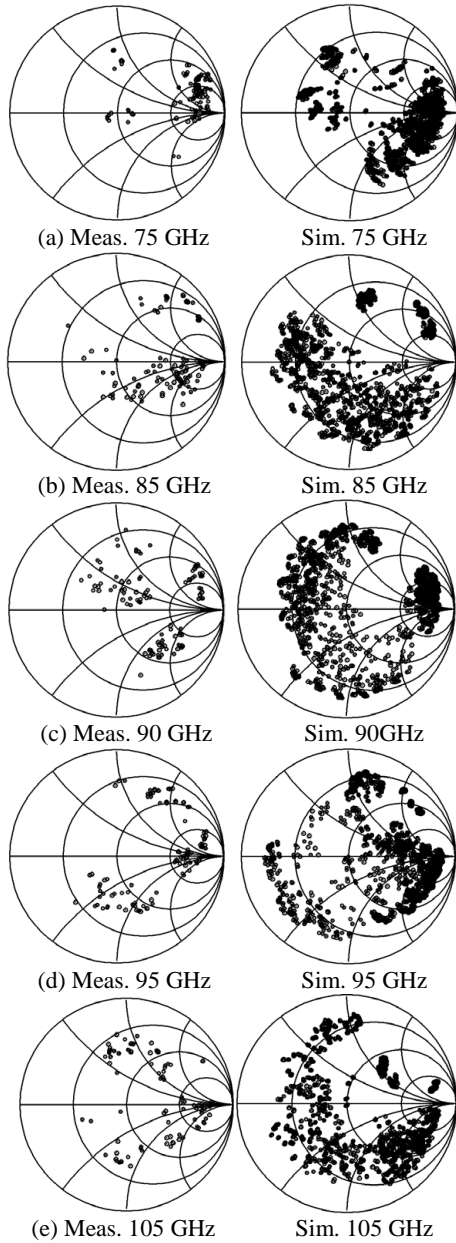
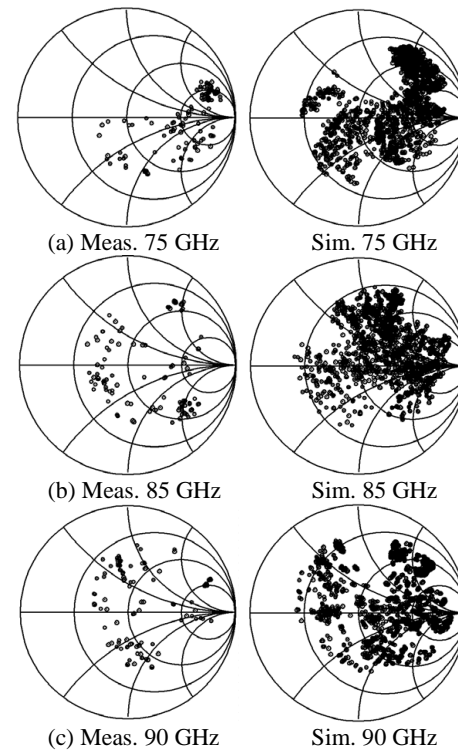


Fig. 5. (a)-(h) Measured (110 points) and simulated (2048 points)  $S_{11}$  impedance coverage of the reconfigurable W-Band double-stub impedance tuner. The tuner was terminated with  $50 \Omega$  at Port 2.



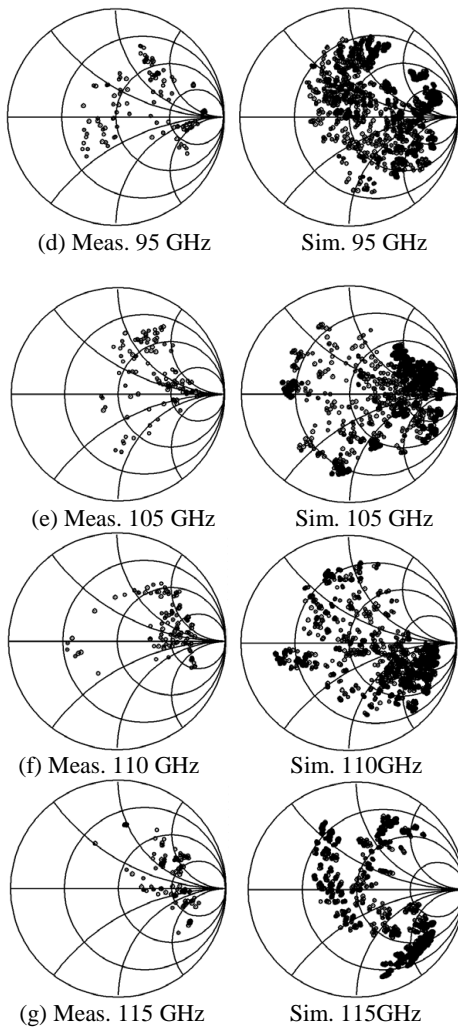


Fig. 6. (a)-(g) Measured (90 points) and simulated (2048 points)  $S_{11}$  impedance coverage of the reconfigurable W-Band triple-stub impedance tuner. The tuner was terminated with  $50 \Omega$  at Port 2.

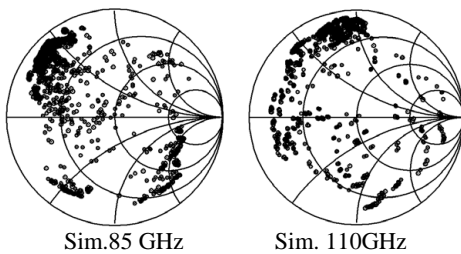


Fig. 7. Simulated impedance coverage for the re-designed triple-stub impedance tuner with  $C_U = 10$  fF and  $C_D = 80$  fF.

The impedance coverage of the tuners can be further improved by decreasing the up-state capacitance ( $C_U = 10$ -15 fF), increasing the down-state capacitance of the switched capacitor ( $C_D = 60$ -80 fF), and re-designing the T-junctions. The measured up-state capacitance was higher than intended because the MEMS switches were curved down a bit. The T-

junctions can be improved by making them more compact and lowering the transmission line impedance. With these improvements, we feel that the double and triple stub tuners can cover the entire Smith chart over the W-band frequency range (see Fig. 7).

#### IV. CONCLUSIONS

Reconfigurable W-Band double- and triple-stub impedance tuners were presented. The tuners were developed for on-wafer noise parameter and load-pull measurement purposes. The electrical tuning of impedance is realized with 11 switched MEMS capacitors, and 2048 ( $2^{11}$ ) different impedances can be generated with the tuners. The tuners are small enough to be integrated inside W-band RF probes.

#### ACKNOWLEDGEMENT

This work has been supported by the ESA/ESTEC contract no. 1655/95/NL/MV at MilliLab, and the DARPA IRFFE program at the University of Michigan.

#### REFERENCES

- [1] M. Kantanen, M. Lahdes, T. Vähä-Heikkilä, J. Tuovinen, "A wideband automated measurement system for on-wafer noise parameter measurements at 50-75 GHz", *IEEE Trans. on Microwave Theory & Tech.*, vol. 51, pp. 1489-1495, June 2003.
- [2] T. Vähä-Heikkilä, M. Lahdes, M. Kantanen, J. Tuovinen, "On-wafer noise parameter measurements at W-band", *IEEE Trans. on Microwave Theory & Tech.*, vol. 51, pp. 1621-1628, June, 2003.
- [3] V. Möttönen, J. Mallat, and A. Räisänen, "Characterisation of European Millimetre-Wave Planar Diodes", *Proceedings of European Microwave Conference 2004*, Amsterdam, Netherlands, pp. 921-924, 2004.
- [4] T. Vähä-Heikkilä, J. Varis, J. Tuovinen, and G. M. Rebeiz, "A 6-20 GHz Reconfigurable RF MEMS Impedance Tuner," *IEEE MTT-S Int. Microwave Symposium Digest*, Forth Worth, TX, pp. 729-732, 2004.
- [5] T. Vähä-Heikkilä, J. Varis, J. Tuovinen, and G. M. Rebeiz, "A 20-50 GHz RF MEMS Single-Stub Impedance Tuner", Accepted for publication to the *IEEE Microwave and Wireless Components Letters*, Nov. 2004.
- [6] T. Vähä-Heikkilä, J. Varis, J. Tuovinen, G. M. Rebeiz, "A V-Band Single-Stub RF MEMS Impedance Tuner", *Proceedings of European Microwave Conference 2004*, Amsterdam, Netherlands, pp. 1301-1304, 2004.
- [7] H.-T. Kim, S. Jung, K. Kang, J.-H. Park, Y.-K. Kim, and Y. Kwon, "Low-Loss Analog and Digital Micromachined Impedance Tuners at the Ka-Band," *IEEE Trans. on Microwave Theory and Techniques*, vol. 49, pp. 2394-2400, Dec. 2001.
- [8] J. Papapolymerou, K. L. Lange, C. L. Goldsmith, A. Malczewski, and J. Kleber, "Reconfigurable Double-Stub Tuners Using MEMS Switches for Intelligent RF Front-Ends," *IEEE Trans. on Microwave Theory & Tech.*, vol. 51, pp. 271-278, 2003.

PUBLICATION P7

**A 4–18 GHz Reconfigurable RF  
MEMS Matching Network for Power  
Amplifier Applications**

In: International Journal of RF and Microwave Computer-  
Aided Engineering 2004. Vol. 14, No. 4, pp. 356–372.  
Reprinted with permission from the publisher.

# A 4–18-GHz Reconfigurable RF MEMS Matching Network For Power Amplifier Applications

Tauno Vähä-Heikkilä,<sup>1,2</sup> Gabriel M. Rebeiz<sup>1</sup>

<sup>1</sup> The University of Michigan, Electrical Engineering and Computer Science Department, Ann Arbor, MI, 48109-2122

<sup>2</sup> VTT Information Technology, P.O. BOX 12021,02044 VTT, Finland

Received 24 September 2003; accepted 19 February 2004

**ABSTRACT:** We have developed a novel reconfigurable matching network based on the loaded-line technique. The network is composed of  $N$ -switched capacitors ( $N = 4–8$ ) with a capacitance ratio of 4–5:1 and is suitable for power amplifiers at 4–18 GHz, or as an impedance tuner for noise parameter and load-pull measurements at 10–28 GHz. The networks are very small, and offer better performance than double or triple stub matching networks. Extensive loss analysis indicates that the 8-element network has a loss of 0.5 dB at 4–12 GHz, and less than 1.5 dB at 18 GHz, even when matching a  $10\Omega$  output impedance to a  $50\Omega$  load. As expected, the 4-element matching network has about half the loss of the 8-element network, but with much less impedance coverage. Both networks were simulated and measured in high VSWR conditions and can handle at least 500 mW of RF power at 4–18 GHz. The application areas are in phased array antennas, reconfigurable power amplifiers, and wideband noise-parameter and load-pull measurement systems. © 2004 Wiley Periodicals, Inc. *Int J RF and Microwave CAE* 14: 356–372, 2004.

**Keywords:** RF MEMS; reconfigurable networks; impedance tuner; matching network; loaded-line; phased arrays; load-pull; noise parameters

## I. INTRODUCTION

Power amplifiers (PAs) with 1–2-W output power and a 5-V power supply have an output impedance of  $10\Omega$ – $20\Omega$ , and are mismatched in  $50\Omega$  systems. Therefore, it is imperative that a low-loss impedance matching network be used to ensure optimum power transfer between the PA and the antenna (Fig. 1). The matching network should be flexible enough to accommodate a changing load impedance or a changing PA output impedance. This is a common problem, for example, in multiband wireless networks where the antennas are placed close to walls or obstacles. An-

other application is in phased arrays where the active input antenna impedance changes with scanning angles and operating frequency. Also, the PA output impedance can change versus frequency due to gain degradation over extended operation times.

A standard narrowband matching network is the CLC network with variable capacitors [1]. Such a network can match a wide range of impedances, but suffers from a narrowband response (single or dual-frequency bands). For wider frequency coverage, one can use reconfigurable networks based on the double-stub or triple-stub tuners [2, 3]. These networks offer excellent performance, but are quite large and employ a large number of MEMS switches (or varactors). Also, depending on the design, they can have a substantial loss component (0.5–3-dB loss), thus resulting in a reduced Smith chart coverage.

Correspondence to: T. Vähä-Heikkilä; email: heikkila@eecs.umich.edu

Published online in Wiley InterScience (www.interscience.wiley.com). DOI 10.1002/mmce.20021

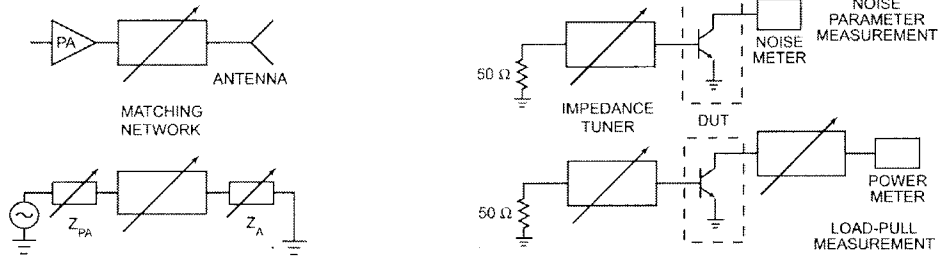


**Figure 1.** A reconfigurable matching network used between a power amplifier and a radiating antenna, or as an impedance tuner in noise or load-pull measurements.

In this work, we present a novel matching network capable of very wideband PA matching (4–18 GHz), and with low loss. The network is based on a loaded transmission-line with  $N$  switched capacitors. The article analyses in detail the loss of matching networks in non-50 $\Omega$  systems, taking in to consideration that they are measured solely using 50 $\Omega$   $S$ -parameter setups. This work also presents simulations and measurements of the power handling and intermodulation distortion of the novel matching network. The reconfigurable network can also be used in noise and load-pull measurement setups. In this case, the network loss is less of a concern, and the important characteristic is that a large range of impedance be synthesized at the transistor input. This article shows that the proposed network can work over a 3:1 frequency range for these applications.

## II. DESIGN AND FABRICATION

### A. Design of the Reconfigurable Loaded-Line

It is well known that the phase velocity and impedance of a transmission line can be changed by capacitive loading. This fact has been used in distributed transmission-line (DMTL) MEMS phase shifters [1, 4, 5] and in tunable filters [6]. The loaded-line idea can also be applied to reconfigurable matching networks: a transmission-line is loaded with  $N$ -switched MEMS capacitors, each having a capacitance  $C_U$  (up-state position) and  $C_D$  (down-state position), and the line impedance is chosen to be approximately 50 $\Omega$  when the MEMS capacitors are in the up-state position (Fig. 2). The capacitance ratio is chosen anywhere from 3:1 to 8:1, depending upon the design. When a MEMS capacitor is actuated to the down-state position, the loading on the t-line increases, thus resulting in a localized low impedance and a high effective dielectric constant (around the region of the MEMS capacitor). Since the loading is increasingly

capacitive with more MEMS switches being actuated, the network will transform a 50 $\Omega$ –60 $\Omega$  load into a low-input impedance (or vice versa, due to reciprocity), and the higher the capacitive loading, the lower the input impedance. A 4- to 8-element design results in 16 to 256 different impedance points on the Smith chart, and the distributed nature of the design ensures wideband-frequency coverage. Also, at high frequency and due to the varying electrical length of the loaded t-line, when the switched capacitors are actuated, the impedance coverage covers the entire Smith chart and not only the low impedance region.

Many different parameters can be optimized in the loaded-line network. In general, a larger number of switched capacitors yield more wideband operation and better Smith chart coverage. However, this also results in increased component size and loss, thus the smallest  $N$  must be chosen to meet the specific application. The highest frequency of operation is limited by the Bragg frequency (see below) of the loaded line, and the lowest impedance which can be matched to 50 $\Omega$  is dependent on the loading capacitance (see section III). A closed-form design technique has not been found, because the location, electrical length, and loaded-line impedance change with the actuation of the MEMS switched capacitors; therefore, Agilent ADS [7] is used extensively for choosing  $C_U$ ,  $C_D$ ,  $s$ , and the number of capacitors. The design is amazingly robust, and a capacitance or a separation change of  $\pm 30\%$  will not affect the performance much, especially if  $N = 6$ –8.

### B. Basic Analysis and Model Fitting

The impedance ( $Z_L$ ) and effective dielectric constant ( $\epsilon_{\text{reff-L}}$ ) of a capacitively loaded t-line is calculated using [8]:

$$K = 1 + \frac{cZ_0C}{s\sqrt{\epsilon_{\text{reff}}}},$$

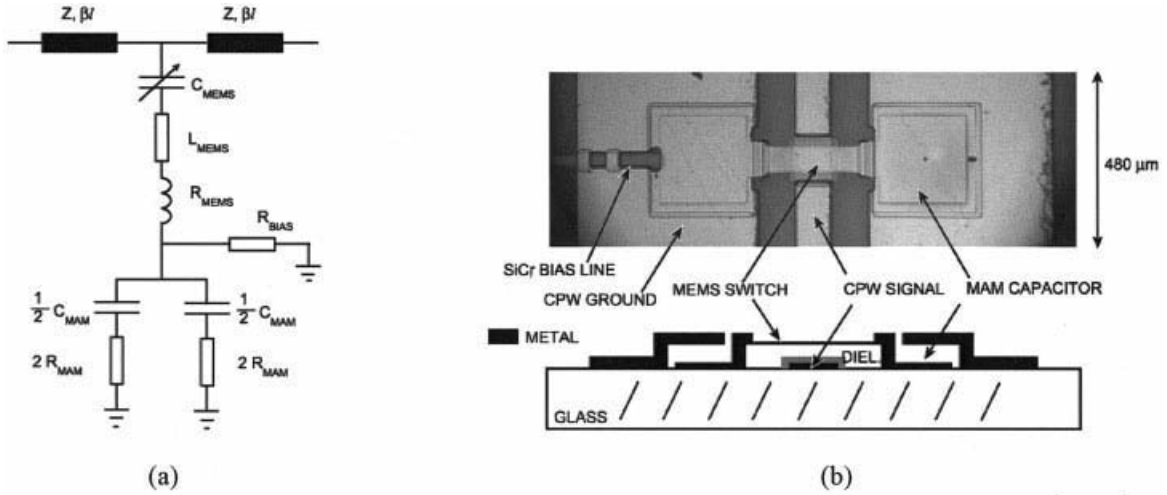


**Figure 2.** (a) Equivalent circuit, and (b) picture and cross-sectional view of a switched MEMS capacitor. The CPW signal line is DC grounded. This represents one cell in the reconfigurable loaded-line matching network.

$$\begin{aligned} \epsilon_{\text{reff-L}} &= \epsilon_{\text{reff}} K, \\ Z_L = Z_U, Z_D &= Z_0 / \sqrt{K}, \end{aligned} \quad (1)$$

where  $c$  is the speed of the light in free space,  $C$  is the capacitance of the switched capacitor ( $C_U, C_D$ ),  $\epsilon_{\text{reff}}$  is the effective dielectric constant of the unloaded line, and  $s$  is the period of the loading structure ( $s = 480 \mu\text{m}$ ). In this design (Fig. 3), the loaded line characteristics are  $Z_U = 45 \Omega$  and  $\epsilon_{\text{reff-U}} = 10$ , and  $Z_D = 23 \Omega$  and  $\epsilon_{\text{reff-D}} = 38.2$ , when the MEMS switches are in the up-state and down-state positions, respectively. The impedance in the up-state was designed to be  $50 \Omega$  but is lower since the MEMS bridges are curved down resulting in a larger loading capacitance.

The Bragg frequency is calculated using [4]:

$$f_B = \frac{cZ_L}{\pi s Z_0 \sqrt{\epsilon_{\text{reff}}}} \quad (2)$$

and is 62.8 GHz and 32.2 GHz in the up-state and down-state positions, respectively. In general, it is good to have a relatively high Bragg frequency in order to obtain good operation over a wide-frequency range. The measured and simulated  $S$ -parameters for

the 8-element matching network are shown in Figure 4, and Agilent ADS is used for fitting the values of the switched MEMS capacitor (see Fig. 2(a) and Table 1).

### C. Fabrication

The MEMS switched capacitor is fabricated using a series combination of a capacitive RF MEMS switch (with a capacitance ratio of 10–30:1) and fixed metal-insulator-metal (MIM) or metal-air-metal (MAM) capacitors. The down-state capacitance is mostly determined by the MIM (or MAM) capacitor (300–900 fF for X-band operation), while the up-state capacitance is set by the MEMS switch (70–80 fF). In this work, MAM capacitors are used for high- $Q$  performance. Figure 2 shows a fabricated MEMS switched capacitor, and is based on a coplanar waveguide (CPW) transmission line with dimensions 100/100/100  $\mu\text{m}$  on a 500  $\mu\text{m}$  glass substrate (see Table 1). The dimensions of the MEMS switch are 280  $\mu\text{m} \times 80 \mu\text{m}$  and the area of each MAM capacitor is 240  $\mu\text{m} \times 235 \mu\text{m}$ . The MEMS bridge is fabricated using a 0.8  $\mu\text{m}$  thick gold membrane suspended 1.1  $\mu\text{m}$  above the t-line, and a 3500 Å silicon-nitride dielectric inter-layer. The fabrication process is based on standard

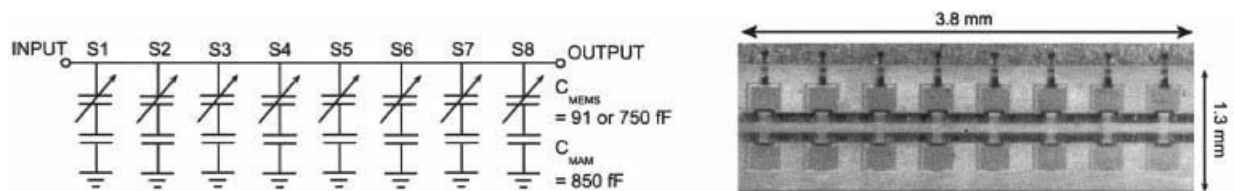


**Figure 3.** Circuit diagram and picture of the eight-element reconfigurable matching network.

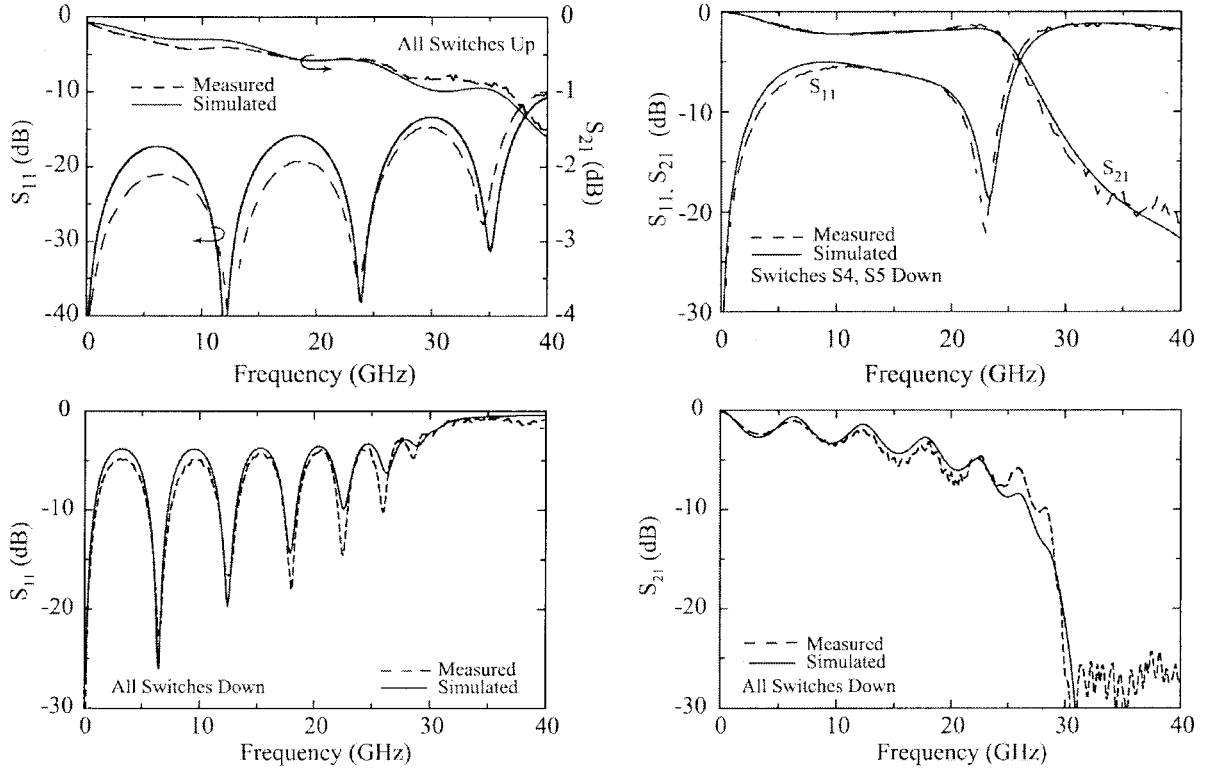


**Figure 4.** Measured and simulated  $S$ -parameters for the 8-switched capacitor reconfigurable MEMS network with different switch combinations.

techniques and is described in [9]. Polymethylmethacrylate (PMMA) is used as a sacrificial layer under the switches and MAM capacitors, and is patterned using oxygen plasma in a reactive ion etcher (RIE). The circuit is electroplated to 3  $\mu\text{m}$ -thick (except the MEMS bridges) to reduce the t-line and MAM capacitor loss. SiCr bias lines with resistance of  $700\Omega$ /

**TABLE I.** Measured T-Line Values From the TRL Calibration (Top), Fitted Values for the Switched MEMS Capacitor (Middle), and Loaded-Line Characteristics (Bottom)

$\epsilon_r$	4.6
$Z_0$ ( $\Omega$ )	86.2
$\epsilon_{\text{reff}}$	2.72
$\alpha$ (dB/cm), 10/20 GHz	0.35/0.52
$C_{\text{MEMS}}$ : $C_{\text{UP}}$ (fF)	91
$C_{\text{MEMS}}$ : $C_{\text{DOWN}}$ (fF)	750
$R_{\text{BIAS}}$ (k $\Omega$ )	>3
$L_{\text{MEMS}}$ (pH)	9.5
$R_{\text{MEMS}} + R_{\text{MAM}}$ ( $\Omega$ )	0.6
$C_{\text{MAM}}$ (fF)	850
$s$ ( $\mu\text{m}$ )	480
$Z_U$ ( $\Omega$ ), $\epsilon_{\text{reff}_U}$	45, 10
$Z_D$ ( $\Omega$ ), $\epsilon_{\text{reff}_D}$	23, 38

square are used for actuating the MEMS switch. The measured pull-down voltage was 15–17 V, and an actuation voltage of 35 V was used for obtaining an excellent metal-to-dielectric coverage in the down-state position. The estimated spring constant is  $k = 40\text{--}50$  N/m from the standard pull-down equation [10]. The estimated residual stress is  $\sigma = 50\text{--}60$  MPa using the formulas in [10].

The measured capacitance ratio of the RF MEMS switch is only 8:1 due to its low height and thick silicon-nitride layer (see Table 1), and the fixed MAM capacitor is 850 fF. This results in  $C_U = 81.2$  fF,  $C_D = 398$  fF and a capacitance ratio 4.9:1. The quality factor of the MEMS switched capacitor is calculated using  $Q = (2\pi f C (R_{\text{MEMS}} + R_{\text{MAM}}))^{-1}$  and at 12 GHz results in  $Q_U = 272$  ( $C_U = 81.2$  fF,  $X = -j163\Omega$ ) and  $Q_D = 56$  ( $C_D = 398$  fF,  $X = -j33.3\Omega$ ) in the up-state and down-state positions, respectively.

### III. IMPEDANCE COVERAGE

#### A. Simulations and Measurements

The measured and simulated input impedances of the 8-element matching network are presented in Figure 5

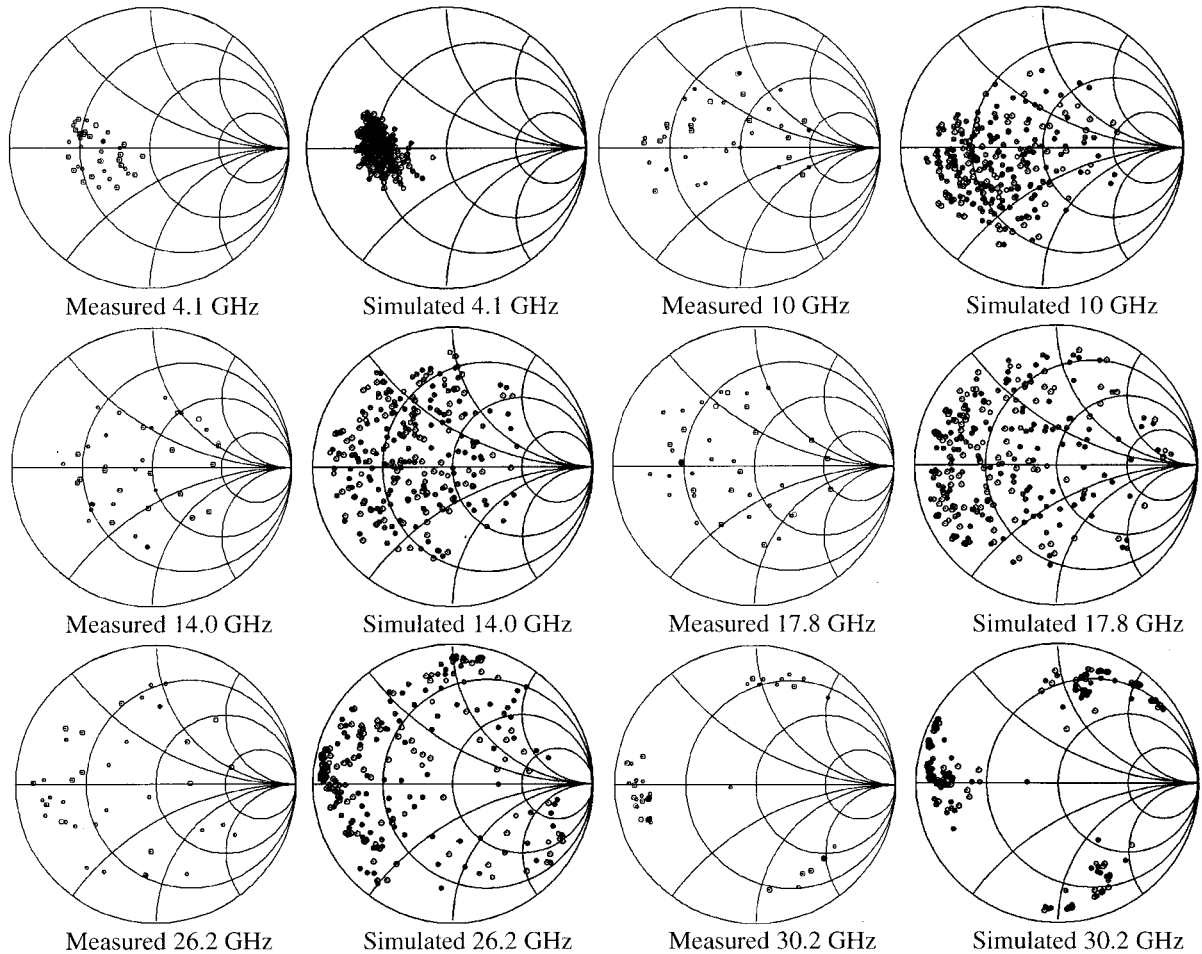


**Figure 5.** Measured (35) and simulated (256) impedances of the 8-element reconfigurable MEMS matching network. The single-cell values are given in Table I.

at 4–30 GHz for a  $50\Omega$  load. The measurements were done on 35 switch settings out of 256 possible combinations, and the results match the simulated results very well. Notice that at 4–8 GHz, the electrical length of the loaded t-line is quite short and the mapped input impedance lies in the low-impedance region of the Smith chart. However, above 8 GHz, the loaded-line is long enough to transform a  $50\Omega$  load into a wide coverage of the Smith chart. Still, the loaded-line design is better suited for low-impedance matching as is evident from a study of the impedance loci at 4–30 GHz (as compared with the coverage at the  $20\Omega$  and  $200\Omega$  areas).

## B. Discussion of Impedance Coverage

**Effect of the MEMS Bridge Height.** The height of the MEMS bridge is usually the most sensitive part in the fabrication process since the value of the fixed MIM or MAM capacitor is achieved with accuracy.

Therefore, the impedance coverage of the 8-element matching network is simulated with a fixed MAM capacitor of 850 fF and a varying up-state MEMS capacitance. It is clear that the impedance coverage of the 8-element network does not change significantly if the MEMS up-state capacitance (and capacitance ratio) is changed from 34 fF to 170 fF (Fig. 6).

**Effect of Loading Capacitance.** The total down-state capacitance controls the lowest input impedance that can be achieved with a  $50\Omega$  load. Figure 7(a) presents the simulations with  $C_D = 200$  fF ( $C_{D-MEMS} = 750$  fF,  $C_{MAM} = 275$  fF),  $C_D = 400$  fF ( $C_{D-MEMS} = 750$  fF,  $C_{MAM} = 850$  fF) and  $C_D = 900$  fF ( $C_{D-MEMS} = 1300$  fF,  $C_{MAM} = 2900$  fF). The other switch and line parameters are the same as Table I. For  $C_D = 900$  fF and  $s = 480$   $\mu\text{m}$ , the minimum input impedance is plotted up to 20 GHz due to Bragg frequency limitations, since above this frequency, the circuit results in very poor coverage of the Smith chart. On the other

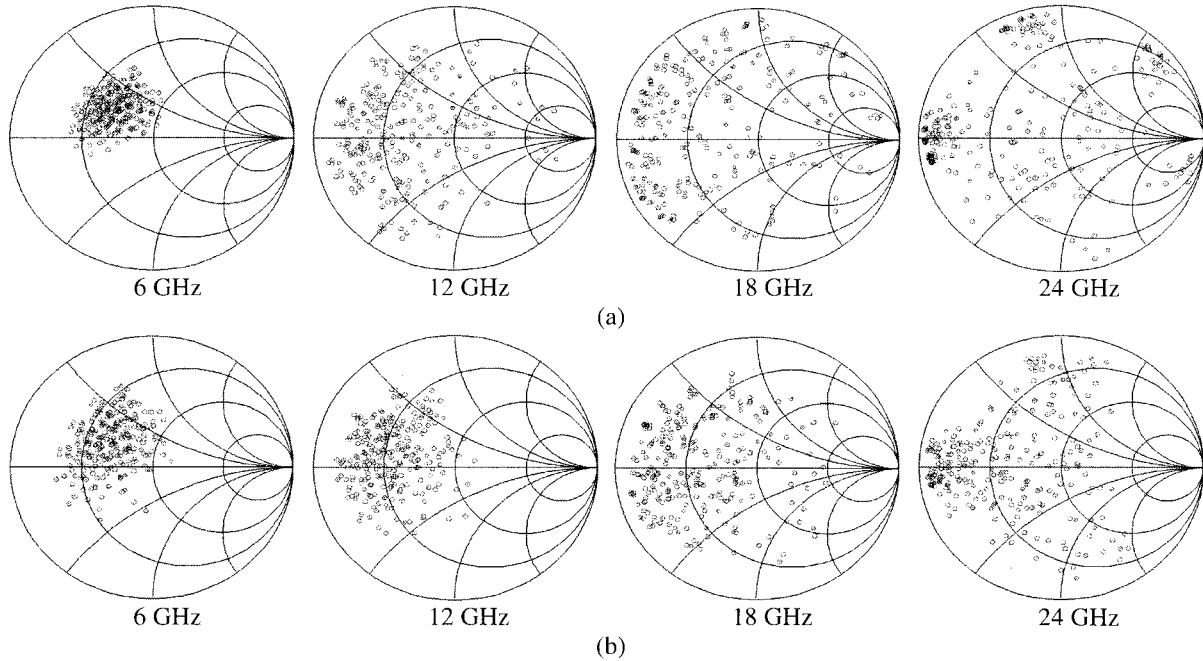


**Figure 6.** Simulated impedance coverage for the 8-element reconfigurable matching network with loading-capacitance ratios of (a) 2.8:1 ( $C_{U-MEMS} = 171$  fF,  $C_{D-MEMS} = 750$  fF,  $C_{MAM} = 850$  fF) and (b) 12.2:1 ( $C_{U-MEMS} = 34$  fF,  $C_{D-MEMS} = 750$  fF,  $C_{MAM} = 850$  fF).

hand, for  $C_D = 200$  fF and  $s = 480$   $\mu\text{m}$ , the circuit results in excellent coverage of the Smith chart up to 36 GHz, but at the expense of a higher input impedance at 6–12 GHz. It is clear that for 6–24 GHz applications, a down-state capacitance of 400–600 fF for  $s = 480$   $\mu\text{m}$  is the best choice for low impedance matching and good Smith chart coverage.

**Effect of Switched-Capacitor Separation.** Figure 7(b) presents the effect of the period  $s$  between the switched capacitors for  $C_D = 400$  fF. Again, for  $s = 900$   $\mu\text{m}$ , the results are plotted to 20 GHz due to Bragg frequency limitations (the circuit is electrically large), and for  $s = 225$   $\mu\text{m}$ , one can extend the operation of the circuit up to 40 GHz. It is seen that the separation does not affect the minimum achievable input impedance at 6–24 GHz, but a closer look at the Smith chart indicates that the best coverage occurs for  $s = 300$ – $600$   $\mu\text{m}$  with  $C_D = 400$  fF in the 6–24-GHz frequency range.

In general, many solutions in the  $s$  and  $C_D$  plane will lead to acceptable results in any frequency band.

#### IV. LOSS ANALYSIS AND CASE STUDIES

The reconfigurable circuit results in a very high reflection coefficient for many different switch combi-

nations; therefore,  $S_{21}$  is not the correct measure of the circuit loss. The loss of any mismatched circuit is defined as:

$$\text{Loss} = 1 - |S_{11}|^2 - |S_{21}|^2 \quad (3)$$

and takes into account the loss in the CPW line, MEMS bridges, and MAM capacitors, and the radiation loss. The loss for different switch combinations can be easily obtained from the  $S$ -parameter measurements and from the circuit model of Figure 2(a) and Table 1, as shown in Figure 8). The peaks in the loss analysis are due to the low-impedance t-line section, which is synthesized in the reconfigurable circuit ( $Z_D = 23$   $\Omega$ ,  $\epsilon_{\text{reff}_D} = 38.2$ ,  $N^*s = N^*480$   $\mu\text{m}$ ) when one or several switched capacitors are actuated. This low impedance section is bound by  $45\Omega$  t-line sections on either side, and will resonate when its effective length is  $n\lambda_g/2$  (half-wave resonator), where  $\lambda_g$  is the guided wavelength in the resonator. For 2, 4, or 8 cascaded switched capacitors, the first resonant frequencies occur at 25.3, 12.6, and 6.3 GHz, respectively (Fig. 8), and is independent of the location of the switched capacitors. The simulated loss using the circuit model agrees very well with the values obtained from the measured  $S$ -parameters (Fig. 8). This allows us to use the circuit model for accurate loss analysis with non- $50\Omega$  loads.

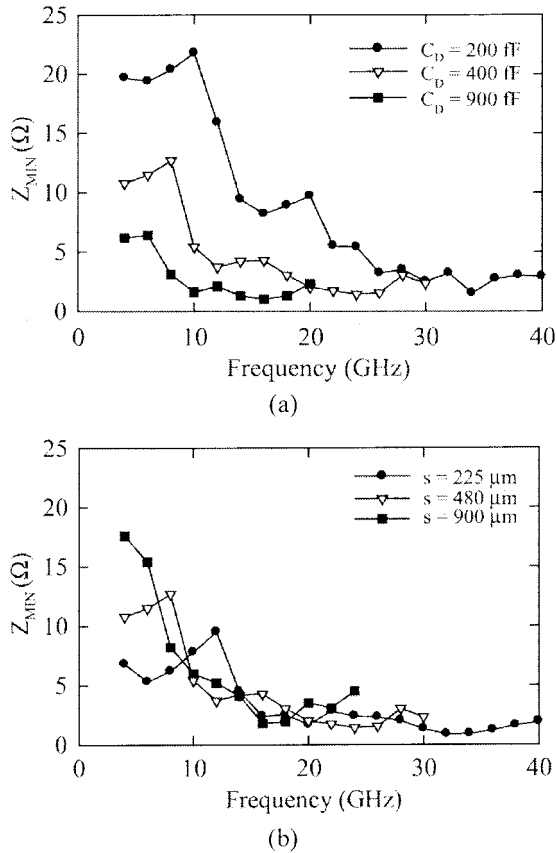


**Figure 7.** Simulated minimum input impedance for the 8-element matching network with a  $50\Omega$  load: (a) with different down-state capacitances and  $s = 480 \mu\text{m}$ ; (b) with different separation distances and  $C_D = 400 \text{ fF}$ .

### A. Case Study: $10\Omega$ and $20\Omega$ Loads

The reconfigurable loaded-line network was terminated with  $10\Omega$  and  $20\Omega$  loads and matched to  $50\Omega$  at 6, 12, 18, and 24 GHz (see Figs. 9 and 10). It is evident that several switch combinations result in a good match at each frequency (Tables 2 and 3). Note that as the frequency increases, the circuit becomes electrically larger and results in a narrower bandwidth (a percentage of the center frequency). The loss increases significantly above 12 GHz, and becomes  $-2 \text{ dB}$  ( $20\Omega$  case) and  $-3 \text{ dB}$  ( $10\Omega$  case) at 24 GHz. The reason is that the circuit is electrically lossy, since the down-state capacitor  $Q$  is only 28 and the t-line loss is  $0.56 \text{ dB/cm}$  at 24 GHz. If operation at 18–24 GHz is needed, then one should employ a much smaller down-state capacitor and a smaller separation  $s$ , thus resulting in a more compact circuit. However, if wide-band operation is needed (6–24 GHz), then it would be best to use a quartz substrate (instead of a glass substrate) with a lower t-line loss. Also, the use of thicker gold plating for the bridges and MAM capac-

itors can decrease the switched capacitor resistance to  $0.3\Omega$  (instead of the current value of  $0.6\Omega$ ). The loss of the reconfigurable circuit with a  $10\Omega$  load is presented in Table 4 for different t-line loss and device resistance values.

The input-reflection coefficient and loss can also be obtained from the measured  $S$ -parameters under different switch combinations (Fig. 11). It is seen that the experimental data agrees quite well with the circuit model of Figure 10, and again shows that the network is excellent up to 18 GHz. The network results in high matching loss for the  $10\Omega$  case at 24 GHz, but this can be solved as discussed above.

### Case Study: $200\Omega$ Load

The 8-element reconfigurable matching network was primarily designed to match low output-impedance amplifiers to  $50\Omega$ . However, the circuit can also be used to match high-impedance components at 10–28 GHz (Fig. 12). The simulated input impedances at the input of the 8-element matching network with a  $200\Omega$  load are shown in Figure 12. A detailed analysis indicates that the bandwidth and loss (which are not presented here) are comparable to the  $10\Omega$  case.

### B. Case Study: $10\Omega$ PA to Varying Antenna Loads ( $10\Omega$ – $200\Omega$ )

An interesting case for power amplifiers is when the load impedance (such as the antenna) varies over a wide impedance range. The matching network still needs to be used when connecting a  $10\Omega$  PA to a  $10\Omega$  load due to its finite length and non- $10\Omega$  impedance. The reconfigurable network is versatile enough that it can easily render such a match possible with several switch combinations, under virtually any load condition (Table 5, Figs. 13 and 14) but at the expense of a reduced bandwidth for the  $10\Omega$ – $200\Omega$  case.

The above case studies prove that the loaded-line reconfigurable network is an extremely versatile design, and is capable of a wide range of impedance matching (even a 20:1 case) over a large frequency band without any excessive loss. Although we have used solely real impedances, the reconfigurable matching network has virtually the same performance for complex loads on the same VSWR circles, and this will not be repeated here for conciseness.

## V. INTERMODULATION MEASUREMENTS

The intermodulation analysis of MEMS switches, varactors, and tunable filters is presented in [11] and will

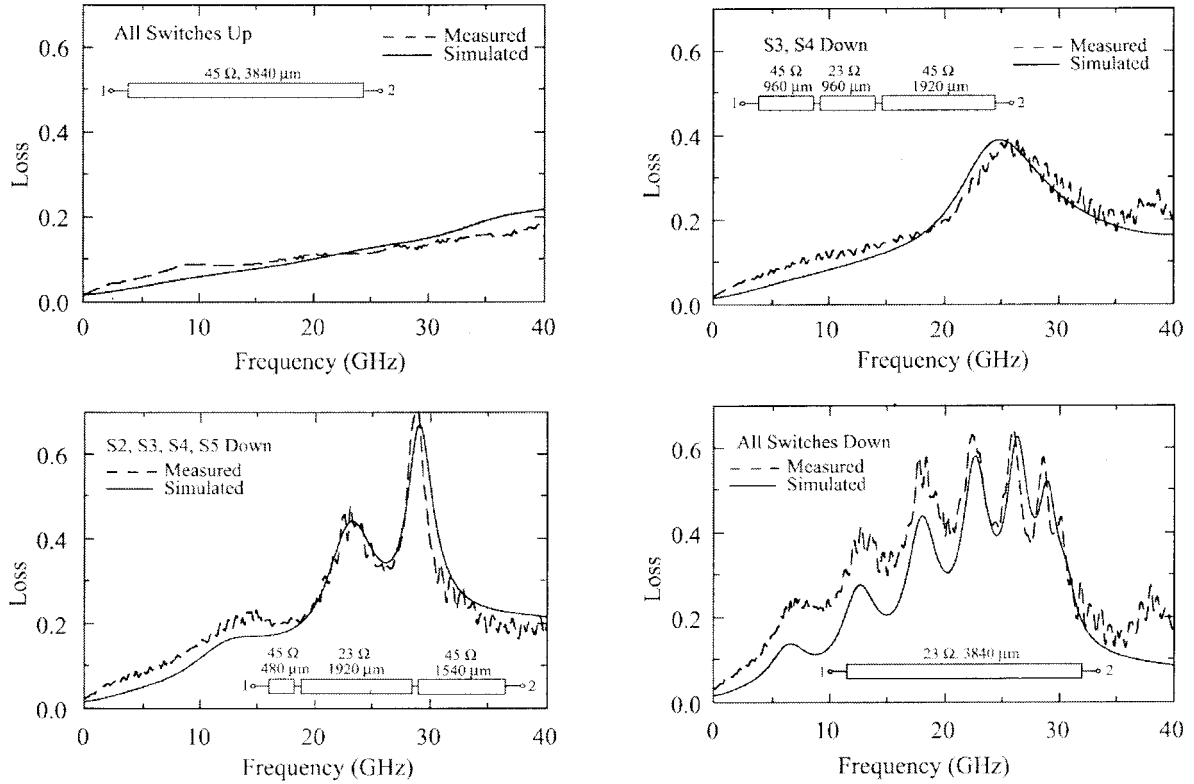


**Figure 8.** Loss of the 8-element matching network obtained from measured *S*-parameters and from the circuit model for different switch combinations.

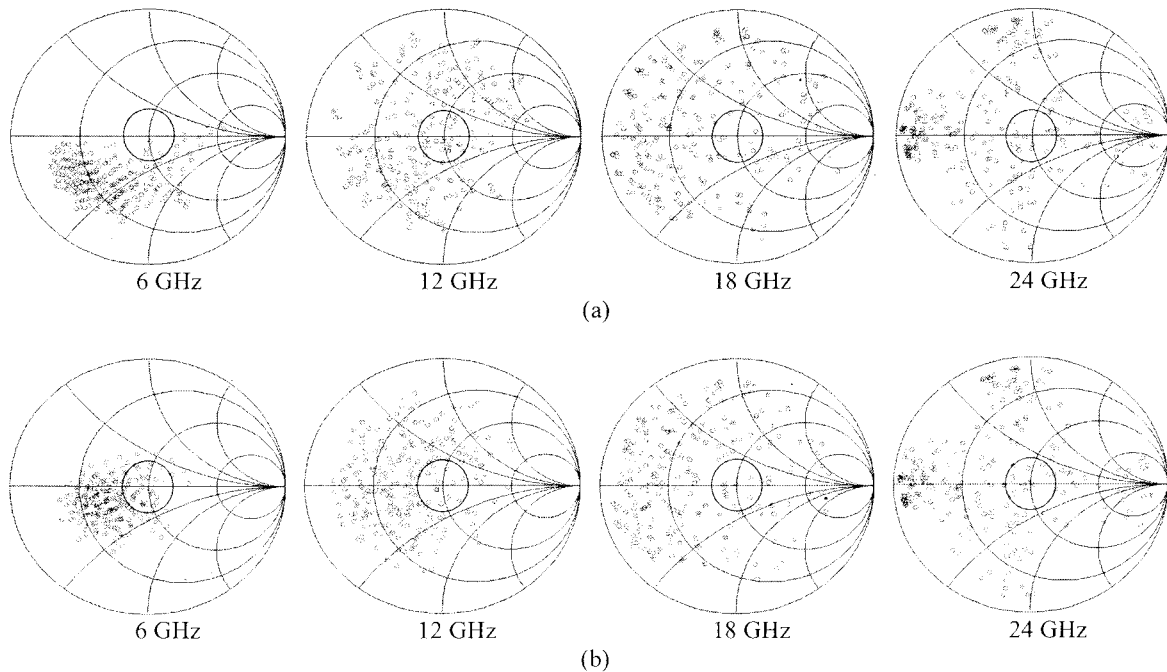


**Figure 9.** Simulated impedances seen at the input of the 8-element matching network with (a)  $10\Omega$  and (b)  $20\Omega$  load (Smith chart is based on  $50\Omega$ ). The circle shows the  $-15$ -dB matching area.

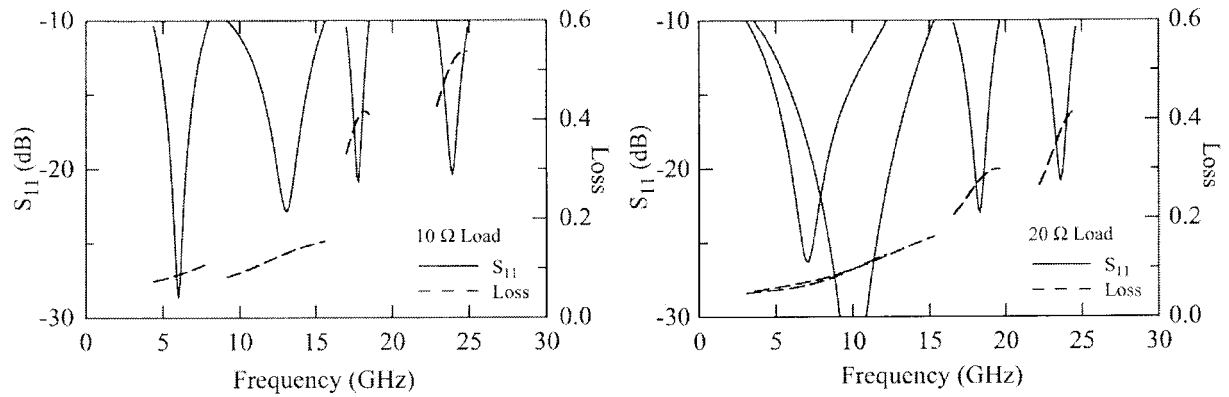


**Figure 10.** Simulated input reflection coefficient and loss of the 8-element matching network at 6, 12, 18, and 24 GHz with (a) 10Ω and (b) 20Ω loads matched to 50Ω. The specific switch combinations are presented in Tables II and III in italics.

not be repeated here. The findings in [11] are that MEMS circuits generate insignificant amount of intermodulation products, especially if the difference  $\Delta f$  is higher than the mechanical resonant frequency of the bridge (90–100 kHz). Intermodulation measurements of the 8-element matching network were done at 8 and 17 GHz (Fig. 14), and the 8-GHz results are shown due to the higher dynamic range. The circuit was terminated with a 50Ω load or with a short circuit. In the case of a short-circuit condition, the intermodulation signal was measured at the input port using a circulator. It is seen that the intermodulation products are truly negligible ( $IIP3 > +30$  dBm), even

under short-circuit conditions (Fig. 15). The  $IIP3$  increases with  $\Delta f^4$  and, therefore, it is expected to be  $> +70$  dBm for a  $\Delta f$  of 1 MHz. This is so low that it is simply unmeasurable in most experimental setups. These findings confirm the results of [11].

## VI. POWER ANALYSIS AND MEASUREMENTS

The position of a MEMS switch changes if a DC or RF voltage is applied between the bridge electrodes, since the electrostatic force is dependent on  $V^2$ , and

**TABLE II. Case Study: 10Ω Load**

Switch Combination	$S_{11}$ at Center Freq. (dB) and $-10$ -dB BW (GHz)	Loss at Center Freq. and Max. Loss in $-10$ -dB Band
<b>6 GHz</b>		
S5, S6, S7	-20.6 (3.1)	0.09 (0.10)
S5, S6, S7, S8	-28.6 (3.6)	0.09 (0.11)
S4, S6, S7, S8	-17.4 (3.2)	0.09 (0.10)
<b>12 GHz</b>		
S7, S8	-17.1 (6.4)	0.12 (0.16)
S3, S6, S7	-44.5 (2.1)	0.21 (0.23)
S1, S4, S7, S8	-23.9 (2.5)	0.19 (0.20)
<b>18 GHz</b>		
S2, S4, S7	-20.0 (1.3)	0.44 (0.47)
S2, S3, S4, S7	-16.5 (1.6)	0.47 (0.49)
S2, S4, S6, S7, S8	-17.6 (1.5)	0.41 (0.42)
<b>24 GHz</b>		
S6, S7	-19.9 (2.0)	0.52 (0.54)
S1, S2, S4	-17.9 (2.3)	0.52 (0.56)
S3, S4, S6, S7, S8	-25.1 (3.5)	0.58 (0.65)

**TABLE III. Case Study: 20Ω Load**

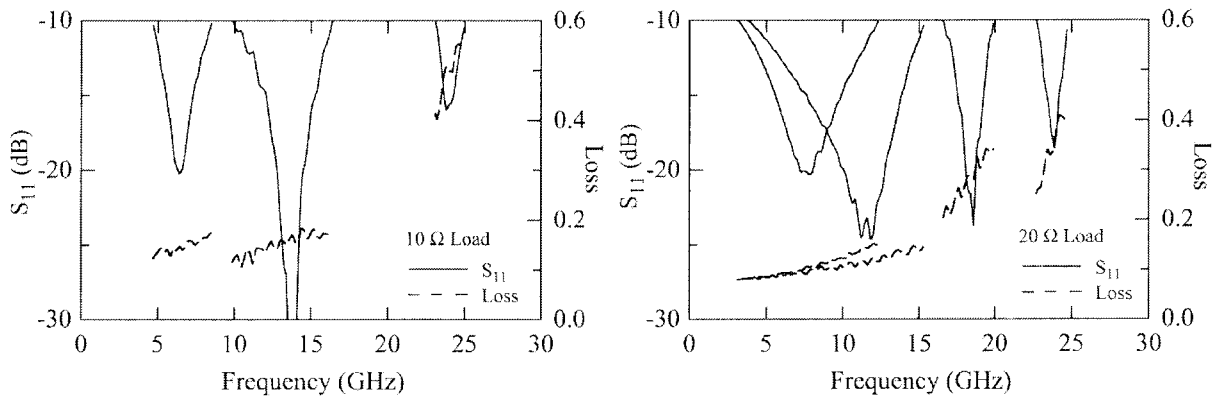
Switch Combination	$S_{11}$ at Center Freq. (dB) and $-10$ -dB BW (GHz)	Loss at Center Freq. and Max. Loss in $-10$ -dB Band
<b>6 GHz</b>		
S6	-20.0 (9.1)	0.06 (0.13)
S5	-23.6 (5.8)	0.06 (0.08)
S5, S7	-21.8 (8.8)	0.07 (0.12)
<b>12 GHz</b>		
S7	-20.1 (11)	0.10 (0.12)
S6, S8	-22.3 (11.7)	0.12 (0.16)
S2, S4, S5, S7	-25.8 (3.5)	0.18 (0.19)
<b>18 GHz</b>		
S4, S6, S8	-18.14 (4.7)	0.29 (0.34)
S5, S6, S7	-20.5 (3.0)	0.27 (0.30)
S3, S4, S5, S7, S8	-20.5 (3.5)	0.34 (0.36)
<b>24 GHz</b>		
S2, S3	-17 (2.4)	0.36 (0.42)
S6, S7	-17.5 (2.6)	0.40 (0.42)
S4, S5, S7, S8	-17.7 (2.6)	0.52 (0.61)

**TABLE IV. Simulated Loss of the Reconfigurable 8-Element Circuit with a 10Ω Load and Different T-Line Loss and Switched Capacitor Resistance**

$\alpha$ at 10/20 GHz (dB/cm)	$R_{MEMS} + R_{MAM}$ (Ω)	Loss, 6 GHz S5, S6, S7, S8	Loss, 12 GHz S7, S8	Loss, 18 GHz S2, S4, S6, S7, S8	Loss, 24 GHz S6, S7
0.35/0.52	0.6	0.09 (0.11)	0.12 (0.16)	0.41 (0.42)	0.52 (0.54)
0.35/0.52	0.3	0.08 (0.10)	0.10 (0.12)	0.32 (0.32)	0.41 (0.42)
0.18/0.27	0.6	0.07 (0.09)	0.10 (0.13)	0.37 (0.38)	0.48 (0.50)
0.18/0.27	0.3	0.06 (0.08)	0.08 (0.10)	0.27 (0.27)	0.35 (0.36)

**TABLE V. Case Study: 10Ω Source and 10Ω or 200Ω Load**

Frequency	Switch Combination	$S_{11}$ at Center Freq. (dB) and -10-dB BW (GHz)	Loss at Center Freq. and Max. Loss in -10-dB Band	Switch Combination	$S_{11}$ at Center Freq. (dB) and -10-dB BW (GHz)	Loss at Center Freq. and Max. Loss in -10-dB Band
10Ω to 10Ω						
6 GHz	S2, S3, S4, S5, S6, S7	-18.3, (1.3)	0.13 (0.14)	All up	-18.7, (1.2)	0.09 (0.10)
12 GHz	S1, S2, S7, S8	-48.3, (5.0)	0.17 (0.23)	S4, S8	-31.8, (0.6)	0.42 (0.42)
18 GHz	S1, S2	-22.6, (1.3)	0.42 (0.43)	S1, S2, S3, S4, S5	-28.1, (1.7)	0.37 (0.37)
24 GHz	S1, S2, S7, S8	-19.1, (2.5)	0.45 (0.47)	S1, S2	-28.3, (1.8)	0.37 (0.38)
200Ω to 10Ω						

**Figure 11.** Input-reflection coefficient and loss obtained from the measured  $S$ -parameters of the 8-element matching network with 10Ω and 20Ω loads. The 10Ω load is matched to 50Ω at 6 GHz using (S5, S6, S7, S8), at 12 GHz (S7, S8), and at 24 GHz (S6, S7). The 20Ω load is matched to 50Ω at 6 GHz using (S6), at 12 GHz (S7), at 18 GHz (S5, S6, S7) and at 24 GHz (S2, S3).

this translates to  $V_{rms}^2$  for RF voltages [10]. If  $V_{rms}$  is equal or greater than the pull-down voltage of the MEMS switch ( $V_p$  is typically 15–30 V), the switch will self-actuate to the down-state position. Another problem related to high RF power is the hold-down voltage in the down-state position ( $V_h$  is typically 5–8 V). This is important for switched capacitors, since the RF voltage across the MEMS switch can be quite high. The reason for this is that the switch is not connected to a ground, and therefore can sustain a high-RF voltage even in the down-state position.

Also, the RF current in the switch in the down-state position can be quite high, and this is especially true in standing-wave circuits. Still, switched-capacitor circuits result in more favorable down-state conditions than standard RF MEMS switches because the impedance to ground at any switch location is quite high ( $X = -j33\Omega$  at 12 GHz), compared to a capacitive short-circuit (around  $X = -j5\Omega$  at 12 GHz).

The rms voltages and currents ( $V_{RF-rms}$ ,  $I_{RF-rms}$ ) for the  $N$ -switched capacitors under different combination can be easily obtained using a circuit simulator

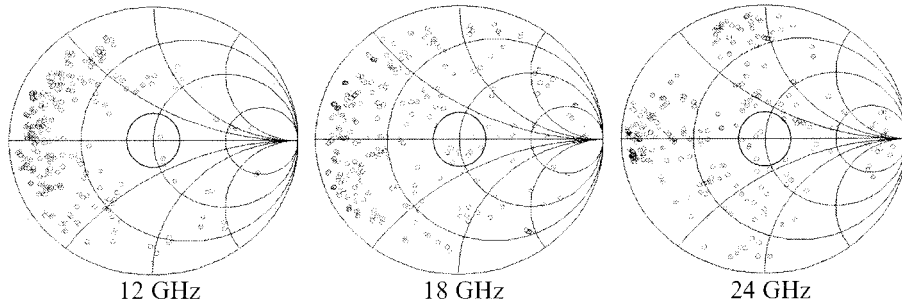


**Figure 12.** Simulated impedances seen by the 50Ω source connected to the 8-element matching network and a 200Ω load.

and the circuit model of Table 1 (Agilent ADS). The 8-element circuit was terminated with 10Ω or 20Ω loads and matched with the same switch combinations as in Tables 2 and 3 (Fig. 16). An input-RF power of +27-dBm (500 mW) was used, but the voltages and current for different powers can be easily obtained, since they are proportional to  $\sqrt{P}$ . From Figure 16, it is easy to locate which switches are in the down-state position from the large simulated current in the switched-capacitors. The simulated voltage is divided between the MEMS switch ( $C_{U-MEMS} = 91$  fF,  $C_{D-MEMS} = 750$  fF) and the MAM capacitor ( $C_{MAM} = 850$  fF), and therefore, the voltage across the MEMS switch is  $0.9 V_{RF-rms}$  and  $0.47 V_{RF-rms}$  for the up-state

and down-state positions, respectively. The current in the MEMS switch is the same as the MAM capacitors (there are two MAM capacitors connected to each MEMS switch). The simulations indicate that the rms voltages across the MEMS switches for the 10Ω and 20Ω loads are below 6 V for the up-state and down-state positions at 6–18 GHz, and therefore, there is no failure due to self-actuation or hold-down. The rms current values are also reasonable (up to 300 mA at 6–18 GHz) which can be easily sustained by 0.8 μm-thick gold bridges [12]. However, at 24 GHz, the down-state voltage and current in S6 and S7 are quite high, and will likely result in a hold-down condition (MEMS switch voltage > 6 V) or a current-failure

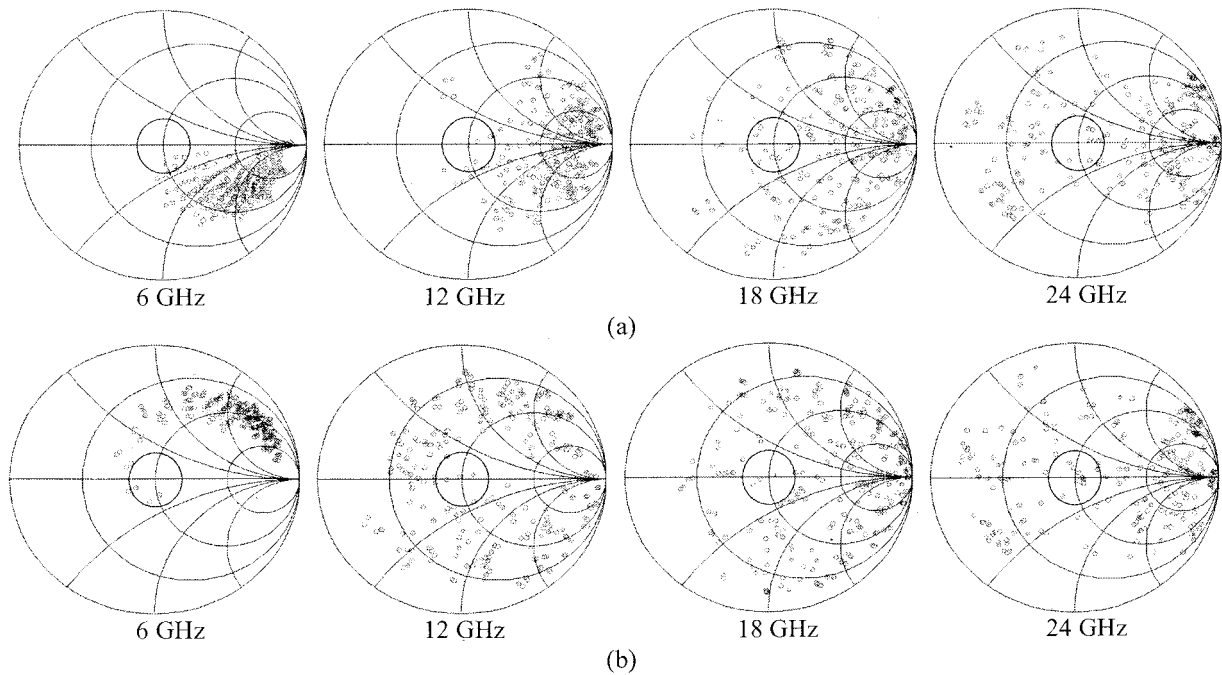


**Figure 13.** Simulated impedances seen by a PA ( $Z_{PA} = 10\Omega$ ) connected to the 8-element matching network and antenna with impedance ( $Z_A$ ) of (a) 10Ω or (b) 200Ω. The Smith chart is a 10Ω chart in both cases above.

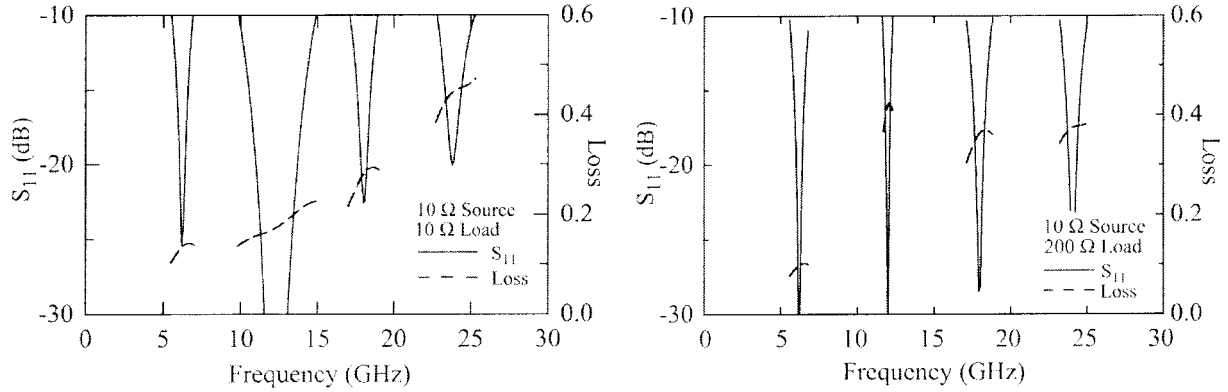


**Figure 14.** Simulated input-reflection coefficient and loss of a PA ( $Z_{PA} = 10\Omega$ ) connected to the 8-element matching network and an antenna impedance ( $Z_A$ ) of  $10\Omega$  or  $200\Omega$ .

condition ( $I_{RF-rms} = 400$  mA). The high current level can be explained by the value of the loading reactance at 24 GHz ( $X = -j16\Omega$ ), which is approaching a short circuit, and the high-voltage levels are due to the electrically long low-impedance resonator, which is

synthesized even with the use of two switches in the down-state position. Again, for  $-20$ -GHz operation, it is best to use a smaller loading capacitance and a shorter separation  $s$ .

Power measurements using on-wafer  $50\Omega$  set-ups are not easily achievable, and if a lumped  $10\Omega$  load is placed at port 2, then  $S_{21}$  cannot be measured, and, most important, the absorbed power in the lumped load cannot be measured unless a precise calorimetric technique is used. Another method is to use a fixed impedance transforming network and a  $50\Omega$  load (that is, power meter) at port 2, with the goal of presenting an effective load of  $10\Omega$  to the reconfigurable network; however, this is quite narrowband, and due to the electrical delay in the CPW probe launchers, one cannot be sure that the impedance seen at port 2 is actually as designed. We have therefore decided to load the reconfigurable network with a standard  $50\Omega$  load (that is, power meter and a CPW probe) and purposely mismatch the input port by selecting different switch combinations. The important value in Figure 17 is the achieved VSWR or  $S_{11}$  under the different switch combinations, since this gives a good idea of the standing waves in the circuit.

The reconfigurable circuit was measured at 8 and 17.6 GHz due to the availability of TWT amplifiers at these frequencies. The measured maximum on-wafer power was  $+29$  dBm at 8 GHz and  $+30.5$  dBm at 17.6 GHz (Fig. 17). At 8 GHz, it is evident that the 8-element circuit can handle up to  $+29$  dBm of RF power (loading reactance is  $X = -j50\Omega$ ) for different VSWR conditions. In this case, the minimum input impedance which can be achieved is about  $13\Omega$  (see Figs. 5 and 7), which corresponds to  $S_{11} = -4.6$  dB. At 17.6 GHz, the circuit starts to self-actuate or hold-down at an RF power of  $+28$ – $29$  dBm when S4 and S7 were actuated ( $S_{11} = -2.6$  dB). The case of (S2,

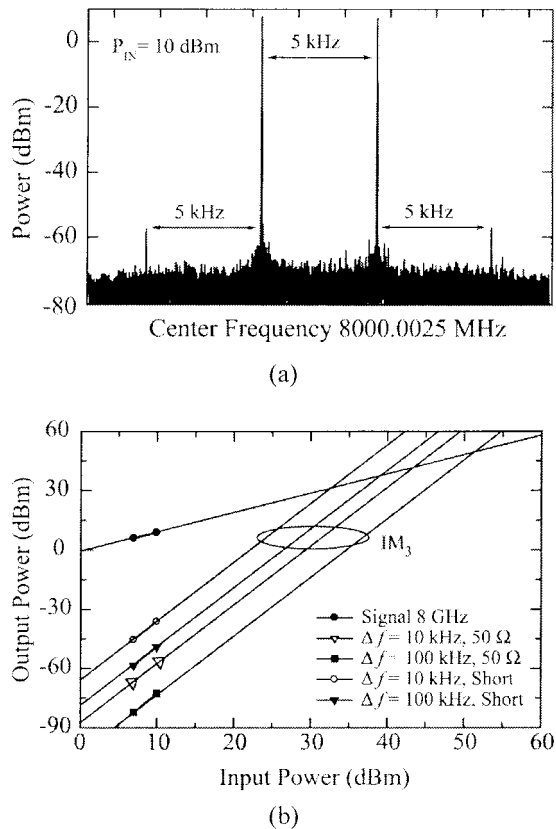


**Figure 15.** (a) Representative measured spectrum of the output ( $50\Omega$ ) or input (short circuit) signals at 8 GHz in the intermodulation setup; (b) measured third-order intermodulation as a function of  $\Delta f$  and the input power level.

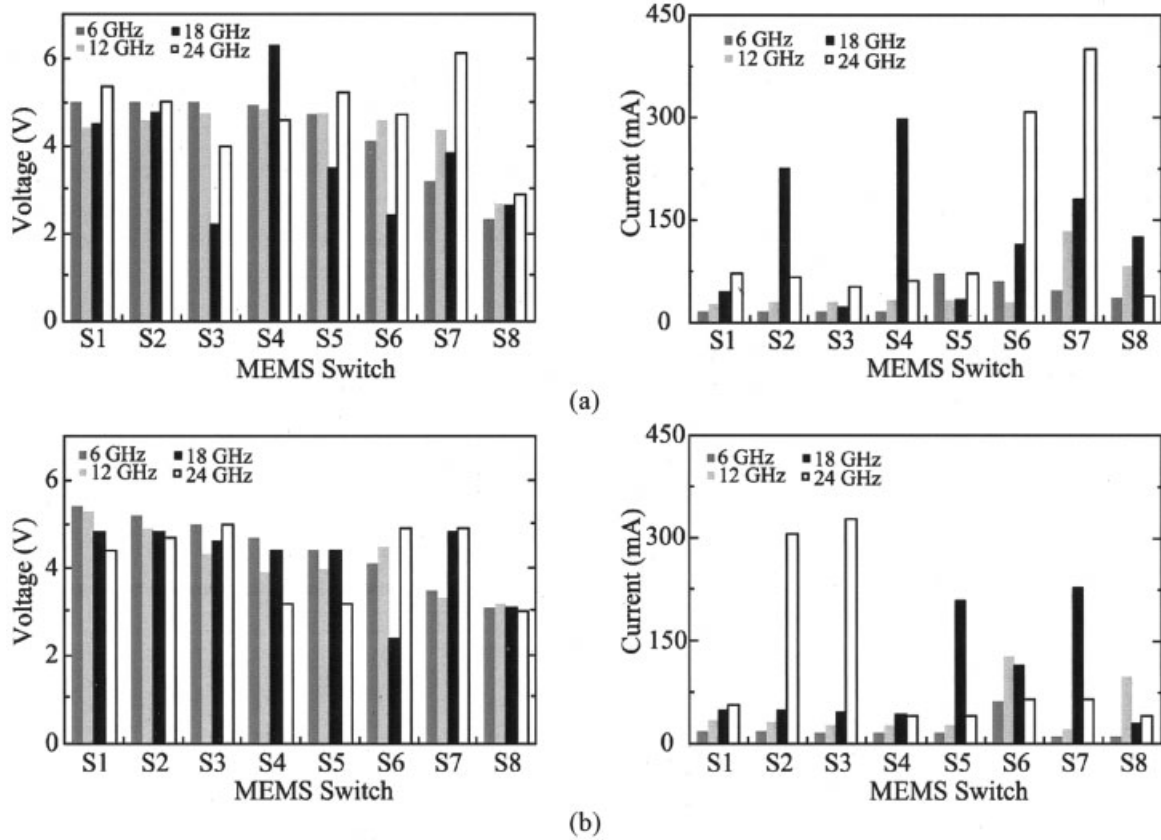


**Figure 16.** Simulated rms voltages and currents for the 8-element matching network with +27-dBm input power at 6, 8, 12, and 24 GHz. The component was terminated with a load of (a) 10Ω or (b) 20Ω, and matched to 50Ω (see Tables II and III, italic entries).

S7) with a VSWR of 13.7 is particularly interesting since one can see an RF self-actuation of several switches at 28.5 dBm thereby changing the reconfigurable circuit impedance (Fig. 18). It is quite hard to determine exactly which switches are actuated as S3

and S4 are starting to be pulled down, the impedance of the network changes and different voltage distribution occurs on the 8-element network. A coupled-microwave-circuit mechanical analysis is needed to find the solution in a dynamic fashion and is not done

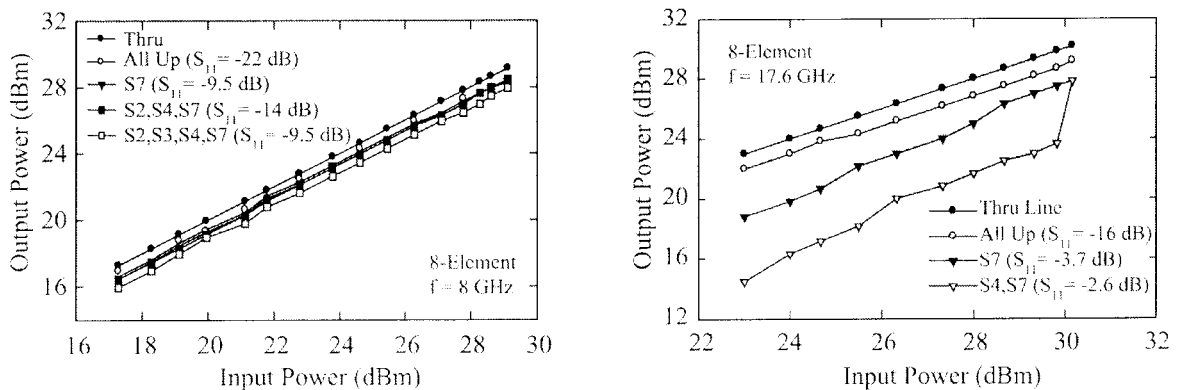


**Figure 17.** The measured power handling of the 8-element MEMS matching networks at 8 and 17.6 GHz under different VSWR ( $S_{11}$ ) conditions.

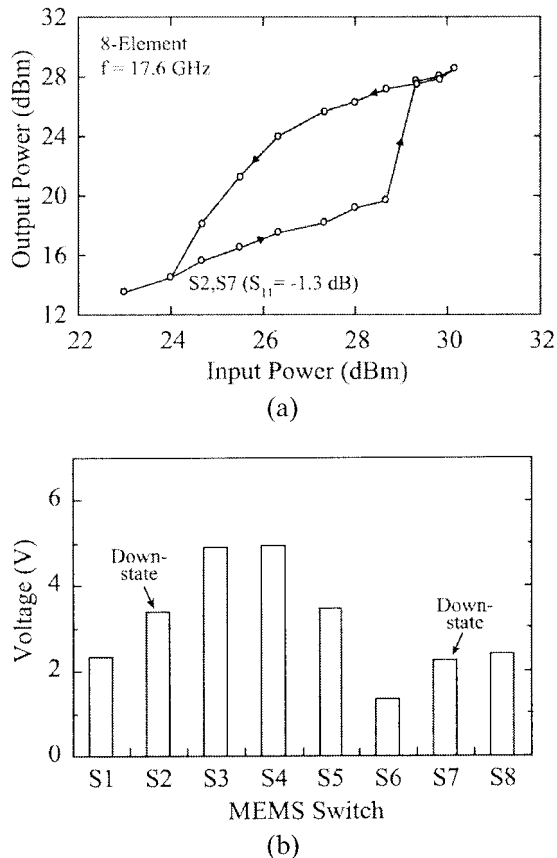


**Figure 18.** An RF self-actuation and hold-down case at 17.6 GHz: (a) measured output power and (b) simulations of the rms circuit voltages when (S2, S7) are actuated at  $P_{IN} = 28.5$  dBm.

in this work. An RF hold-down is present in this new circuit until the power is reduced to 24 dBm, where these particular switches are released to the up-state position and the circuit returns to its initial condition.

We feel confident that the 8-element reconfigurable network with  $g_0 = 1.1 \mu\text{m}$ ,  $V_p = 15\text{--}20$  V, and  $V_h = 6\text{--}8$  V, can handle  $>1$  W of RF power at 8 GHz, and around 600 mW at 18 GHz under different VSWR conditions. If higher-power handling is required, then the pull-down and hold-down voltages must be increased, and this can be done by increasing  $g_0$  or the spring constant of the bridge. Another solution at 18 GHz is to reduce the loading capacitance to  $C_D = 200$  fF (see Fig. 7). This will result in less standing waves and higher power handling, and can still match a  $10\Omega$  impedance at 18 GHz. However, if a wideband 6–18-GHz matching network is needed, then one has to accept the fact that the network will handle more RF power at the low end of the band than at the high end.

## VII. EXTENSION TO 4-ELEMENT NETWORKS

A 4-element tuning network with 16 possible states was also developed for power-amplifier applications. The element values are exactly as Table 1 and the dimensions of the 4-element network are  $1.9 \text{ mm} \times 1.3 \text{ mm}$  (see Fig. 3). The main advantage of this network is a reduced loss at the expense of less impedance coverage.

The measured impedance values with a  $50\Omega$  load agree very well with simulations over a wide frequency range (Fig. 19). The effect of the MEMS bridge capacitance  $C_{U\text{-MEMS}}$ , loading capacitance  $C_D$ , and separation  $s$  are the same as the 8-element network and will not be repeated here. A detailed loss calculation based on the circuit model and the measured  $S$ -parameters shows a loss of 0.25–0.5 dB up to 12 GHz and 1.0–1.5 dB at 18 GHz for  $10\Omega$  and  $20\Omega$  loads (Fig. 20). The impedance match at these frequencies is around  $-15$  to  $-20$  dB, since the network results in only 16 possible combinations. Still, this is excellent for most power amplifiers operating at 4–18 GHz.

Power measurements were also done on the 4-element network (Fig. 21). At 8 and 17.6 GHz, the network can handle at least +29 and +31 dBm of input power under a large range of  $S_{11}$  and VSWR values. Notice that the TWT amplifier was unlevelled and this explains the deviations in linearity even at low-RF input powers.

## VIII. CONCLUSION

This article has presented a novel reconfigurable matching network based on 4- and 8-element loaded-line networks for 4–18 GHz power amplifier applications. The 8-element network presents 256 impedance combinations, including a  $50\Omega$  impedance, and is also applicable for noise-parameter and load-pull measurement systems over a 3:1 frequency band. The 4-element network results in about 66% loss in the 8-element design, but with a smaller impedance coverage (which can be a limitation if the both the PA and antenna impedances varies). Still, it may be an excellent design for PA applications driving a constant load. The designs are quite robust (especially the 8-element network), and can be easily scaled to 18–50 GHz by reducing the loading capacitance and the switched-capacitor separation. It is possible that a 6-element network with 64 impedance points may ultimately be the best compromise between imped-

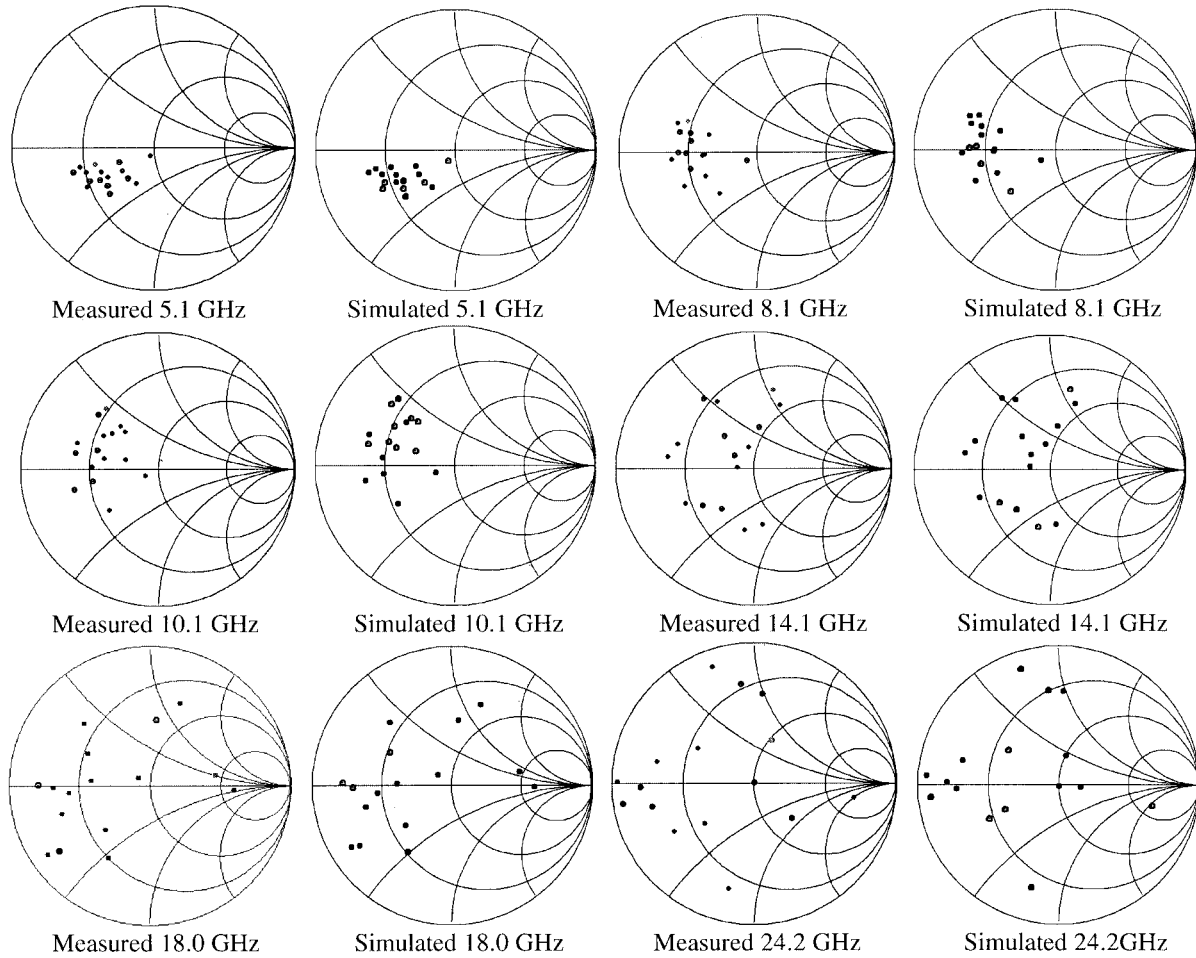


**Figure 19.** Measured (16) and simulated (16) impedances of the 4-element reconfigurable MEMS matching network. The single-cell values are given in Table I.

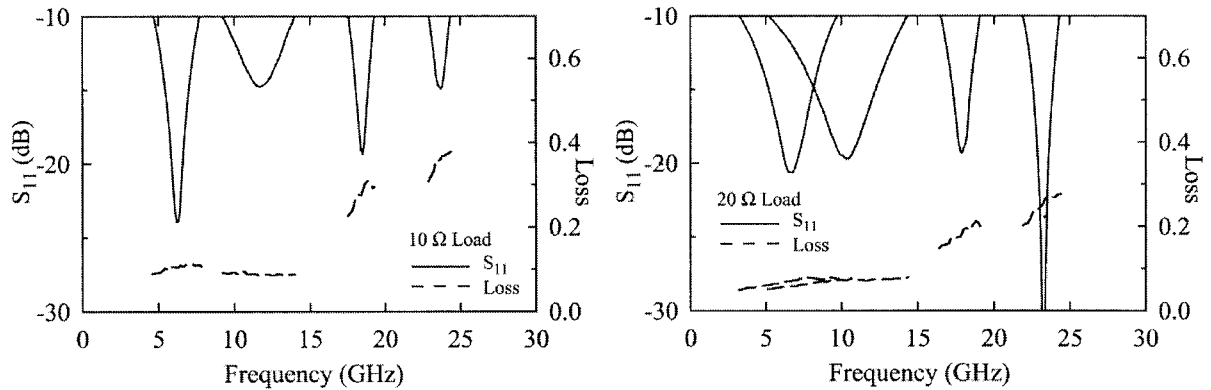


**Figure 20.** Input-reflection coefficient and loss obtained from measured  $S$ -parameters of the 4-element matching network with  $10\Omega$  and  $20\Omega$  loads. The  $10\Omega$  load is matched to  $50\Omega$  at 6 GHz using (S1, S2,S3), at 12 GHz (S3), at 18 GHz (S1, S2, S3), and at 24 GHz (S2, S3). The  $20\Omega$  load is matched to  $50\Omega$  at 6 GHz using (S1, S3), at 12 GHz (S3), at 18 GHz (S1, S2, S3), and at 24 GHz (S2, S3).

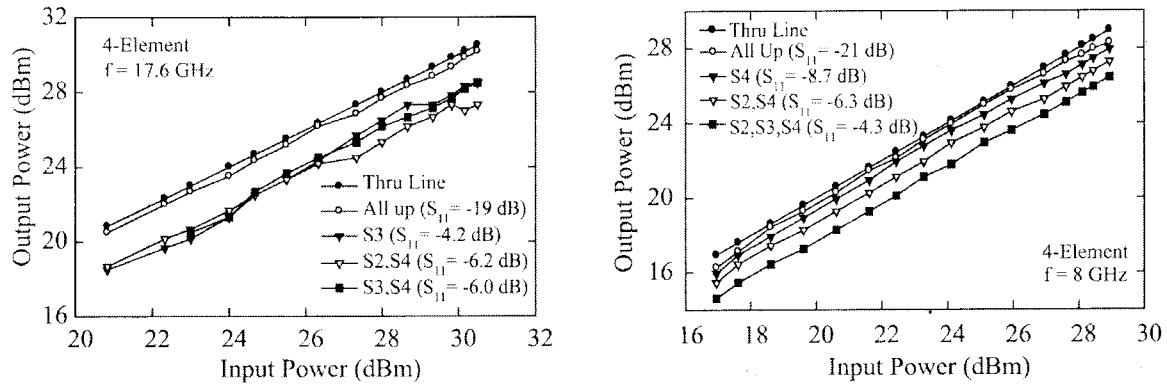


**Figure 21.** Power handling of the 4-element MEMS matching networks at 8 and 17.6 GHz under different VSWR ( $S_{11}$ ) conditions.

ance flexibility and network loss in PA to antenna applications.

## ACKNOWLEDGMENTS

This work was funded under the DARPA IRFFE program, under a subcontract from BAE; Dr. Edgar Martinez was Program Manager. The authors thank Donna Ryan and Richard Millard, BAE, for their technical inputs.

## REFERENCES

1. N.S. Barker and G.M. Rebeiz, Optimization of distributed MEMS transmission line phase shifters — U-band and W-band designs, *IEEE Transactions on Microwave Theory and Techniques*, vol. 48, Nov. 2000, pp. 1957–1966.
2. H.T. Kim, S. Jung, K. Kang, J.H. Park, Y.K. Kim, and Y. Kwon, Low-loss analog and digital micromachined impedance tuners at the Ka-band, *IEEE Transactions on Microwave Theory and Techniques*, vol. 49, pp. 2394–2400, Dec. 2001.
3. J. Papapolymerou, K.L. Lange, C.L. Goldsmith, A. Malczewski, and J. Kleber, Reconfigurable double-stub tuners using MEMS switches for intelligent RF front-ends, *IEEE Transactions on Microwave Theory and Techniques*, vol. 51, pp. 271–278, Jan. 2003.
4. J.S. Hayden and G.M. Rebeiz, Very low-loss distributed X-band and Ka-band MEMS phase shifters using metal-air-metal capacitors, *IEEE Transactions on Microwave Theory and Techniques*, vol. 51, Jan. 2003, pp. 309–314.
5. Y. Liu, A. Borgioli, A.S. Nagra, and R.A. York, K-band 3-bit low-loss distributed MEMS phase shifter, *IEEE Microwave and Guided Wave Lett.*, vol. 10, Oct. 2000, pp. 415–417.
6. A. Abbaspour-Tamijani, L. Dussopt, and G.M. Rebeiz, Miniature and tunable filters using MEMS capacitors, *IEEE Transactions on Microwave Theory and Techniques*, vol. 51, July 2003, pp. 1878–1885.
7. *Advanced Design System 2002*, Agilent Technologies, Santa Clara, CA, USA, 2002.
8. R. E. Collin, *Foundations for microwave engineering*, 2<sup>nd</sup> edition, New York, McGraw-Hill, 1992.
9. J.B. Rizk, W-band RF MEMS switches, phase shifters and antennas, Ph.D. dissertation, Dept. Elect. Eng. Univ. of Michigan at Ann Arbor, MI, 2003.
10. G.M. Rebeiz, *RF MEMS theory, design, and technology*, John Wiley & Sons, New York, 2003.
11. L. Dussopt, G.M. Rebeiz, Intermodulation distortion and power handling in RF MEMS switches, varactors and tunable Filters, *IEEE Transactions on Microwave Theory and Techniques*, vol. 51, April 2003, pp. 1247–1256.
12. J.B. Rizk, E. Chaiban, G.M. Rebeiz, Steady state thermal analysis and high-power reliability considerations of RF MEMS capacitive switches, *microwave symposium digest, IEEE MTT-S International Meeting*, June 2, Seattle, WA, 2002, pp. 239–242.

## BIOGRAPHIES

**Tauno Vähä-Heikkilä** was born in Finland in 1977. He received his B.S. and M.S. degrees in Physics from the University of Turku in 2000 and 2001, respectively. From 2000 to 2001 he was a Trainee Research Scientist, and since 2001 has worked as a Research Scientist at the Millimeter Wave Laboratory of Finland–MilliLab, VTT TECHNICAL RESEARCH CENTER OF FINLAND. He was a Visiting Scholar at the Radiation Laboratory, the University of Michigan at Ann Arbor in 2002 and 2003. His research interests include development of reconfigurable RF MEMS circuits and millimeter wave on-wafer noise parameter and cryogenic measurements of active devices.

**Gabriel M. Rebeiz** (Fellow, IEEE) earned his Ph.D. degree in electrical engineering from the California Institute of Technology, Pasadena, and is a Full Professor of EECS at the University of Michigan, Ann Arbor. His research interests include applying microelectromechanical systems (MEMS) for the development of novel RF and microwave components and sub-systems. He is also interested in Si RFIC design for radar and communication systems, and in the development of millimeter-wave front-end electronics planar antennas, imaging systems and phased-arrays.

Prof. Rebeiz was the recipient of the National Science Foundation Presidential Young Investigator Award in April 1991, and the URSI International Isaac Koga Gold Medal Award in August 1993. Prof. Rebeiz was selected by the students as the 1997–1998 Eta-Kappa-Nu EECS Professor of the Year. In October 1998, he received the Amoco Foundation Teaching Award, given yearly to one or two faculty at the University of Michigan, for excellence in undergraduate teaching. Prof. Rebeiz is the co-recipient, with Prof. Scott Barker, of the IEEE 2000 Microwave Prize. In 2003, he received the Outstanding Young Engineer Award of the IEEE MTT Society. Prof. Rebeiz is a Distinguished Lecturer for the IEEE MTT Society.

PUBLICATION P8

**A 20–50 GHz Reconfigurable  
Matching Network for Power  
Amplifier Applications**

In: 2004 IEEE MTT-S International Microwave Symposium  
Digest, Forth Worth, TX, USA, 2004. Pp. 717–721.  
© 2004 IEEE. Reprinted with permission from the publisher.

# A 20-50 GHz Reconfigurable Matching Network for Power Amplifier Applications

T. Vähä-Heikkilä<sup>1,2</sup> and G. M. Rebeiz<sup>1</sup>

<sup>1</sup>University of Michigan, Ann Arbor, MI, 48105, USA

<sup>2</sup>MilliLab, VTT Information Technology, P.O.BOX 12021, 02044 VTT, Finland

**Abstract** — A reconfigurable matching network has been developed and it is based on loaded line techniques. It consists of 8 switched MEMS capacitors producing 256 ( $2^8$ ) different impedances and is only 1x2.5 mm in size on a glass substrate. The network is ideally suited to match power amplifiers with 10-20  $\Omega$  output impedance to 50-60  $\Omega$  systems at 20-50 GHz. The estimated loss of the network is only 1-1.5 dB at 40 GHz while matching a 10-20  $\Omega$  load to a 50  $\Omega$  load. The reconfigurable network can also be used as an impedance tuner in noise parameter and load-pull measurements of active devices at 30-65 GHz.

**Index Terms** — RF MEMS, impedance tuner, noise parameters, load-pull, matching network, phased array.

## I. INTRODUCTION

The output impedance of power amplifiers (PA) with 1-2 W output power and a 5 V power supply is typically between 10 and 20  $\Omega$ , and are mismatched in 50  $\Omega$  systems. Optimum power transfer from the PA to an antenna can be ensured with a wideband low-loss impedance matching network (Fig. 1). Both the output impedance of the PA ( $Z_{PA}$ ) and the input impedance of the antenna ( $Z_A$ ) can vary and the matching network should be flexible to maintain optimum power transfer in the both cases.  $Z_{PA}$  can change as a function of frequency and with different bias conditions.

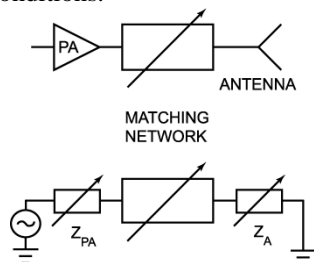


Fig. 1. A reconfigurable matching network used between a power amplifier and a radiating antenna.

In addition to matching applications, reconfigurable matching networks can be used as impedance tuners in noise parameter and load-pull measurements of active devices. Commercial impedance tuners are usually either coaxial or waveguide structures requiring large space [1].

Reconfigurable impedance matching networks/ tuners are typically based on the double-stub [2,3] or triple-stub topologies [4] and can be made using MMIC or RF MEMS technologies. A problem related to MMIC varactor or transistor based matching networks is limited tuning range because of the resistance of active devices. Also, MMIC matching networks have electrical noise and intermodulation products which affects the system performance.

In this work, a novel reconfigurable RF MEMS matching network, based on a transmission line (t-line) loaded with 8 identical switched MEMS capacitors is presented. The network is capable of very wideband PA matching with low loss at 20-50 GHz.

## II. DESIGN

The phase velocity and impedance of a t-line can be changed by loading it capacitively. This idea has been used successfully in distributed transmission-line (DMTL) MEMS phase-shifters [5]. The loaded line technique can be applied to reconfigurable matching networks by loading a t-line with  $N$  digitally controlled switched MEMS capacitors each having capacitances  $C_U$  (up-state position) and  $C_D$  (down-state position). The line impedance is chosen to be approximately 50  $\Omega$  when the MEMS capacitors are in the up-state position. When a MEMS capacitor is actuated to the down-state position, the loading on the t-line increases thus resulting in a localized low impedance and a high effective dielectric constant (around the region of the MEMS capacitor). Since the loading is increasingly capacitive with more MEMS switches being actuated, the network will transform a 50-60  $\Omega$  load into a low input impedance (or vice versa due to reciprocity), and the higher the capacitive loading, the lower the input impedance. A 4 to 8-element design results in 16 to 256 ( $2^N$ ) different impedance points on the Smith Chart, and the distributed nature of the design ensures wideband frequency coverage. Also, at high frequencies and due to the varying electrical length of the loaded t-line, when the switched capacitors are actuated, the

impedance coverage covers the entire Smith chart and not only the low impedance region.

The equivalent circuit and picture of a switched MEMS capacitor are shown in Figs. 2-3. The switched capacitor is a combination of a capacitive MEMS switch attached fixed metal-air-metal (MAM) capacitors. Typically, the capacitance ratio of a capacitive MEMS switch is 30:1, and this can be lowered using fixed capacitors in series with a capacitive MEMS switch. The fabricated switched capacitor is based on a coplanar waveguide (CPW) with dimensions 100/100/100  $\mu\text{m}$  (G/W/G) on a 500  $\mu\text{m}$  glass substrate ( $\epsilon_r = 4.6$ ). Dimensions of the MEMS switch are 250  $\mu\text{m}$  x 80  $\mu\text{m}$  x 0.8  $\mu\text{m}$ . Fabrication of the switched MEMS capacitor is based on standard surface MEMS techniques and is identical as used in [4]. Fitted (based on measurements) values for the equivalent circuit of switched MEMS capacitor and t-line properties are presented in Table 1. The measured capacitance ratio of the RF MEMS switch is 8:1 due to its low height and the thick silicon-nitride layer. The total up-state and down-state capacitances of the switched capacitor ( $C_{\text{MEMS}}$  in series with  $C_{\text{MAM}}$ ) are  $C_U = 45.1$  fF and  $C_D = 129$  fF, respectively, resulting in a capacitance ratio of 2.9:1. The quality factor of the switched MEMS capacitor is calculated using  $Q = (2\pi f C (R_{\text{MEMS}} + R_{\text{MAM}}))^{-1}$  and at 30 GHz results in up and down states values of  $Q_U = 168$  ( $C_U = 45.1$  fF,  $X = -j118 \Omega$ ) and  $Q_D = 59$  ( $C_D = 129$  fF,  $X = -j41.3 \Omega$ ).

There are many different parameters that can be optimized in the loaded-line network. The highest frequency of operation is limited by the Bragg frequency (see below) of the loaded-line, and the lowest impedance, which can be matched to 50  $\Omega$  is dependent on the loading capacitance. A closed-form design technique has not been found since the location, electrical length, and loaded-line impedance change with the actuation of the MEMS switched capacitors, and therefore, Agilent ADS [6] is used extensively for choosing  $C_U$ ,  $C_D$ ,  $s$ , and the number of capacitors. The design was optimized to have 8 switched capacitors and is presented in Fig. 4.

In this design, the loaded line characteristics are  $Z_U = 47 \Omega$  and  $\epsilon_{\text{reff}_U} = 9.1$ , and  $Z_D = 31 \Omega$  and  $\epsilon_{\text{reff}_D} = 21$ , when the MEMS switches are in the up-state and down-state positions, respectively. The impedance in the up-state was designed to be 50  $\Omega$  but it is lower since the MEMS bridges are curved down resulting in a larger loading capacitance. The Bragg frequency is calculated using [5]:

$$f_B = \frac{cZ_L}{\pi s Z_0 \sqrt{\epsilon_{\text{reff}}}} \quad (1)$$

and is 105 GHz and 69.5 GHz when all the bridges are in the up-state and down-state positions, respectively. In general, it is desirable to have a relatively high Bragg frequency to obtain good operation over a wide frequency range.

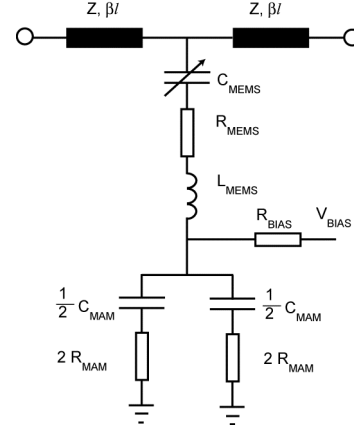


Fig. 2. Equivalent circuit a switched MEMS capacitor.

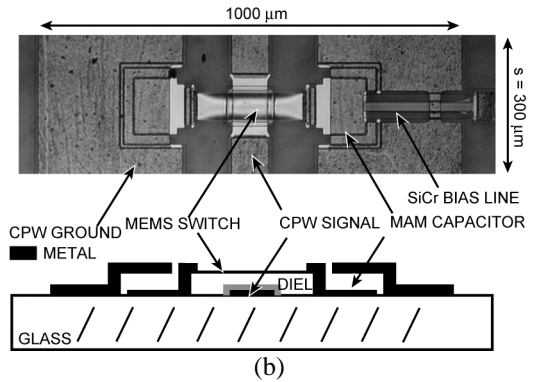


Fig. 3. Picture and cross-section of a switched MEMS capacitor.

TABLE 1  
MEASURED T-LINE PROPERTIES FROM THE TRL CALIBRATION, FITTED VALUES FOR THE SWITCHED MEMS CAPACITOR, AND LOADED LINE CHARACTERISTICS.

$\epsilon_r$	4.6
$Z_0 (\Omega)$	86.2
$\epsilon_{\text{reff}}$	2.72
$\alpha$ (dB/cm), 20/30/40 GHz	0.52/0.78/1.1
$C_{\text{MEMS}}$ Up State- $C_{\text{UP}}$ (fF)	61
$C_{\text{MEMS}}$ Down State- $C_{\text{DOWN}}$ (fF)	500
$R_{\text{BIAS}}$ (k $\Omega$ )	> 3
$L_{\text{MEMS}}$ (pH)	9.5
$R_{\text{MEMS}} + R_{\text{MAM}}$ ( $\Omega$ )	0.7
$C_{\text{MAM}}$ (fF)	167
$s$ ( $\mu\text{m}$ )	300
$Z_U (\Omega), \epsilon_{\text{reff}_U}$	47, 9.1
$Z_D (\Omega), \epsilon_{\text{reff}_D}$	31, 21

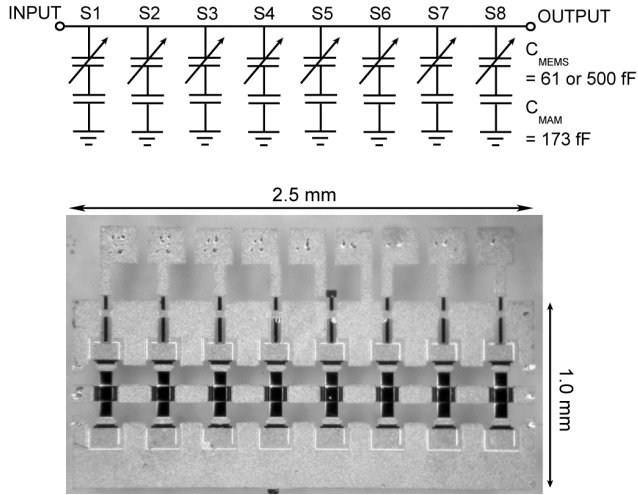


Fig. 4. Schematics and picture of the reconfigurable matching network with 8 switched MEMS capacitors (S1-S8).

The measured and simulated S-parameters for the 8-element matching network are shown in Fig. 5. Agilent ADS is used for fitting the values of the switched MEMS capacitor (Fig. 2 and Table 1).

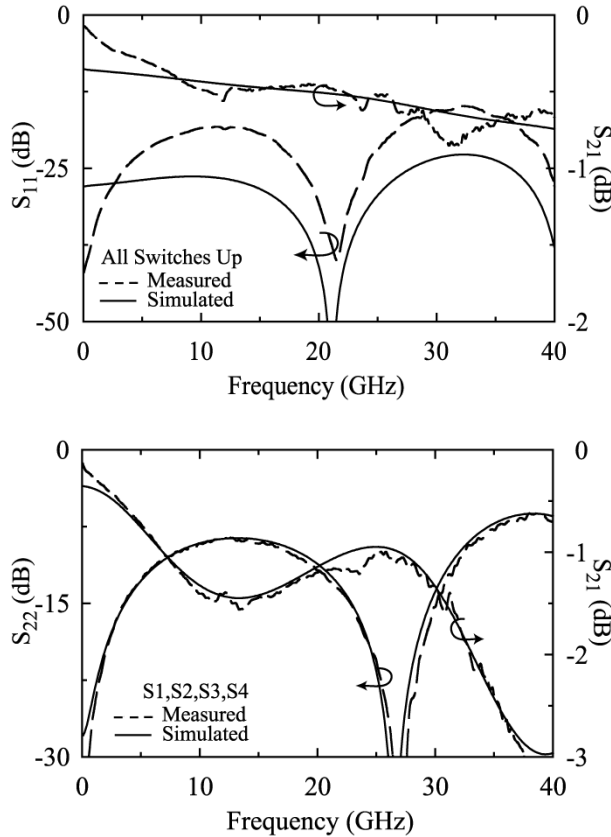
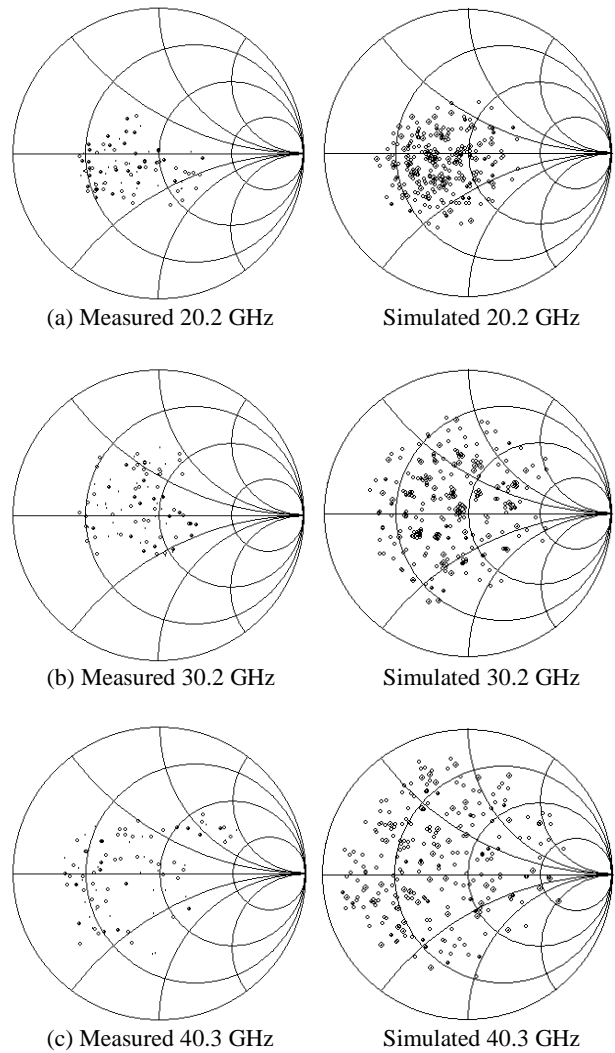


Fig. 5. Measured and simulated S-parameters for the reconfigurable matching network with two different switch combinations. The combinations are written in the figures.

### III. IMPEDANCE COVERAGE AND MATCHING

#### A. Impedance coverage

The measured (90 points) and simulated (256 points) impedance coverage of the reconfigurable distributed matching network is presented in Fig. 6 at 16-60 GHz. The measurements were done up to 40.3 GHz with 90 different switch settings out of 256 possible combinations, and only simulated results are presented above 40 GHz. Other data at 24, 28, 34, and 38 GHz are not shown, but they all agree well with simulations. Notice that the network is ideally suited for matching low impedance loads at all frequencies up to 60 GHz.



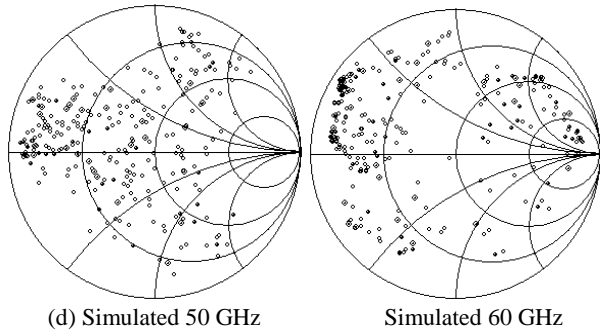


Fig. 6. (a)-(d) Measured (90 points) and simulated (256 points) impedance coverage of the reconfigurable distributed impedance matching network.

### B. Case study: Matching 10 and 20 $\Omega$ loads to 50 $\Omega$

The accurate circuit model can also be used to analyze different matching conditions. 10 and 20  $\Omega$  loads are matched to 50  $\Omega$  at different frequencies separately and the input reflection coefficient (seen from the 50  $\Omega$  source) and loss of the network are shown in Fig. 7. The loss in dB is defined as  $10\log(1-\text{loss})$  and a loss of 0.2 results in a 1 dB loss. For a 20  $\Omega$  load, the loss is 0.7-1.25 dB from 10 to 40 GHz, which is indeed very low. For a 10  $\Omega$  load, the loss is 1.2 dB up to 40 GHz and only 1.4-1.6 dB at 50-55 GHz. This is also very low for a 5:1 impedance match. The reason is that the network is electrically and physically very short and the loaded capacitors have a high Q. Also, no short circuits are induced in the MEMS components, and a capacitance change of 3:1 with  $X = -j120$  to  $X = -j40$  is present on the network. To our knowledge, this work represents state-of-the-art performance at 20-60 GHz.

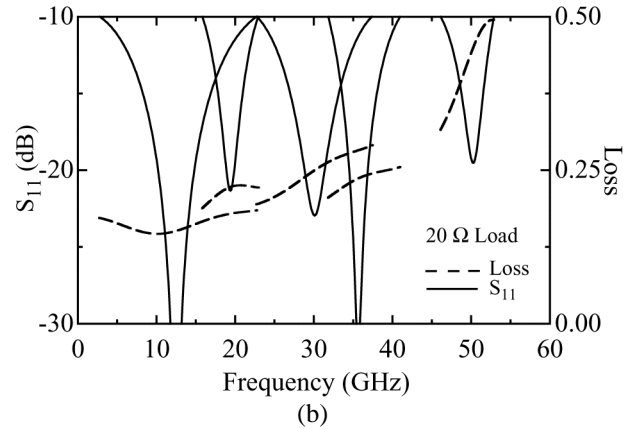
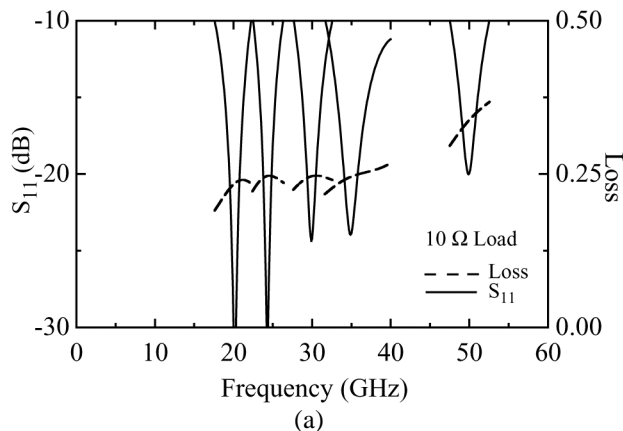


Fig. 7. Simulated input reflection coefficient and loss of the distributed matching network with a 10  $\Omega$  (a) or 20  $\Omega$  (b) load matched to 50  $\Omega$  separately at different frequencies with different switch combinations.

## CONCLUSIONS

This paper presented a novel reconfigurable matching network. It is based on loaded-line techniques and it was realized with 8 switched MEMS capacitors producing 256 ( $2^8$ ) different impedances. The loaded-line reconfigurable networks are much more efficient than double or triple stub networks (less space and elements) and are ideally suited for wideband low-impedance power amplifier matching.

## REFERENCES

- [1] M. Kantanen, M. Lahdes, T. Vähä-Heikkilä, J. Tuovinen: "A wideband automated measurement system for on-wafer noise parameter measurements at 50-75 GHz", *IEEE Transactions on Microwave Theory and Techniques*, vol. 51, pp. 1489-1495, June, 2003.
- [2] H.-T. Kim, S. Jung, K. Kang, J.-H. Park, Y.-K. Kim, and Y. Kwon, "Low-Loss Analog and Digital Micromachined Impedance Tuners at the Ka-Band," *IEEE Transactions on Microwave Theory and Techniques*, vol. 49, pp. 2394-2400, Dec. 2001.
- [3] J. Papapolymerou, K. L. Lange, C. L. Goldsmith, A. Malczewski, and J. Kleber: "Reconfigurable Double-Stub Tuners Using MEMS Switches for Intelligent RF Front-Ends," *IEEE Transactions on Microwave Theory and Techniques*, vol. 51, pp. 271-278, Jan. 2003.
- [4] T. Vähä-Heikkilä, J. Varis, J. Tuovinen, and G. M. Rebeiz, "A 6-20 GHz Reconfigurable RF MEMS Impedance Tuner," *submitted to IEEE Microwave Symposium 2004*.
- [5] N. S. Barker and G. M. Rebeiz "Optimization of distributed MEMS transmission line phase shifters — U-band and W-band designs" *IEEE Transactions on Microwave Theory and Techniques*, vol. 48, pp. 1957-1966, Nov. 2000.
- [6] Advanced Design System 2002, Agilent Technologies, Santa Clara, CA, USA, 2002.

Author(s) Vähä-Heikkilä, Tauno			
Title <b>MEMS tuning and matching circuits, and millimeter wave on-wafer measurements</b>			
Abstract The focus of this thesis is on the development of on-wafer measurement techniques for millimeter wave device and circuit characterization as well as on the development of MEMS based impedance tuning circuits both for measurement and telecommunication applications. Work done in this thesis is presented with eight scientific articles written by the author. The summary of the thesis introduces the field of on-wafer measurements and impedance tuning methods, and is followed by the articles.  Wide-band on-wafer measurement systems have been developed for noise parameter measurement at room temperature at W-band, and for cryogenic S-parameter measurements at 50–110 GHz and 20–295 K. Using the developed systems, noise parameters of an InP HEMT have been measured and results are shown in the frequency band of 79–94 GHz. These are the first published noise parameter measurement results for an active device at W-band, and first on-wafer measurement results at cryogenic conditions and at 50–110 GHz.  Novel RF MEMS impedance tuners have been developed for instrumentation and measurement applications to improve measurement automation and accuracy in on-wafer measurements. Several integrated impedance tuners have been realized to cover 6–120 GHz frequency range. RF MEMS technology has also been used for reconfigurable matching networks. Reconfigurable distributed 4–18 GHz and 30–50 GHz matching networks have been designed, fabricated, and characterized. These are based on switched 4 or 8 MEMS capacitors producing 16 or 256 different impedances. The matching networks are ideal for multi-band and wide impedance range amplifier as well as for antenna matching and tuning applications. Both the tuners and matching networks have shown state-of-the-art performance for circuits realized with integrated circuit technologies.			
Keywords RF MEMS, on-wafer measuring techniques, millimeter wave devices, impedance tuning, instrumentation, noise parameter measurements, reconfigurable matching networks, W-band measurement, double-stub tuners, triple-stub tuners, amplifier applications			
ISBN 951–38–6704–8 (nid.) 951–38–6705–6 (URL: <a href="http://www.vtt.fi/publications/index.jsp">http://www.vtt.fi/publications/index.jsp</a> )			
Series title and ISSN VTT Publications 1235–0621 (nid.) 1455–0849 (URL: <a href="http://www.vtt.fi/publications/index.jsp">http://www.vtt.fi/publications/index.jsp</a> )			Project number
Date March 2006	Language English, Finnish abstr.	Pages 86 p. + app. 82 p.	Price D
Name of project MEMSTUNER		Commissioned by	
Contact VTT Technical Research Centre of Finland Tietotie 3, P.O. Box 1000, FI-02044 VTT, Finland Phone internat. +358 20 722 111 Fax +358 20 722 7012		Sold by VTT Technical Research Centre of Finland PL 1000, 02044 VTT Puh. 020 722 4404 Faksi 020 722 4374	

Tekijä(t) Vähä-Heikkilä, Tauno			
Nimeke <b>Mikromekaaniset viritys- ja sovituspierit sekä millimetri- aaltoalueen suoraan kiekolta tehtävät mittaukset</b>			
Tiivistelmä Väitöskirjatyössä kehitettiin suoraan kiekolta tehtäviä millimetriaaltoalueen mittauksia sekä mikromekaanisia (MEMS) impedanssin säätö- ja sovituspierijä.  Mittauslaitteistoja ja -menetelmiä kehitettiin suoraan kiekolta tehtäviin mittauksiin millimetriaaltoalueelle. Kohinaparametrien mittaamiseksi kehitettiin laitteisto W-alueelle (75–110 GHz), ja mittaustulokset esitetään InP HEMT -transistorille 79–94 GHz taajuusalueella. Sirontaparametrien mittaamiseksi kryogeenisissä olosuhteissa kehitettiin laitteisto W-alueelle, ja laajakaistaiset sekä kahden aaltoputkikaistan kattavat mittaustulokset esitetään InP HEMT -transistoreille 50–110 GHz:n taajuusalueella ja 20–295 K:n lämpötiloissa. Sekä molemmat mittauslaitteistot että esitettävät tulokset ovat ainutlaatuisia näillä taajuuksilla.  Kohinaparametrimittauslaitteistojen kehittämiseksi ja mittausten automatisoimiseksi väitöskirjatyössä suunniteltiin ja valmistettiin integroitua mikromekaanisia impedanssiviritimiä. Impedanssiviritimillä tuotetaan erilaisia impedansseja, ja niitä voidaan kontrolloida sähköisesti. Impedanssin säätö perustuu MEMS-kondensaattoreihin, ja kehitetyillä piireillä saadaan tuotettua tuhansia erilaisia impedansseja riippuen MEMS-kondensaattoreiden lukumäärästä. Impedanssiviritimiä kehitettiin usealle eri taajuusalueelle taajuuksien 6 ja 120 GHz välille. Virittimien tuottama heijastuskertoimen on parhaimmillaan lähellä yhtä mitatun seisovan aallon suhteen ollessa 199 taajuudella 30 GHz. Työssä myös sovellettiin MEMS-kondensaattoreita impedanssinsovituspierisiin tehovahvistimen ja antennin sovitamiseksi. Piireissä integroidun siirtolinjan sähköistä pituutta ja impedanssia muutetaan. Mitatut tulokset osoittavat, että piireillä voidaan sovittaa paljon erilaisia impedansseja pienin häviöin ja lineaarisesti.			
Avainsanat RF MEMS, on-wafer measuring techniques, millimeter wave devices, impedance tuning, instrumentation, noise parameter measurements, reconfigurable matching networks, W-band measurement, double-stub tuners, triple-stub tuners, amplifier applications			
ISBN 951-38-6704-8 (nid.) 951-38-6705-6 (URL: <a href="http://www.vtt.fi/publications/index.jsp">http://www.vtt.fi/publications/index.jsp</a> )			
Avainnimeke ja ISSN VTT Publications 1235-0621 (nid.) 1455-0849 (URL: <a href="http://www.vtt.fi/publications/index.jsp">http://www.vtt.fi/publications/index.jsp</a> )			Projektinumero
Julkaisu-aika Maaliskuu 2006	Kieli Englanti, suom. tiiv.	Sivuja 86 s. + liitt. 82 s.	Hinta D
Projektin nimi MEMSTUNER		Toimeksiantaja(t)	
Yhteystiedot VTT Tietotie 3, PL 1000, 02044 VTT Puh. vaihde 020 722 111 Faksi 020 722 7012		Myynti VTT PL 1000, 02044 VTT Puh. 020 722 4404 Faksi 020 722 4374	

This work deals with millimeter wave on-wafer measurement techniques for device and circuit characterization as well as with MicroElectroMechanical Systems (MEMS) based impedance tuning and matching circuits both for measurement and telecommunication applications. This thesis work has produced new knowledge and scientific results in the following areas: 1) cryogenic on-wafer measurements at millimeter wavelengths; 2) on-wafer noise parameter measurement methods and a system for W-band device characterization; 3) novel impedance tuners for measurement applications based on RF MEMS technology; and 4) novel reconfigurable matching networks for telecommunication applications based on RF MEMS technology. The work includes on-wafer measurement system development, RF MEMS circuit design, fabrication, and characterization which are described in the thesis.

---

Tätä julkaisua myy	Denna publikation säljs av	This publication is available from
VTT PL 1000 02044 VTT Puh. 020 722 4404 Faksi 020 722 4374	VTT PB 1000 02044 VTT Tel. 020 722 4404 Fax 020 722 4374	VTT P.O. Box 1000 FI-02044 VTT, Finland Phone internat. +358 20 722 4404 Fax +358 20 722 4374

---

ISBN 951- 38- 6704- 8 (soft back ed.)  
ISSN 1235- 0621 (soft back ed.)

ISBN 951- 38- 6705- 6 (URL: <http://www.vtt.fi/inf/pdf/>)  
ISSN 1455- 0849 (URL: <http://www.vtt.fi/inf/pdf/>)